Photo source: West Channel of the Hay River, Town of Hay River, NT (NHC, 2023)

Kátł'odeh (Hay River) Flood Hazard Mapping Study

Summary Report

Prepared by:

Northwest Hydraulic Consultants Ltd.
9819 – 12 Avenue SW
Edmonton, AB T6X 0E3
Tel: 780.436.5868
www.nhcwater.com

Prepared for:

Government of Northwest Territories
Environment and Climate Change
Yellowknife, NT X1A 2L9

May 15, 2025
Summary Report

NHC Reference No. 1008469

Report prepared by:

Agata Hall, MSc, PEng
Associate

Darshan Logithasan, EIT
Project Engineer-in-Training

Dan Healy, PhD, PEng
Principal

Report reviewed by:

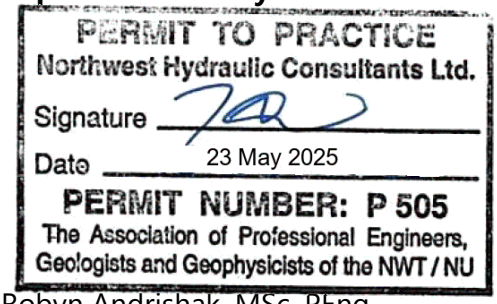

Robyn Andrishak, MSc, PEng
Principal
Branch Manager

DISCLAIMER

This report has been prepared by Northwest Hydraulic Consultants Ltd. for the benefit of Government of Northwest Territories for specific application to the Kátł'odeh (Hay River) Flood Hazard Mapping Study. The information and data contained herein represent **Northwest Hydraulic Consultants Ltd.'s** professional judgment in light of the knowledge and information available to **Northwest Hydraulic Consultants Ltd.** at the time of preparation and were prepared in accordance with generally accepted engineering and geoscience practices.

Except as required by law, this report and the information and data contained herein are to be treated as confidential and may be used and relied upon only by Government of Northwest Territories, its officers, and employees. **Northwest Hydraulic Consultants Ltd.** denies any liability whatsoever to other parties who may obtain access to this report for any injury, loss, or damage suffered by such parties arising from their use of or reliance upon this report or any of its contents.

CREDITS AND ACKNOWLEDGEMENTS

The authors would like to thank the Government of Northwest Territories for initiating this study as well as the Government of Canada for funding through the Flood Hazard Identification and Mapping Program.

The following agencies were key contributors of information supporting this work.

- Natural Resources Canada (NRCan)
- Government of Northwest Territories (GNWT)
- Environment and Climate Change Canada (ECCC)
- Water Survey of Canada, ECCC (WSC)
- Town of Hay River
- Kátł'odeeche First Nation
- West Point First Nation

We are grateful for the support provided during the project, in particular:

- Anna Coles – GNWT
- Shawne Kokelj – GNWT
- Jad Saade – GNWT
- Michele Culhane – GWNT
- Ryan Connon – GNWT
- Melanie Desjardins – GNWT
- Kyle Little – GNWT
- Christy Fung – GNWT
- Brian Perry – NRCan
- Sara Karam – NRCan
- Joshua Wiebe – ECCC
- Apurba Das – ECCC
- Marcena Croizier – WSC
- Travis Wright – Town of Hay River

The primary author of this report was Agata Hall of Northwest Hydraulic Consultants, under the direction of Dan Healy. Darshan Logithasan provided significant contributions to report writing and figures. Mariza Costa-Cabral provided expert review and most of the documentation pertaining to climate change assessment

TABLE OF CONTENTS

TABLES

FIGURES

APPENDICES

1 INTRODUCTION

1.1 Project Overview

Northwest Hydraulic Consultants Ltd. (NHC) was retained by the Government of the Northwest Territories (GNWT) Department of Environment and Climate Change to develop flood hazard maps for the communities of Hay River, Kátł'odeeche First Nation, Fort Simpson, and Aklavik. This project was funded in part under the Flood Hazard Identification and Mapping Program (FHIMP) with additional support from the GNWT. The intended use of these flood hazard maps is for community infrastructure planning and other flood mitigation measures, and emergency preparedness.

This report provides the results of the flood hazard mapping study for the Town of Hay River and Kátł'odeeche First Nation and includes the following: a summary of the data collection and review; results of the 2024 river cross section survey; ice jam flood hydrology; hydraulic modelling; and the development of flood inundation and flood hazard maps. Potential impacts of climate change are also discussed.

1.2 Study Area

The Town of Hay River and Kátł'odeeche First Nation are situated within a small delta formed as the Hay River enters Great Slave Lake (**Figure 1**), approximately 200 km south of Yellowknife. Within this delta, the main channel of the Hay River splits into the East and West Channels which flow around Vale Island, the largest of the delta islands within the area. The East Channel is an extension of the main channel as it conveys most of the flow. The West Channel has higher bed elevations as compared to the East Channel and behaves like a by-pass channel. Close to the entrance to Great Slave Lake, the West Channel splits into three smaller channels. The west arm is referred to as the Rudd Channel, the east arm is the West-Fishing Village Channel, and the channel with higher bed elevations located between these two arms is known as the Island Channel.

In the spring, the snowmelt which originates in the upper basin to the south creates increased discharges within the channel. The formation of ice jams often results as water and ice move downstream towards an ice-covered Great Slave Lake. The mechanics of ice breakup within the Hay River delta are very complex. There are numerous areas where ice jams can form, and the location and extent of flooding is determined by these dynamic interactions. Severe flooding of Vale Island in 1963 prompted the development of a new townsite farther upstream on the left (west) bank of the Hay River main stem (Environment Canada, 1983). The most recent flooding event occurred in 2022 with rising water levels prompting the evacuation of Hay River and Kátł'odeeche First Nation. The extensive flooding caused extensive damage to private and public property with an estimated total cost of $170,900,000 (GNWT, 2024).

As outlined in the Request for Proposals (RFP), the study area encompasses the Main Channel of the Hay River from just upstream of Paradise Gardens down to the mouths of the West and East channels at Great Slave Lake. The total reach lengths within the study area are approximately 45 km, 5 km, and 6 km along the Main, West, and East channels, respectively.

1.3 Study Basin

The Hay River basin (**Figure 2**) originates in the Rocky Mountains of northwestern Alberta, briefly flows into and out of northeastern British Columbia, and enters the southern portion of the Northwest Territories. Within Alberta, the Hay River flows thought the wetland complex of Hay-Zama Lakes. Downstream of Hay-Zama Lakes, the Hay River is joined by a major tributary, the Chinchaga River. From the Chinchaga River confluence, the Hay River flows generally in a northeasterly direction to and through the Northwest Territories (NWT) before entering Great Slave Lake at the Town of Hay River and Kátł'odeeche First Nation. According to the Water Survey of Canda (WSC) gauge station #07OB001 Hay River near Hay River, the Hay River drains an area of approximately 51,700 km^2 before it enters Great Slave Lake. In addition to flow and level data reported at WSC station #07OB001, WSC gauge station #07OB002 Great Slave Lake at Hay River reports lake level data.

2 DATA COLLECTION AND REVIEW

The following describes the relevant information and data sets collected and reviewed during this study. Much of the information and data were used to support understanding of the river ice regime, document the flood history, and inform our methodology for estimating ice jam flood frequencies. Available geospatial data and historical flood elevation data were used to inform planning of our cross-section survey program, and the surveyed data were used to develop the hydraulic model.

2.1 Studies, Reports, and Accounts Specific to Study Site

Relevant studies, reports, and accounts, specific to the study site, are listed below in chronological order. Items are annotated with a description of information relevant to the study. These documents informed our understanding of the river ice regime and flood history. Some of the documents provide historical flood information and data used for model calibration.

1959. Civil Engineering Report on Flooding of Hay River Townsite, NWT. Stanley, Grimble, Roblin Ltd.

- Documentation of reports, data, opinions, and observations related to flooding up to 1959.
- Several flood mitigation concepts were presented for further investigation, including re-opening the West Channel by constructing a bridge and removing the highway fill placed in 1947.

1963. Engineering Report on Flood Protection at Hay River, NWT. Stanley, Grimble, Roblin Ltd.

- Description of state of flood protection in 1963: (1) None of the flood mitigation concepts presented in the 1959 report above were completely implemented, and (2) Construction of a bridge over the West Channel began in 1962, with fill still in place in 1963.
- Three factors identified which affect the occurrence and severity of flooding at Hay River, including: magnitude, condition of ice, and "random" occurrence of ice jams.
- Three approaches for controlling flooding suggested, including: upstream control works on the Hay River, channel improvement at Hay River, and diking on Vale Island.

1978. Flood Risk Mapping for Hay River, Northwest Territories. Underwood McLellan Ltd.

- Modelling was used to simulate water levels and develop flood maps for five specific flood conditions including: open water, three ice jam flooding scenarios, and the 1963 flood event.
- In the absence of gauge data, a hydrologic assessment of snowmelt runoff was used to synthesize flood peak discharges between 1936 and 1963.
- 1977 field survey program collected: 36 cross sections, flow measurements, open water and ice-affected profiles upstream to Paradise Gardens, and breakup observations from April and May.
- Ice jam profiles available through the Hay River delta from 1951, 1956, and 1963.

1983. Hay River Flood Risk Study for Canada-Northwest Territories Flood Damage Reduction Program. Inland Water Directorate Western and Northern Region, Environment Canada.

- Model simulation of a regulatory flood profile (100-year open water flow under conditions of a floating stable ice jam) and mapping of the flood risk area along the Hay River.
- Since both the 1963 flood elevations at Vale Island and the Kátł'odeeche First Nation, and 1974 flood levels in the West Channel exceeded those of the regulatory flood, it was recommended that historic flood levels be used in these areas instead of calculated regulatory flood levels (100-yr open water flow under conditions of a floating stable ice jam).

1983. Hay River Historical Flood Review. Draft report prepared by the Water Resources Division, Indian and Northern Affairs Canada. Jasper, J. N.

- Hay River Flood Risk Mapping previously completed by Underwood McLellan was deemed inadequate for defining flood risk zone; thus, Inland Water Directorate were retained.
- Thorough review of physical evidence, photographs, personal recollections, and historical documents to describe past flood events and list all completed channel modifications.
- Recommendation for designation of Hay River based on the 1963 East Channel flood, the 1974 West Channel flood, and Inland Water Directorate (1983) regulatory flood profile.
- Note included confirming that Hay River Flood Risk Area was designated in May 1984.

1985. Flood Levels 1985 Hay River, NWT. Underhill Engineering Ltd.

- Documentation and mapping of highwater levels throughout the Hay River area in May 1985.

1988. 1985 Hay River Flood Report NWT. J.H. Wedel Water Planning and Management, Environment Canada.

- Documentation of May 1985 flood event chronology and analysis of the causes of flooding.
- Documentation of highest daily discharge estimate on May 6, 1985: 1,350 m^3/s.
- Suggestions for flood forecasting and mitigation; recommendations included redesignation of the Hay River floodplain on Vale Island.

1988. Ice Jams and Flood Forecasting, Hay River, NWT – Phase 1: Final Report. Gerard, R. and Stanley, S.

- Identification and assessment of processes that precede flooding in Hay River to develop a flood forecast procedure for three salient locations within the delta.
- Historical ice jam flood data review, including: (1) ice jam profiles from 1947, 1951, 1956, 1963, and (2) highwater elevations at three locations in the Hay River delta dating back to 1894.
- Field observations of the delta ice regime and field surveys of the delta channels and nearshore lake bathymetry led to determination of salient features of ice jam flooding.

1992. Flood Mitigation Hay River, NWT. Lee Maher Engineering Associates Ltd.

- Proposed mitigation measures to reduce flooding, evaluated through a cost benefit analysis.

1993. Update of Ice Jam Flood Database, Hay River, NWT. Jasek, M., Stanley, S., and Gerard, R.

- Documentation of the 1990, 1992, and 1992 breakup events' chronology and observations.

- Historical ice jam flood data review, including water level profiles and highwater marks from the breakups in 1963, 1985, 1987, 1988, 1989, 1990, 1991, and 1992.

1993. Hay River Flood Control, Hay River, NWT. Jasek, M.

- Resident's views and recollection of the 1985 ice jam flood along the West Channel.
- Overview of the physical aspects of breakup in the West Channel Delta.
- Updated relationship between stage at the West Channel Bridge and the discharge measured at the WSC Gauge.

2011. Patterns of River Breakup Timing and Sequencing Hay River, NWT. Kovachis, N.

- Historical ice jam flood data review, including ice jam profiles in the: following (1) Main and East Channels from 1947, 1951, 1963, 1985, 1989, 1992, 2008, 2009, 2010, and (2) West Channel from 1985, 1989, 1992, 2008, 2009, 2010.
- Consolidation of historical breakup records at the Town of Hay River from 1894 to 2010.
- EMO point gauges' (West Channel Bridge, Kátł'odeh Bridge (formerly Pine Point Bridge), Paradise Gardens, and Alexandra Falls) breakup water level hydrographs from 2003 to 2010.
- Summary of typical breakup sequencing along the Hay River.
- Breakup progression assessment based on degree-day analysis.

2011. 2-D Hydraulic and Ice Process Modeling at Hay River, NWT, Canada. Brayall, M.

- Documentation of the 2008 and 2009 breakup events' chronology and observations.
- River 2D hydraulic model with a computed flow split relationship at the Hay River East-West Channel split during open water and ice jam conditions.
- Historical ice jam flood data review, including ice jam profiles from the breakups in 1963, 1985, 1988, 1989, 1990, 1992, 2008, and 2009.
- Comparison of ice volumes on Hay River before breakup and in the final ice jam configuration.

2024. The 2022 Spring Breakup and Extreme Flooding Event on the Hay River, Canada: A Description of Event Progression. Sandeman, A., Nafziger, J., Connon, R., Coles, A., and Kokelj, S.

- Documentation of the 2022 breakup event's chronology and causes of flooding.
- Interpretation of the 2022 breakup progression through satellite remote sensing imagery.

2.2 Hydrometric Data

The two main water quantity variables collected at hydrometric gauge sites include water level and streamflow (also known as discharge). The following section outlines data sources accessed to build our understanding of the lower Hay River.

2.2.1 National Water Data Archive

Hydrometric data were extracted from National Water Data Archive HYDAT database (Version 1.0 April 16, 2024) for WSC stations #07OB001 Hay River near Hay River and #07OB002 Great Slave Lake at Hay River. The HYDAT data includes annual maxima and daily data. The daily data was supplemented with continuous unpublished data (e.g. 15-minute to 1-hour interval) provided by WSC staff during this project. **Table 1** lists the WSC hydrometric stations for which HYDAT data collected and reviewed for this study. The period of record for which flow and level is available is also listed. Locations of these stations are depicted on **Figure 2**.

Table 1 WSC Hydrometric Stations

Station ID	Station Name	Period of Record
07OB001	Hay River near Hay River	Flow: 1963 – 2023 [61 years] Level: 2002 – 2023 [24 years]
07OB002	Great Slave Lake at Hay River	Level: 1959 – 2023 [53 years]

Supplementary Hydrometric Data

Water level is the parameter of primary interest for estimation of ice jam flood level frequencies. As the published record of water level data is limited, additional data were acquired. Unpublished, hydrometric data was provided by WSC staff for the gauges listed in **Table 2**. These data included continuous, uncorrected, flow and level data. These data were used to supplement the published data from the HYDAT database. Daily data provide estimates of the average flows over a 24-hour period. Continuous level data (5- and 15-minute frequency) provide a time series of discrete point measurements – each with an associated time stamp.

Table 2 Supplementary Hydrometric Data

ID	Data Description	Period of Record
#07OB001 Hay River near Hay River		
	Preliminary WSC Data Unpublished Daily Level Unpublished Continuous Level	Flow: 2023-2024 Level: 2023 Daily Level: 1976-1996 15-min Level: 1996-2010 15-min Level: 2011-2020 5-min Level: 2021-2022
#07OB002 Great Slave Lake at Hay River		
	Unpublished Daily Level Unpublished Continuous Level	Level: 2023-2024 60-min Level: 1996-2001 15-min Level: 2002-2017 5-min Level: 2018-2022

Canadian River Ice Database

The Canadian River Ice Database (CRID) was initiated by the Water Science and Technology Directorate of Environment and Climate Change Canada as a *long-term effort to compile, archive and extract river ice related information from hydrometric records*. The information was accessed online (Canadian River Ice Database - ECCC Data Catalogue). The program and data are detailed by de Rham et. al (2020). Additional supporting information relating to the program was made available during this study by University of Alberta researcher, Dr. Jennifer Nafziger. Supplementary breakup water level data was available in the CRID datasets for WSC Station #07OB001 Hay River near Hay River. This data set provided valuable information on breakup dates and the associated peak flood level and discharge at this gauge site.

2.2.2 Other Project Specific Data

The following provides a brief description of other project specific data received from GNWT, including hydrometric and river ice data. The information obtained from 2022 was instrumental in informing our understanding of the sequence of events during breakup that year.

Peak Stage Data for 07OB001 Hay River near Hay River

Listing of peak stage measurements collected at the #07OB001 Hay River near Hay River gauge with corresponding date and approximate time. Notes describing additional information are included.

07OB001 (Hay River near Hay River) Stage Data

Unpublished daily stage measurements collected at the WSC gauge ranging from copies of original records from 1963 through to preliminary data for 2022. These data are valuable because published WSC data is only available from 2002 onward.

2022 ENR Spring Breakup Reports (Hay River). Environment and Natural Resources, GNWT.

Daily breakup monitoring reports published between May 5 and May 12, 2022, which include breakup description, sequence of events, provisional water level data and photographs at select hydrometric gauges.

2022 Town of Hay River Gauge Stations

Hydrometric and photographic data for the Hay River are available for the 2022 event, including water level data collected at the following three Town of Hay River gauge stations: Alexandra Falls, Paradise Gardens, and Kátł'odeh Bridge (formerly Pine Point Bridge). While these data do not reference any known surveyed elevations, they provide local context. Data from the gauge station located at the Synchro Lift were not available during breakup in 2022.

2022 Town of Hay River Breakup Updates

Daily breakup updates issued by the Town of Hay River between May 2 and May 15, 2022, which include details of breakup description and sequence of events. Evacuation alerts and evacuation orders for various areas are supplemental to these updates.

Hay River Ice Thickness 1963 – 2000

River ice datasets for the Hay River which include discharge and ice thickness measurements recorded several times per ice covered season at the WSC gauge station #07OB001 Hay River near Hay River for the period between 1963 through 2000.

Hay River Ice Readings 2007 – 2022

Spring ice thickness measurements collected in late March / early April for each year between 2007 through 2022 at 16 locations within the Hay River delta. These data were collected by or under the supervision of Travis Wright of the Town of Hay River.

2021 and 2020 Ice Classification Data – Hay River

Collection of river ice classification products from May of 2020, and April and May 2021, which were obtained by the Government of Canada (GOC) and classified by NRCan.

2022 River Ice Classification Data

Collection of river ice classification products from May 2022 classified by C-CORE for the GNWT. These images helped build an understanding of the sequence of events on a macro scale.

2.3 Geospatial Data

Various geospatial data was collected in support of model development and flood hazard mapping. The following includes a description of the geospatial data received from GNWT in support of this study.

Base Data

Information was accessed through the GNWT's ATLAS (Administration of the Territorial Land Acts System) interactive web-based mapping service to support reporting and flood hazard mapping, including road network, hydrography (water bodies and water courses), and administrative boundaries.

Digital Terrain Model Data

A digital terrain model (DTM) with a 1-m resolution based on bare earth LiDAR data collected by McElhanney Ltd. on July 7, 2020, was received as a series of georeferenced tiff files.

Coarse DEM data with 30 m point resolution was obtained from Northwest Territories Centre for Geomatics.

Orthophotos

The most recent orthorectified imagery (20 cm) for Hay River were collected by McElhanney Ltd. on July 7, 2020, and received as georeferenced tiff files and in ECW format.

Optical Radar Satellite, Optical Satellite, and Aerial Imagery

Available images from the European Space Agency (ESA) Sentinel-1 and Sentinel-2 missions were collected for May 2022. Together with river ice classification data, this imagery captured during the 2022 flood event was used to build an understanding of the sequence of ice movement along the Hay River.

Previous (Existing) Flood Mapping (1984)

Scans of the existing 1:10,000 scale flood map and 1:2,000 scale flood maps for Hay River (1984) were provided by GNWT. These provided reference information for flood hazard mapping updates.

2.4 Field Data

The following includes a description of the local hydrometric gauge stations and field data received from GNWT for Hay River as part of the study. These documents are briefly described below and included in the database provided with this case study.

Highwater Marks

Previous studies (**Section 2.1**) contain highwater mark data collected along the Hay River. There are several locations at which these data have been routinely observed, including: (1) East-West Channel split, (2) East Channel near the mouth, and (3) West Channel near the mouth. Highwater marks resulting from ice jams along the Hay River are available in the Main and East Channels for 1947, 1951, 1963, 1985, 1989, and 1992, and in the West Channel for 1985, 1989, and 1992. Researchers from the University of Alberta collected ice jam profile data during breakup in 2008, 2009, 2010, 2011 and 2013.

2022 Highwater Marks Hay River and Kátł'odeeche First Nation

Ollerhead and Associates Ltd. surveyed highwater marks as identified by silt markings left on structures and witness testimony throughout the Town of Hay River and Kátł'odeeche First Nation. These data are documented in a report with accompanying raw data files.

Hydrometric Gauge Photos

Timelapse photo series taken during the 2022 breakup at WSC gauge stations #07OB001 Hay River near Hay River and #07OB008 Hay River near Alta/NWT Boundary.

2022 Flood Photography and Videography

The following field data helped inform our understanding of the 2022 flood events within the Town of Hay River and Kátł'odeeche First Nation:

- May 6 - May 19: Ground and flight photos from Travis Wright of the Town of Hay River
- May 10: Video from drone flight capturing flooding occurring in Paradise Gardens
- May 10: Videos from the Aaron Tambour Photography Facebook page
- May 12: Video from Mikey McBryan capturing flooding throughout Town of Hay River
- May 14: Photos and videos from the Canadian Coast Guard

2.5 Previous Flood Mapping

Jasper (1983) recommended the following flood profiles for designation of Hay River flood mapping: 1963 East Channel flood, the 1974 West Channel flood, and Inland Water Directorate (1983) regulatory flood profile. The flood risk area for Hay River was designated on 29 May 1984, with delineation based on the recommended combination of historical flood levels and backwater simulations (Coles, 2020a). Electronic geospatial files (ESRI shapefile format) delineating floodway and flood fringe extents for these Flood Damage Reduction Program (FDRP) maps were provided by GNWT. It was acknowledged that a relatively short historical record of flooding had been used to produce the maps in 1984, and redesignation of Hay River was considered as a result of a major flood which occurred in May 1985 (Coles, 2020a). This

prompted further studies of ice jams, including those carried out by Dr. Larry Gerard and others of the University of Alberta.

3 FIELD SURVEY

The survey program was completed between May 27th and June 4th, 2024. The objective was to survey channel cross sections along the study reaches to support the development of a hydraulic model, which includes both open water and ice jam scenarios. The following summarizes the field survey work and methodology employed to collect the data.

3.1 Survey Procedures and Methodology

Ground positioning for the survey was measured using Global Navigation Satellite Systems (GNSS) and Trimble R10 and R12 Real Time Kinematic (RTK) GNSS receivers. Bathymetric surveys were performed in water areas typically deeper than 0.3 meters using a CeeEcho echo sounder mounted on a jet boat to measure water depth under the transducer. The position and height of the transducer were recorded with the RTK GNSS receiver mounted directly above it and paired through the HYPACK software. Riverbed elevations were derived by subtracting sounding depths from the transducer elevations. In shallower, wadable areas, elevations were obtained directly with the RTK GNSS receiver attached to a survey rod. The surveyed cross-sections included the riverbanks, and extended into the floodplain, overlapping with the DTM provided by GNWT.

3.1.1 Coordinate System and Datum

Horizontal positions were referenced to the Universal Transverse Mercator (UTM) Zone 11N projection. The UTM 11N projection is part of the Canadian Spatial Reference System (CSRS) North American Datum of 1983 (NAD83). Orthometric heights are based on the Canadian Geodetic Vertical Datum of 2013 (CGVD2013a; Epoch 2010.0).

3.1.2 Control Network

A control point network was established from local available WSC benchmarks and GNSS surveying to provide a spatial reference for the survey program. Seven WSC benchmarks, and four NHC project survey control points were tied into the survey. A list of the control point coordinates is provided in **Table 3**.

Table 3 Control point summary

Name	Type	Easting (m)	Northing (m)	Elevation (m)	Measurement Type
NHC 1	Project Control Point	566,223.804	6,742,996.381	166.190	Long term static measurement with PPP (≥ 4 hours).
NHC 2		560,796.924	6,733,357.233	181.216	
NHC 3		553,721.494	6,725,811.134	203.709	
NHC 4		567,493.029	6,745,638.518	162.716	
SIBM1	WSC Benchmark	562,173.663	6,734,685.878	170.188	Shorter term, 6 to 300 second, RTK observation.
NT94-428		562,184.938	6,734,700.964	170.223	
NT84-402		568,750.983	6,747,827.956	158.338	
NTP-2022-287		568,772.293	6,747,861.010	157.835	
NT97-1		568,747.182	6,747,855.634	157.828	
NTP-2022-286		568,748.587	6,747,855.932	157.849	
VCM-5		568,785.524	6,747,810.729	157.834	

Coordinates of the four NHC control points were determined by running the GNSS receivers in static mode for over at least 4 hours at each point. This enabled high accuracy precise point positioning (PPP) results from the CSRS for each control point. The data were then post-processed using Trimble Business Center software to adjust the network by establishing baselines between these control points.

A free adjustment of the base control network was completed, and the error from the adjustment was distributed equally throughout the network. The horizontal and vertical errors at the control points, following post-processing and adjustments to the reference CSRS-PPP values, are summarized in **Table 4**. The largest horizontal error was 0.0012 m, and the largest vertical error was 0.0053 m.

Table 4 Control network errors

Control Point	Horizontal		Vertical
	Easting (m)	Northing (m)	Elevation (m)
NHC 1	0.0006	0.0010	0.0048
NHC 2	0.0008	0.0012	0.0050
NHC 3	0.0006	0.0008	0.0037
NHC 4	0.0008	0.0012	0.0053

A comparison between the surveyed elevations (after post-processing and adjustment) and WSC benchmark elevations documented in benchmark history reports received by WSC on June 4, 2024, are provided in **Table 5.** Horizontal coordinates are not published by WSC or within documents received by WSC for these benchmarks, and therefore, the comparison is limited to the elevations.

Table 5 Comparison between surveyed and published WSC benchmark elevations

Name	Description	Elevation Difference in m (Surveyed Minus Published)
SIBM1	WSC #07OB001 Gauge Benchmark	0.146
NT94-428		0.173
NT84-402	WSC #07OB002 Gauge Benchmark	0.326
NTP-2022-287		0.332
NT97-1		0.337
NTP-2022-286		0.321
VCM-5		0.339

The differences between the surveyed and published elevations at the WSC #07OB001 Hay River near Hay River gauge were found to be reasonably close to the equivalent CGVD28 to CGVD2013a datum conversion of −0.12 m for the area (Ollerhead and Associates 2022). Therefore, it was assumed that the WSC datum for the #07OB001 gauge is equivalent to CGVD28 and the conversion of −0.12 m was applied to water levels recorded by this gauge.

The differences between the surveyed and published elevations at the WSC #07OB002 Great Slave Lake at Hay River gauge exceeded the expected CGVD28 to CGVD2013a datum conversion of −0.19 m for the area (Ollerhead and Associates 2022). Therefore, it was assumed that the WSC datum for the #07OB002 was not equivalent, instead a *project-specific* datum

conversion was estimated. The project-specific datum conversion was calculated by averaging the elevation difference between surveyed and published benchmark (i.e., −0.33 m) and the elevation difference between surveyed water level at the gauge site and gauge heights published by WSC at the time of the survey (i.e., −0.23 m). This approach resulted in a project specific-datum conversion of −0.28 m for the #07OB002 gauge location.

3.2 Survey Accuracy and Error

The Trimble RTK GNSS receivers used in the survey are capable of accuracies of ±0.02 meters under optimal conditions, such as a stable mounting (e.g. tripod) with a clear view of the sky, clear communication with enough satellites, and long sample time over a static location. Under normal field conditions, errors are introduced when the receiver is off-level or obstructed by trees and vegetation. Operator errors can be introduced such as an incorrectly entered receiver height (an error that can be corrected during data post processing). Much of the ground-based surveyed data was collected under favourable conditions, with good satellite coverage, and errors were expected to be about ±0.05 meters. Larger errors were experienced on a few occasions where satellite coverage was poor, such as, in dense vegetation or alongside very high steep banks. The digital echo sounder used for the boat-based surveys can achieve accuracies of ±0.01 meters under optimal conditions. The dominant source of error was due to pitch and roll of the boat during data collection. The error associated with depth sounding was expected to be about 0.07 meters. Considering the various sources and range of possible accuracy errors of the surveyed elevation data was about 0.10 m to 0.15 m.

3.3 Digital Terrain Model

For this study, NHC acquired a hydro-flattened 1m-grid Digital Terrain Model (DTM), along with the corresponding LAS file from GNWT. The data was constructed from airborne LiDAR data gathered by McElhanney (2020) in July 2020. The mean point density of these data is 14 pts/m^2 with variation depending on the canopy closure, understory density, and topographic features.

Elevations extracted from the DTM were compared with selected ground surveyed points collected by NHC on roads and other dry ground areas. A summary of the comparison is shown in **Table 6**. Ground survey points were slightly lower than the elevations extracted from the DTM; and the average difference was approximately 0.10 m. The differences are small, and therefore, and elevations of the project LiDAR DTM (provided by GNWT) was considered to be in good agreement with NHC-surveyed ground elevations.

Table 6 Comparison between LiDAR DTM and surveyed LiDAR check points

Name	Point Description	Horizontal Easting (m)	Horizontal Northing (m)	NHC Survey Elevation (m)	DTM Elevation (m)	Surveyed minus DTM (m)
100	Lidar Check	553,739.2	6,725,808.586	204.714	204.794	-0.080
105	Lidar Check	555,948.1	6,727,003.039	199.347	199.457	-0.110
106	Lidar Check	558,261.5	6,728,110.307	194.068	194.204	-0.136
107	Lidar Check	560,512.9	6,731,373.487	187.606	187.741	-0.135
108	Lidar Check	561,912.6	6,734,372.424	180.033	180.131	-0.098
109	Lidar Check	563,451.7	6,736,406.606	173.309	173.428	-0.119
1000	Lidar Check	564,470.2	6,740,486.626	169.254	169.297	-0.043
1001	Lidar Check	565,571.1	6,741,322.883	167.969	168.031	-0.062
1002	Lidar Check	565,960.0	6,741,996.125	166.835	166.885	-0.050
1003	Lidar Check	566,675.1	6,742,978.288	166.492	166.608	-0.116
1004	Lidar Check	566,462.0	6,743,706.133	166.086	166.169	-0.083
10353	Ground	568,676.6	6,748,021.555	157.424	157.594	-0.170
10571	Ground	565,980.8	6,747,692.376	158.936	159.078	-0.142
19414	Berm Crest	565,775.3	6,747,235.762	159.933	160.047	-0.114
19244	Ground	566,304.3	6,743,919.489	162.488	162.531	-0.043
20261	Top of Bank	567,520.5	6,745,631.149	162.692	162.836	-0.144

3.4 Orthophoto (Aerial Photograph)

Orthophotos were provided by GNWT for this project, which were acquired for GNWT by McElhanney in July 2020.

3.5 Cross Section Survey

Cross section locations were selected to ensure adequate representation of the channel geometry to be used in the hydraulic model. The cross sections were spaced according to the active channel width and slopes, with adjustments to capture historical cross sections, hydraulic structures, meander bends, and other important channel or floodplain features. The alignments were identified by desktop analysis with the available DTM and Orthophotos. Some adjustments

were made based on the conditions observed in the field during the survey. All cross sections were surveyed between May 7 and June 4, 2024. A summary of the surveyed cross-sections in each study reach is provided in **Table 7**.

Table 7 Cross section survey summary

Reach	Approximate Reach Length (km)	Number of Cross Sections	Average Spacing (m)	Minimum Spacing (m)	Maximum Spacing (m)
Hay River Main Channel	44	104	427	34	1,517
Hay River East Channel	6.5	32	203	112	266
Hay River West Channel	3.2	24	127	14	167
Hay River West – Fishing Village Channel	2.3	21	108	77	148
Hay River West – Rudd Channel	1.3	12	109	75	173

A total of 192 cross sections were surveyed to support the development of a hydraulic model. The cross sections were grouped into five distinct sub-reaches— Hay River Main Channel, Hay River East Channel, Hay River West Channel, Hay River West-Fishing Village Channel, and Hay River West-Rudd Channel. The locations of these cross sections are discussed in more detail in sub-section 5.2.1.

3.6 Project and Model River Station Conventions

The project river station convention was established to align with that which was previously used by University of Alberta researchers (Nafziger 2018, Kovachis 2011, Brayall 2011). The starting point of this convention lies within the Hay River ‘s headwaters in northeastern British Columbia. To maintain consistency with previous research, a river station value of 1108 (km) was adopted at the location of the Hay River flow split into the East and West channels.

The coordinates of this location using the NAD 1983 CSRS UTM Zone 11N coordinate system are as follows:

- Easting (X) = 566,776.012 m
- Northing (Y) = 6,743,721.853 m

Channel centrelines using this river station convention follow the same path as those of the model cross sections. **Table 8** provides a comparison between the project river stations (km) the model river stations (m).

Table 8 Comparison between project and model river station convention

River Segment	Model River	Model Reach	River KM (km) (downstream to upstream)	Model RS (m) (downstream to upstream)
Hay River East Channel	Hay	East	1114.5 to 1108	0 to 6500
Hay River Main Channel	Hay	Main	1108 to 1064	6500 to 50490
Fishing Village Channel	West-Fishing	Fishing	1113.5 to 1111.2	0 to 2300
Hay River West Channel	West-Fishing	West	1111.2 to 1108	2300 to 5500
Rudd Channel	Rudd	Rudd	1112.5 to 1111.2	0 to 1300

3.7 Hydraulic Structures

The hydraulic structures were measured as a part of the survey, which includes two bridges listed in **Table 9**. Survey data collected for the bridge included: span length; deck width; top of curb or solid guardrail elevation; and photographs of the bridge.

Table 9 Hydraulic structure summary

Reach	River Station (km)	Crossing Description	Structure Type
Hay River – Main Channel	1098.1	Kátł'odeh Bridge	Bridge
Hay River - West Channel	1108.4	West Channel Bridge	Bridge

3.8 Additional Data

Additional data collected during the field survey included water level measurements, taking site photographs, and elevations of existing benchmarks.

3.8.1 Water Level Measurements

Water level measurements were obtained at each cross section on both the left and right banks. This provided a surveyed water surface elevation profile, which will aid in the calibration of the open water model. The surveyed water levels at the gauge locations were also used to estimate datum conversions at the following gauges sites: # 07OB001Hay River near Hay River, and #07OB002 Great Slave Lake at Hay River.

3.8.2 Site Photographs

Representative photographs of the reaches were captured during the site inspection and survey. Selected photos with annotations are provided in **Appendix B.**

3.8.3 Existing Benchmarks

Existing benchmarks identified at both WSC gauging stations (#07OB001 and #07OB002), were surveyed for comparison with published elevation data. The results of the comparisons are listed in **Table 3** and **Table 5**, respectively. No additional benchmark was surveyed in this program.

4 FLOOD HYDROLOGY

This section details the flood hydrology of the Hay River. An understanding of the flood history, complete with flood frequency analysis carried out for open water flooding along the Hay River, and ice regime is presented. In addition, a flood level frequency is also carried out for ice jam flooding using two different approaches.

4.1 Flood History

The following section will focus on recounting the details of ice jam induced flooding events. It is understood that Vale Island experienced some open water flooding due to record highwater levels on Great Slave Lake between 2020 and 2022; however, past flood accounts suggest that open water flooding has been limited within the Hay River and Kátł'odeeche First Nation area and not associated with impactful flooding events.

Ice Jam Flooding

The most impactful flooding within the Town of Hay River and Kátł'odeeche First Nation has been associated with ice jams during breakup. Water Survey of Canada (WSC) gauge station #07OB001 Hay River near Hay River has been operational since June 28, 1963. This station is located 12.5 km upstream of the East-West Channel split, and water levels recorded at this location do not capture the full effects of ice jam activity occurring throughout the Town of Hay River and Kátł'odeeche First Nation. To gain an understanding of flood levels within the delta region, available highwater mark data was accessed for various sources, including: Jasek et al (1993), Kovachis (2011), and Ollerhead and Associates (2022). These sources present highwater marks and flood profiles resulting from noteworthy ice jam flooding events since 1894.

Jasek et al. (1993) presented comparisons of water level data made at the following three locations:

- East-West Channel split (West Channel bridge) from 1947,
- East Channel near the mouth (Old Town and the Indian Village) from 1894, and
- West Channel near the mouth (the Fishing Village) from 1964.

Highwater mark and flood profile data was considered at these locations throughout this study. A flood was considered "significant" if it surpassed a specified threshold at any of the three sites. These threshold values were based on the "perception stage" presented in Jasek et al. (1993) and the following elevations were adopted: 163.0 m at the East-West Channel Split and 159.0 m at each of the East Channel near the mouth and West Channel near the mouth. This analysis determined that up to 1993, the highest measured flood events occurred between late April and mid-May of the following years: 1904, 1914, 1951, 1963, 1974, 1985, 1986, 1989, 1992.

This analysis was corroborated and extended with the flood accounts detailed in Kovachis (2011), Hay River Hub newspaper, and reports of flood damage available from Public Safety Canada (2023) and GNWT (2024). These data determined that there were two more significant flood events caused by ice jams since 1992 and these included events from 2003 and 2008.

A highwater mark survey was carried out by Ollerhead and Associates following the unprecedented flood event of 2022. Highwater marks were compared with flood level data at each of the three locations listed above and confirmed the flood event of 2022 resulted in the highest levels at each site.

Table 10 contains a summary of the most significant flooding events experienced throughout the Hay River area, occurring between late-April and mid-May. Context is provided about the impact of each flood event on the surrounding area, along with a list of reference documents.

Table 10 Significant flood events resulting from ice jams during breakup

Year	Description	Reference
1904	Much of Old Indian Village flooded.	Wedel (1988)
1914	Flooding of lower parts of Village.	Wedel (1988)
1951	Considerable damage along East Channel: airport flooded and out of commission, downtown was under water; washouts along Mackenzie Highway. Land was raised and new buildings were built on piles following this event.	Stanley, Grimble, Roblin Ltd. (1959)
1963	Entire community of 1,800 was evacuated. Flooding along East Channel: Airstrip was under water; wash outs along causeway link to the Mackenzie Highway; flooding in Old Indian Village. New town site formed following this event.	Public Safety Canada (2023); GNWT (2024); Wedel (1988)
1974	Evacuation of residents along West Channel ahead of flooding in that area. Ice jam was blasted, and residents returned.	Public Safety Canada (2023); GNWT (2024); Wedel (1988)
1985	Record high flows on the Hay River. Serious and sudden flooding along West Channel prompts evacuation of residents in that area, including use of canoe.	Public Safety Canada (2023); GNWT (2024); Wedel (1988)
1986	Highest water levels within the West Channel up to 1993; water levels at East-West Channel split that are slightly lower than those measured in 1985.	Jasek, M., Stanley, S., and Gerard, R. (1993)
1989	Water levels at East-West Channel split that are slightly lower than those measured in 1985 and 1986.	Jasek, M., Stanley, S., and Gerard, R. (1993)
1992	Large ice jam at the mouth of the West Channel and ice jamming along the East and Main channel results in evacuation of 100 residents.	Public Safety Canada (2023); GNWT (2024); Jasek, M., Stanley, S., and Gerard, R. (1993)
2003	Localized flooding and evacuations within community of Hay River and Hay River Reserve.	GNWT (2024)
2008	Voluntary evacuation of 600 people from Vale Island. Flooding knocked Old Anglican Church off foundation, affected the Roman Catholic Church, and caused damage to public and private property.	Public Safety Canada (2023); GNWT (2024)
2022	Threat of severe flooding prompts evacuation for all of Hay River. Extensive flooding caused widespread damage. Highwater marks identified by GNWT and ECCC were surveyed by Ollerhead and Associates Ltd.	GNWT (2024)

2022 Breakup Chronology

The 2022 ice jam event caused the greatest flooding within the Town of Hay River and Kátł'odeeche First Nation (**Table 10**), as based on accounts and corresponding highwater marks from records dating back to 1894, and flood profile data collected since 1947. Our understanding of this event is based largely on ENR Reports for Hay River, Town of Hay River Breakup Updates, observation camera data, as well as photos and videos collected by individuals. Sandeman et al (2024) present a detailed account of event progression which includes a description of antecedent conditions, rain events, interpretation of satellite remote sensing imagery, and commentary on the event magnitude.

Figure 3 provides a chart of the 2022 breakup water levels recorded at station #07OB001 Hay River near Hay River which captures the entire flood event in the Town of Hay River and Kátł'odeeche First Nation between May 7 and May 12, 2022. Water levels at the WSC gauge #07OB002 Great Slave Lake at Hay River are also shown; however, these data are only available up to May 7, 2022. The water level data is expressed in geodetic elevations as per each gauge.

The following provides a brief summary of the sequence of events over the 2022 breakup period, as based on the sources described above:

- On Thursday, May 6, a large section of local ice released near the Hay River Golf Course and accumulated in the Hay River delta. A significant ice run was observed at WSC Station #07OB001 near midnight and continued overnight. A storm system with a significant amount of precipitation was forecasted within the basin. An evacuation notice was put in place for residents of Vale Island and the West Channel.
- On Friday, May 7, ice flowed into the East and West Channels in the morning and continued shoving through the day, forming an ice jam in both channels. The ice pushed out onto Great Slave Lake through the West Channel. Overnight, the head of the ice jam reached WSC Station #07OB001. At 1:32 am on May 7, a local state of emergency due to the potential flooding was declared. This was followed by an evacuation order for Vale Island and the West Channel. Ice continued to run, jam, and release along sections of the Hay River. At this time, pushes were frequently resulting in localized flooding along the West and East Channel areas and at Paradise Gardens.
- On the morning of May 8, two ice jams were in place: (1) a 13.3 km long jam extending from toes in the East Channel and West Channel and (2) a second jam forming just upstream of the head of the downstream jam. The head of the second jam reached Paradise Gardens in the afternoon and measured 29.9 km in length. By the evening, it was 41.4 km long. On May 8, an evacuation order was issued for Paradise Gardens, followed by an evacuation alert for all Riverfront properties. Significant flooding occurred in the evening at Paradise Gardens from a large surge of ice and water into the area.
- On May 9, the two ice jams that formed on May 7 and 8 remained in place for the day. More ice and water were anticipated to release and make contact with the downstream jam.

- On May 10, water levels continued to rise slowly within Town boundaries, and the two ice jams remained in place locally. More flooding was anticipated with pending increases in water and future pushes and releases of ice jams.
- On May 11, ice jams remained in place locally, extending from the lake to a few kilometers south of Paradise Gardens. The upstream ice jam began to move downstream and flowed into the downstream jam. In the evening, the downstream ice jam pushed farther downstream, and the upstream jam released. At 11:00 pm, an evacuation order was issued for all of Hay River.
- On May 12, ice from both upstream and downstream jams pushed downstream overnight. This resulted in a new jam within the Hay River delta and caused extensive flooding and damage. Remaining pushes were anticipated to cause more flooding through the community. Water levels began to recede upstream through the Paradise Gardens area. Water levels at WSC Station #07OB001 dropped more than 4 m over the course of the day.
- Residents were allowed to return to Hay River in the evening of May 15.

4.2 Open Water Flood Frequency

An open water flood frequency analysis was completed at #07OB001 Hay River near Hay River. Flood level frequency analysis coincident with peak open water flooding was carried out for #07OB002 Great Slave Lake at Hay River. These data were used to estimate the 100-year open water regulatory flood for hazard mapping.

4.2.1 07OB001 Hay River near Hay River

Annual peak discharges reported by the WSC for Station #07OB001 are listed in **Table 11** and illustrated in **Figure 4**. The data series includes years 1963 to 2023; however, the 1963 peak value was not included in this assessment as the record begins in the month of July, after the peak discharge in that year occurred. Where instantaneous peaks are not reported, the instantaneous peak values were calculated by regression analysis between instantaneous (Q_i) and daily discharges (Q_d) from the historical data series. This relationship ($Q_i = 1.01Q_d$) is illustrated in **Figure 5**.

UMA (1978) conducted a flood study which extended the WSC peak flow record by deriving a unit hydrograph based on snowmelt runoff. This produced additional flood peaks for the period of 1936 to 1963 and extended the existing record by 27 years. Environment Canada (1983) also included these synthesized flood peaks in the dataset for the Hay River Flood Risk Study. For consistency with the previous flood studies, these synthesized flood peaks were included as part of this data series and are summarized in **Table 11** and illustrated in **Figure 4.** These data were assumed to correspond to the instantaneous discharge dataset and are presented as such.

Table 11 Annual peak instantaneous and daily discharges for #07OB001 Hay River near Hay River including the synthesized UMA (1978) data series

Year	Peak Instantaneous Discharge (m^3/s)	Date	Peak Daily Discharge (m^3/s)
1936	*470*[2]		
1937	*560*[2]		
1938	*660*[2]		
1939	*770*[2]		
1940	*630*[2]		
1941	*660*[2]		
1942	*750*[2]		
1943	*700*[2]		
1944	*590*[2]		
1945	*780*[2]		
1946	*710*[2]		
1947	*890*[2]		
1948	*840*[2]		
1949	*770*[2]		
1950	*830*[2]		
1951	*770*[2]		
1952	*730*[2]		
1953	*340*[2]		
1954	*690*[2]		
1955	*1,230*[2]		
1956	*550*[2]		
1957	*780*[2]		
1958	*940*[2]		
1959	*690*[2]		
1960	*600*[2]		
1961	*840*[2]		
1962	*1,250*[2]		
1963	*900*[2]		

Year	Peak Instantaneous Discharge (m^3/s)	Date	Peak Daily Discharge (m^3/s)
1964	**732**[1]		725
1965	**758**[1]		750
1966	**626**[1]		620
1967	**909**[1]		900
1968	**523**[1]		518
1969	**898**[1]		889
1970	**378**[1]		374
1971	**606**[1]		600
1972	**1,030**[1]		1,020
1973	**657**[1]		650
1974	**1,252**[1]		1,240
1975	**687**[1]		680
1976	**692**[1]		685
1977	1,080	15-Jun	1,080
1978	**826**[1]		818
1979	**1,131**[1]		1,120
1980	**121**[1]		120
1981	**798**[1]		790
1982	**664**[1]		657
1983	**556**[1]		550
1984	621	08-Jul	617
1985	**1,010**[1]		1,000
1986	**655**[1]		649
1987	**806**[1]		798
1988	1,360	09-Jul	1,080
1989	**914**[1]		905
1990	**566**[1]		560
1991	**603**[1]		597
1992	**909**[1]		900
1993	710	18-Aug	705

Year	Peak Instantaneous Discharge (m^3/s)	Date	Peak Daily Discharge (m^3/s)
1994	**800**[1]		792
1995	**343**[1]		340
1996	**651**[1]		645
1997	**682**[1]		675
1998	435	23-Jul	426
1999	389	17-Jun	385
2000	393	02-Jun	391
2001	437	07-May	430
2002	**568**[1]		562
2003	**682**[1]		675
2004	211	06-May	209
2005	779	30-Apr	758
2006	**964**[1]		954
2007	**832**[1]		824
2008	900	10-May	893
2009	964	14-May	952
2010	440	01-May	436
2011	555	16-May	550
2012	393	03-May	332
2013	1,020	19-May	1,010
2014	**628**[1]		622
2015	**281**[1]		278
2016	714	26-Jun	706
2017	305	23-May	303
2018	393	10-May	391
2019	**204**[1]		202
2020	**899**[1]		890
2021	980	15-May	975
2022	1,740	18-May	1,730
2023	277[3]	30-Apr	164

Notes:

1. The bolded and underlined peak instantaneous discharges were estimated from daily values based on the established relationship of Qi=1.01Qd.
2. Synthesized flood peaks from the UMA (1978) flood study are presented in italics and rounded to the nearest ten. These data were assumed to correspond with the instantaneous discharge dataset.
3. Provisional values provided by WSC may be subject to change.

Results

Three parameter log-normal (3LN) distribution was found to provide a good fit to the observed data and was used to estimate the 100-year open water flood frequency. Flood frequency distributions for the Hay River are depicted on **Figure 6**. The adopted 3LN curve is shown in **Figure 7** along with it 95% confidence limits. Flood frequency estimates are provided in **Table 12** for the 2-, 5-, 10-, 20-, 50-, 100-, 200-, and 500-year open water floods, for Hay River near Hay River including the synthesized UMA (1978) data series.

Table 12 Flood frequency estimates for Hay River near Hay River including the UMA (1978) synthesized data series

Return Period (Years)	Annual Probability of Exceedance (%)	Peak Instantaneous Discharge (m^3/s)	
		Value	95% Confidence Limit
500	0.2	1,710	1,340-2,090
200	0.5	1,570	1,280-1,870
100	1	1,470	1,230-1,710
50	2	1,350	1,160-1,540
20	5	1,200	1,070-1,330
10	10	1,070	970-1,170
5	20	930	850-1,000
2	50	690	630-750

Comparison to Previous Flood Studies

Table 13 shows the results of the above flood frequency analysis compared to the prior flood studies. The UMA (1978) and Environment Canada (1983) flood frequency magnitude estimates are 13% to 26% less than those estimated using the current data series. The difference between the current flood frequency results and the previous flood studies flood frequency likely is a result of two factors:

- The first factor is the length of record. The UMA (1978) flood study used a gauged record from 1964 to 1976, with an additional synthesized dataset extending from 1936 to 1963,

resulting in a total length of data of 40 years. The Environment Canada (1983) flood study used the same data series as the UMA (1978) flood study, with the addition of 6 years, extending the record to 1982. This resulted in 46 years of record. Compared to the record used in this study, which included the synthesized UMA (1978) data series used in both prior studies, along with a gauged record from 1964 to 2023. This resulted in a total period of record of 88 years, which is 42 years longer than the most recent flood study conducted for Environment Canada.

- The second factor is that the two largest floods on record occurred in 1988 and 2022, after the completion of both prior flood studies. The inclusion of these two floods, especially the 2022 flood, has likely skewed the fitted curve high.

Table 13 Comparison with previous flood frequency estimates for Hay River at Hay River including the synthesized UMA (1978) data series

Return Period (Years)	Peak Instantaneous Discharge (m^3/s)		
	This Study	Environment Canada Flood Study (1983)	UMA Flood Study (1978)
100	1,470	1,250	1,282
50	1,350	1,210	1,203
20	1,200	1,120	1,090

Notes:
1. This frequency values for this study and the UMA (1978) study were based off the three-parameter log-normal distribution while the Environment Canada (1983) study was based off the Log-Pearson III distribution.

4.2.2 07OB002 Great Slave Lake at Hay River

Table 14 presents Great Slave Lake water levels which are coincident with the peak flows for the Hay River Main Channel upstream listed in **Table 11**. The WSC gauge #07OB002 Great Slave Lake at Hay River is located near the mouth of the East Channel of the Hay River and is influenced by river discharge upstream. This is made apparent by a very pronounced and relatively rapid spike in water level readings, which can begin days before the peak event. Therefore, during breakup, this gauge may not accurately reflect water levels on Great Slave Lake. There were also numerous data gaps in the record. To address these issues, the #07OB002 dataset considered values measured up to one week before and after the timing of the peak event at #07OB001 Hay River near Hay River. Additionally, a correlation was made with #07SB001 Great Slave Lake at Yellowknife Bay to help confirm representative values and fill in data gaps.

Table 14 #07OB002 Great Slave Lake water level data series corresponding to annual peak discharges for # 07OB001 Hay River near Hay River

Year	Date	Great Slake Lake Water Level[1] (m)	Comment
1964	08-May	156.475	
1965	02-May	156.612	
1966	10-May	156.451	
1967	11-May	156.326	
1968	06-May	156.542	
1969	07-May	156.390	
1970	03-May	156.292	
1971	01-May	156.341	Correlation with 07SB001
1972	09-May	156.307	Correlation with 07SB001
1973	27-Apr	156.545	Correlation with 07SB001
1974	02-May	156.451	Correlation with 07SB001
1975	30-Apr	156.716	Correlation with 07SB001
1976	30-Apr	156.606	Correlation with 07SB001
1977	15-Jun		
1978	03-May	156.582	Correlation with 07SB001
1979	05-Jun	156.711	Correlation with 07SB001
1980	28-Apr	156.371	Correlation with 07SB001
1981	04-May	156.372	Correlation with 07SB001
1982	09-May	156.204	Correlation with 07SB001
1983	30-Apr	156.275	Correlation with 07SB001
1984	09-Jul	156.603	
1985	07-May	156.789	Value on 5/1/1985
1986	07-May	156.752	Value on 4/30/1986
1987	27-Apr	156.600	Value on 4/25/1987
1988	09-Jul	157.031	
1989	08-May	156.960	
1990	28-Apr	156.799	Value on 4/26/1990
1991	23-Jun	157.005	

Year	Date	Great Slake Lake Water Level[1] (m)	Comment
1992	28-Apr	157.013	Value on 4/25/1992
1993	18-Aug	156.706	Correlation with 07SB001
1994	29-Apr	156.848	Correlation with 07SB001
1995	02-May	156.580	
1996	08-May	156.619	Correlation with 07SB001
1997	10-Aug	157.223	
1998	23-Jul	156.797	
1999	17-Jun	156.722	
2000	02-Jun	156.553	
2001	07-May	156.657	Value on 4/30/2001
2002	22-May	156.687	Correlation with 07SB001
2003	02-May	156.954	Value on 4/27/2003
2004	06-May	156.725	
2005	30-Apr	156.784	
2006	10-Jun	156.912	
2007	14-May	156.781	
2008	10-May	156.840	
2009	13-May	156.884	
2010	01-May	156.737	
2011	16-May	156.481	
2012	03-May	156.658	Correlation with 07SB001
2013	19-May	156.802	
2014	08-May	156.646	Correlation with 07SB001
2015	26-Apr	156.484	Correlation with 07SB001
2016	26-Jun	156.673	
2017	23-May	156.842	
2018	10-May	156.669	
2019	05-Aug	156.502	Value on 8/11/2019
2020	14-Jul	157.182	Value on 7/12/2020
2021	15-May	157.344	

Year	Date	Great Slake Lake Water Level[1] (m)	Comment
2022	18-May	157.239	Correlation with 07SB001
2023	30-Apr	156.707	Value on 4/28/2023

Note:
1. Elevations at gauge #07OB002 Hay River near Hay River reference the Geodetic Survey of Canada datum (local 1982 adj.).

Results

The Log-Pearson III (LP3) distribution was found to provide a good fit to the observed data and was used to estimate the 100-year open water level frequency. Flood level frequency distributions for the Hay River are depicted on **Figure 8**. The adopted LP3 curve is shown in **Figure 9** along with it 95% confidence limits. Flood level frequency estimates for #07OB002 Great Slave Lake at Hay River coinciding with peak instantaneous discharges along the #07OB001 Hay River near Hay River are provided in **Table 15**.

Table 15 Water level frequency estimates for #07OB002 Great Slave Lake at Hay River coinciding with peak instantaneous discharges along the #07OB001 Hay River near Hay River

Return Period (Years)	Annual Probability of Exceedance (%)	Water Level[1] (m)	
		Value	95% Confidence Limit
500	0.2	157.55	157.26 - 157.85
200	0.5	157.44	157.21 - 157.68
100	1	157.35	157.16 - 157.55
50	2	157.26	157.10 - 157.42
20	5	157.12	157.01 - 157.24
10	10	157.01	156.93 - 157.10
5	20	156.89	156.82 - 156.96
2	50	156.67	156.61 - 156.72

Note:
1. Elevations at gauge #07OB002 Hay River near Hay River reference the Geodetic Survey of Canada datum (local 1982 adj.).

4.3 Ice Regime

Freeze-up

Freeze-up of the Hay River generally occurs in early November, with ice first forming in the deep sections at the mouths of the East and West Channels in the delta. Frazil pans travelling

downstream accumulate at these locations and form a rough ice cover which has a locally increased depth (Gerard and Stanley 1988). A solid ice cover first forms around these areas. As water levels decrease due to decreasing discharge throughout the winter, the West Channel freezes to the bed in the shallower sections. Freeze-up begins on Great Slave Lake around the same time as the Hay River and the lake is frozen over by around mid-December. During this time, wave action creates conditions for offshore ice ridges, or areas of increased ice thickness, to form on the lake in the vicinity of the mouth of the Hay River (Gerard and Stanley 1988).

Breakup

Breakup of the Hay River typically occurs between mid-April and early May, which is earlier than the breakup of ice on Great Slave Lake (Gerard and Stanley 1988). Kovachis (2011) outlines a typical breakup sequence based on site observations made by University of Alberta researchers since 2005, earlier research conducted in the area, and information provided by residents of Hay River. This sequence is comprised of ten stages which are summarized below:

1. The sequence begins with melting in the headwaters, which refers to the increase in discharge due to snowmelt runoff in southern, upstream portion of the basin.
2. This is followed by thermal deterioration of snow on the ice cover and ice along the channel margins due to warm spring weather.
3. During this period, significant ice melt can occur in the West Channel as the ice is frozen to the bed and the channel is relatively dry.
4. Transverse cracking occurs next throughout the river as the increased runoff lifts and breaks the intact ice cover creating large individual ice sheets which are then shifted downstream.
5. As the ice sheets move downstream, sheet accumulations occur and cause localized water level fluctuations.
6. This action develops into mini-jams (0.5 to 2 km long) that occur upstream of intact ice segments, and commonly in areas such as the Kátł'odeh Bridge (formerly Pine Point Bridge).
7. Localized fluctuations trigger ice jams that are 5 to 20 km in length. Areas where significant jams occur include: downstream of Alexandra and Louise Falls (approximately 80 km upstream of the Hay River mouth), within the East Channel, and along most, or all, of the West Channel.
8. Some of the ice jams formed in the upstream reaches will release and travel downstream at a high speed, with an ice run either pushing through an intact ice cover or stalling to form a new ice jam (re-jamming).
9. Within the Hay River delta, ice runs from upstream typically shove primarily into the West Channel and cause the toe of the initial East Channel jam to push downstream. Ultimately, these jam(s) cause the peak stage which may result in flooding.

10. Finally, once all the ice runs have consolidated in the delta, the ice jam(s) thermally deteriorate.

Factors affecting Ice Jam Flooding Severity

Past research has pointed towards ice jam flood severity being a factor of the following:

- Condition and configuration of the ice pack in the delta when the peak discharge arrives (Gerard and Stanley 1988), including how far the toes of the jams shove down the East and West Channels and if ice and water are able to discharge onto the lake (Kovachis 2011).
- Timing of the arrival of the peak snowmelt discharge (Kovachis 2011) as well as its magnitude while ice jams are in place, which may be augmented by ice jam releases in the mid-reaches of the river and runoff from spring rain (Gerard and Stanley 1988).
- Presence of intact, solid ice offshore in Great Slave Lake (Wedel 1988; Gerard and Stanley 1988).

In the East Channel, severe flooding has been linked to a high discharge moving the toe of the jam to the mouth of the river while there is still much ice accumulated in the area; in the West Channel, flooding takes place when ice jams are present in both the West and East Channels and a high discharge is experienced (Gerard and Stanley 1988).

Based on local observations, Gerard and Stanley (1988) concluded that it is not likely anthropogenic changes made to channels since 1947 have significantly influenced ice jam flooding in the region.

4.4 Ice Jam Data Preparation

4.4.1 07OB001 Hay River near Hay River

Breakup discharge and water level data at #07OB001 Hay River near Hay River were inspected on a year-by-year basis to determine the maximum breakup level, breakup discharge, and characterize breakup mechanism type. The methodology for assessing continuous water level hydrographs (1996 to 2023) and pen recorder charts (1965 to 1996) to characterize the breakup mechanism, as either thermal breakup, an ice run, or ice jam, is as follows:

- Years in which the breakup hydrograph showed a relatively gradual rise in water level were interpreted as thermal breakup.
- Years in which the breakup hydrograph showed a rapid rise in water level followed by a rapid or gradual fall were interpreted as an ice run.
- Years in which the breakup hydrograph showed a rapid rise in water level with a sustained peak water level for four hours at minimum were interpreted as an ice jam.

Past literature was also accessed, including observations on the extents of ice jams, severity of flooding, and visual observations. There was insufficient data for the years 1971, 1975, 1979, 1980, and 2003; therefore, breakup mechanisms for these seasons were not characterized. The results of the analysis are listed in **Table 16**.

Additionally, a review of past literature was completed to characterize the breakup mechanism within the Hay River Delta region, specifically along the East and West Channels. Detailed observational accounts which are well documented in Appendix A of Kovachis (2011) were used as the primary source of data up to 2011. These results are also listed in **Table 16**.

Table 16 Peak Spring Breakup Summary – #07OB001 Hay River near Hay River, Hay River East Channel, and Hay River West Channel

Season	WSC Gauge #07OB001					East Channel	West Channel
	Date	Water Level[1] (m)	Discharge (m3/s)	Breakup Type	Data Source	Breakup Type[2]	Breakup Type[2]
1964	1964-05-07 4:00	166.351	566	Ice Run	CRID	Thermal	Ice Run
1965	1965-05-02 20:00	167.244	750	Ice Run	CRID	Ice Jam	Ice Jam
1966	1966-05-09 2:00	163.608	550	Thermal	CRID	Thermal	Thermal
1967	1967-05-10 20:30	164.302	850	Ice Run	CRID	Ice Run	Ice Run
1968	1968-04-30 16:45	165.982	328	Ice Run	CRID	Ice Run	Ice Run
1969	1969-04-25 0:00	165.114	623	Ice Run	CRID	Ice Jam	Ice Run
1970	1970-05-03 0:00	165.373	374	Ice Run	CRID /WSC	Ice Run	Ice Run
1971	ND	ND	ND	Ice Run	ND	Ice Run	Ice Run
1972	1972-05-08 17:00	165.193	566	Ice Run	CRID	Ice Run	Ice Run
1973	1973-04-28 14:00	164.117	629	Ice Run	WSC	ND	ND
1974	1974-05-01 0:00	166.433	1,100	Ice Run	CRID	Ice Jam	Ice Jam
1975	ND	ND	ND	Thermal	ND	Ice Run	Ice Run
1976	1976-04-22 13:30	164.181	152	Ice Run	CRID	Ice Run	Ice Run
1977	1977-04-27 13:25	165.443	530	Ice Jam	CRID	Ice Jam	Ice Run
1978	1978-05-05 11:15	165.307	767	Ice Run	CRID	Ice Jam	Ice Run
1979	ND	ND	ND	ND	ND	Ice Jam	Ice Run
1980	ND	ND	ND	ND	ND	Ice Run	Ice Run

Season	WSC Gauge #07OB001					East Channel	West Channel
	Date	Water Level[1] (m)	Discharge (m3/s)	Breakup Type	Data Source	Breakup Type[2]	Breakup Type[2]
1981	1981-05-04 0:00	165.425	775	Ice Run	CRID	Ice Jam	Ice Run
1982	1982-05-09 0:00	166.047	657	Ice Run	CRID	Ice Run	Ice Run
1983	ND	164.572	370	Ice Run	CRID	Ice Run	Ice Run
1984	1984-04-21 0:00	161.643	172	Ice Run	CRID	Ice Run	Ice Run
1985	1985-05-06 19:50	167.752	1,350	Ice Run	CRID	Ice Jam	Ice Jam
1986	1986-05-06 20:44	167.813	900	Ice Run	CRID	Ice Jam	Ice Run
1987	1987-04-28 9:23	166.552	832	Ice Run	CRID	Ice Jam	Ice Jam
1988	1988-04-27 13:59	165.602	800	Ice Run	CRID	Ice Jam	Ice Jam
1989	1989-05-03 5:42	168.680	800	Ice Jam	CRID	Ice Jam	Ice Jam
1990	1990-04-27 14:59	166.280	350	Ice Jam	CRID	Ice Jam	Ice Jam
1991	1991-04-24 21:50	165.429	200	Ice Jam	CRID	Ice Jam	Ice Jam
1992	1992-04-28 9:23	167.823	900	Ice Jam	CRID	Ice Jam	Ice Jam
1993	1993-04-30 8:30	163.142	159	Ice Run	CRID	Ice Run	Ice Run
1994	1994-04-28 9:46	168.556	770	Ice Jam	CRID	Ice Jam	Ice Jam
1995	1995-05-04 15:03	165.479	320	Ice Run	CRID	Ice Jam	Ice Run
1996	1996-05-02 13:30	163.603	200	Ice Jam	CRID	Ice Run	Ice Run
1997	1997-05-03 10:45	166.606	515	Ice Run	CRID	Ice Run	Ice Jam
1998	1998-04-21 16:00	164.298	360	Ice Jam	CRID	Ice Run	Ice Run
1999	1999-04-26 9:45	161.799	181	Ice Run	CRID	ND	ND
2000	2000-04-29 22:45	163.754	180	Ice Run	CRID	ND	ND
2001	2001-05-04 11:50	166.587	410	Ice Jam	CRID	Ice Run	Ice Jam
2002	2002-05-15 17:25	166.577	460	Ice Jam	CRID	Ice Run	Ice Jam
2003	ND	ND	ND	ND	ND	Ice Run	Ice Jam
2004	2004-05-01 2:10	164.553	155	Ice Jam	CRID	Thermal	Thermal
2005	2005-04-24 2:00	164.790	436	Ice Run	CRID	Ice Jam	Ice Run
2006	2006-04-25 19:15	165.493	370	Ice Jam	CRID	Ice Run	Ice Jam
2007	2007-04-27 11:15	165.975	380	Ice Run	WSC	Ice Jam	Ice Jam

Season	WSC Gauge #07OB001					East Channel	West Channel
	Date	Water Level[1] (m)	Discharge (m3/s)	Breakup Type	Data Source	Breakup Type[2]	Breakup Type[2]
2008	2008-05-05 19:15	167.064	700	Ice Run	WSC	Ice Jam	Ice Jam
2009	2009-05-06 13:50	165.396	630	Ice Run	CRID	Ice Jam	Ice Jam
2010	2010-04-25 15:25	165.822	250	Ice Run	CRID	Ice Jam	Ice Jam
2011	2011-05-08 16:05	165.267	478	Ice Jam	CRID	ND	ND
2012	2012-05-02 15:20	164.999	112	Ice Jam	CRID	ND	ND
2013	2013-05-11 13:05	162.950	186	Ice Run	WSC	ND	ND
2014	2014-05-04 13:10	166.406	283	Ice Jam	CRID	ND	ND
2015	2015-04-26 2:50	163.597	278	Ice Run	CRID	ND	ND
2016	2016-04-28 21:30	164.373	250	Ice Run	WSC	ND	ND
2017	2017-05-02 23:05	163.088	180	Ice Jam	WSC	ND	ND
2018	2018-05-04 8:45	162.274	198	Thermal	WSC	ND	ND
2019	2019-04-17 17:05	160.851	26	Ice Run	WSC	ND	ND
2020	2020-05-05 11:10	166.311	602	Ice Run	WSC	ND	ND
2021	2021-05-10 4:15	168.335	885	Ice Jam	WSC	ND	ND
2022	2022-05-12 6:55	170.900	1,460	Ice Jam	WSC	Ice Jam	Ice Jam
2023	2023-04-30 9:10	162.338	133	Ice Run	WSC	ND	ND

Legend:

CRID = Canadian River Ice Database

WSC = Water Survey of Canada

ND = No Data

Notes:

1. Elevations at gauge #07OB001 Hay River near Hay River reference the Geodetic Survey of Canada datum (local 1985 adj.).
2. Breakup type characterization for both the Hay River East and West Channels were based on observational accounts documented in Kovachis (2011).

4.4.2 07OB002 Great Slave Lake at Hay River

Table 17 presents Great Slave Lake water levels which are coincident with the breakup peak flows listed in **Table 16**. As with the peak discharge data, the #07OB002 dataset considered values measured up to one week before and after the timing of the peak event at #07OB001.

Additionally, a correlation was made with #07SB001 Great Slave Lake at Yellowknife Bay to help confirm representative values and fill in data gaps.

Table 17 #07OB002 Great Slave Lake water level data series corresponding to breakup peak discharges for #07OB001 Hay River near Hay River

Year	Date	Great Slake Lake Water Level[1] (m)	Comment
1964	05-07	156.475	Value on 5/7/1964
1965	05-02	156.612	
1966	05-09	156.451	Value on 5/10/1966
1967	05-10	156.326	Value on 5/7/1964
1968	04-30	156.542	Value on 5/6/1968
1969	04-25	156.292	
1970	05-03	156.292	
1971	ND	-	
1972	05-08	156.307	Correlation with 07SB001
1973	04-28	156.545	Correlation with 07SB001
1974	05-01	156.451	Correlation with 07SB001
1975	ND	-	
1976	04-22	156.606	Correlation with 07SB001
1977	04-27	156.600	Correlation with 07SB001
1978	05-05	156.582	Correlation with 07SB001
1979	ND	-	
1980	ND	-	
1981	05-04	156.372	Correlation with 07SB001
1982	05-09	156.204	Correlation with 07SB001
1983	ND	156.275	Correlation with 07SB001
1984	04-21	156.533	Correlation with 07SB001
1985	05-06	156.789	Value on 5/1/1985
1986	05-06	156.752	Value on 4/30/1986
1987	04-28	156.600	Value on 4/25/1987
1988	04-27	156.719	
1989	05-03	156.960	Value on 5/8/1989

Year	Date	Great Slake Lake Water Level[1] (m)	Comment
1990	04-27	156.799	Value on 4/26/1990
1991	04-24	156.799	Value on 4/26/1991
1992	04-28	157.013	Value on 4/25/1992
1993	04-30	156.903	
1994	04-28	156.848	Correlation with 07SB001
1995	05-04	156.580	Value on 5/2/1995
1996	05-02	156.619	Correlation with 07SB001
1997	05-03	156.875	
1998	04-21	157.132	
1999	04-26	156.582	
2000	04-29	156.561	
2001	05-04	156.657	Value on 4/30/2001
2002	05-15	156.687	Correlation with 07SB001
2003	ND	-	
2004	05-01	156.725	Value on 5/6/2004
2005	04-24	156.784	Value on 4/30/2005
2006	04-25	156.907	
2007	04-27	156.652	Value on 4/23/2007
2008	05-05	156.840	Value on 5/10/2008
2009	05-06	156.884	Value on 5/13/2009
2010	04-25	156.737	Value on 5/1/2010
2011	05-08	156.481	Value on 5/16/2011
2012	05-02	156.658	Correlation with 07SB001
2013	05-11	156.802	Value on 5/19/2013
2014	05-04	156.646	Correlation with 07SB001
2015	04-26	156.484	Correlation with 07SB001
2016	04-28	156.568	Value on 4/27/2016
2017	05-02	156.844	
2018	05-04	156.669	Value on 5/10/2018
2019	04-17	156.584	

Year	Date	Great Slake Lake Water Level[1] (m)	Comment
2020	05-05	156.918	Value on 5/7/2020
2021	05-10	157.344	Value on 5/15/2021
2022	05-12	157.239	Correlation with 07SB001
2023	04-30	156.707	

Note:
1. Elevations at gauge #07OB002 Hay River near Hay River reference the Geodetic Survey of Canada datum (local 1982 adj.).

4.5 Ice Jam Flood Frequency

Whereas flood *flow* (stream discharge) is the parameter of interest for open water analysis, flood *level* is the parameter of interest for ice jam flood analysis. This is because it is not possible to ascribe a unique flood level to each breakup flood flow. For a particular breakup discharge there are a range of flood levels owing to different ice-affected backwater conditions. And so, for ice jam flood level frequency analysis, the more meaningful parameter is *level*. While the parameter used to express flood magnitude (level versus discharge) differs, the resulting flood frequency magnitudes are technically equivalent.

Two different approaches were considered to estimate ice jam flood frequency for this study: a *direct method* based on observed flood levels and an *indirect* method based on flood levels derived from a very large population of synthesized flood levels. The indirect method was ultimately used in the development of the flood hazard maps.

4.5.1 Direct Method

07OB001 Hay River near Hay River

The direct method was an intuitive approach that undertook a simple frequency analysis of the peak breakup levels. This approach relied solely on peak water level data at breakup without consideration of the breakup ice conditions associated with the peak. The direct method analysis provides an initial estimate of flood level frequencies at the gauge. For this approach, the Cunnane plotting position formula (**Equation 1**) was applied to the ranked annual maximum flood levels to estimate the probability of non-exceedance, $\boldsymbol{P_i}$, for each rank, i, and total number of samples, $\boldsymbol{N}$ using the Cunnane plotting position parameter where , $\boldsymbol{a}$, is 0.4 (Stedinger et al. 1993).

$$\boldsymbol{P_i = \frac{i-a}{N+1-2a}} \qquad \textbf{Equation 1}$$

The results of the analysis are depicted as a probability plot on **Figure 10**. The data for the Hay River were all part of the systematic record.

The flood frequencies implied by the probability plot are indicative of the flood level magnitudes over a range of flood recurrence intervals at the gauge site. The indirect methods, which will be described below, were used to fit a flood frequency distribution to these observed data and extend regulatory flood levels at the gauges throughout the entire study area.

07OB002 Great Slave Lake at Hay River

The Log-Pearson III (LP3) distribution was found to provide a good fit to the observed data presented in **Table 17** and was used to estimate the peak breakup water level frequency. Breakup flood level frequency distributions for the Hay River are depicted on **Figure 11**. The adopted LP3 curve is shown in **Figure 12** along with it 95% confidence limits. Flood level frequency estimates for #07OB002 Great Slave Lake at Hay River coinciding with breakup peak discharges along the #07OB001 Hay River near Hay River are provided in **Table 18**.

Table 18 Water level frequency estimates for #07OB002 Great Slave Lake at Hay River coinciding with peak instantaneous discharges along the #07OB001 Hay River near Hay River

Return Period (Years)	Annual Probability of Exceedance (%)	Water Level (m)	
		Value	95% Confidence Limit
500	0.2	157.46	157.21 - 157.73
200	0.5	157.36	157.16 - 157.56
100	1	157.28	157.11 - 157.46
50	2	157.20	157.06 - 157.34
20	5	157.08	156.97 - 157.18
10	10	156.97	156.89 - 157.06
5	20	156.86	156.79 - 156.92
2	50	156.65	156.60 - 156.70

Note:
1. Elevations at gauge #07OB002 Hay River near Hay River reference the Geodetic Survey of Canada datum (local 1982 adj.).

4.5.2 Joint Probability Analysis

There are many different drivers impacting the magnitude of ice jam flooding including the following.

- Antecedent conditions preceding breakup, such as competency of the ice cover (thickness, type, and state of decay) and/or discharge and corresponding water levels.

- The prevailing meteorological conditions during their development and the potential for a concurrent major rainfall event.
- The resulting breakup mechanism (e.g. mechanical or thermal) and evolution of the ice jam accumulation.

The relative contribution of each factor on flood magnitude (directly or indirectly) is complex. There are no practical equations available to quantify relationships between many of the important drivers and flood level magnitude. It is not practical to explicitly account for all the various driving factors by a typical joint probability analysis.

The current state of practice for estimation of flood frequency magnitude is to rely on historical hydrometric data. For ice jam floods, the combined effect of all the different drivers impacting ice jam flood magnitude is ultimately expressed as flood level at the gauge. Fortunately, there exists historic flood level data with a relatively long record at the WSC gauge within the study reach.

The indirect method used to determine ice jam flood frequency in this study, is a type of joint probability analysis. The procedure followed a Monte Carlo approach that uses statistical methods to quantify the combined effects of the dominant drivers (or causative factors) that contribute to the whole set of flood level data. The adopted methodology follows that described by Healy and Kovachis (2023) and is detailed in the next section.

4.5.3 Indirect Method – Monte Carlo Analysis

The indirect method attempted to quantify the causative factors that contribute to the characteristics of the whole set of data rather than individual events and follows an approach similar to the so-called G-C method described by Beltaos (2021). The approach accounts for the variation in ice conditions at breakup and relies on a range of ice-affected flood level conditions along the study reach according to breakup type.

The analysis begins with preparation of the data used by the Monte Carlo workflow as follows.

1. Conduct a year-by-year inspection of the breakup data at the #07OB001 Hay River near Hay River gauge to determine the peak breakup level, corresponding discharge, and dominant breakup mechanism (or *type*). Complete a year-by-year review of anecdotal evidence to determine the dominant breakup mechanism (or *type*) for both the East and West Channels. In this study, three different breakup types were identified as thermal, mechanical resulting in a fully developed ice jam, and mechanical resulting in an ice-run or partially developed ice jam.
2. Determine the breakup discharge frequency relationship. A comparison of the different breakup flood frequency distributions and the adopted flood frequency distribution for the Hay River study reach are depicted on **Figure 13** and **Figure 14**, respectively.

3. Estimate the relative ratios of breakup types throughout the study reach based on the breakup types determined in step 1. These provide the probability of occurrence factors for the various breakup types used by the Monte Carlo analysis. For this study, the probability of occurrence factors for each reach is summarized by breakup type in **Table 19**.

4. Develop a family of ice-affected flood level profiles for each breakup type. This was achieved by computing water level profiles over a range of ice conditions and breakup discharges using the calibrated hydraulic ice jam model. This provides a set of rating curves at each model cross section according to breakup type

Table 19 Summary of Probability of Occurrence Factors for Hay River

Reach	Probability Factor by Breakup Type		
	Thermal	Mechanical	
		Ice Jam	Ice Run
Hay River Main Channel (KM 1064.0 to KM 1089.9)	5%	10%	86%
Hay River Main Channel (KM 1089.9 to KM 1095.0)	5%	Exponential transition from 10% to 31%	Exponential transition from 86% to 64%
Hay River Main Channel (KM 1095.0 to KM 10981.1)	5%	31%	64%
Hay River Main Channel (KM 10981.1 to KM 1108.0)	5%	Linear transition from 31% to 52%	Linear transition from 64% to 43%
Hay River Main Channel (KM 1108.0)	5%	52%	43%
Hay River East Channel (KM 1108.0 to KM 1110.4)	5%	52%	43%
Hay River East Channel (KM 1110.4 to KM 1113.0)	Linear transition from 5% to 8%	Linear transition from 52% to 20%	Linear transition from 43% to 0%
Hay River East Channel (KM 1113.0 to KM 1114.4)	8%	20%	0%

Reach	Probability Factor by Breakup Type		
	Thermal	Mechanical	
		Ice Jam	Ice Run
Hay River West Channel (KM 1108.2 to KM 1111.2)	5%	45%	50%
Hay River West Fishing Village Channel (KM 1111.2 to KM 1112.8)	5%	45%	50%
Hay River West Fishing Village Channel (KM 1112.8 to KM 1113.3)	Linear transition from 5% to 8%	Linear transition from 45% to 20%	Linear transition from 50% to 0%
Hay River West Fishing Village Channel (KM 1113.3 to KM 1113.4)	8%	20%	0%

Note:
1. Transitions are relative to project river station (km) distances.

The Monte Carlo workflow preceded according to the following steps which are illustrated in **Figure 15**. The workflow resulted in a very large population of breakup flood levels that was used to estimate the ice jam flood frequency distribution – it was completed separately for the Main, East, and West Channels.

1. Randomly select a value from the breakup discharge frequency distribution (recall **Figure 14**).
2. Randomly select a breakup mechanism at each cross section based on the probability factors for the various breakup types (recall step 3 above).
3. Determine the breakup flood level at each cross section associated with the randomly selected breakup discharge value and randomly selected breakup type according to the breakup rating curves pre-calculated in step 4 above.
4. Store the breakup flood levels to the synthesized population of breakup levels for and repeat the process many, many, times (i.e. 20,000 iterations). The degree of statistical confidence increases with a very high number of iterations. It limits the variation in the flood level magnitudes associated with the extreme AEP values by ensuring samples are selected within the extreme range.
5. Rank and plot the series at each cross section with a standard plotting position formula to form a distribution of breakup flood levels and compare to the estimated breakup flood levels based on observational data.

6. Repeat steps 1 to 5 twice to obtain three separate distributions of breakup flood levels. From the ranked series store the corresponding 100-year and 200-year breakup flood levels at each cross section for each distribution. Calculate the average 100-year and 200-year breakup flood levels at each cross section between the three sets of distributions.
7. To mitigate local adverse slopes that aren't hydraulic possible apply smoothing techniques through an adjusted average approach of breakup flood levels where required.

The resulting Monte Carlo distributions as compared to the observational data are provided in **Figure 16** and **Figure 17** which display the Hay River Main Channel discharge and flood level at #07OB001 Hay River near Hay River gauge, respectively. Note **Figure 17** provides an example Monte Carlo distribution for the gauge location on a cross-section.

5 OPEN WATER HYDRAULICS

The first step towards development of the ice jam model was to create an open water model calibrated to surveyed water levels. The following describes the steps taken to develop the open water model.

5.1 Data Preparation

The hydraulic modelling relied on bed and overbank elevation data gathered by NHC in the summer of 2024 (detailed in a previous section) for the main channel geometry and the received DTM for the overbank geometry. The received orthorectified aerial imagery was also used to assist in aligning the model cross sections and channel centreline.

5.1.1 Model DTM

The project DTM (McElhaney 2020) sufficiently covered the mapping domain and channel cross sections, and no additional DTM data sources were required. The project DTM was used to inform the channel geometry and complete the subsequent flood mapping.

5.1.2 Highwater Marks

Highwater mark observations serve as documentation of the highest water levels reached at specific locations during a particular flood event. These observations are instrumental in calibrating and validating hydraulic models, as they allow for comparisons between simulated water levels and actual highwater mark elevations along the study reach.

Water levels associated with open water flood events have not resulted in significant flooding of settled areas; therefore, these data are not often collected. Recorded highwater mark observations for an open water event which occurred in July 1977 are available in UMA (1978);

however, due to the poor quality of the digital maps and lack of documentation in the report, it was not possible to extract this dataset.

5.1.3 Previous Models

In some cases, an existing hydraulic model can be found from a previous study and these previously developed models can provide useful information for a new or updated model. Salient conclusions determined from these efforts are included below.

Flow Split Determination

The work of Gerard and Stanley (1988) found that East Channel is the main channel and typically carries about 65-75% of the flow passing through the Hay River delta. The West Channel behaves as a high-level by-pass, as its bed is substantially higher than that of the East Channel. The West Channel becomes dry during low flows in the summer and freezes to the bed during winter. There is a notable and sudden deepening of both the East and West Channels near their mouths.

Discharge in the West Channel is largely controlled by the water level in the East Channel. Based on field observations, Gerard and Stanley (1988) developed relationships between water level at the East-West Channel split and the discharge in the West Channel of Hay River under open water and ice jam conditions. This work suggested two extreme conditions: 1) a fully developed ice jam in both the East and West Channel up to the split; and (2) fully developed jam along the East Channel up to the split and open water downstream of the split on the West Channel.

More recently, two dimensional (2D) models have been used to model the flow and ice split between the East and West Channels of the delta. Brayall (2011) developed 2D models of the Hay River delta using both CRISSP2D and River2D. Brayall (2011) determined various relationships and compared results with those of Gerard and Stanley (1988) and Jasek (1993). Ultimately, a relationship was developed between the total discharge and the East Channel discharge under open water and ice jam conditions (Brayall 2011). Like past researchers Brayall (2011) found that the East Channel is the primary flow route through the Hay River delta, carrying about 72%-81% under open water and 63%-74% under ice jam conditions. This relationship was further explored by Decoste (2017) using River1D and it compared well to the original using River2D by Brayall (2011).

5.2 Open Water Model Construction

The U.S. Army Corps of Engineer's Hydrologic Engineering Center River Analysis System (HEC-RAS) computer program (Version 6.5, 2024) was used to perform hydraulic modelling for this study. The basic inputs required by HEC-RAS are cross sections spaced throughout the study reach that represent the geometry of the river channel and floodplain, roughness coefficients for the channel and overbank areas at each cross section, a specified water level, rating curve, slope at the downstream boundary, and an inflow discharge, at the upstream boundary.

HEC-RAS can perform one-dimensional (1D), two-dimensional (2D), or combined 1D and 2D hydraulic calculations for a network of channels with or without hydraulic structures. For the open water condition, a 1D model was constructed to compute water surface profiles for steady-state flows.

5.2.1 Geometric Layout

The approach followed to develop key components of the model geometric layout was:

- The channel centreline was defined along the middle of the main channel and was digitized using ArcGIS tools and visual referencing of the DTM, hillshade, and aerial imagery. A single continuous centreline was created to represent each modelled reach. Five reaches were modelled for this study. The modelled reaches are as follows.
  - *Hay River Main Channel* reach extending from the upstream study limit (near Enterprise) to East-West flow split location. The total reach length is approximately 44 km.
  - *Hay River East Channel* reach extending from the East-West flow split location to the confluence with the Great Slave Lake. The total reach length is approximately 6.5 km.
  - *Hay River West Channel* reach extending from East-West flow split location to the Rudd-Fishing flow split location. The total reach length is approximately 3.2 km.
  - *Hay River (West) Rudd Channel* reach extending from the Rudd- Fishing flow split location to the confluence with the Great Slave Lake. The total reach length is approximately 1.3 km.
  - *Hay River (West) Fishing Channel* reach extending from the Rudd- Fishing flow split location to the confluence with the Great Slave Lake. The total reach length is approximately 2.3 km.
- Flow paths were created coincident with the river centerline and along the left and right floodplains, representing the length of the main channel, left overbank, and right overbank flow paths. Distances between cross sections were measured along flow path lines. The model requires these distances for estimating energy losses between cross sections within the main channel and the left and right overbank areas.
- Model cross section transects were digitized at each surveyed cross section as follows. First, a main channel portion was digitized across the main channel overtop of the surveyed channel and bank point data. Then, the main channel portion was extended left and right across the floodplain (overbank areas). The overbank portions were aligned perpendicular to the anticipated path of the floodplain flows. Cross section elevation values from the survey point data were projected onto the cross-section lines using the RAS Mapper GIS toolset through a conflation process. Elevations in the overbank areas were determined by extracting elevation values from the underlying DTM along the cross-section polylines. The available bare-earth DTM was used for the model construction.

The cross sections were spaced according to the active channel width and slopes, with adjustments to capture historical cross sections, hydraulic structures, meander bends, and other important channel or floodplain features.

The determination of the left and right banks, referred to as model bank stations, involved examining the geometry of cross sections and analyzing the DTM of the channel. These model bank stations were strategically positioned to delineate the boundaries of the modelled left overbank, main channel, and modelled right overbank sections of the cross sections. Additionally, they were placed to reflect variations in roughness within both the channel and floodplains. It's important to note that while these model bank stations serve to represent hydraulic conditions within the channel and floodplain, they may not precisely align with the actual banks of the main channel. Their primary function is to simulate the hydraulic behavior of the channel and its surrounding floodplains within the model framework. The resulting model cross sections and model channel centreline for the Hay River are shown on **Figure 18** through **Figure 31**.

5.2.2 Channel and Overbank Roughness

Manning's roughness values were used to simulate roughness in the modelled reaches. Manning's roughness is an empirical coefficient used to account for energy losses due to a combination of factors including surface roughness and channel sinuosity. Manning's roughness also varies somewhat with discharge. The Manning's roughness values adopted for the present study are discussed further in a subsequent section on model parameters.

5.2.3 Expansion and Contraction Coefficients

To account for the effect of flow contraction or expansion losses on the energy balance between successive cross sections, HEC-RAS multiplies the absolute difference in velocity head by a coefficient. These coefficients range from 0.10 for gradual transitions to 0.80 for abrupt transitions (Brunner, 2016).

5.2.4 Boundary Conditions

Boundary conditions are required at the inflow (upstream) and outflow (downstream) boundaries of the model. The inflow boundary condition is the discharge. The outflow boundary condition could be a water level (through fixed stage or rating curve) or a friction slope with which the water level will be calculated by HEC-RAS assuming a normal depth approximation.

5.2.5 Ineffective Flow Areas

Ineffective flow areas can be specified within portions of cross sections where water will pond but there is no appreciable flow. One common example of using ineffective flow area is in cross sections upstream and downstream of a bridge or culvert where flow is obstructed by elevated road embankments. In HEC-RAS, ineffective flow areas can be defined as either a permanent or

non-permanent type. Permanent ineffective flow areas stay ineffective regardless of the water surface elevation, whereas temporary ineffective flow areas become effective when water surface elevation exceeds a defined elevation. The configuration of ineffective flow areas depends on site-specific circumstances and engineering judgement.

5.2.6 Geometric Database

The geometric database provides all the components of the HEC-RAS model geometry, including cross sections, internal hydraulic structures, and boundary conditions. Each component is described below. Additional information and data are provided as part of the electronic deliverables of the study.

Cross Section Data

A total of 192 cross sections were created and used to construct the model for this study. The steps taken to generate the cross section data were as follows:

- Cross section alignments within the channel were established generally following the alignments of the cross section survey. The overbank portions were aligned perpendicular to the anticipated flow direction.
- Two separate station-elevation data sets were created for each cross section.
- The first data set was created by projecting surveyed data points perpendicularly onto the channel portion of the cross section line.
- The second data set was created by extracting elevation values from the DTM along the cross section lines excluding the channel portion covered by the survey data.
- The two station-elevation data sets were combined. For each cross section, the number of elevation points for the overbanks were reduced using the minimize-area-change point filter option in HEC-RAS, so that the total number of the points is within the HEC-RAS limit of 500 points.
- Distances between consecutive cross sections were established within the HEC-RAS model following the established channel centerline and central flow paths for the left and right overbank areas.

Hydraulic Structures

The constructed model comprises two bridge crossings: Kátł'odeh Bridge and West Channel Bridge. The alignments and locations of the hydraulic structures were established based on the survey data and available record drawings.

Key design information of these structures that was incorporated into the model, including: abutments, high and low chords defining the bridge deck and the superstructure, and the arrangement, shape, and dimensions of the piers. Key design information was primarily based

on survey data, with supplemental details such as low chord elevation and pier geometry (when its shape is varied) from record drawings as needed. The cross section line that defined the centreline of this highway crossing was extended linearly to include the approach roadway on both banks.

5.2.7 Model Calibration

Calibrating the model involved selecting various parameters to accurately simulate observed water levels within the study reach under both high and low flow conditions. The following parameters were modified as part of calibration:

- Manning's roughness coefficients for the channel and floodplain.
- Ineffective flow areas at each model cross section.
- Expansion and contraction loss coefficients.
- Discharge coefficients for flow overtopping roadway crossings and embankments.

Of these parameters, Manning's roughness for the river channel is typically the primary calibration parameter. Challenges and limitations inherent in the calibration process included:

- Availability and accuracy of the calibration data.
- Proper identification of highwater mark locations.
- Uncertainties in estimates of the flood peak discharge.
- Insufficient channel geometry data.

The general calibration approach involved adjusting Manning's roughness values to ensure computed water levels closely matched observed levels for selected events. Adjustments were made on a reach-averaged basis. High flow events were preferred for calibration, although WSC gauge rating curve data and/or low flow events could also be utilized.

In this study, the primary challenge affecting calibration efforts was the absence of highwater mark data for open water flood events within the study reaches. However, it is possible to extract a water surface profile from the non-hydroflattened LiDAR DTM from July 7, 2020. The mean daily flow on this date was recorded as 505 m^3/s at the WSC #07OB001 Hay River near Hay River gauge location. A comparison of the computed water levels to the extracted LiDAR surface for the same discharge in HEC-RAS is shown in **Figure 32** though **Figure 35**. Note while this discharge is relatively high for the summer flow period, it is still lower than the 2-year flood frequency event (690 m^3/s). Furthermore, it is expected that some elevation errors are present within the non-hydroflattened LiDAR water surface profile as wet surfaces typically reflect a LiDAR pulse differently than dry ground. While the extracted profile likely provides a reasonable representation of the water surface during the time of the LiDAR flight, it is not comparable to

the data quality that is achieved by topographic GPS surveys and should therefore be interpreted with caution.

A low flow calibration has been completed utilizing the water level measurements collected as part of the May/June 2024 field survey by NHC. Water levels were surveyed at each cross section, typically along both the left and right banks. A comparison of the surveyed water surface profile to the simulated water surface profile using the discharges below can be found in in **Figure 32** though **Figure 35**.

Additionally, the provided rating curve table from the WSC gauge #07OB001 Hay River near Hay River was used to calibrate the Hay River locally. Included in the WSC rating curve tables were the direct measurements used to synthesize the WSC curve. These values were found to be more relevant for calibration than just the curve. **Figure 36** provides a comparison of computed HEC-RAS water surface profiles to the WSC rating curve data and corresponding direct measurements collected at the gauging site.

5.3 Model Parameters and Options

The following sections describe the key model parameters and options adopted in the HEC-RAS model. These include Manning's roughness values for channel and overbank areas; contraction and expansion loss coefficients; ineffective areas; and roadway weir coefficient.

5.3.1 Manning's Roughness Coefficient

Manning's roughness is used to account for an array of energy losses that may vary with respect to discharge. A minimum of three (one channel and two overbank) roughness values were used within each cross section. Where appropriate, roughness was varied horizontally across the section to capture changes in river and floodplain characteristics. **Table 20** summarizes the selected channel and floodplain roughness values at each model cross section.

Table 20 Description of bed material and land cover types within the study reach

Reach Description	River Station (km)	Channel Roughness	Channel Remarks	Overbank Roughness	Overbank Remarks
Hay River Main Channel reach	1108 to 1064	0.032	Natural gravely channel	0.080-0.10	Mostly treed area with some development.
Hay River East Channel reach	1114.5 to 1108	0.032	Natural gravely channel	0.040-0.10	Combination of development (within Town) and treed areas.
Hay River West Channel reach	1108 to 1111.2	0.032	Natural gravely channel	0.060-0.10	Combination of treed and grass area
Hay River (West) Rudd Channel	1111.2 to 1112.5	0.032	Natural gravely channel	0.080-0.10	Combination of mostly treed and some grass area
Hay River (West) Fishing Channel	1111.2 to 1113.5	0.032	Natural gravely channel	0.060-0.10	Combination of development and treed areas.

The channel and overbank roughness values mentioned in the table above are directly utilized for all flood frequency flows.

5.3.2 Expansion and Contraction Coefficients

To account for the effect of flow contraction and expansion losses on the energy balance between successive cross sections, HEC-RAS multiplies the absolute difference in velocity head by a coefficient. The default values of 0.1 and 0.3 (for expansion and contraction coefficients, respectively) were utilized throughout the model domain. One exception is for cross sections located at bridge crossings. At these locations, expansion and contraction coefficients were increased to 0.3 and 0.5, respectively.

5.3.3 Weir Coefficient

HEC-RAS uses a broad crested weir formulation to represent flow overtopping road, rail, or similar embankments crossing the flow path. Typical discharge coefficients range between 1.45 to 1.8, with larger values generating less backwater. Flow overtopping a bridge deck is not an ideal broad crested weir, and it is generally recommended that lower values be used when an increased resistance to flow from obstructions such as bridge railings, curbs, and debris is

anticipated. The resistance of flow is believed to be moderate for this study, and a weir coefficient of 1.6 was assigned for all hydraulic structure embankments.

5.3.4 Boundary Conditions

A water level boundary condition was applied at the downstream boundary of the Hay River East Channel, Hay River (West) Rudd Channel and Hay River (West) Fishing Channel. For the high flow calibration event, the observed water level from July 7, 2020 of 156.91 m CGVD2013a from the non-hydroflattened LiDAR DTM has been used to represent the downstream boundary at the mouth. For the low flow calibration event, the surveyed water level of 155.87 m CGVD2013a at the East Channel was selected as downstream boundary for all reaches. Given the relatively high water levels within Great Slave Lake during LiDAR collection, the downstream boundary selected for the 100-year flood frequency scenario was set to 156.95 m to facilitate ease of hazard mapping. Based on the flood frequency analysis completed on Great Slave Lake water levels during the open water season, this is equivalent to a water level with an approximately 50-year return period.

A specified discharge is required at the upstream end of each modelled reach. An inflow discharge was assigned at the upstream boundary of the Hay River Main Reach and at the lower sub-reaches respectively. For the calibration events single flow inputs of 505 m^3/s (June 7, 2020) and 18.2 m^3/s (May 29, 2024) have been selected respectively while a flow input of 1,470 m^3/s has been applied for the 100-year event. Additional flow change locations were required at the upstream limits of the lower sub-reaches to capture noticeable changes in river discharges within the study area. The flow change locations assigned in the HEC-RAS model are summarized in **Table 21**.

Table 21 Summary of flow change locations

Stream Name	Reach	River Station (km)	Flow Split Relationship Basis	Description
Hay River	Main Channel	1064	No flow split	Hay River above the East-West Channel Flow Split Location.
	East Channel	1108	Brayall (2011)	Hay River below the East-West Channel Flow Split Location.
	West Channel	1108	Brayall (2011)	Hay River below the East-West Channel Flow Split Location.
	West Channel - Rudd	1111.2	50% of West Channel flow	Hay River West Channel below the Rudd-Fishing West Channel Flow Split Location.
	West Channel – Fishing Village	1111.2	50% of West Channel flow	Hay River West Channel below the Rudd-Fishing West Channel Flow Split Location.

5.3.5 Blocked Obstructions

Blocked obstructions in the floodplain, such as buildings, walls, storage tanks, or elevated foundations were not specified in the HEC-RAS model. Obstructions associated with bridge piers and structural members were modelled using the standard bridge editor specifications in HEC-RAS.

5.3.6 Ineffective Flow Areas

Ineffective flow areas were specified at cross sections in the HEC-RAS model based on a review of the local terrain and floodplain features both at and between cross sections. Ineffective flow areas can be specified within portions of cross sections where water is expected to pond, and where the velocity of that water, in the downstream direction, is expected to be close to or equal to zero (Brunner, 2016). The downstream direction is taken relative to the cross-section lines defined in the model, so the orientation of cross sections was considered when specifying ineffective flow areas.

Ineffective flow areas in the model may be specified as either permanent or non-permanent. Permanent ineffective flow areas apply regardless of the water surface elevation, whereas non-permanent ineffective flow areas become effective above a defined elevation. The configuration of permanent and non-permanent ineffective flow areas were specified depending on site-specific circumstances and engineering judgement.

The general principles for determining ineffective flow areas were as follows:

- Non-permanent ineffective flow areas were used to "fill" local depressions on the floodplain that are obstructed by higher ground upstream or downstream. These areas were assumed to become engaged in the active flow area (or effective) once the water level exceeded the elevation of the adjacent ground.
- Permanent ineffective flow areas were used to permanently "fill" relic channels, tributary channels or excavated holes that would otherwise have incorrectly added flow area to the cross section.
- Permanent ineffective flow areas were defined where flow patterns were likely to be influenced by nearby bridge abutments and roadway embankments crossing the floodplain. These types of obstructions tend to direct flows towards the bridge opening. Several site-specific factors were taken into account when configuring ineffective flow areas at bridges and culverts in the study area, including: distance from the cross section to the bridge, terrain features, bridge geometry, and skew of the bridge opening relative to the river.
- Ineffective flow areas behind railroad and highway embankments were assessed on a case by case basis. Aerial imagery, LiDAR, and historic information were used to determine if there were indications of flow behind and/or above embankments. Areas behind and below the height of the embankment were modelled as effective flow only if there was no downstream obstruction or if there was an indication of flow moving in the downstream direction. Otherwise, permanent ineffective flow areas were set to the top of embankment elevation, allowing areas behind embankments (assumed permeable) to be shown as wet and isolated but not conveying flow. Areas above embankments generally conveyed flow once the embankment was overtopped, unless an upstream or downstream obstruction was present causing local ponding or dead zones with limited flow.

5.3.7 Flow Splits, Islands and Diversions

The study reaches were adequately represented without flow splits around smaller islands. Where a cross section intersected an island, the HEC-RAS model assumed equal water level on both sides of an island based on the composite channel conveyance properties and computed energy losses. This assumption is most valid once flood magnitudes increase, and the island becomes inundated.

For the larger Vale Island along the Hay River, both the Rudd and Fishing channels have been modelled as separate river reaches to account for varying water surface profiles and energies between them.

Diversions may include avulsion channels or flow paths that reduce the total discharge carried by the main channel along a portion of the study reach. There were no such diversions encountered within the study area, and all open-water flood flows were confined to the cross sections modelled along the study reaches.

5.4 Open Water Flood Profiles

The hydraulic model was used to generate open water flood profiles for the 100-year return period. The computed flood frequency water levels at each surveyed cross section on the Hay River are provided in **Appendix C**. These results are plotted graphically in **Figure 37** through **Figure 39** for the different Hay River reaches.

6 ICE JAM MODEL DEVELOPMENT

The basic inputs required by the ice model are much the same as those required by an open water model (i.e., river cross sections along known lengths of channel, roughness coefficients for the channel and overbank areas at each cross section, a specified or computed water level at the downstream model boundary, and a discharge at all upstream model boundaries). In addition to these basic inputs, the ice model requires at each model cross section: a prescribed ice cover condition, under ice roughness, and a set of ice jam parameters characterizing the properties of the ice jam. These ice model inputs are used to solve for the under ice hydraulics and ice jam stability relationship. As this is the case, it was considered acceptable to use the calibrated open water model previously discussed, with some adjustments to better facilitate the modelling of ice conditions.

6.1 Model Refinements

While the open water model was generally considered acceptable for use in the ice jam model, certain modifications were necessary to better facilitate ice jam modelling. These model refinements may include adjustment to the bank stations to better represent the ice jam "width" and the addition of extra cross sections, typically created by interpolating existing surveyed cross sections.

6.1.1 Main Channel Widths

The ice jam profile computations were found to be sensitive to abrupt changes in channel width. Bank stations from the open water model stage were adjusted along the study reach to improve model stability and to provide for a more representative ice jam width. Adjustments were made so that the modelled main channel (portion between left bank and right bank stations) was representative of an average ice jam width along the river and so that changes in the ice jam width were gradual. The main channel was constrained to a single channel alongside islands and banks stations were placed within the constrained channel except for the West Fishing Village Channel. Along this reach, the bank stations were set to the most outer banks which encompassed the islands since the active jam width commonly spanned overtop these islands. This provides a reasonable approximation as based on field observations of ice jam widths, as indicated by the presence of longitudinal shear walls. Observed shear wall lines generally follow

a smooth pattern with gradual transitions. As ice jams form alongside islands, it is common for the ice to accumulate and shove first down one side of the island and then the other. Bank stations within the open water main channel were set to allow for the transition from single channels to island splits and to ensure gradual changes in ice jam widths for model stability.

6.1.2 Cross Sections

Additional cross sections may be necessary to perform a stable ice thickness assessment. Due to the surveyed cross sections having a relatively uniform spacing and being positioned at major changes within the river morphology, it was found unnecessary to interpolate additional cross sections.

Model tests found that the presence of bridge structures introduced instabilities in the ice thickness computations. Therefore, closely spaced cross sections at bridges were removed to facilitate ice jam modelling. The removal of the bridges had negligible effect on the computed ice jam profiles because the bridge structure spans the main channel (i.e., the embankments only encroach the overbank areas) and does not impact the ice jam width used for the ice thickness computation.

6.2 Ice-Specific Model Parameters

Aside from the model refinements, ice jam specific parameters are necessary to produce a stable ice jam model. These include composite roughness, which was determined through calibration to known ice jam events. In addition, other required parameters include initial ice thickness (t), internal friction angle (ϕ), ice jam porosity (p), coefficient of lateral to longitudinal stress (k_1), and maximum under ice velocity (V_{max}).

Composite Roughness

The composite ice roughness (n_o) is a product of the bed roughness (n_b) and the under ice roughness (n_i). For this study, the bed roughness calibrated for the open water model was held constant and the adjustments were made to the under ice roughness. Hydraulic calculations by the model rely on the composite roughness which is calculated internally by the model following the Sabeneev relationship as follows:

$$n_o = \left(\frac{n_i^{3/2} + n_b^{3/2}}{2}\right)^{2/3} \quad (1)$$

where n_b and n_i are the bed and bottom of ice roughness values, respectively.

Initial Ice Thickness

A fully developed ice jam profile was prescribed between the downstream boundary and upstream boundary by specifying a wide-river ice jam condition between these boundaries. Fixed thickness values at the boundaries are required inputs to the model. For all calibration

profiles, the thickness at the upstream boundary was set to 1 m. An initial ice thickness is required by the model at every cross section in the model domain and this thickness also prescribes the minimum allowable thickness at each section. To achieve a realistic thickness profile, the user must prescribe initial values that are below the fully developed ice thickness values. An initial thickness of 0.7 m was chosen to ensure that initial values were not set to values larger than the fully developed ice thickness values; thus, ensuring the computed thickness profile was not artificially constrained by the initial thickness.

Model tests found that the computed ice jam profiles were somewhat sensitive to the downstream boundary thickness:

- Downstream ice thickness values that under-predicted the thickness at the downstream boundary would tend to steepen the profile in the lower reach resulting in over-predicted (thicker) ice thickness values and under-predicted (lower) water levels.
- Values that over predicted the ice thickness would create a local backwater effect resulting in under-predicted (thinner) ice thickness values and over-predicted (higher) water levels.

An initial assumption of 1.5 m was adopted for the toe thickness which was iterated until reasonable convergence with upstream cross sections.

Jam Stability Parameters

The jam stability parameters are required as input to the HEC RAS model to solve for the ice jam thickness profile. These include: (1) the internal friction angle of the jam; (2) the ice jam porosity; and (3) the coefficient of lateral to longitudinal stress in the jam. Ice jam strength properties can not be measured directly in the field and consequently they are not reported for observed events. Default values were selected for the jam stability parameters in this model.

Ice Jam Porosity: Ice jam porosity represents the volume fraction of the interstitial spaces in the ice accumulation. It is assumed to be the same above and below the water surface. The default value in HEC-RAS of p = 0.4 was adopted for this study.

Internal Friction and Coefficient of Lateral to Longitudinal Stress: The default parameters in HEC-RAS for the internal friction angle and stress coefficient are ϕ = 45° and k_1 = 0.33.

Flow-Split Relationships

Brayall (2011) developed a River2D model of the Hay River Delta using data from historical ice jam profiles. The hydraulic model determined a flow-split relationship between the East and West Channels under ice jam conditions and this relationship was adopted for the study. An equal flow split was assumed between the West-Fishing Village Channel and the Rudd Channel, where the flow was evenly split between the two channels. Further downstream, when the West-Fishing Village channel encounters another split, it was assumed that 40% of the flow was diverted to the Island Channel while the remaining 60% of the flow continued along the West-Fishing Village Channel.

7 ICE JAM MODEL CALIBRATION

The ice jam profiles using the above parameters were generated and calibrated to known ice jam highwater marks.

7.1 Summary of Highwater Marks

Historical highwater data resulting from ice jams in the Town of Hay River and Kátł'odeeche First Nation were available from various sources. Data was recorded along the Hay River at the following locations: Main and East Channels for 1947, 1951, 1963, 1985, 1989, and 1992, and in the West Channel for 1985, 1989, and 1992. Researchers from the University of Alberta collected ice jam profile data during breakup in 2008, 2009, 2010, 2011 and 2013. Most recently, highwater marks were collected after the flood event which occurred in 2022.

Highwater and top of ice data from the following events were used for calibration of ice jams along the Hay River:

- 2022 (Ollerhead and Associates 2022),
- 2009 (Kovachis 2011),
- 2008 (Kovachis 2011),
- 1992 (Jasek, M. et al. 1993), and
- 1985 (Underhill Engineering Ltd. 1985).

7.2 Calibration Approach

Using parameters listed above, the ice jam profiles were adjusted to match the highwater marks and top of ice data points collected during the events listed above. These data points were visually compared to one another. Calibration was achieved by modifying a reach representative under ice roughness to match the surveyed highwater marks or top of ice data at the peak flood level in the main channel area within a tolerance of 0.25 m. Data points notably exceeding this tolerance were primarily in off channel areas or not associated with the peak flood level.

7.3 Calibration Results

The ice jam profile was determined based on the calibration approach and highwater marks or top of ice data points from the events listed above. **Table 22** summarizes the setup of the breakup ice jam calibration runs. The following section provides a summary of the calibration results for the Hay River during breakup.

Table 22 Breakup Ice Jam Calibration Setup

Breakup Event	Observation Type	Number of Observations	Hay River Discharge (m^3/s)	Downstream Boundary Water Surface Elevation (m)
2022 (Assumed May 12)	Highwater Marks	65	1,460	158.18
2022 (Assumed May 8)	Highwater Marks	16	1,030	156.79
2009	Top of Ice	61	540	156.47
2008	Top of Ice	27	800	156.18
1992	Highwater Marks	34	900	156.78
1985	Highwater Marks	79	1,350	157.70

7.3.1 2022 Hay River Breakup

The 2022 breakup jam caused the greatest recorded flooding within the Town of Hay River and Kátł'odeeche First Nation. A calibration was carried out using the data collected by Ollerhead and Associates (2022). Flows on WSC gauge #07OB001 Hay River near Hay River recorded a maximum instantaneous water level on May 12, 2022, with a corresponding daily average discharge of 1,460 m^3/s. Calibration of 2022 breakup ice jam event used this daily discharge and a downstream boundary condition of 158.178 m CGVD2013a for all reaches based on highwater mark data collected by Ollerhead and Associates (2022). It was found that an under ice roughness (n_i) of 0.074 matched the highwater marks recorded for this event reasonably well along the East, West, and Rudd Channels. The resulting composite roughness coefficient (n_c) was 0.055. The ice pack upstream of Main Channel River Station 1101.2 km was assumed to come from above the falls, and a smoother under ice roughness (0.045) was adopted for the upstream reach of the Main Channel. **Figure 40** through **Figure 42** present a comparison between the computed and recorded ice jam profiles for the 2022 breakup ice jam event for the Main and East Channels, West and West-Fishing Village Channels, and West and Rudd Channels. Observations indicate that the head of jam on May 12 was just upstream of the WSC Gauge #07OB001 Hay River near Hay River (Sandeman et al. 2024), therefore, the highwater marks upstream of the gauge likely resulted from prior ice jam activity (labelled as Ice Jam B). The WSC gauge #07OB001 Hay River near Hay River recorded daily average discharge of 1,030 m^3/s on May 8, 2022 and downstream boundary condition of 156.788 m CGVD2013a for all reaches as recorded at WSC gauge #07OB002 Great Slave Lake at Hay River was used for the calibration of Ice Jam B. It was found that an under ice roughness (n_i) of 0.074 matched the highwater marks recorded for the Ice Jam B event reasonably well along the Main Channel which corresponds to a composite roughness coefficient (n_c) of 0.055.

7.3.2 2009 Hay River Breakup

The University of Alberta collected top of ice profiles on May 3, 5, and 7 of 2009 (Kovachis 2011). The top of ice data collected on May 5 was selected for calibration. The reported daily discharge on May 5 from the WSC gauge #07OB001 Hay River near Hay River was 540 m^3/s. The corresponding water level from the WSC gauge #07OB002 Great Slave Lake at Hay River reported an elevation of 156.57 m CGVD2013a. **Figure 43** through **Figure 45** present a comparison between the computed and recorded top of ice jam profiles for the 2009 breakup ice jam event on May 5 for all sub-channels. An under ice roughness of 0.074 (composite roughness of 0.055) was found for the East, West, and Rudd Channels, while an under ice roughness value of 0.045 agreed well for the Main Channel from the East-West Channel split up to the head of the jam.

7.3.3 2008 Hay River Breakup

The University of Alberta collected top of ice profiles on May 5 and May 6, with the latter date selected for calibration. The reported daily discharge on May 6 from the WSC gauge #07OB001 Hay River near Hay River was 800 m^3/s. The corresponding water level from the WSC gauge #07OB002 Great Slave Lake at Hay River reported an elevation of 156.49 m CGVD2013a. **Figure** 46 through **Figure 48** show a comparison between the computed and recorded top of ice jam profiles for the 2008 breakup ice jam event on May 6 for all sub-channels. Agreement was found with an under ice roughness of 0.074 (composite roughness of 0.055) for the East and Main Channels, 0.065 (composite roughness of 0.050) for the West-Fishing Village Channel, and 0.082 (composite roughness of 0.060) for the Rudd Channel.

7.3.4 1992 Hay River Breakup

The 1992 breakup ice jam was composed of two primary types of broken ice: ice from above the falls which is smoother, and ice below the falls which is typically rougher (Gerard and Stanley, 1988). During the 1992 breakup jam the West Channel toe advanced onto Great Slave Lake which led to smoother broken ice accumulating upstream of the split and along most of the West Channel, as deduced through photographs.

The WSC Gauge #07OB001 Hay River near Hay River recorded a maximum instantaneous water level on April 28, with a corresponding daily average discharge of 900 m^3/s. A downstream boundary condition of 157.00 m CGVD2013a was applied for all sub-channels. **Figure 49** through **Figure 51** show a comparison between the computed water surface profile and recorded highwater marks for the 1992 breakup ice jam event for all sub-channels. Resulting under ice roughness (and composite) values included: 0.090 (0.065), 0.045 (0.039), 0.082 (0.060), and 0.099 (0.070) for the East, Main, West-Fishing Village, and Rudd channels, respectively.

7.3.5 1985 Hay River Breakup

There have been noted discrepancies regarding the discharge measurement for the 1985 breakup ice jam, with discharges values ranging from 1,000 m^3/s to 1,350 m^3/s (Wedel 1988). A discharge of 1,350 m^3/s was used for calibration. A downstream boundary water surface elevation of 157.70 m CGVD2013a was applied for all sub-channels. **Figure 52** through **Figure 54** present a comparison between the computed water surface profiles and recorded highwater marks for the 1985 breakup ice jam event. Resulting under ice roughness (and composite) values included: 0.065, 0.074, and 0.099 for the East, West-Fishing Village, and Rudd channels, respectively.

7.3.6 Hay River Rating Curve Calibration

An ice jam affected rating curve was developed using the estimated maximum water levels and corresponding discharges determined for breakup at the WSC gauge #07OB001 Hay River near Hay River. Discharges associated with the rating curve ranged from 100 m^3/s to 1,800 m^3/s. Starting with an under ice roughness matching the bed roughness of 0.032, the roughness was gradually increased until it enveloped most of the available breakup water level data. It was found that an ice roughness of 0.075 enveloped most of the available data, resulting in a composite roughness of 0.055. The resulting ice jam rating curve, compared to the available ice affected breakup data and direct measurements collected by WSC are depicted on **Figure 55**.

7.3.7 Calibration Results Summary

A summary of under ice coefficients for the various reaches of the Hay River under the flood events described above is shown in **Table 23.**

Table 23 Summary of calibration results

Flood Event	Under Ice Roughness Coefficient (n_i)			
	East Channel	Main Channel	West-Fishing	Rudd
2022 (Assumed May 12)	0.074	0.074/0.045 (RS13340)	0.074	0.074
2022 (Assumed May 8)	-	0.074	-	-
2009	0.074	0.045	0.074	0.074
2008	0.074	0.074	0.065	0.082
1992	0.090	0.045	0.082	0.099
1985	0.065	-	0.074	0.082

Based on the results of the calibration runs above, an under ice roughness coefficient of 0.075 was adopted for the calibrated ice jam hydraulic model.

7.4 Sensitivity Analysis

A sensitivity analysis was completed on the calibrated ice jam model to determine the effects of changing the dominant model calibration parameter, Manning's roughness, on computed flood levels. Mannings roughness values were varied for open water, thermal ice, and ice jam conditions over the ranges listed in **Table 24**. The resulting sensitivity of the computed water levels to changes in Manning's roughness are illustrated by the calculated rating curves at the WSC gauge #07OB001 Hay River near Hay River the WSC gauge, depicted in **Figure 56**. The computed water levels vary by approximately ± 0.2 m for flood events associated with a 100-year to 200-year regulatory flood magnitude.

Table 24 Range of Manning's roughness values for sensitivity tests

Test	Manning's Roughness		
	Calibrated	Low Value	High Value
Open Water	0.032	0.027 (-0.05)	0.037 (+0.05)
Thermal Ice	0.015	0.010 (-0.05)	0.020 (+0.05)
Ice Jam	0.075	0.070 (-0.05)	0.080 (+0.05)

7.5 Ice Jam Flood Profiles

Using the results of the Monte Carlo analysis, the 100-year and 200-year ice jam flood profiles were generated. These water levels at each surveyed cross section on the Hay River are provided in **Appendix C**. Results are plotted graphically in **Figure 57** through **Figure 62**. The probabilities of dynamic breakup and ice jams if there is a dynamic breakup were determined based on the characterization of breakup type carried out for each reach (**Table 16**). Additionally, each of the assumed transition zones are shown.

8 FLOOD MAPPING

The following section outlines the steps taken to produce flood hazard maps based on the flood profiles generated through calibration of the hydraulic model and Monte Carlo analysis.

8.1 Inundation Mapping

The methodology used to create the flood inundation maps followed these steps, details of which are provided in the subsequent sections. Inundation mapping was completed in ArcGIS Pro, using the results of the hydraulic modelling calibration and Monte Carlo analysis above.

1. Create a 3D water surface elevation (WSE) triangular irregular network (TIN) that is representative of a contiguous flood level profile along modelled reaches, floodplain, and overland flow areas.
2. Create a 2D WSE grid with elevation values assigned to grid cells based on the values found in the WSE TIN (3D surface).
3. Create a 2D depth grid based on the WSE grid and underlying DTM.
4. Create inundation polygons based on the depth grid such that the polygon extents delineate positive depth areas, with polygon edges following zero depth contours.
5. Adjust the inundation polygons manually for areas where depths and hydraulic connectivity cannot be adequately resolved by the preceding steps.
6. Finalize the inundation extents, including smoothing and removal of isolated areas.

8.1.1 Mapping of Overland Areas within Hay River Delta

The WSE TIN inputs (for step 1) were derived from flood levels computed in the hydraulic model. A 1D model was used to compute flood levels along the Hay River main reaches. A decoupled 1D-2D hydrodynamic model was used to construct a water surface flood level profiles that were representative of the 100-year and 200-year ice jam regulatory flood profiles through the Hay River delta. A 1D model network was used to synthesize flood levels along the mainstem of the Hay River and the East and West channels. A 2D model configuration was used to synthesize flood levels in the overbanks of the East and West channels (including Vale Island). The 2D model provided a more realistic representation of the overbank flow pattern and corresponding water surface profile than could otherwise be represented with 1D cross sections extending from the main channel and into the overbank areas. **Figure 63** through **Figure 68** show a comparison between the 100-year ice jam design water surface elevations at each cross section and the 2D model generated profile.

8.1.2 Water Surface Elevation TIN

The TIN inputs were based on the model geometry and water levels calculated for each cross section. Additional geometry was included to define the limits of the model and mapping domain. The inputs used to create the TIN are listed below. Feature information used to inform the TIN is included in parenthesis.

- Cross section lines (isoline with constant water surface elevation along cross section line). Cross section lines were extended from each end to ensure the TIN surface covered areas of ineffective flow between cross sections (e.g. backwater areas and small tributaries).
- Perimeter feature for clipping mapping results to the mapping domain.

Additional manual editing features used to modify the TIN were as follows.

- Polygons around areas of constant water surface elevation to inform manual edits for backwater and level pools – used to model backwater into the Snye.
- Breakline features to inform TIN interpolation. For example, a bounding polygon was used for local backwater areas to ensure features used to inform the backwater elevation did not influence elevations elsewhere that were based on the flood elevation profile along the main channel.

The above inputs were then combined to create a WSE TIN with standard GIS TIN creation tools.

8.1.3 WSE and Depth Grids

The WSE grid was created directly from the WSE TIN using ArcGIS Pro tools. The WSE grid provides a raster data set with water surface elevation values at the same cell resolution and is congruent with the underlying Digital Terrain Model (DTM). The depth grid was created by subtracting the underlying DTM elevation values from the WSE grid values. WSE and depth values are based on the Canadian Geodetic Vertical Datum of 2013 (CGVD2013a; Epoch 2010.0).

8.1.4 Inundation Polygons

Inundation polygons were created through a series of steps, described as follows.

Filtered Depth Mask: The first step was to create an inundation mask of wetted areas found within the depth grids. This step is based solely on positive depth values with no filtering. Negative depth values indicate dry cells and are assigned a *NoData* value. Positive depth values denote wet cells and were assigned a value of 1. This mask was denoted as the positive depth mask. The positive depth mask was further processed and filtered to aggregate contiguous areas of wet cells and remove patchy dry areas. This also minimizes the creation of small self-intersecting loops and knots in the resulting inundation polygon. This final mask was denoted as the filtered depth mask.

Inundation Polygons: Inundation polygons are created through a series of steps, beginning with conversion of the filtered depth mask into polygons. These initial inundation polygons were further processed by: ensuring there are no multipart polygons and dissolving contiguous polygon features; removing small, isolated polygon areas; and, filling small holes inside polygons.

Inundation Areas Classification: The inundation polygons were then examined and visually classified as direct inundation areas or isolated areas of inundation (which were subsequently removed from the final inundation polygon). Areas disconnected by roads, railways, or other embankments (including non-engineered flood protection structures) were classified as direct since these areas would otherwise be directly connected. The final polygon area (isolated areas removed) was then used to mask the WSE and depth gridded datasets.

Final Inundation Extents: The final polygon areas (areas of direct inundation) were then smoothed to create the final inundation extents. Further visual checks were conducted to ensure proper nesting of flood extent limits across the range of flood frequency estimates.

8.2 Flood Hazard Mapping

8.2.1 Floodway and Flood Fringe Terminology

The following provides terminology adopted for this study pertaining to the flood hazard mapping. The descriptions below provide an additional detail to the general definitions provided in the guidelines. The floodway and flood fringe were delineated in ArcGIS Pro using the results of the inundation mapping above.

Flood Hazard Map

A flood hazard map defines the areas at risk of flooding (flood hazard area) for the specified regulatory flood and subdivides that flood hazard area into the floodway and flood fringe. Flood hazard maps may include additional flood hazard information (e.g., high hazard flood fringe) to support community planning.

Floodway

The floodway carries most of the discharge during the regulatory flood event. Under open water conditions, it is the area where the flow is deepest, fastest, and typically most destructive. For ice conditions it also includes areas exposed to moving ice – it is difficult to envision a condition under which moving ice would not be considered dangerous and destructive. Criterion based on flow velocities would rarely apply or be impractical since high velocities would most always be associated with depths greater than 1 m or a moving ice condition.

Flood Fringe

The flood fringe depicts areas of flood hazard area outside of the floodway. The flood fringe typically represents areas with shallower, slower, and less destructive flooding but it may contain areas considered to be of significant hazard. Under ice-affected conditions, the flood fringe may or may not be occupied by ice. This will depend on whether the ice thickness exceeds the water depth into specific areas of the flood fringe.

8.2.2 Regulatory Floods

The regulatory flood typically represents a severe flood with a low annual exceedance probability, such as AEP = 1% or AEP = 0.5%. Equivalent flood magnitudes, expressed as a recurrence interval, are the 100-year or 200-year regulatory floods, respectively.

As detailed in previous sections, flood profiles were created for the following scenarios:

- 100-year open water flood (AEP = 1%).
- 100-year ice jam flood (AEP = 1%).
- 200-year ice jam flood (AEP = 0.5%).

For this study, the 100-year open water, 100-year ice jam, and 200-year ice jam flood scenarios were adopted as the regulatory floods used for development of the flood hazard maps. The resulting flood profiles for these scenarios, along with the simulated 2022 inundation levels (NHC 2023b), are plotted in **Figure 69** through **Figure 71**. The calculated flood elevations for each of these scenarios are tabulated in **Appendix C**.

8.2.3 Floodway Determination

The following criteria were considered in determination of the floodway.

- **Depth and Velocity:** Areas where depths exceed 1 m or where flow velocities are greater than 1 m/s were considered to be part of the floodway. When the regulatory flood is an ice jam flood, depth become the dominant criteria.
- **Hydraulic Smoothing:** In some instances, exceptions to the depth and velocity criterion can be made to support creation of a hydraulically smooth floodway. Consideration for these adjustments are typically limited to small backwater areas or ineffective flow areas.
- **Active Channel:** The floodway must always include the main channel.
- **Previously Defined Floodway:** When a floodway is being updated (from a previously defined floodway) consideration must be given for potential need for additional criteria pertaining to the previously defined floodway. The need for, and definition of, any additional criteria should be determined with the project manager in consultation with the community.
- **Areas in the Floodway:** The floodway extends fully across the channel. Areas within the floodway extents that do not exceed the floodway determination criteria (e.g. small islands or areas not exceeding the 1 m depth or 1 m/s velocity) are included in the floodway. Exceptions may be made for larger islands with extensive dry areas or areas protected by engineered flood control structures. Determination of these areas was done with approval by the project manager and in consultation with the community.

For this study, the 1 m depth criterion governed the floodway extents for each of the 100-year open water, 100-year ice jam, and 200-year ice jam flood scenarios.

8.2.4 Flood Hazard Maps

The resulting flood hazard maps are included in **Appendix D**, **Appendix E**, and **Appendix F** for the 1% AEP (100-year) open water, 1% AEP (100-year) ice jam, and 0.5% AEP (200-year) ice jam floods, respectively. The floodway is depicted on the flood hazard mapping as a darker shade of red than the surrounding flood fringe areas which are depicted in a lighter red to pink tone.

9 CLIMATE CHANGE CONSIDERATIONS

9.1 Objective

The objective of this assessment is to present a qualitative review of foreseeable or plausible climate change impacts pertaining to ice jam flooding experienced by the Kátł'odeeche First Nation and other communities on the lower Hay River. To meet this objective, we review the technical literature on ice jam flooding most pertinent to this region, as well as the quantitative climatic projections for seasonal air temperature and streamflow made available by the Canadian government. The resulting review presents a qualitative assessment of the future evolution of ice jam flood risk under climate change and a first picture of the factors to consider towards a more quantitative assessment.

The goals of the Government of the Northwest Territories Climate Change Strategic Framework[1] are as follows:

1. Transition to a strong, healthy economy that uses less fossil fuel, thereby reducing greenhouse gas emissions by 30% below 2005 levels by 2030.
2. Improve knowledge of the climate change impacts occurring in the NWT.
3. Build resilience and adapt to a changing climate.

The context and motivation for this assessment follows, primarily, under the second goal. Further details pertaining to goal 2 are provided in **Appendix G**.

9.2 Climate Setting

The Hay River, a tributary of the Mackenzie River system, flows primarily in a Northeast direction from its confluence with the Chinchaga River in Alberta. It continues its course until it reaches

[1] https://www.gov.nt.ca/ecc/en/services/climate-change/2030-nwt-climate-change-strategic-framework

the Great Slave Lake at the Town of Hay River and Kátł'odeeche First Nation. The breakup sequence typically begins in late April or early May at Alexandra Falls and progresses northeastward within a week. The river's northward flowing and delta characteristics creates conditions favourable for the development of ice jams and associated flooding. Significant ice jam floods have occurred during spring breakup on the Hay River. The community of Hay River is often at risk of ice jam flooding over spring breakup.

With climate change, arctic regions are warming well above global average rates. If this apparent trend continues it would influence the breakup progression. The outcome of a shift in the breakup progression with respect to ice jam frequency and severity is uncertain.

The Hay River experiences most of its rainfall between May and September each year. While snowfall can occur in any month, most of the snowfall occurs from October to April. Maximum flood levels on the Hay River are dominated by freshet peaks which come between May and July while minimum flows are experienced over the winter recession.

9.3 Climate Change Information

This section provides an overview of the available data and key findings of relevant studies pertaining to climate change in a northern setting, characteristic of this study. The review emphasized information relating to river ice processes influencing breakup ice jam flooding.

9.3.1 Climate Projection Data

The most scientifically defensible method for obtaining projections of climatic variables for any specific global region utilizes computerized models of the earth's climate, known as global climate models (GCMs) or, more recently, referred to as earth system models (ESMs) – a name that reflects that they now include more detailed representations of interactions between the land surface and the atmosphere including geochemical cycles and climate feedback. Different ESMs have been developed in research institutions around the world and are continuously being improved upon with the incorporation of new findings and datasets. The results of several dozen ESMs from multiple institutions are compiled every few years and available to the public.

A new report is released every few years by the Intergovernmental Panel on Climate Change (IPCC) summarizing the ESMs' projections, as well as peer-reviewed research based on those projections and environmental monitoring. The most recent is the IPCC's Sixth Assessment report released in 2021-2023, and its various volumes are available from the government of Canada data portal online[2]. Downscaled seasonal air temperature and precipitation data were downloaded for the Hay River watershed from the Canadian government's IPPC data portal. The projection data informing this study arose from the Coupled Model Intercomparison Project

[2] https://www.ipcc.ch/

no. 6 dataset (CMIP6). Further explanation of the CMIP6 datasets and associated emission scenarios, rationale for the choice in downscaled data sets, and associated emission scenarios are detailed in **Appendix G**. The emission scenarios, referred to herein, are explanatory storylines referred to as *shared socio-economic pathways* (SSPs) that relate to different future greenhouse gas concentrations scenarios, denoted as *representative concentration pathways* (RCPs). The scenarios adopted for this study are listed on Table 25 Adopted Global Emission Scenarios (adopted from Riahi et al., 2017)**Table 25**.

Table 25 Adopted Global Emission Scenarios (adopted from Riahi et al., 2017)

Scenario	Description
Low Emissions SSP1-2.6	The world shifts gradually, but pervasively, toward a more sustainable path, emphasizing more inclusive development that respects perceived environmental boundaries. Management of the global commons slowly improves, educational and health investments accelerate the demographic transition, and the emphasis on economic growth shifts toward a broader emphasis on human well-being. Driven by an increasing commitment to achieving development goals, inequality is reduced both across and within countries. Consumption is oriented toward low material growth and lower resource and energy intensity.
Moderate Emissions SSP2-4.5	The world follows a path in which social, economic, and technological trends do not shift markedly from historical patterns. Development and income growth proceeds unevenly, with some countries making relatively good progress while others fall short of expectations. Global and national institutions work toward but make slow progress in achieving sustainable development goals. Environmental systems experience degradation, although there are some improvements and overall the intensity of resource and energy use declines. Global population growth is moderate and levels off in the second half of the century. Income inequality persists or improves only slowly and challenges to reducing vulnerability to societal and environmental changes remain.

Projections of seasonal mean temperature and precipitation corresponding to the study watershed above the project area are depicted on **Figure 72** and **Figure 73**, respectively. The data corresponds to the Lower Hay River subbasin which was found to be representative of the entirety of the watershed. Projections for other portions of the watershed were checked (though not shown) and projected trends were found to be sufficiently similar and offered no additional interpretive value (and thus, are not shown herein).

The season's mean ensemble values for each year are represented by the solid lines. Ensemble simulations for the historical period are represented in black (ensemble mean) and the grey shaded area (which ranges from the lowest to highest value of the individual ESMs). This historical period, for which the projections have been bias-corrected to approximately match

observations, ranges from 1950 to 2013. Starting in 2014, the blue and green lines indicate projections for SSP1-2.6 and SSP2-4.5, respectively. The shaded blue and green areas range from the lowest to highest value of the individual ESMs. Warming in the contemporary period (2011-2040) is similar for the two SSPs, but in future periods becomes more pronounced for SSP2-4.5 compared to the lower-emissions SSP1-2.6. Rates of warming are considerable for all seasons, and especially large for the winter season. The sharpest rate of temperature rise is seen in the contemporary period, 2011-2040. In the Lower Hay River, the projected warming is about 1.4°C in summer and 2°C in all other seasons.

Projected air temperatures of ensemble mean projections (indicated by the solid blue and green lines of (**Figure 72**) for the fall and spring seasons were found to be crossing the 0°C line into non-freezing temperatures in the contemporary period (2011-2040). For precipitation, moderate increases are projected for all seasons, for both SSPs, with SSP2-4.5 tending toward larger increases (as depicted in **Figure 73**). The combination of projected higher air temperature and higher precipitation will produce higher mean streamflow in the fall and spring. Further, a progressive thawing of the permafrost could further exacerbate the impacts on seasonal flows. Shorter winter seasons could result in thinner, weaker ice covers. The potential for winter rainfall events could lead to the occasional mid-winter breakup event.

9.3.2 Study-specific Climate Research

The foreseeable outcomes of the climate projections, implied by the data in previous section, on ice jam flood frequency and severity were explored on the basis of review of the scientific literature found to be most relevant to this topic and study area. Ice jams on the lower Hay River have been studied over time, and Burrell et al. (2015) provides a list of 16 different studies, spanning 1959 to 2012. Notable from this list are theses and peer-reviewed publications by students of Prof. Faye Hicks at University of Alberta, dating from 2011 and 2012. NHC consulted these studies for the present assessment, having found that the doctoral thesis by Zhao (2012) contains important observations-based interpretation of the hydro-climatic factors associated with ice jam flooding on the Hay River, which will be discussed in further detail in **Appendix G**. **Appendix G** also provides supplementary information on particular aspects of river ice processes. The review was documented in the context of the following processes considered important (for this study) towards understanding the impacts of climate change on ice jam frequency and severity.

- Snow accumulation and snowmelt
- Streamflow
- Ice formation and growth
- Breakup characteristics
- Channel morphology
- Lake effects

Snow accumulation and snowmelt

The climate projections indicate a shorter winter period with increased temperature and increased precipitation. The possible increase in snowfall may be prominent at the Great Slave Lake due to lake effect snow. Lake effect snow refers to the enhancement of snowfall after a cold air mass passes through open water and becomes saturated with moisture, hence dropping extra snow on nearby areas. Rühland et al. (2023) presented a recent account of the climatic changes affecting the Great Slave Lake. These suggest the following trends.

- A reduced snowpack with less snow water equivalent available for the spring melt can contribute to a decrease in spring runoff peaks.
- For a projected increase in temperature and precipitation, the rate of snowmelt, attributed to thermal processes and rain-on-snow conditions, would also increase – suggesting an increase in spring runoff peaks.
- A reduced snow thickness on established ice covers which would increase the rate of heat transfer between the solid ice cover and air. This would tend to increase the rate of thermal ice growth over periods of freezing temperatures and increase the rate of thermal decay during episodes of above zero temperatures.
- An increase in snowfall particularly in river water can lead to the formation of slush, later resulting in thicker river ice cover (Turcotte et al., 2012). A thicker and denser snowpack promotes the formation of thicker river ice due to higher albedo (Bush and Lemmen, 2019).

These projections present competing trends in both peak spring runoff rates and ice cover growth. For this desktop review, it is not apparent as to whether there is a dominant process (in either mechanism) to suggest a clear trend in either ice thickness and or spring runoff peaks.

Streamflow

As a result of warming in the fall and spring, seasonal flows throughout Hay River will experience changes in their seasonal means and seasonal peak flow frequencies. Warming of the fall season, where the average air temperature is crossing above 0°C, implies a progressive transition from snowfall to rainfall and higher mean seasonal flows and peak flows in this season. Von de Wall et al. (2010) noted a trend toward earlier arrival of the spring freshet throughout the Hay River basin.

Potential implications of permafrost warming are potentially significant to changes in streamflow. St. Jacques and Sauchyn (2009) surmised that a progressive thawing of permafrost will increase infiltration capacity and amplify the subsurface component of the hydrograph, which may augment minimum flows in winter. Permafrost thaw can also amplify surface runoff response and therefore peak flows, due to increased surface connectivity. Changes in the landscape following permafrost thaw may result in landforms with higher and more rapid rainfall runoff response through a range of mechanisms that are too broad in scope for this study (such

as a potential increase in forest fire activity arising from a shift in tree type coupled with increase in pine beetle infestations).

Climate projections on temperature and precipitation indicate an increase in both seasonal average and peak runoff rates though the ice-affected period and breakup. These changes in the streamflow hydrograph have implications on river ice which are described within the relevant processes that follow.

Ice formation and growth

Ice formation begins in the fall as freezing temperatures cool the water to just below 0°C (denoted as a *supercooled* condition) at which time the ice begins to form in the river and collect on the surface to form a cover. This cover of ice continues to grow in thickness over the winter period until it eventually decays and breaks up in the spring. A list of potential effects of climate projections relating to ice formation and growth are as follows.

- Increase in flows in late autumn and early winter can delay and prolong freeze-up resulting in thicker yet potentially less stable ice covers (Prowse et al., 2007; Burrell et al., 2023). Thicker covers advance upstream at a slower rate and a less stable cover is more prone to breakup.
- The growth of the cover over the winter season relies on persistently freezing temperatures. It is intuitive that as mean temperatures increase, initial ice formation (the fall freeze-up) is delayed, and winter ice growth diminishes.

Breakup characteristics

Climate projections indicate changes in the breakup characteristics in response to an increase in freeze-up level, an earlier onset of breakup, and an increase in peak runoff rates. The changes are described as follows. An expanded description of these deductions are provided by (Beltaos et al., 2006; Turcotte et al., 2019; and Zhao, 2012).

- A higher freeze-up level would require a higher streamflow threshold capable of initiating ice breakup which can potentially reduce the frequency of ice jams. However, when ice jams do occur, they will tend to be more severe due to the incrementally higher flows.
- An earlier onset of breakup could present comparatively weaker covers due to limited thermal thickening over a shortened winter period. This suggests an increase in the frequency of mechanical breakups and possibly an increase in the rate of the advancing breakup front. However, it is not apparent to the authors as to how this may impact ice jam severity.

Channel morphology

Climate projections indicate an increase in the rate of permafrost melt, which can result in a weakening of the banks and change in sediment supply (Ettema and Day, 2004). While these changes are expected to lead to some degree of morphological change, those changes are site-specific, and can vary along the reach. It is uncertain how these changes may affect ice jam frequency and severity (Turcotte et al., 2019).

Lake effects

The Great Slave Lake presents several effects on the frequency and severity of ice jam flooding. At a local basin scale, its thermal inertia indirectly moderates seasonal climatic changes, reducing temperature fluctuations across seasons (Huziy and Sushama, 2017). Furthermore, the lake's presence can contribute to increased snowfall during the ice-free fall season through "lake effect snow". Snowfall directly into rivers often forms slush, later resulting in thicker river ice cover (Turcotte et al., 2012). A thicker and denser snowpack promotes the formation of thicker river ice due to higher albedo (Bush and Lemmen, 2019). Direct effects near the lake include the lake levels and lake ice conditions. Higher spring lake levels generally intensify backwater effects and increase the risk flooding in surrounding areas near the Great Slave Lake. While thicker lake ice raises the threshold discharge required to facilitate breakup, it may also increase the severity and frequency of ice jam floods locally near the lake.

9.4 Trends in Historical Breakup Data

Historical data developed for this study (peak breakup discharge, and peak breakup water levels) were examined for trends. Annual time series of peak breakup levels for both Hay River and Great Slave Lake, peak breakup discharge, and associated breakup dates are depicted on **Figure 74**, **Figure 75**, **Figure 76**, and **Figure 77**, respectively. The trends found in the historical data are as follows.

- The linear fit to the historical breakup **water level** data suggests a downward trend in the Hay River breakup levels. However, the P-Value for this trend (0.4995) indicates a high probability (50%) there is no trend in the data. Therefore, it is not possible to reliably discern a trend in breakup levels from the historical data.
- The linear fit to the historical spring **water level** data indicates an upward trend in the Great Slave Lake spring levels. The low P-Value (<0.00001) indicates a low probability there is no trend in the data (<0.001%). Therefore, it is possible to reliably discern a trend in spring lake levels from the historical data.
- For historical breakup **discharge**, there is a downward trend in the historical data for Hay River (P-Value = 0.0356). The relatively low P-Value (less than 0.05) indicates a low probability the dataset had no trend.

- The linear trend fit to historical **breakup dates** (expressed in Julian days) suggests there is no significant trend to the onset of breakup. Moreover, the P-Value for this trend (0.9200) indicates a high probability (92%) there is no trend in the data. Therefore, it is not possible to discern a trend in breakup dates from the historical data.

9.5 Qualitative Assessment

The qualitative assessment considers the climate projections for both temperature and precipitation (recall **Figure 72** and **Figure 73**) and trends in the historical breakup data (recall **Figure 74**, **Figure 75**, **Figure 76**, and **Figure 77**). Inferences were made from the trend analyses to assess their impacts on ice jam flood frequency and severity. The following is based on the authors' understanding of river ice processes and is supported by the relevant research reviewed during this study. The key findings from the qualitative assessment are provided below.

- Historical breakup **water level** data for Hay River does not have a reliable trend to discern from based on the trend fit's relatively high P-Value.
- Historical breakup **lake level** data for Great Slave Lake suggests an upward trend in spring lake levels with high confidence, shown by its low P-Value (<0.00001). Higher spring lake levels may locally intensify backwater effects and increase the risk of flooding locally at surrounding areas near the lake.
- Historical breakup **discharge** data for Hay River suggests a downward trend in discharge with relatively high confidence shown by its low P-Value (0.0356). Lower breakup discharges can reduce the severity and frequency of ice jam flooding.
- Historical **breakup dates** for Hay River suggests no significant trend in the timing of breakup.
- **Temperature** projections indicate a warming in the fall season with mean air temperatures reaching 0° C in the contemporary period (2011-2040) for both SSPs.
- **Precipitation** projections indicate "small" to "moderate" increases in mean precipitation in the fall and winter seasons in the contemporary period (2011-2040) and mid-century period (2041-2070), respectively for both SSPs.
- The **combined** effects of these temperature and precipitation projections lead to the following.
    - An increase in mean streamflow over freeze-up, and a prolonged freeze-up period. This can contribute to thicker, more competent ice covers on average or at usual lodging points.
    - An increase in peak flows over breakup causing an increase in the frequency of mechanical breakups and more severe ice jams.

- A reduction in thermal ice growth leading to the development of less competent ice covers over the winter period. This is attributed to warmer temperatures, insulating effects of increased snow cover, and a shorter ice growth period.
- An increase in freeze-thaw cycles over winter which could lead to the creation of mid-winter breakup jams or secondary consolidation of existing freeze-up ice jams.
- A progressive thawing of the permafrost.

9.6 Uncertainty

This qualitative assessment provides an overview of the potential trends in ice jam severity and frequency for the Lower Hay River near the delta where the Town of Hay River resides. The potential trends and salient findings of the assessment suggests a changing climate that will influence the frequency and severity of ice jam flooding, the degree to which is uncertain. The main sources of uncertainty are unknown future emissions of greenhouse gases; limitations of current scientific knowledge and the formulation of the earth system models used. As detailed in **Appendix G**, climate projections for temperature and precipitation are uncertain, particularly for precipitation. Further, the projected impacts of these projections on ice jam severity and frequency should not be considered to persist indefinitely. Somewhat implicit in the assumptions by the authors under this assessment is that the current physiography, hydrography, and to some extent, ice regime, also represent a future condition associated with the climate projections. This may be reasonable for the nearer contemporary period (2011-2040) however, it may become less likely as we progress towards the end of the mid-century period (2041-2070). In addition, the potential effects of Great Slave Lake on the regional climate may not be well represented by the CMIP6 earth system models – lake effects could moderate climatic changes (Huziy an Sushama, 2017).

9.7 Summary

The results of this assessment do not indicate a definitive trend in both the severity and frequency of ice jam flooding arising from trends in the historical observations and projected climate scenarios. It is difficult to discern which responses to climate change are dominant; however, most tend to point towards an increase in ice jam frequency. Additional analysis supported with a more comprehensive review of the findings of other researchers would be required to determine the dominant responses and attempt to quantify the incremental change in ice jam flood frequency and severity.

Nevertheless, the trends found in this qualitative study indicate that an increase in both magnitude and severity of ice jam floods are plausible, if not likely. As such, it is prudent to anticipate more frequent ice jam flooding in the future. The trends identified herein are indicative of the contemporary and future terms (2011-2070) and are not considered applicable

beyond the future period (approaching 2070 and later), that is, the frequency and severity of ice jam flooding are not forever increasing.

10 REFERENCES

Beltaos, S. 1995a. Breakup forecasting. Proceedings of the 8th Workshop on River Ice Winter Environments of Regulated River, Kamloops, British Columbia, 463-482. .

Beltaos, S. 1995b. River ice jams. Highlands Ranch, Colorado, USA.

Beltaos, S. 2002. Effects of climate on mid winter ice jams. Hydrological Processes. 16(4), 789–804.

Beltaos, S. 2003. Threshold between mechanical and thermal breakup of river ice cover. Cold Regions Science and Technology, 37(1), 1–13. doi:10.1016/S0165-232X(03)00010-7.

Beltaos, S. 2007. Hydro-climatic impacts on the ice cover of the lower Peace River. Hydrological Processes, 22(17), 3252–3263.

Beltaos, S. 2021. Assessing the Frequency of Floods in Ice-Covered Rivers under a Changing Climate: Review of Methodology. Geosciences. 2021(11)514-33, https://doi.org/10.3390/geosciences11120514

Beltaos, S., and Bonsal, B. 2021. Climate change impacts on Peace River ice thickness and implications to ice-jam flooding of Peace-Athabasca Delta, Canada. Cold Regions Science and Technology, 186, 103279. doi:10.1016/j.coldregions.2021.103279.

Beltaos, S., and Burrel, B. 2002. Climatic change and river ice breakup. Canadian Journal of Civil Engineering, 30(1).

Beltaos, S., Carter, T., and Rowsell, R. 2012. Measurements and analysis of ice breakup and jamming characteristics in the Mackenzie Delta, Canada. Cold Regions Science and Technology, 82, 110–123. doi:http://dx.doi.org/10.1016/j.coldregions.2012.05.013.

Beltaos, S., and Prowse, T. 2009. River-ice hydrology in a shrinking cryosphere. Hydrological Processes, 23(1), 122–144. doi:10.1002/hyp.7165.

Beltaos, S., Prowse, T., Bonsal, B., MacKay, R., Romolo, L., Pietroniro, A., and Toth, B. 2006. Climatic effects on ice-jam flooding of the Peace-Athabasca Delta. Hydrological Processes, 20(19), 4031–4050. doi:10.1002/hyp.6418.

Blackburn, J and She, Yuntong. 2023. The Simulation of Ice Jam Profiles in Multi-channel Systems using a One-Dimensional Network Model, Cold Regions Science and Technology, 208(4):103796.

Brayall, M. and Hicks, F. 2009. 2-D Modelling of Ice Processes on the Hay River NWT. CGU HS Committee on River Ice Processes and the Environment.

Brayall, M. 2011. 2-D Hydraulic and Ice Process Modeling at Hay River, NWT, Canada. M.Sc. Thesis. Water Resources Engineering, Department of Civil Engineering, University of Alberta, Edmonton.

Brown, L. C., and Duguay, C. R. 2010. The response and role of ice cover in lake-climate interactions. Progress in Physical Geography: Earth and Environment, 34(5), 671–704. doi:10.1177/0309133310375653.

Brunner, G.W. 2016. HEC-RAS, River Analysis System Hydraulic Reference Manual, US Army Corps of Engineers, Hydrologic Engineering Center Report CPD-69, February 2016, 547 pp.

Burn, D. H., Abdul Aziz, O. I., and Pietroniro, A. 2004. A Comparison of Trends in Hydrological Variables for Two Watersheds in the Mackenzie River Basin. Canadian Water Resources Journal.

Burrell, B. C., Beltaos, S., and Turcotte, B. 2023. Effects of climate change on river-ice processes and ice jams. International Journal of River Basin Management, 21(3), 421–441. doi:10.1080/15715124.2021.2007936.

Burrell, B. C., Hokuna, M., Beltaos, S., Kovachis, N., Turcotte, B., and Jasek, M. 2015. Flood Hazard and Risk Delineation of Ice-Related Floods: Present Status and Outlook. CGU HS Committee on River Ice Processes and the Environment 18th Workshop on the Hydraulics of Ice Covered Rivers, Quebec City, QC, Canada.

Bush, E., and Lemmen, D. S. 2019. Canada's Changing Climate Report, Government of Canada, ON, 444p.

Chen, D. et al. 2021. Framing, context, and methods. Chapter 1. In Climate Change 2021: The Physical Science Basis, 147–286 (Cambridge University Press, 2021). [online] Available from: https://www.ipcc.ch/report/ar6/wg1/downloads/report/IPCC_AR6_WGI_Chapter01.pdf.

Coles, A. 2020a. Flood Maps of the Northwest Territories: Background Paper on the History of the Existing (c. 1980s) FDRP Flood Maps. Draft Report.

Coles, A. 2020b. NWT Flood Events. Draft Report.

Connon, R. F., Quinton, W. L., Craig, J. R., and Hayashi, M. 2014. Changing hydrologic connectivity due to permafrost thaw in the lower Liard River valley, NWT, Canada. Hydrol.

Processes, 28: 4163–4178. doi: 10.1002/hyp.10206. Hydrological Processes, 28, 4163–4178. doi:10.1002/hyp.10206.

Das, A., and Lindenschmidt, K.-E. 2021. Modelling climatic impacts on ice-jam floods: a review of current models, modelling capabilities, challenges, and future prospects. Environmental Reviews, 29(3), 378–390. doi:10.1139/er-2020-0108.

Das, A., Rokaya, P., and Lindenschmidt, K.-E. 2020. Ice-jam flood risk assessment and hazard mapping under future climate. Water Resources Planning and Management, 146.

Dessai, S., and Hulme, M. 2004. Does climate adaptation policy need probabilities? Climate Policy, 4(2), 107–128.

De Coste, M. 2017. Modelling Flood Levels Associated with Ice Consolidation Events Triggered by Upstream Ice Jam Release Waves in the Hay River Delta, NWT. M.Sc. Thesis. Water Resources Engineering, Department of Civil Engineering, University of Alberta, Edmonton.

Dibike, Y., Prowse, T., Saloranta, T., and Ahmed, R. 2011. Response of Northern Hemisphere lake-ice cover and lake-water thermal structure patterns to a changing climate. Hydrological Processes, 25(19), 2942–2953. doi:10.1002/hyp.8068.

Environment and Climate Change Canada (ECCC). 2023. Environment Canada Data Explorer. [Online resource: https://www.canada.ca/en/environment-climate-change/services/water-overview/quantity/monitoring/survey/data-products-services/explorer.html]

Environment Canada. 1983. Hay River Flood Risk Study. For Canada-Northwest Territories Flood Damage Reduction Program.

Ettema, R., and Daly, S. F. 2004. Sediment Transport Under Ice. Hanover, N.H. 63 pp.

Flato, G.M. and Gerard, R.. 1986. Calculation of Ice Jam Thickness Profiles. Proceedings of the 4th Workshop on the Hydraulics of Ice Covered River.

Gerard R. and Karpuk E. 1979. Probability analysis of historical flood data. The Journal of Hydraulics Division, 105 (9), pp. 1153-1165, ASCE, 1979.

Gerard, R. and Stanley, S. 1988. Ice Jams and Flood Forecasting, Hay River, NWT – Phase 1: Final Report. Report for Environment Canada, Inland Waters Directorate, NWT Programs and Indian and Northern Affairs Canada, Water Resources Division. Yellowknife NWT. [Online resource: https://publications.gc.ca/site/archivee-

archived.html?url=https://publications.gc.ca/collections/collection_2021/eccc/En36-535-88-6-eng.pdf]

Gidden, M. J. et al. 2019. Global emissions pathways under different socioeconomic scenarios for use in CMIP6: a dataset of harmonized emissions trajectories through the end of the century. Geosci. Model Dev., 12, 1443–1475.

Gillett, N. P. 2024. Halving of the uncertainty in projected warming over the past decade. npj Climate and Atmospheric Science, 7(1), 1–3. doi:10.1038/s41612-024-00693-3.

Government of Northwest Territories (GNWT). 2024. Northwest Territories Hazard Identification Risk Assessment. [Online resource: https://www.maca.gov.nt.ca/en/services/hazard-identification-risk-assessment]

Government of Northwest Territories (GNWT). 2023. Administration of the Territorial Lands Act System (ATLAS). [Online resource: https://www.maps.geomatics.gov.nt.ca/HTML5Viewer/index.html?viewer=ATLAS]

Guo, X., Stoesser, T., Zhang, C., Fu, C., and Nian, T. 2022. Effect of opening and wall boundaries on CFD modeling for submarine landslide-ambient water-pipeline interaction. Applied Ocean Research, 126. doi:10.1016/j.apor.2022.103266.

Healy, D. and Kovachis, N. (2023). Case Studies on Ice Jam Flood Frequency Estimation. Conference: 22nd Workshop on the Hydraulics of Ice Covered Rivers, Canmore, Alberta.

Huard, D., Fyke, J., Capellán-Pérez, I., Matthews, H. D., and Partanen, A.-I. 2022. Estimating the likelihood of GHG concentration scenarios from probabilistic integrated assessment model simulations. Earth's Future, 10. doi:10.1029/2022EF002715. [online] Available from: https://doi.org/10.1029/2022EF002715.

Huziy, O., and Sushama, L. 2017. Lake–river and lake–atmosphere interactions in a changing climate over Northeast Canada. Climate Dynamics, 48(9–10), 3227–3246. doi:10.1007/s00382-016-3260-y.

Inland Waters Directorate (IWD) Western and Northern Region, Environment Canada. 1983. Hay River Flood Risk Study for Canada-Northwest Territories Flood Damage Reduction Program.

Jasek, M. 1993. Hay River Flood Control, Hay River, NWT. Report for the Town of Hay River, NWT.

Jasek, M., Stanley, S., and Gerard, R. 1993. Update of Ice Jam Flood Database, Hay River, NWT. Report for Indian and Northern Affairs Canada, Yellowknife, NWT.

Jasper, J.N. 1983. Hay River Historical Flood Review. Water Resources Division, Indian and Northern Affairs Canada. Draft Report for the Northwest Territories Technical Committee,

Flood Damage Reduction Program. Yellowknife, August 1983. With revisions and edits made in August 1988.

Jumikis, A. R. 1977. Thermal Geotechnics.

J.H. Wedel Water Planning and Management (Wedel). 1988. 1985 Hay River Flood Report NWT. Report for Environment Canada, NWT Programs, Inland Waters Directorate Conservation and Protection, Yellowknife NWT.

Kovachis, N., 2011. Patterns of River Breakup Timing and Sequencing, Hay River, NWT. M.Sc. Thesis. Water Resources Engineering, Department of Civil Engineering, University of Alberta, Edmonton.

Kwong, J., and Gan, Y. T. 1994. Northward Migration of Permafrost Along the Mackenzie Highway and Climatic Warming. Climatic Change, 26(4), 399–419.

Lee Maher Engineering Associates Ltd. 1992. Flood Mitigation Hay River, NWT. Report for the Government of Northwest Territories, Department of Municipal and Community Affairs.

Meliefste, C. and Hicks, F. 2005. Bathymetric Survey of the Hay River Delta, 2005. River Ice Engineering Report RIE:06-01, Department of Civil and Environmental Engineering, University of Alberta, Edmonton, Alberta, Canada, pp.29

Michel, B. 1971. Winter Regime of Rivers and Lakes. Hanover, NH, USA.

Nafziger, J. 2018. Unsteady Ice Processes in Complex River Systems. Ph.D. Thesis. Water Resources Engineering, Department of Civil Engineering, University of Alberta, Edmonton.

Nakićenović, N. et al. (2000). Special Report on Emissions Scenarios. Cambridge University Press. [online] Available from: https://www.ipcc.ch/site/assets/uploads/2018/03/sres-en.pdf.

Natural Resources Canada (NRCan). 2023. Federal Hydrologic and Hydraulic Procedures for Flood Hazard Delineation. Version 2.0. [Online resource: https://ostrnrcan-dostrncan.canada.ca/handle/1845/267304]

Northwest Hydraulic Consultants Ltd. (NHC). 2023a. Northwest Territories Ice Jam Flood Mapping Guidelines. Report prepared for Natural Resources Canada and Government of Northwest Territories.

Northwest Hydraulic Consultants Ltd. (NHC). 2023b. Northwest Territories Ice Jam Flood Mapping Case Studies. Report prepared for Natural Resources Canada and Government of Northwest Territories.

Ollerhead and Associates Ltd. 2022. Spring 2022 Flood Level Mapping in the communities of Hay River and Kátł'odeeche First Nation, NWT. Report for the Government of Northwest Territories.

O'Neil, H. C. L., Prowse, T. D., Bonsal, B. R., and Dibike, Y. B. 2017. Spatial and temporal characteristics in streamflow-related hydroclimatic variables over western Canada. Part 2: future projections. Hydrology Research, 48(4), 932–944. doi:10.2166/nh.2016.045.

O'Neill, B. C., Kriegler, E., Riahi, K., Ebi, K. L., Hallegatte, S., Carter, T. R., Mathur, R., and van Vuuren, D. P. 2014. A new scenario framework for climate change research: the concept of shared socioeconomic pathways. Climatic Change, 122(3), 387–400. doi:10.1007/s10584-013-0905-2.

Park, H., Yoshikawa, Y., Oshima, K., Kim, Y., Ngo-Duc, T., Kimball, J. S., and Yang, D. 2016. Quantification of warming climate-induced changes in terrestrial Arctic River ice thickness and phenology. Journal of Climate, 29(5), 1733–1754.

Prowse, T. D., Bonsal, B. R., Duguay, C. R., and Lacroix, M. P. 2007. River-ice break-up/freeze-up: a review of climatic drivers, historical trends and future predictions. Annals of Glaciology, 46, 443–451. doi:10.3189/172756407782871431.

Public Safety Canada. 2023. Canadian Disaster Database. [Online resource: https://cdd.publicsafety.gc.ca/srchpg-eng.aspx]

Riahi, K., van Vuuren, D. P., Kriegler, E., Edmonds, J., O'Neill, B. C., Fujimori, S., Bauer, N., Calvin, K., Dellink, R., Fricko, O., Lutz, W., Popp, A., Cuaresma, J. C., Kc, S., Leimbach, M., Jiang, L., Kram, T., Rao, S., Emmerling, J., Ebi, K., Hasegawa, T., Havlik, P., Humpenöder, F., Da Silva, L. A., Smith, S., Stehfest, E., Bosetti, V., Eom, J., Gernaat, D., Masui, T., Rogelj, J., Strefler, J., Drouet, L., Krey, V., Luderer, G., Harmsen, M., Takahashi, K., Baumstark, L., Doelman, J. C., Kainuma, M., Klimont, Z., Marangoni, G., Lotze-Campen, H., Obersteiner, M., Tabeau, A., and Tavoni, M. (2017). The Shared Socioeconomic Pathways and their energy, land use, and greenhouse gas emissions implications: An overview. Global Environmental Change, 42, 153–168. doi:10.1016/j.gloenvcha.2016.05.009.

Rokaya, P., Lindenschmidt, K.-E., Pietroniro, A., and Clark, M. 2022. Modelling of ice jam floods under past and future climates: A review. Journal of Hydrology X, 15(1). doi:https://doi.org/10.1016/j.hydroa.2022.100120.

Rühland, K. M., Evans, M., and Smol, J. P. 2023. Arctic warming drives striking twenty-first century ecosystem shifts in Great Slave Lake (Subarctic Canada), North America's deepest lake. Proceedings of the Royal Society B: Biological Sciences, 290(2007), 20231252. doi:10.1098/rspb.2023.1252.

Sandeman, A., Nafziger, J., Connon, R., Coles, A., and Kokelj, S. 2024. The 2022 Spring Breakup and Extreme Flooding Event on the Hay River, Canada: A description of event

progression. Proceedings of the 27th IAHR International Symposium on Ice, Gdańsk, Poland. [Online resource: https://www.iahr.org/library/infor?pid=30419]

Shiogama, H., Fujimori, S., Hasegawa, T., Hayashi, M., Hirabayashi, Y., Ogura, T., Iizumi, T., Takahashi, K., and Takemura, T. 2023. Important distinctiveness of SSP3–7.0 for use in impact assessments. Nature Climate Change, 13. doi:10.1038/s41558-023-01883-2.

Stanley, Grimble, Roblin Ltd. 1959. Civil Engineering Report on Flooding of Hay River Townsite, NWT. Report for Department of Northern Affairs and National Resources, Northern Administration Branch, Engineering Division.

Stanley, Grimble, Roblin Ltd. 1963. Engineering Report on Flood Protection at Hay River, NWT. Report for Department of Public Works Canada.

Stanley, S. 1988. Ice Jam Analysis of a Complex Reach: A Case Study. M.Sc. Thesis. Department of Civil Engineering, University of Alberta, Edmonton.

Stedinger, J.R., Vogel, R.M., and Foufoula-Georgious, E. (1993). "Frequency analysis of extreme events", chapter 18 of Handbook of Hydrology(ED. Maidment, D. R.), 18.1-18.66, McGraw-Hill, New York.

Stefan, J. 1891. Über die Theorie der Eisbildung, insbesondere über die Eisbildung im Polarmeere. Annalen der Physik und Chemie, 42, 269–286.

St. Jacques, J., and Sauchyn, D. J. 2009. Increasing winter baseflow and mean annual streamflow from possible permafrost thawing in the Northwest Territories, Canada. Geophysical Research Letters, 36(1), 2008GL035822. doi:10.1029/2008GL035822.

Turcotte, B., Burrell, B., and Beltaos, S. 2019. The Impact of Climate Change on Breakup Ice Jams in Canada: State of knowledge and research approaches. Conference: 20th Workshop on the Hydraulics of Ice Covered Rivers.

Turcotte, B., Morse, B., and Anctil, F. 2012. Impacts of precipitation on the cryologic regime of stream channels. Hydrological Processes, 26(17), 2653–2662. doi:10.1002/hyp.9438.

Turcotte, B., Morse, B., Bergeron, N. E., and Roy, A. G. 2011. Sediment transport in ice-affected rivers. Journal of Hydrology, 409(1–2), 561–577. doi:10.1016/j.jhydrol.2011.08.009.

Underhill Engineering Ltd. 1985. Flood Levels 1985 Hay River, NWT. Report for Water Resources Division Department of Indian and Northern Affairs, Northern Affairs Program.

Underwood MacLellan and Associates (UMA). 1978. Flood risk mapping for Hay River Northwest Territories. Report to the Inland Water Directorate, Environment Canada.

USGS. 2018. Guidelines for Determining Flood Flow Frequency – Bulletin 17C, U.S. Geological Survey, Reston, Virginia.

Venmans, F., and Carr, B. 2024. Literature-informed likelihoods of future emissions and temperatures. Climate Risk Management, 44, 100605. doi:10.1016/j.crm.2024.100605.

Von de Wall, S. J., de Rham, L. P., and Prowse, T. D. 2010. The river ice break-up season in Canada: Variations in water levels and timing. Hancock, MA, pp. 11.

van Vuuren, D. P., Edmonds, J., Kainuma, M., Riahi, K., Thomson, A., Hibbard, K., Hurtt, G. C., Kram, T., Krey, V., Lamarque, J.-F., Masui, T., Meinshausen, M., Nakicenovic, N., Smith, S. J., and Rose, S. K. 2011. The representative concentration pathways: an overview. Climatic Change, 109(1–2), 5–31. doi:10.1007/s10584-011-0148-z.

Warden, J. W., Rezvani, R., Najafi, M. R., and Shrestha, R. R. 2024. Projections of rain-on-snow events in a sub-arctic river basin under 1.5°C–4°C global warming. Hydrological Processes, 38(8), e15250. doi:10.1002/hyp.15250.

Zhao, L. 2012. River ice breakup forecasting using artificial neural networks and fuzzy logic systems (Doctor of Philosophy Thesis thesis). University of Alberta.

FIGURES

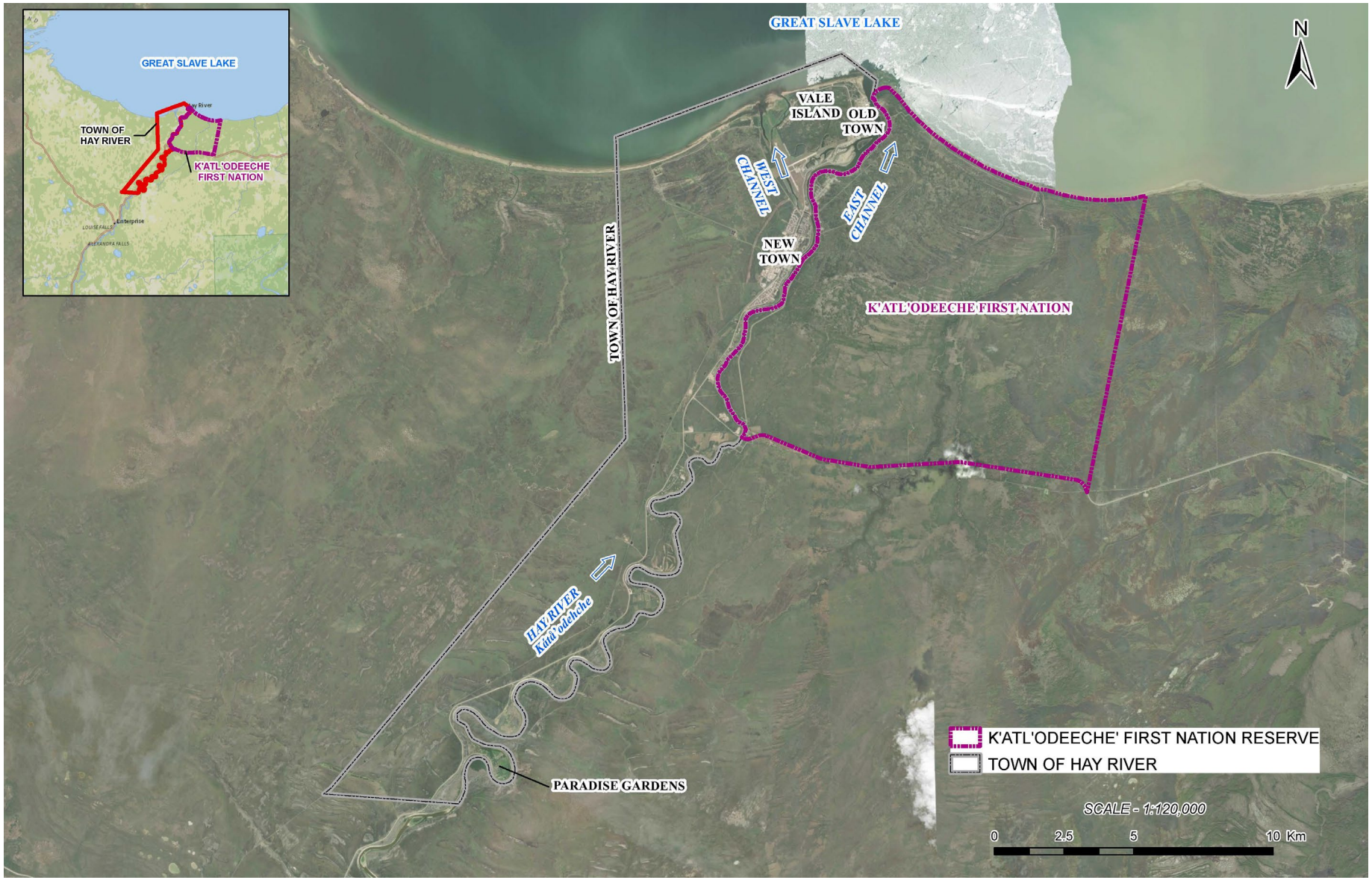

Government of Northwest Territories / Gouvernement des Territoires du Nord-Ouest; Canada; nhc	SCALE – AS SHOWN	KÁTŁ'ODEH (HAY RIVER) FLOOD HAZARD MAPPING STUDY ***HAY RIVER STUDY AREA***
	Job: 1008469	*Date: Feb-2025*
		FIGURE 1

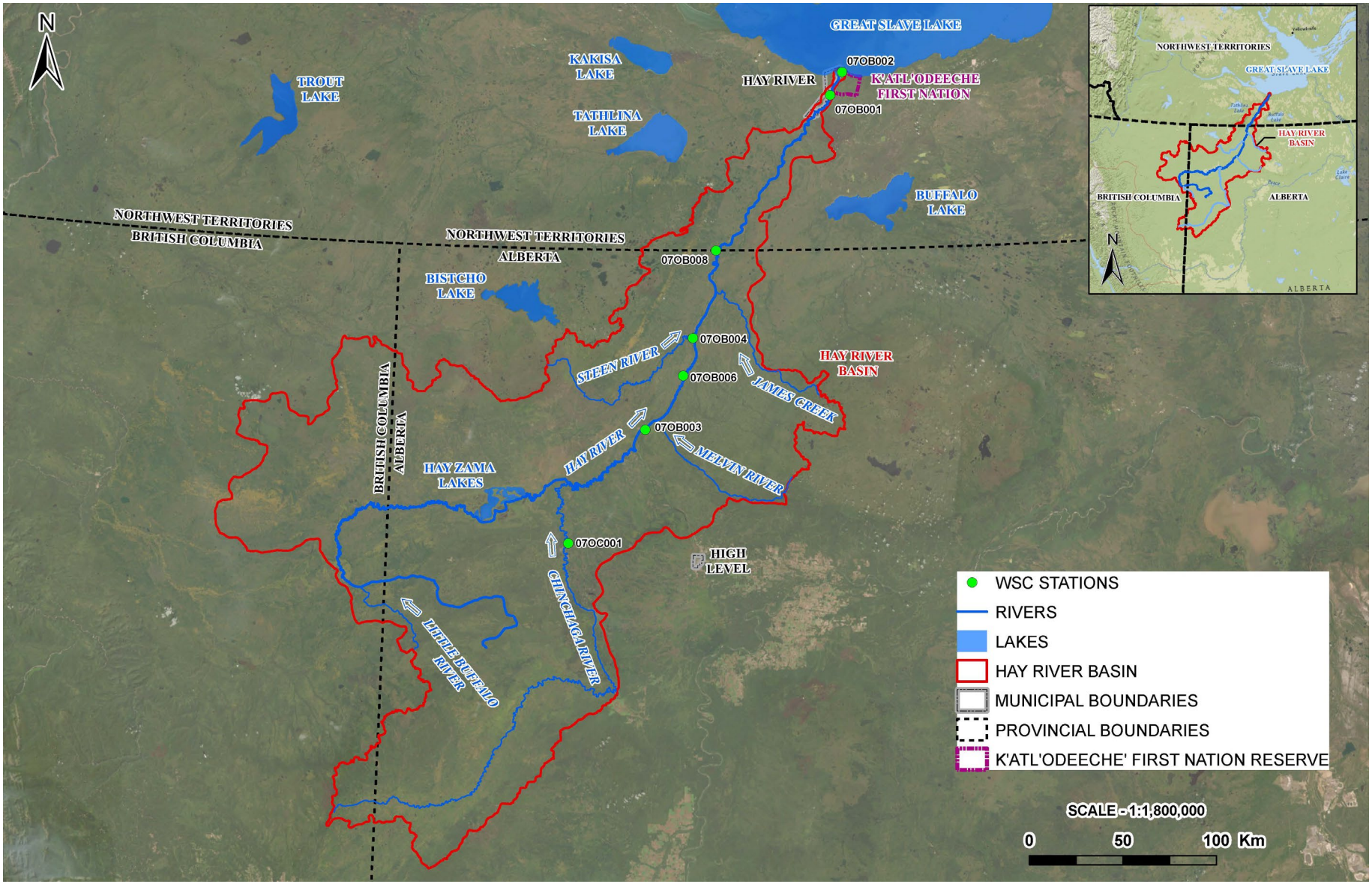

Government of Northwest Territories
Gouvernement des Territoires du Nord-Ouest

Canada

nhc

SCALE – AS SHOWN

KÁTŁ'ODEH (HAY RIVER)
FLOOD HAZARD MAPPING STUDY

HAY RIVER BASIN OVERVIEW

Job: 1008469

Date: Feb-2025

FIGURE 2

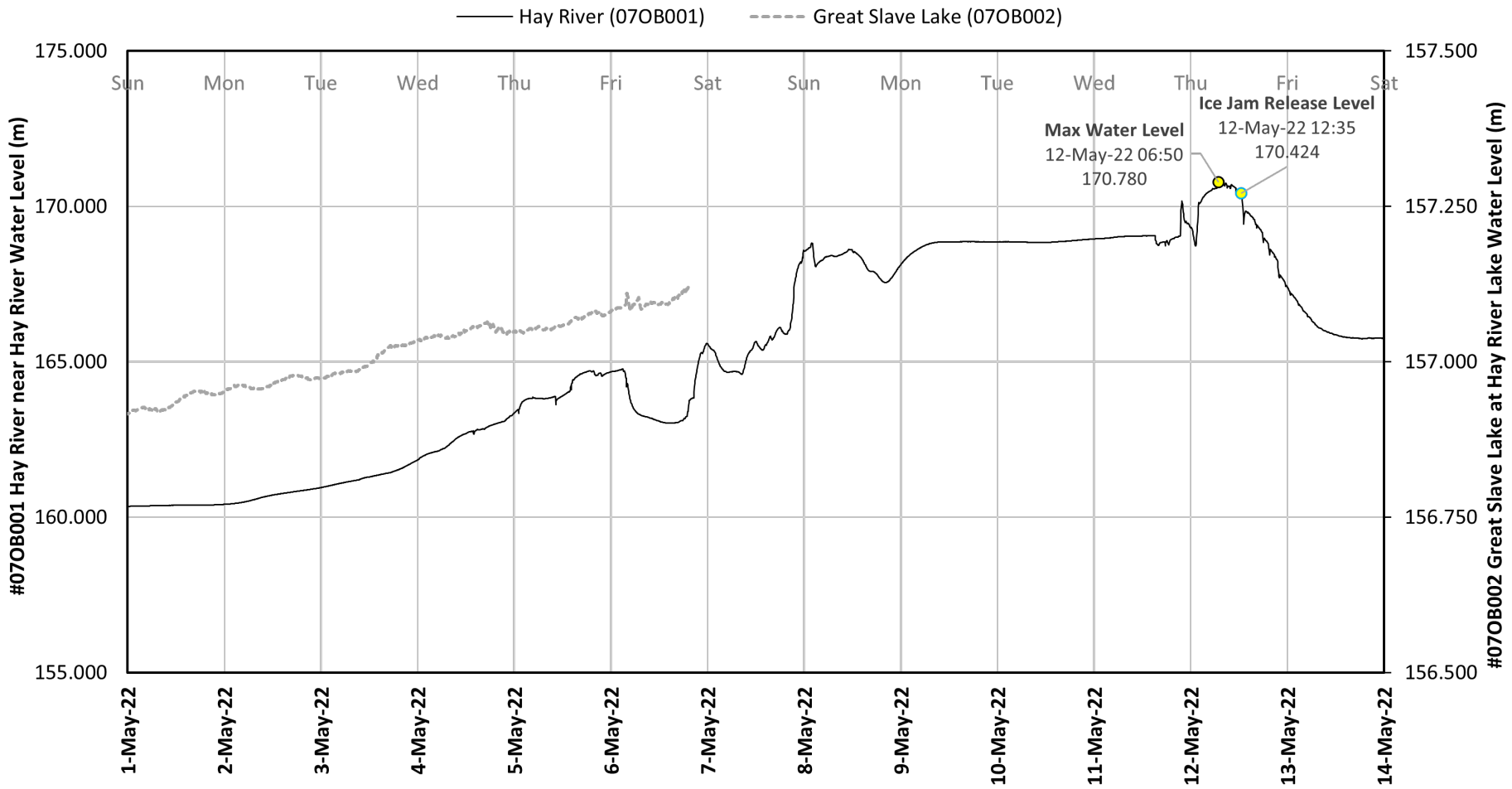

Government of Northwest Territories
Gouvernement des Territoires du Nord-Ouest

Canada

nhc

UNITS – AS SHOWN

VERTICAL ELEVATION DATUM: CGVD2013a

Job: 1008469

Date: Feb-2025

KÁTŁ'ODEH (HAY RIVER)
FLOOD HAZARD MAPPING STUDY

2022 BREAKUP LEVELS: #07OB001 HAY RIVER NEAR HAY RIVER AND #07OB002 GREAT SLAVE LAKE AT HAY RIVER

FIGURE 3

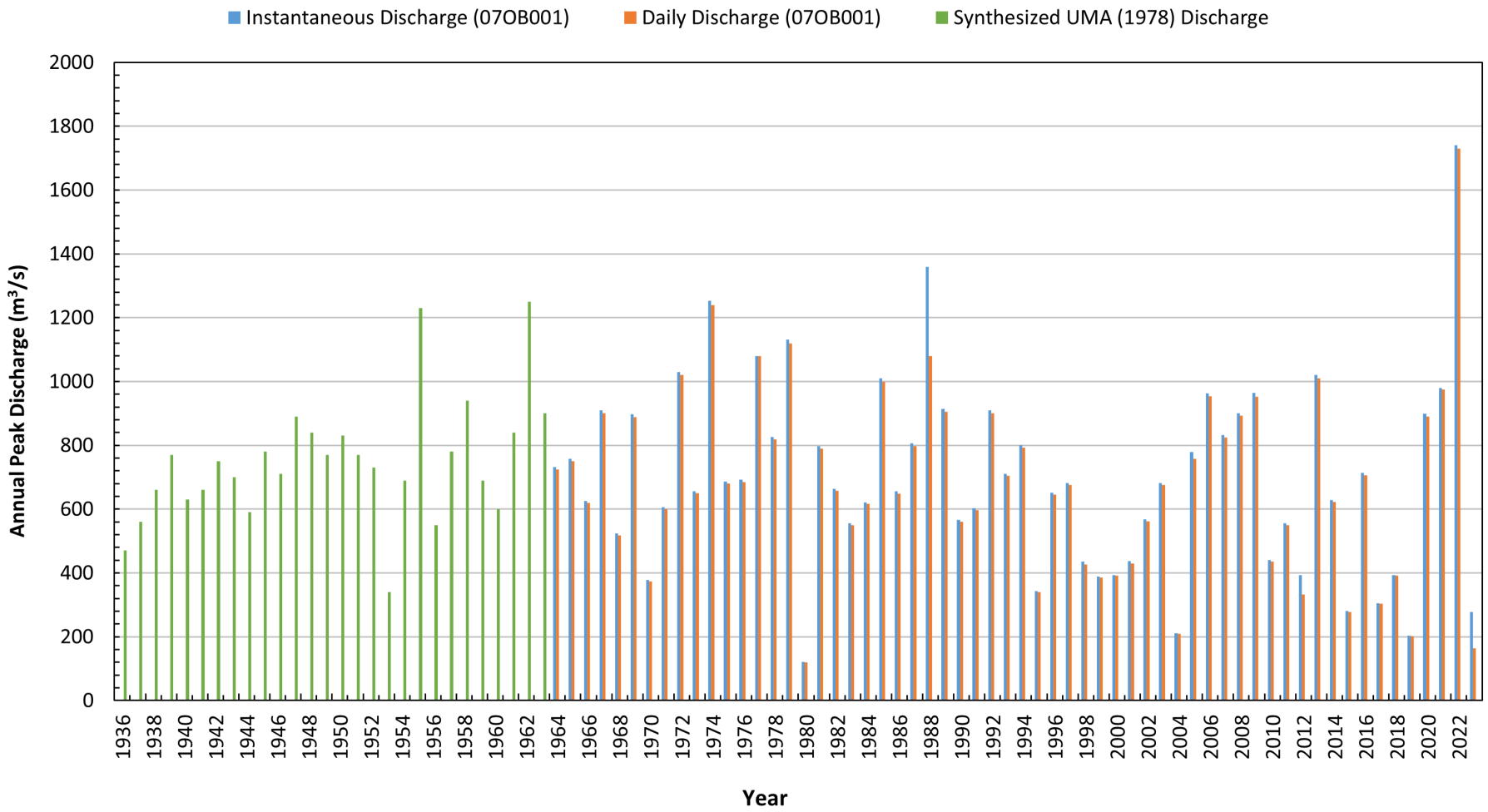

Government of Northwest Territories / Gouvernement des Territoires du Nord-Ouest

Canada

nhc

UNITS – AS SHOWN

Job: 1008469

Date: Feb-2025

KÁTŁ'ODEH (HAY RIVER)
FLOOD HAZARD MAPPING STUDY

ANNUAL PEAK DISCHARGES FOR #07OB001 HAY RIVER NEAR HAY RIVER INCLUDING THE SYNTHESIZED UMA (1978) DATA SERIES

FIGURE 4

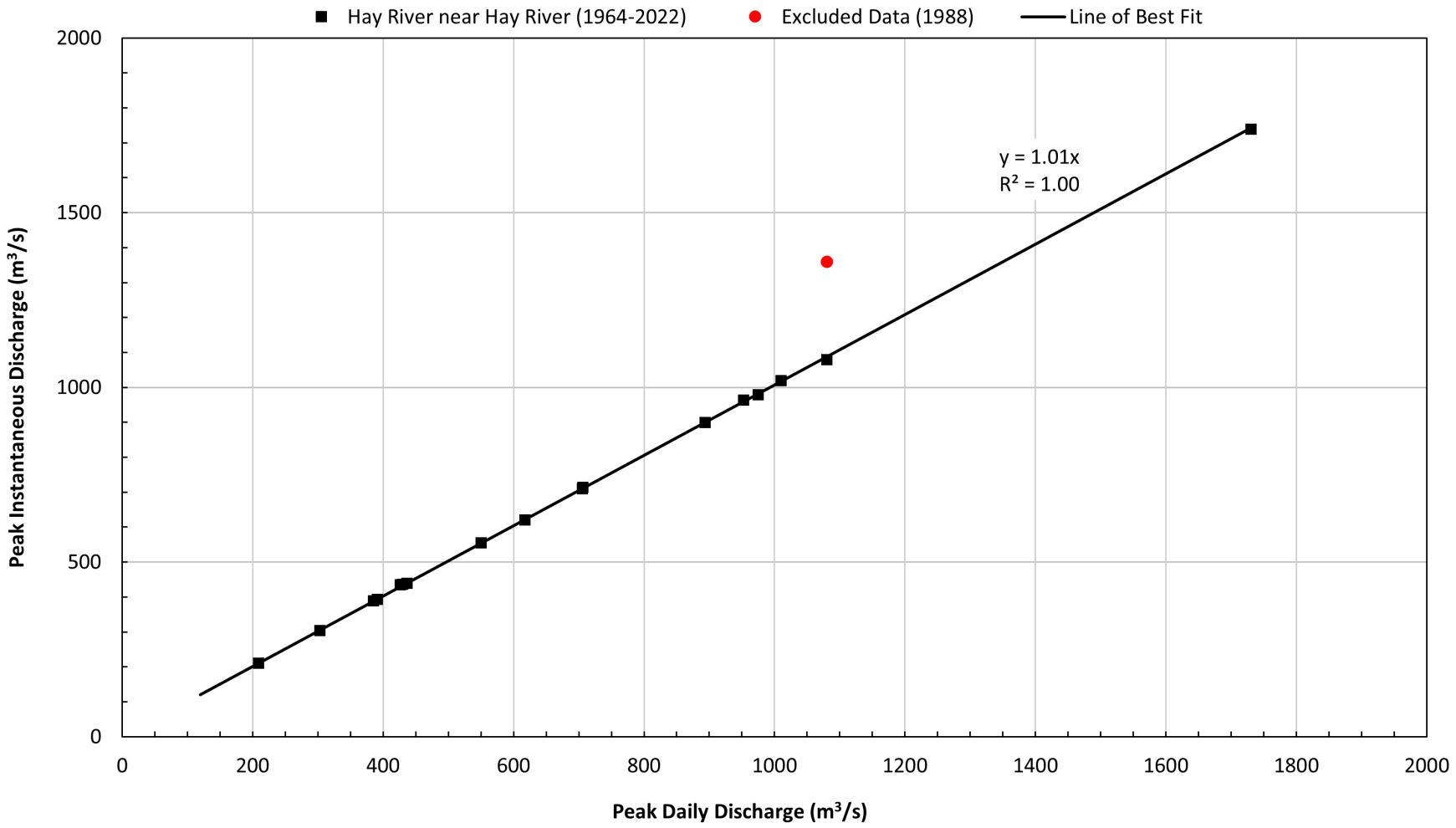

Government of Northwest Territories / Gouvernement des Territoires du Nord-Ouest

Canada

nhc

UNITS – AS SHOWN

Job: 1008469

Date: Feb-2025

KÁTŁ'ODEH (HAY RIVER)
FLOOD HAZARD MAPPING STUDY

CORRELATION BETWEEN ANNUAL MAXIMUM DAILY AND PEAK INSTANTANEOUS DISCHARGES AT #07OB001 HAY RIVER NEAR HAY RIVER

FIGURE 5

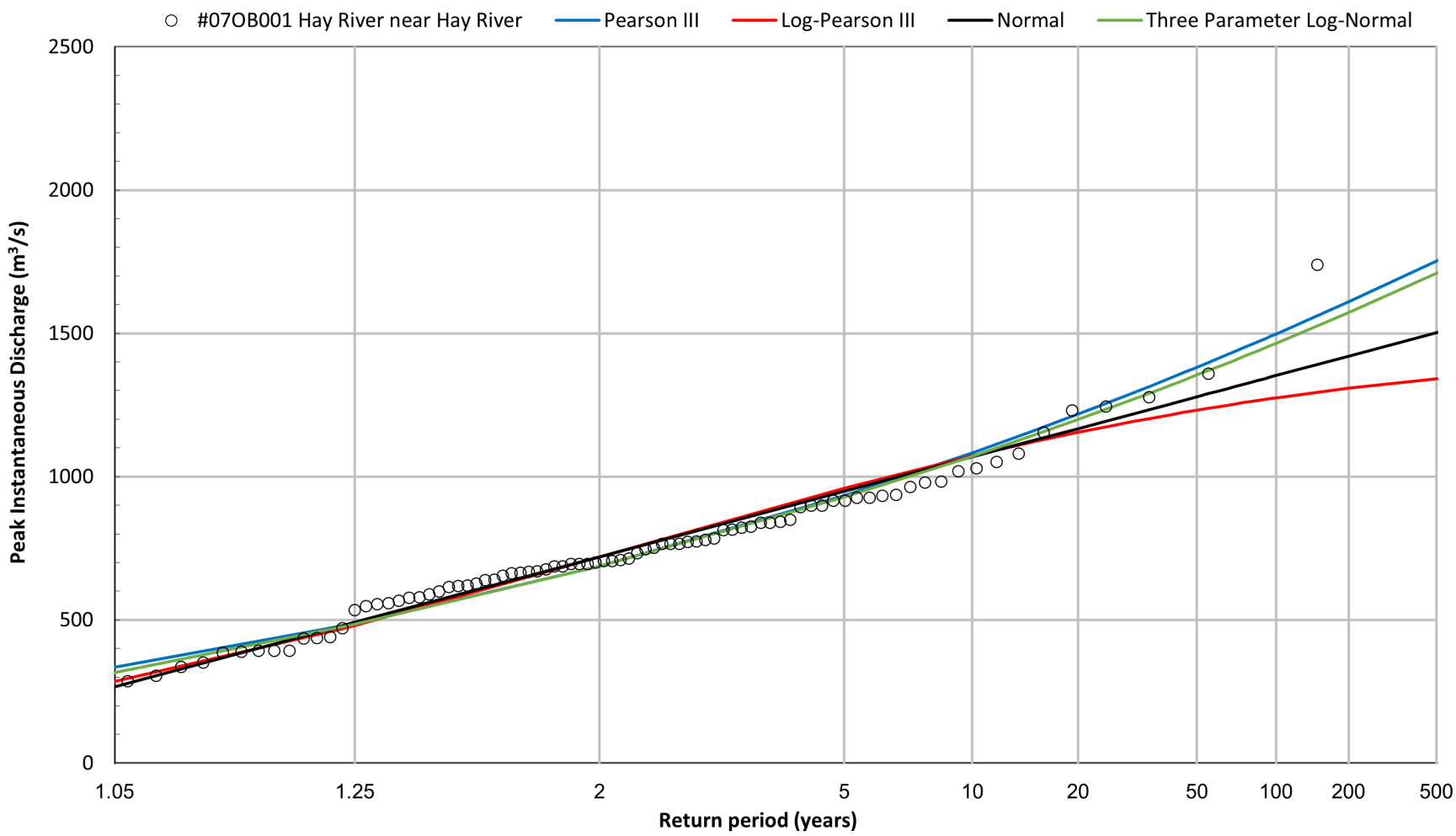

Government of Northwest Territories
Gouvernement des Territoires du Nord-Ouest

Canada

nhc

UNITS – AS SHOWN

Job: 1008469

Date: Feb-2025

KÁTŁ'ODEH (HAY RIVER)
FLOOD HAZARD MAPPING STUDY

COMPARISON OF SELECTED FLOOD FREQUENCY CURVES FOR #07OB001 HAY RIVER NEAR HAY RIVER INCLUDING UMA (1978) SYNTHESIZED DATA SERIES

FIGURE 6

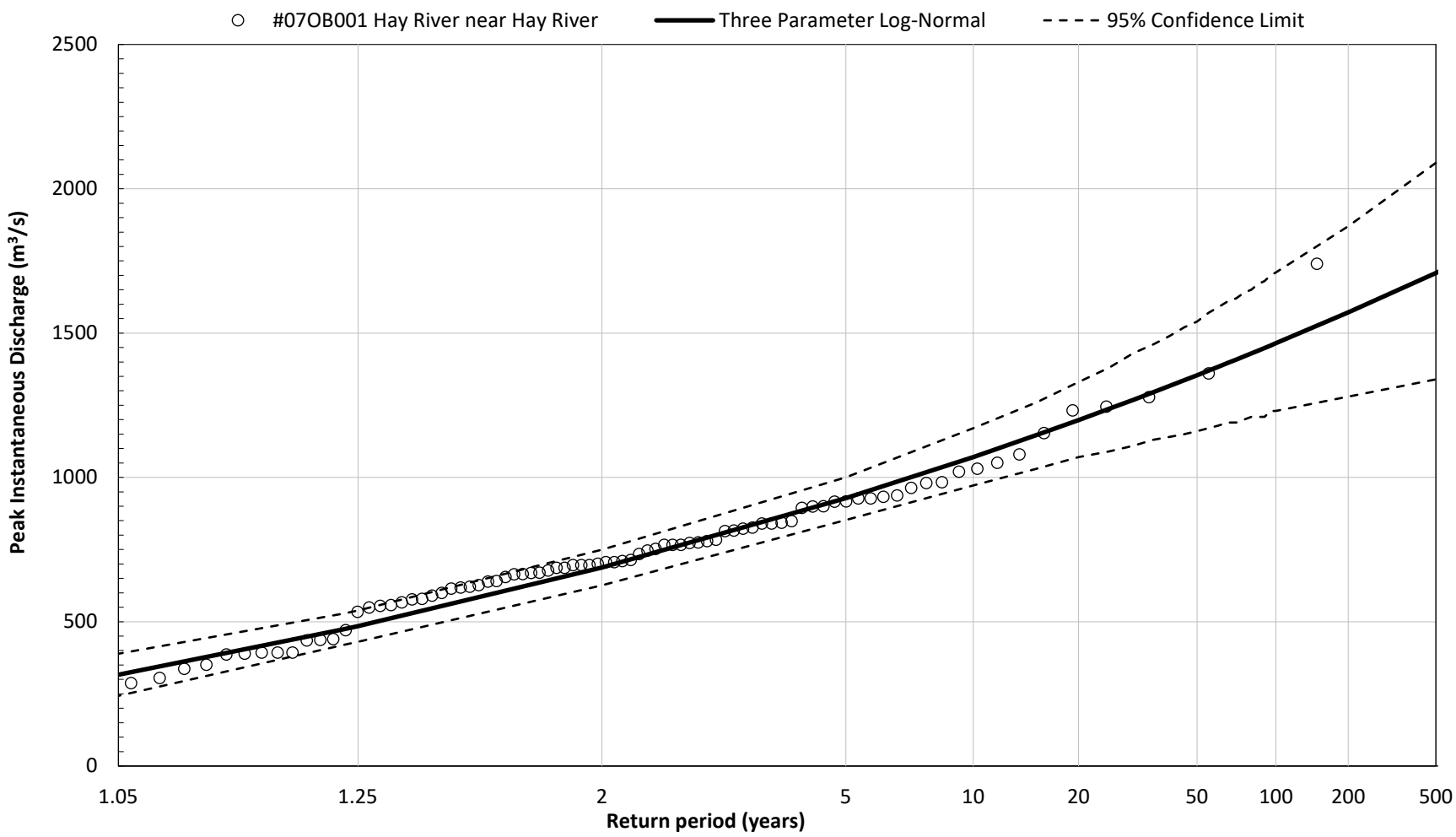

Government of Northwest Territories
Gouvernement des Territoires du Nord-Ouest

Canada

nhc

UNITS – AS SHOWN

Job: 1008469

Date: Feb-2025

KÁTŁ'ODEH (HAY RIVER)
FLOOD HAZARD MAPPING STUDY

ADOPTED 3LN FLOOD FREQUENCY CURVES FOR #07OB001 HAY RIVER NEAR HAY RIVER

FIGURE 7

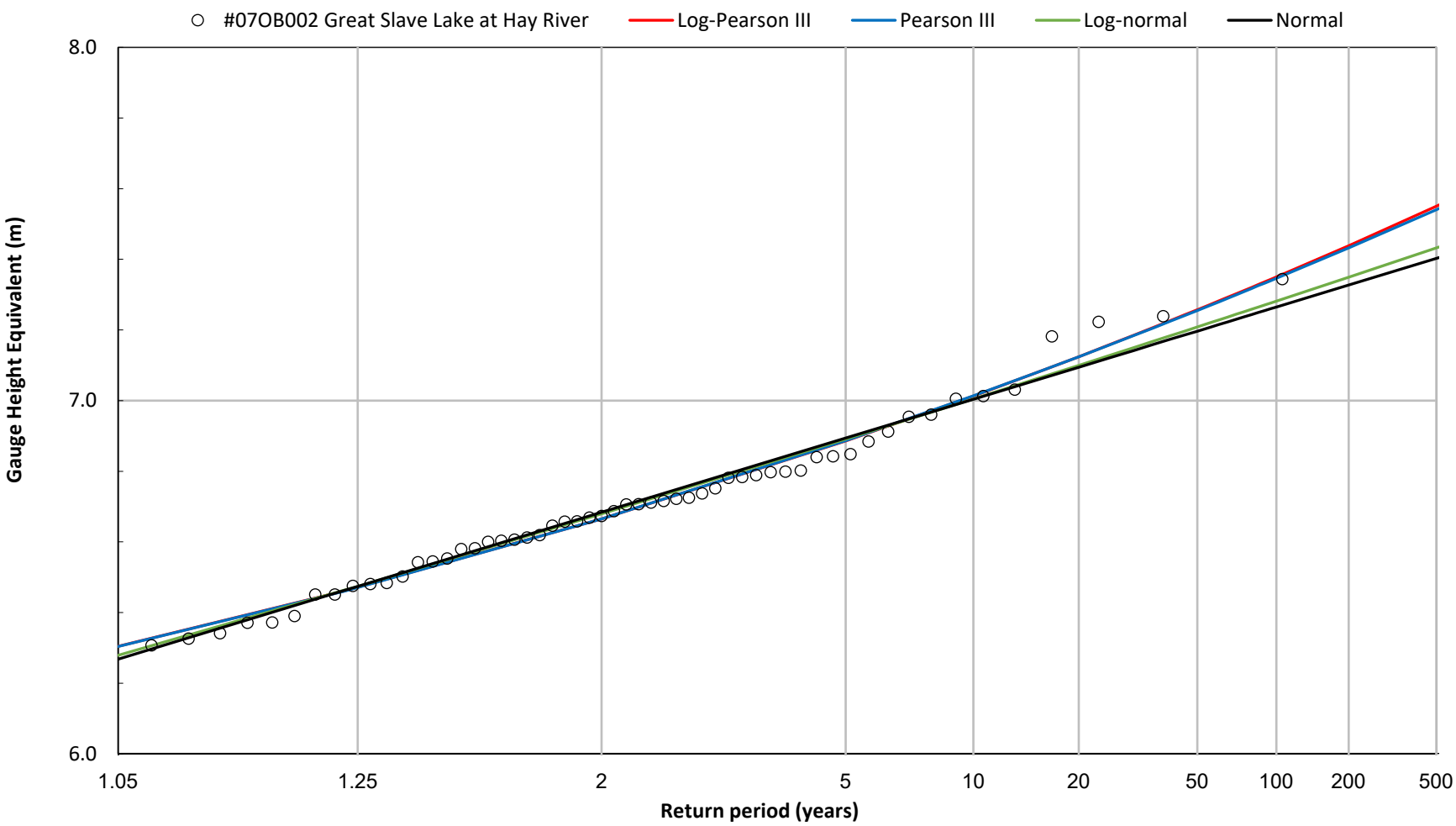

Notes: 1. A conversion to a gauge height equivalent has been adopted based off a gauge height adjustment (1985) during the years of record. The gauge height equivalent is equal to the CGVD28 elevation minus 150.000 m.

Government of Northwest Territories / Gouvernement des Territoires du Nord-Ouest; Canada; nhc	UNITS – AS SHOWN VERTICAL ELEVATION DATUM: GAUGE HEIGHT EQUIVALENT	KÁTŁ'ODEH (HAY RIVER) FLOOD HAZARD MAPPING STUDY ***COMPARISON OF FLOOD LEVEL FREQUENCY CURVES FOR #07OB002 GREAT SLAVE LAKE AT HAY RIVER***
	Job: 1008469 / *Date: Feb-2025*	FIGURE 8

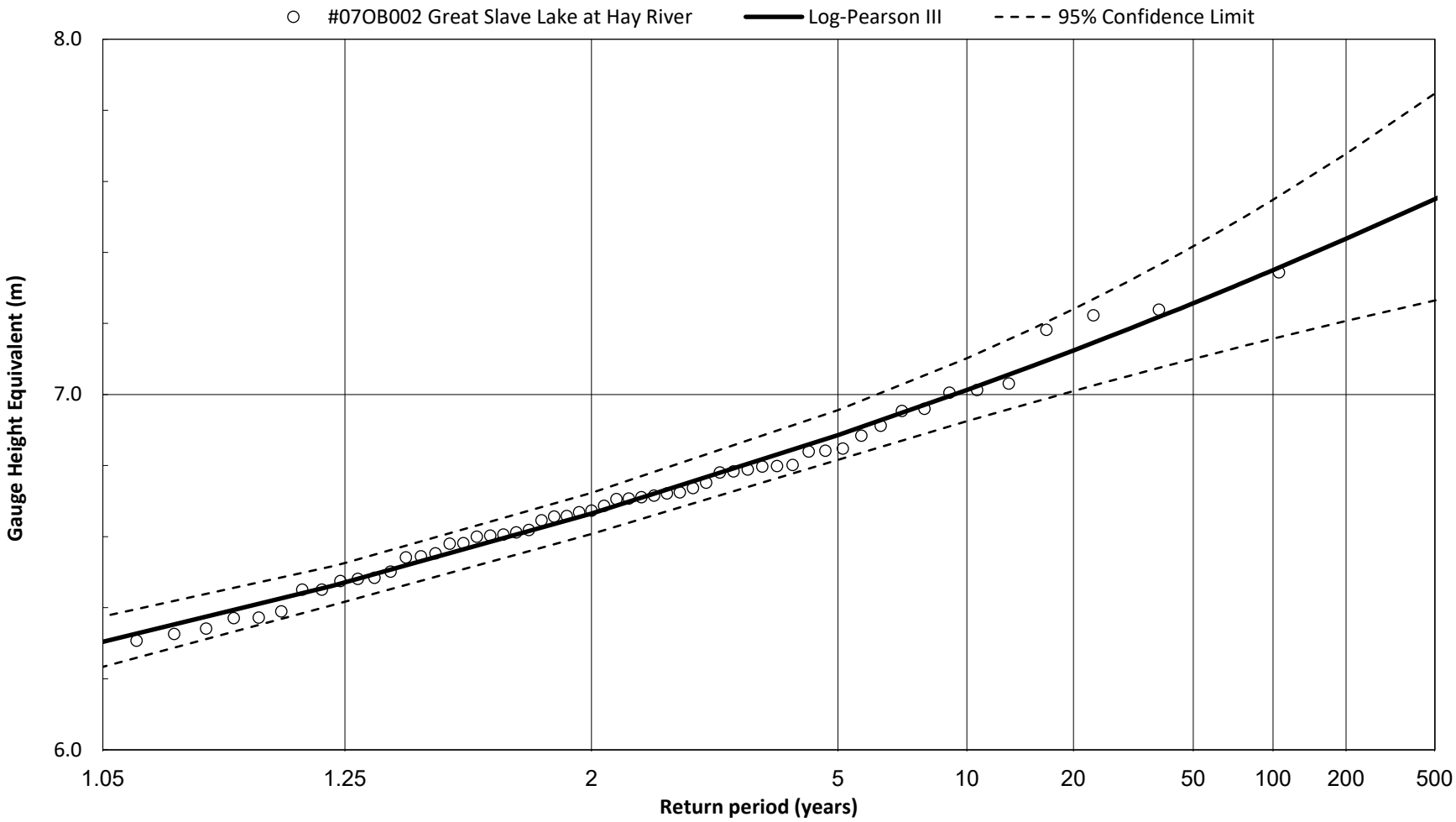

Notes: 1. Gauge height equivalent refers to the Geodetic Survey of Canada datum (local 1982 adj.) at WSC gauge #07OB002 Great Slave Lake at Hay River minus 150.000 m.

Government of Northwest Territories / Gouvernement des Territoires du Nord-Ouest

Canada

nhc

UNITS – AS SHOWN

VERTICAL ELEVATION DATUM: GAUGE HEIGHT EQUIVALENT

Job: 1008469

Date: Feb-2025

KÁTŁ'ODEH (HAY RIVER)
FLOOD HAZARD MAPPING STUDY

ADOPTED FLOOD LEVEL FREQUENCY CURVE FOR #07OB002 GREAT SLAVE LAKE AT HAY RIVER

FIGURE 9

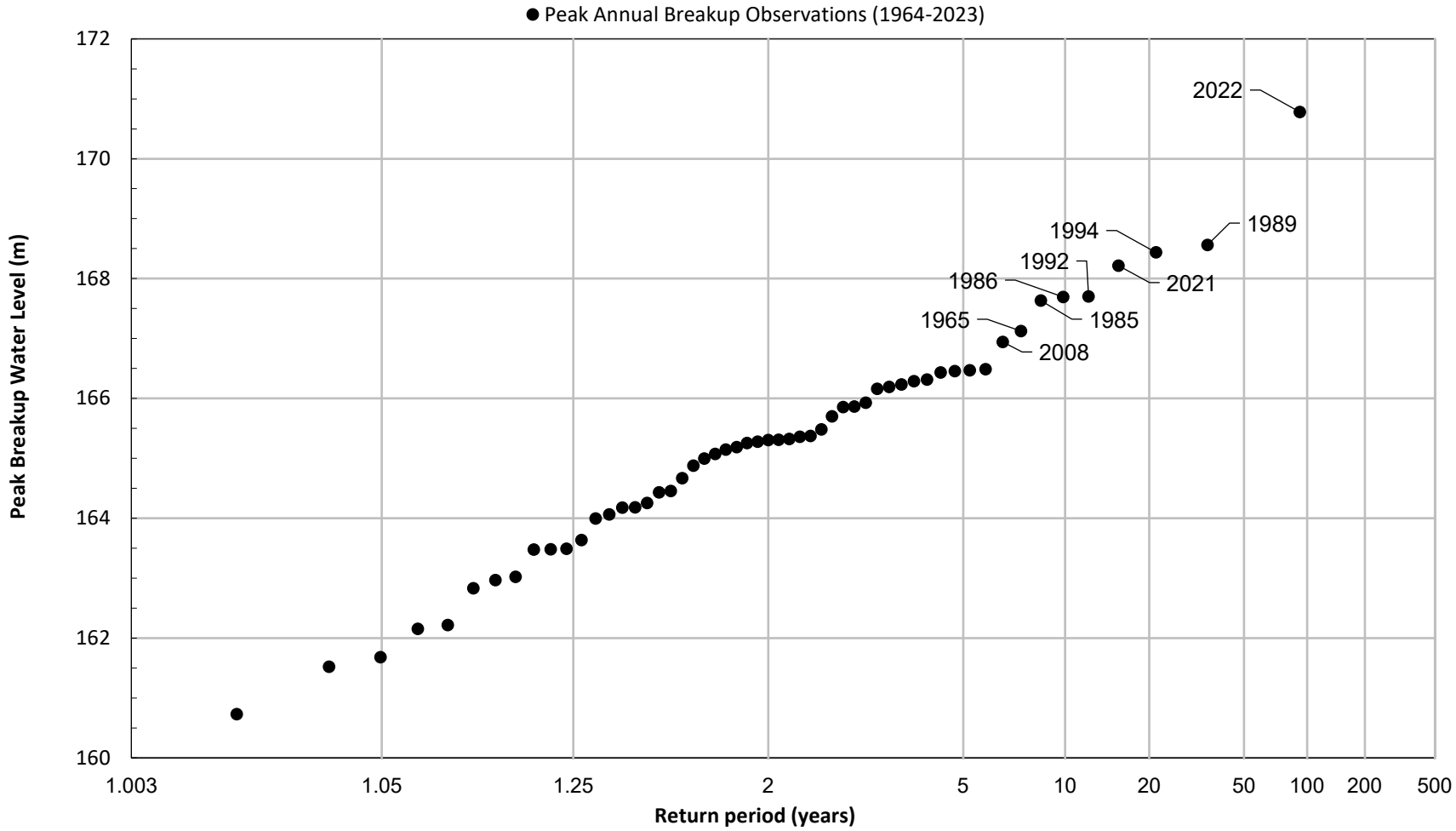

Government of Northwest Territories / Gouvernement des Territoires du Nord-Ouest; Canada; nhc	UNITS – AS SHOWN VERTICAL ELEVATION DATUM: CGVD2013a	KÁTŁ'ODEH (HAY RIVER) FLOOD HAZARD MAPPING STUDY ***FLOOD LEVEL FREQUENCY LEVELS*** ***#07OB001 HAY RIVER NEAR HAY RIVER***
	Job: 1008469 / *Date: Feb-2025*	FIGURE 10

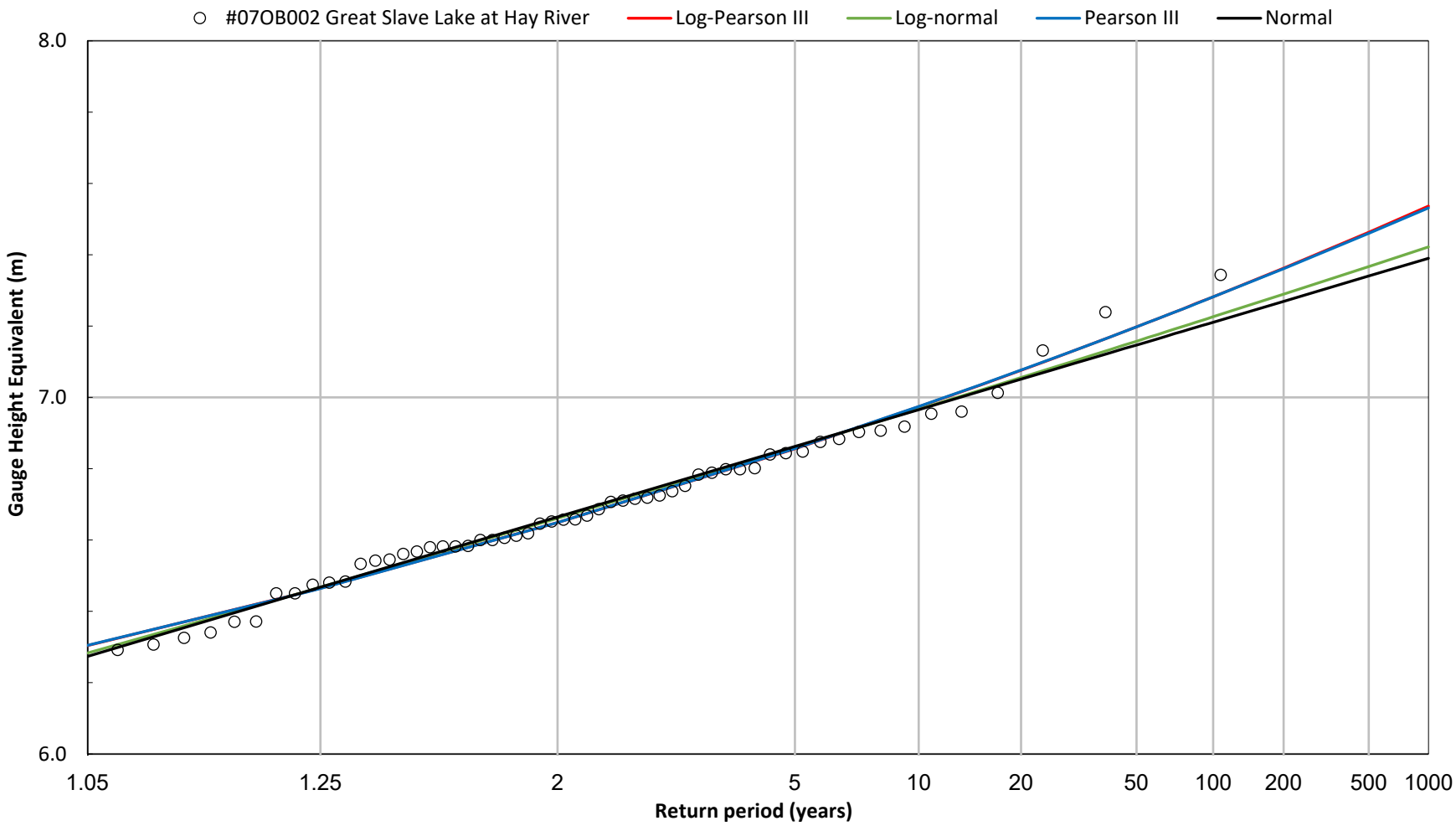

Notes: 1. A conversion to a gauge height equivalent has been adopted based off a gauge height adjustment (1985) during the years of record. The gauge height equivalent is equal to the CGVD28 elevation minus 150.000 m.

Government of Northwest Territories / Gouvernement des Territoires du Nord-Ouest; Canada; nhc	UNITS – AS SHOWN VERTICAL ELEVATION DATUM: GAUGE HEIGHT EQUIVALENT	KÁTŁ'ODEH (HAY RIVER) FLOOD HAZARD MAPPING STUDY ***COMPARISON OF SPRING BREAKUP FLOOD LEVEL FREQUENCY CURVES FOR #07OB002 GREAT SLAVE LAKE AT HAY RIVER***
	Job: 1008469 / *Date: Feb-2025*	FIGURE 11

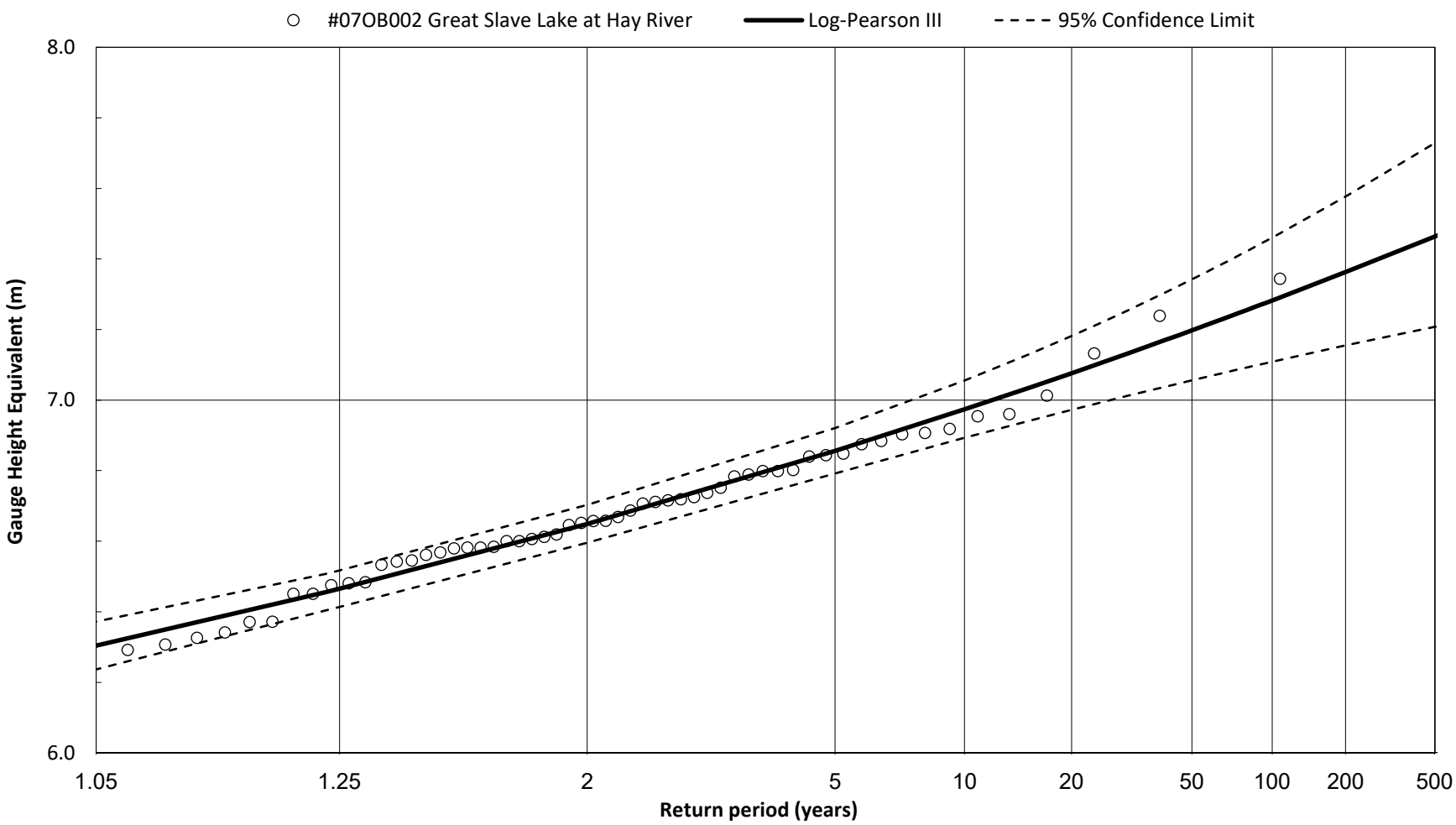

Notes: 1. Gauge height equivalent refers to the Geodetic Survey of Canada datum (local 1982 adj.) at WSC gauge #07OB002 Great Slave Lake at Hay River minus 150.000 m.

Government of Northwest Territories / Gouvernement des Territoires du Nord-Ouest

Canada

nhc

UNITS – AS SHOWN

VERTICAL ELEVATION DATUM: GAUGE HEIGHT EQUIVALENT

Job: 1008469

Date: Feb-2025

KÁTŁ'ODEH (HAY RIVER)
FLOOD HAZARD MAPPING STUDY

ADOPTED SPRING BREAKUP FLOOD LEVEL FREQUENCY CURVE FOR #07OB002 GREAT SLAVE LAKE AT HAY RIVER

FIGURE 12

Determine peak breakup level and discharge by year and characterize by breakup mechanism.

Year	Breakup Discharge (m^3/s)	Peak Breakup Gauge Height (m)	Breakup Mechanism
...	...	...	...
2018	198	4.132	Thermal
2019	26	2.709	Ice Run
2020	602	8.169	Ice Run
2021	885	10.193	Ice Jam
2022	1460	12.758	Ice Jam
...	...	...	...

Develop a family of ice-affected flood level profiles for each breakup mechanism (rating curves).

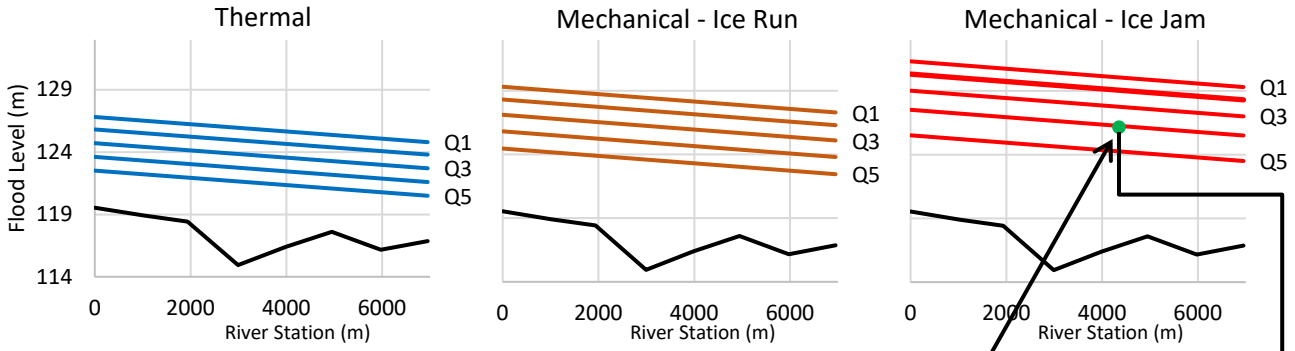

Determine probability factors by breakup mechanism.

$P_{mechanical} = 0.95$, $P_{thermal} = 0.05$

$P_{jam\ if\ mechanical} = 0.33$, $P_{ice\ run\ if\ mechanical} = 0.67$

Estimate breakup discharge frequency distribution.

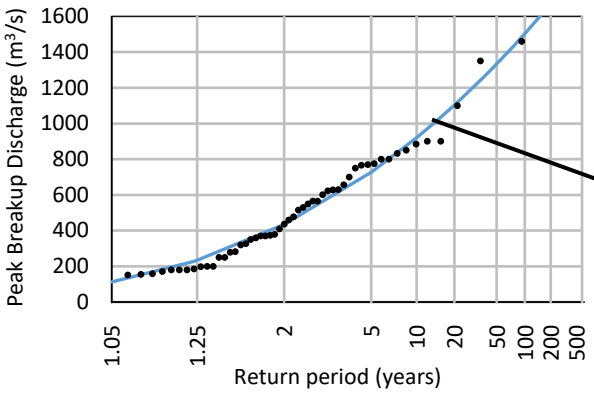

1. Randomly select a value from the breakup discharge frequency distribution

2. Randomly select a breakup mechanism based on probability factors.

3. Determine the ice-affected flood level based on the breakup type and the respective breakup discharge – water level relationship.

4. Store the breakup flood level to the synthesized population of breakup levels for each section and repeat the process (e.g. 10,000 + iterations).

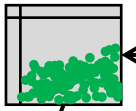

5. Rank and plot the series with a standard plotting position formula to form a distribution of breakup flood levels and compare to the estimated breakup flood levels based on observational data.

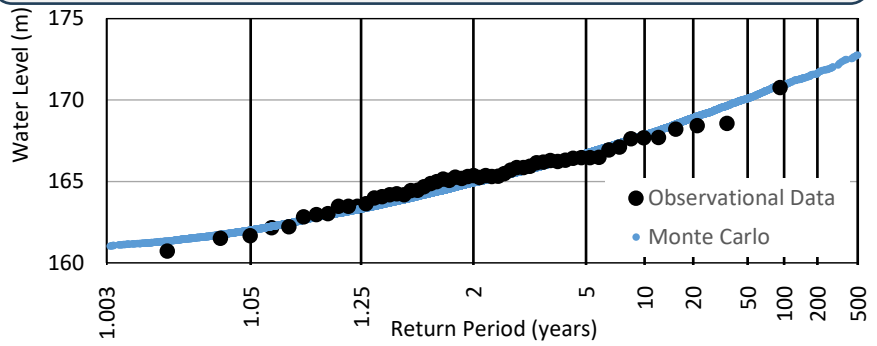

NOTE: All values in this figure are hypothetical and are for information only.

KÁTŁ'ODEH (HAY RIVER)
FLOOD HAZARD MAPPING STUDY

MONTE CARLO ANALYSIS WORKFLOW

Job: 1008469

Date: Feb-2025

FIGURE 13

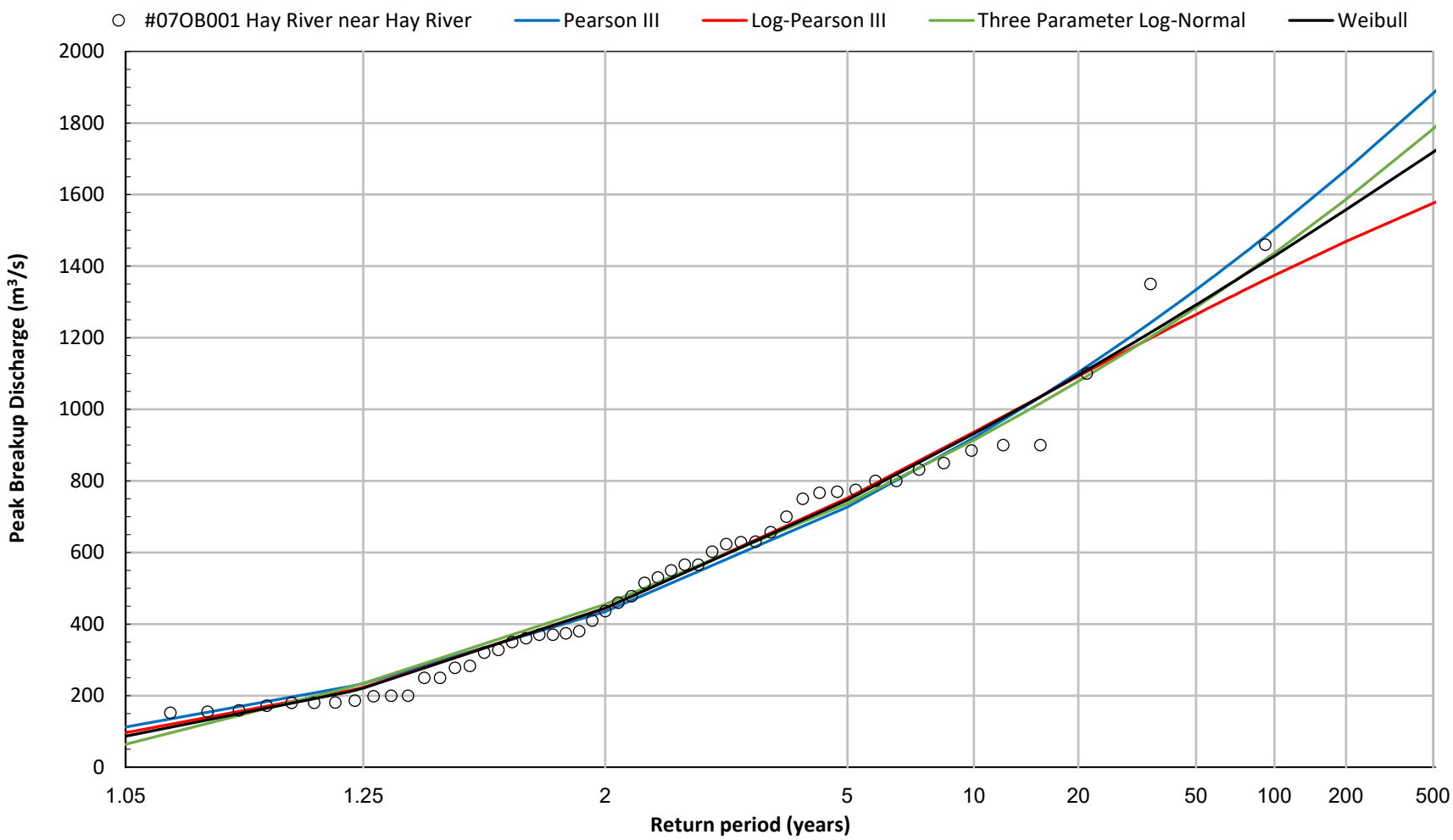

Government of Northwest Territories / Gouvernement des Territoires du Nord-Ouest

Canada

nhc

UNITS – AS SHOWN

Job: 1008469

Date: Feb-2025

KÁTŁ'ODEH (HAY RIVER)
FLOOD HAZARD MAPPING STUDY

COMPARISON OF BREAKUP DISCHARGE FLOOD FREQUENCY CURVES #07OB001 HAY RIVER NEAR HAY RIVER

FIGURE 14

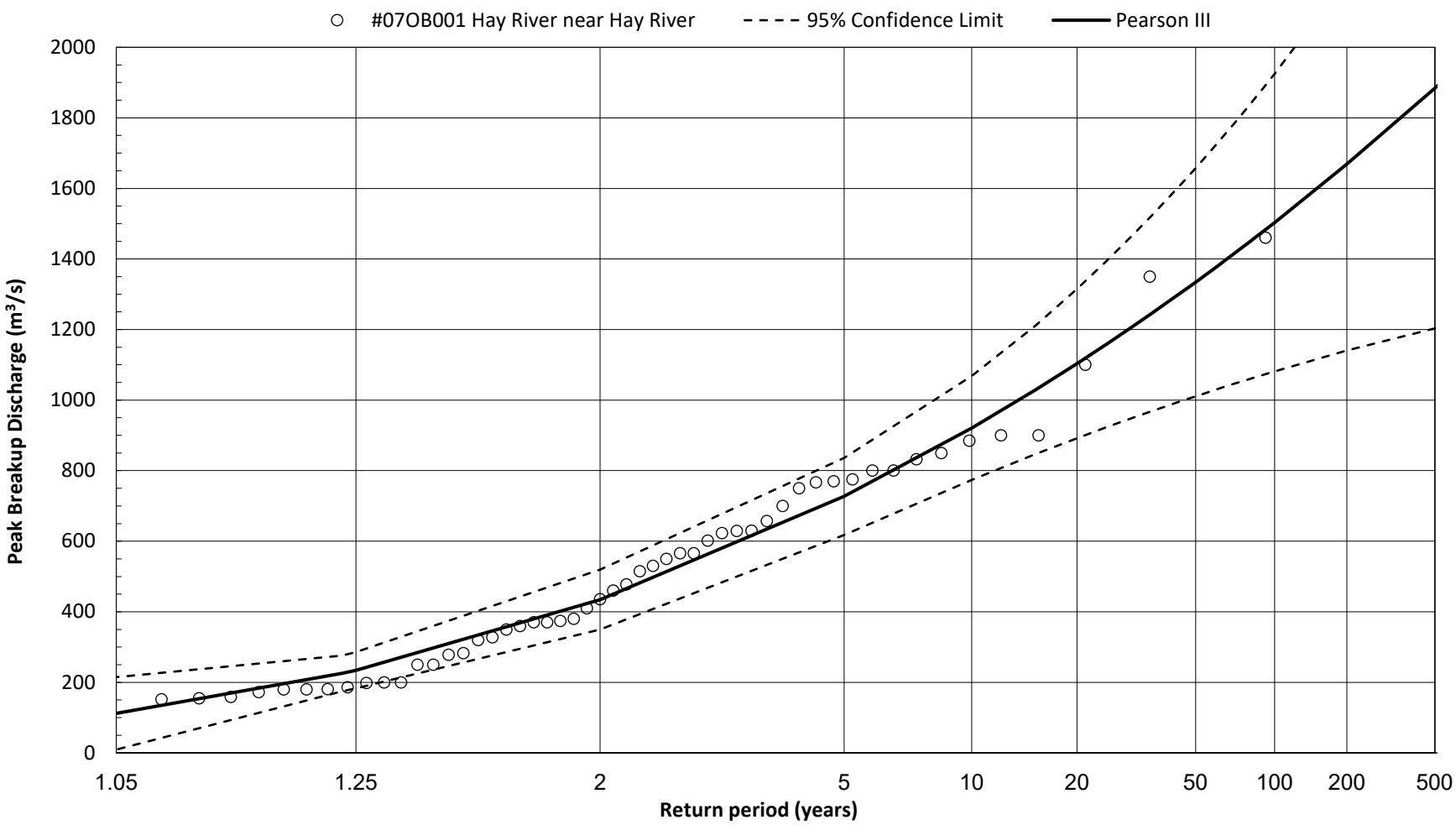

Government of Northwest Territories
Gouvernement des Territoires du Nord-Ouest

Canada

nhc

UNITS – AS SHOWN

Job: 1008469

Date: Feb-2025

KÁTŁ'ODEH (HAY RIVER)
FLOOD HAZARD MAPPING STUDY

ADOPTED BREAKUP DISCHARGE FLOOD FREQUENCY
#07OB001 HAY RIVER NEAR HAY RIVER

FIGURE 15

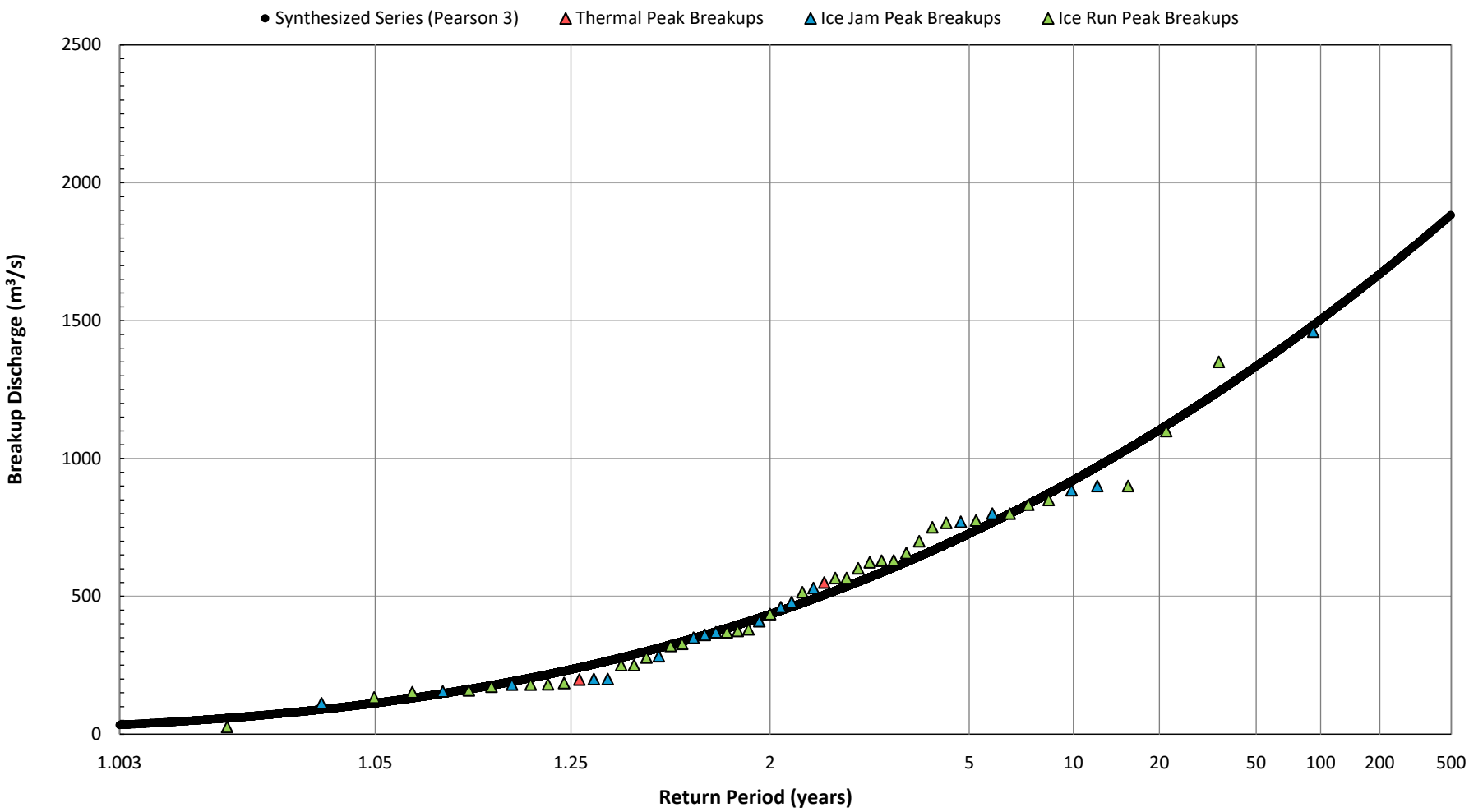

Government of Northwest Territories
Gouvernement des Territoires du Nord-Ouest

Canada

nhc

UNITS – AS SHOWN

Job: 1008469

Date: Feb-2025

KÁTŁ'ODEH (HAY RIVER)
FLOOD HAZARD MAPPING STUDY

MONTE CARLO
SYNTHESIZED DISCHARGE DISTRIBUTIONS

FIGURE 16

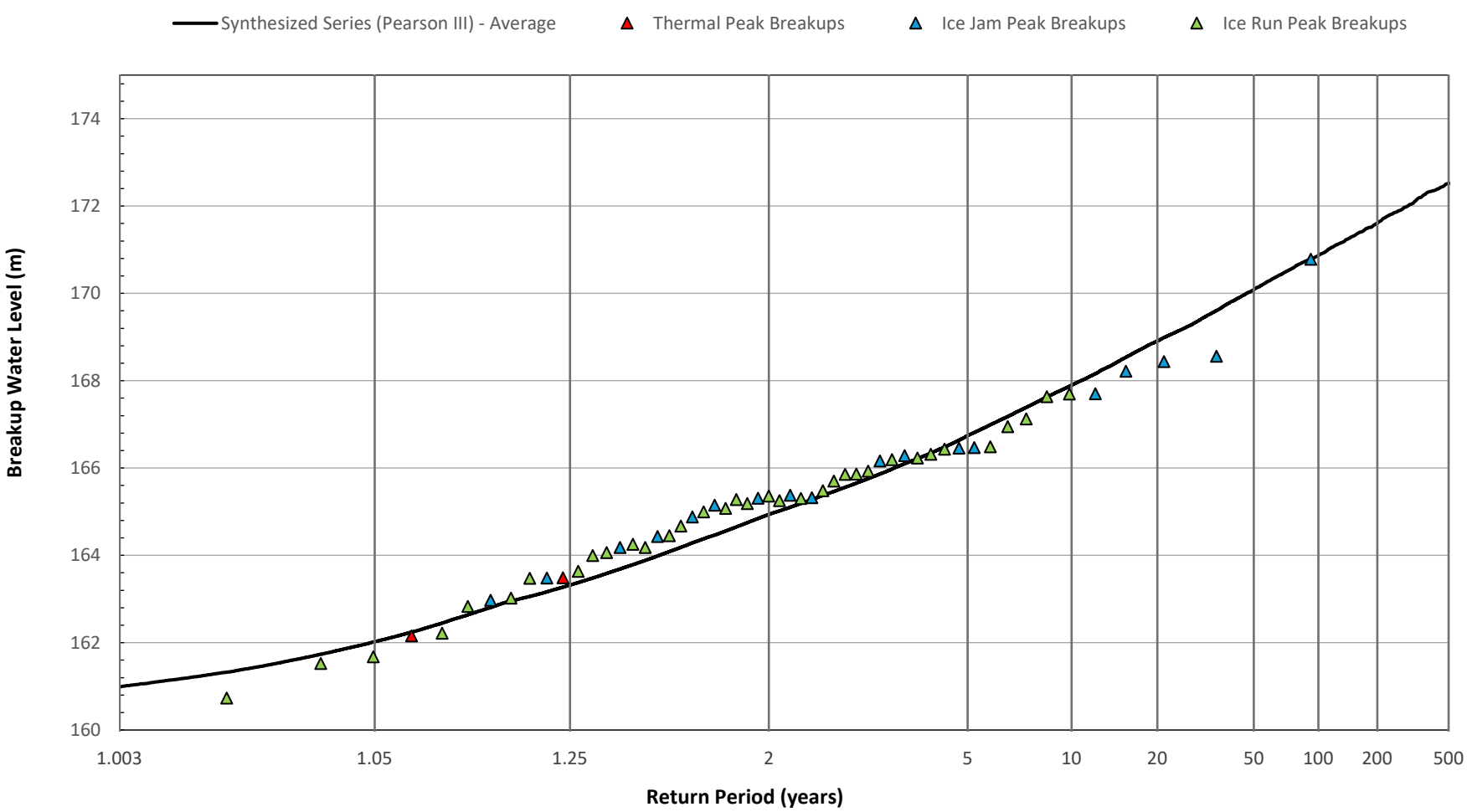

Government of Northwest Territories
Gouvernement des Territoires du Nord-Ouest

Canada

nhc

UNITS – AS SHOWN

VERTICAL ELEVATION DATUM: CGVD2013a

Job: 1008469

Date: Feb-2025

KÁTŁ'ODEH (HAY RIVER)
FLOOD HAZARD MAPPING STUDY

MONTE CARLO – WATER LEVEL FREQUENCY DISTRIBUTION AT #07OB001 HAY RIVER NEAR HAY RIVER

FIGURE 17

Notes: 1. RS refers to model cross section river stations in metres.

Government of Northwest Territories / Gouvernement des Territoires du Nord-Ouest; Canada; nhc	SCALE – AS SHOWN	KÁTŁ'ODEH (HAY RIVER) FLOOD HAZARD MAPPING STUDY
		RIVER CENTRELINES AND MODEL CROSS SECTIONS HAY RIVER EAST CHANNEL (REACH 1 OF 3)
	Job: 1008469 / *Date: Feb-2025*	FIGURE 18

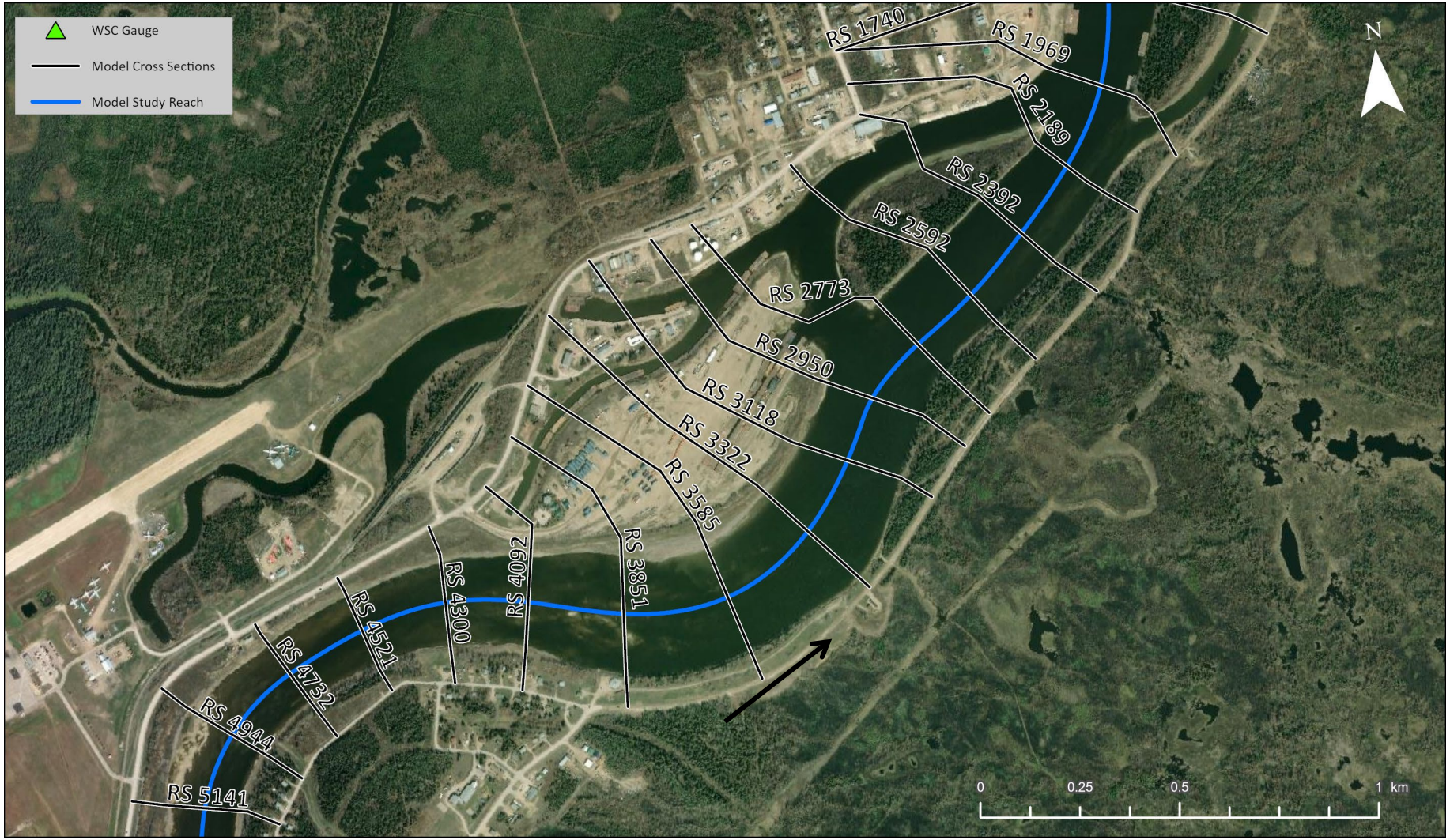

Notes: 1. RS refers to model cross section river stations in metres.

Government of Northwest Territories / Gouvernement des Territoires du Nord-Ouest; Canada; nhc	SCALE – AS SHOWN	KÁTŁ'ODEH (HAY RIVER) FLOOD HAZARD MAPPING STUDY
		RIVER CENTRELINES AND MODEL CROSS SECTIONS HAY RIVER EAST CHANNEL (REACH 2 OF 3)
	Job: 1008469 / *Date: Feb-2025*	FIGURE 19

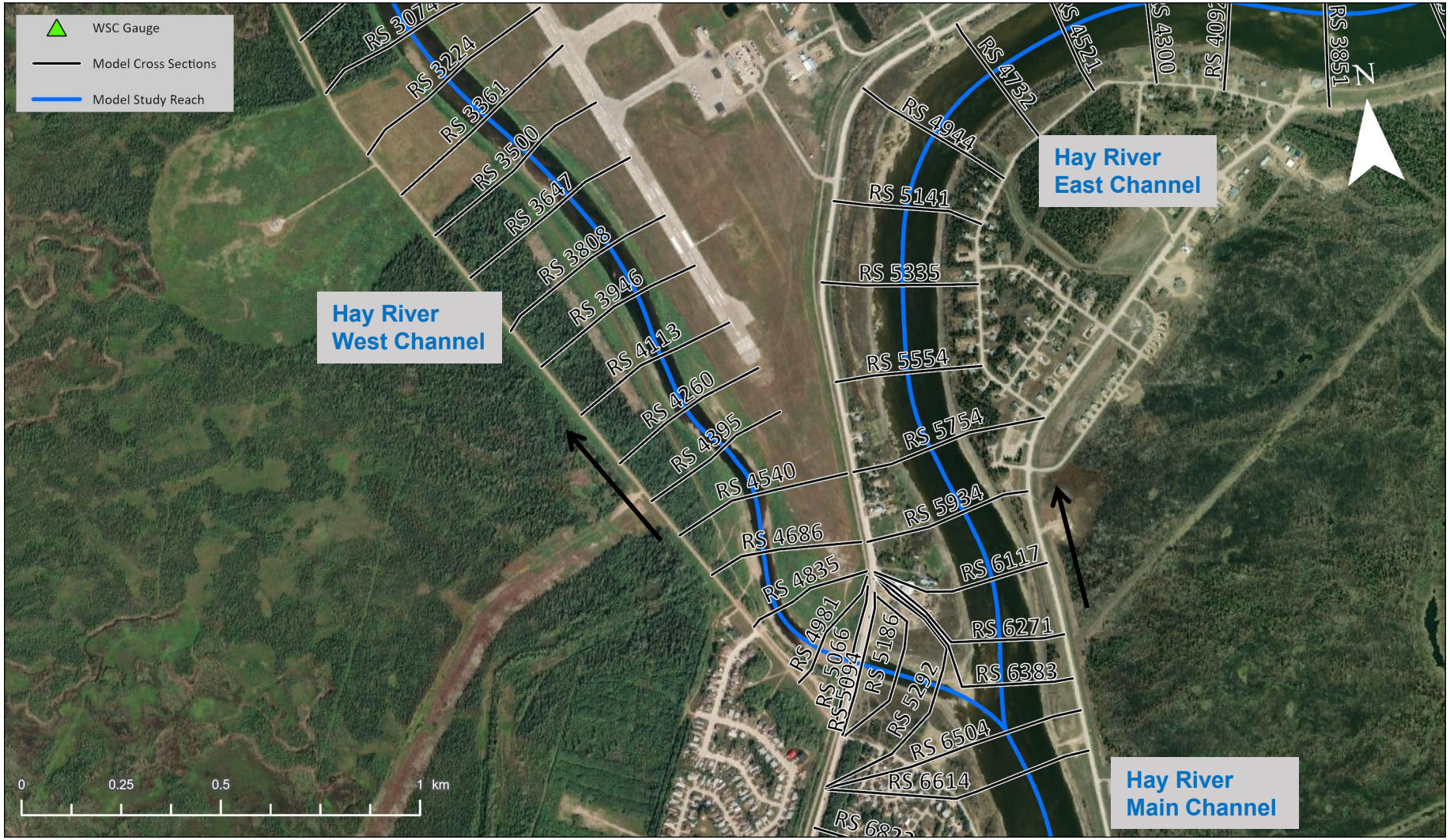

Notes: 1. RS refers to model cross section river stations in metres.

Government of Northwest Territories / Gouvernement des Territoires du Nord-Ouest; Canada; nhc	SCALE – AS SHOWN	KÁTŁ'ODEH (HAY RIVER) FLOOD HAZARD MAPPING STUDY
		RIVER CENTRELINES AND MODEL CROSS SECTIONS HAY RIVER EAST CHANNEL (REACH 3 OF 3)
	Job: 1008469 / *Date: Feb-2025*	FIGURE 20

Notes: 1. RS refers to model cross section river stations in metres.

Government of Northwest Territories / Gouvernement des Territoires du Nord-Ouest; Canada; nhc	SCALE – AS SHOWN	KÁTŁ'ODEH (HAY RIVER) FLOOD HAZARD MAPPING STUDY
		RIVER CENTRELINES AND MODEL CROSS SECTIONS HAY RIVER WEST FISHING VILLAGE AND RUDD CHANNELS (REACHES 1 OF 1)
	Job: 1008469 / *Date: Feb-2025*	FIGURE 21

Notes: 1. RS refers to model cross section river stations in metres.

Government of Northwest Territories / Gouvernement des Territoires du Nord-Ouest; Canada; nhc	SCALE – AS SHOWN	KÁTŁ'ODEH (HAY RIVER) FLOOD HAZARD MAPPING STUDY
		RIVER CENTRELINES AND MODEL CROSS SECTIONS HAY RIVER WEST CHANNEL (REACH 1 OF 2)
	Job: 1008469 / *Date: Feb-2025*	FIGURE 22

Notes: 1. RS refers to model cross section river stations in metres.

Government of Northwest Territories / Gouvernement des Territoires du Nord-Ouest; Canada; nhc	SCALE – AS SHOWN	KÁTŁ'ODEH (HAY RIVER) FLOOD HAZARD MAPPING STUDY
		RIVER CENTRELINES AND MODEL CROSS SECTIONS HAY RIVER WEST CHANNEL (REACH 2 OF 2)
	Job: 1008469 / *Date: Feb-2025*	FIGURE 23

Notes: 1. RS refers to model cross section river stations in metres.

Government of Northwest Territories / Gouvernement des Territoires du Nord-Ouest; Canada; nhc	SCALE – AS SHOWN	KÁTŁ'ODEH (HAY RIVER) FLOOD HAZARD MAPPING STUDY
		RIVER CENTRELINES AND MODEL CROSS SECTIONS HAY RIVER MAIN CHANNEL (REACH 1 OF 8)
	Job: 1008469 / *Date: Feb-2025*	FIGURE 24

Notes: 1. RS refers to model cross section river stations in metres.

Government of Northwest Territories / Gouvernement des Territoires du Nord-Ouest; Canada; nhc	SCALE – AS SHOWN	KÁTŁ'ODEH (HAY RIVER) FLOOD HAZARD MAPPING STUDY
		RIVER CENTRELINES AND MODEL CROSS SECTIONS HAY RIVER MAIN CHANNEL (REACH 2 OF 8)
	Job: 1008469 — *Date: Feb-2025*	FIGURE 25

Notes: 1. RS refers to model cross section river stations in metres.

Government of Northwest Territories / Gouvernement des Territoires du Nord-Ouest; Canada; nhc	SCALE – AS SHOWN	KÁTŁ'ODEH (HAY RIVER) FLOOD HAZARD MAPPING STUDY
		RIVER CENTRELINES AND MODEL CROSS SECTIONS HAY RIVER MAIN CHANNEL (REACH 3 OF 8)
	Job: 1008469 / *Date: Feb-2025*	FIGURE 26

Notes: 1. RS refers to model cross section river stations in metres.

Government of Northwest Territories / Gouvernement des Territoires du Nord-Ouest; Canada; nhc	SCALE – AS SHOWN	KÁTŁ'ODEH (HAY RIVER) FLOOD HAZARD MAPPING STUDY
		RIVER CENTRELINES AND MODEL CROSS SECTIONS HAY RIVER MAIN CHANNEL (REACH 4 OF 8)
	Job: 1008469 / *Date: Feb-2025*	FIGURE 27

Notes: 1. RS refers to model cross section river stations in metres.

Government of Northwest Territories / Gouvernement des Territoires du Nord-Ouest; Canada; nhc	SCALE – AS SHOWN	KÁTŁ'ODEH (HAY RIVER) FLOOD HAZARD MAPPING STUDY
		RIVER CENTRELINES AND MODEL CROSS SECTIONS HAY RIVER MAIN CHANNEL (REACH 5 OF 8)
	Job: 1008469 / *Date: Feb-2025*	FIGURE 28

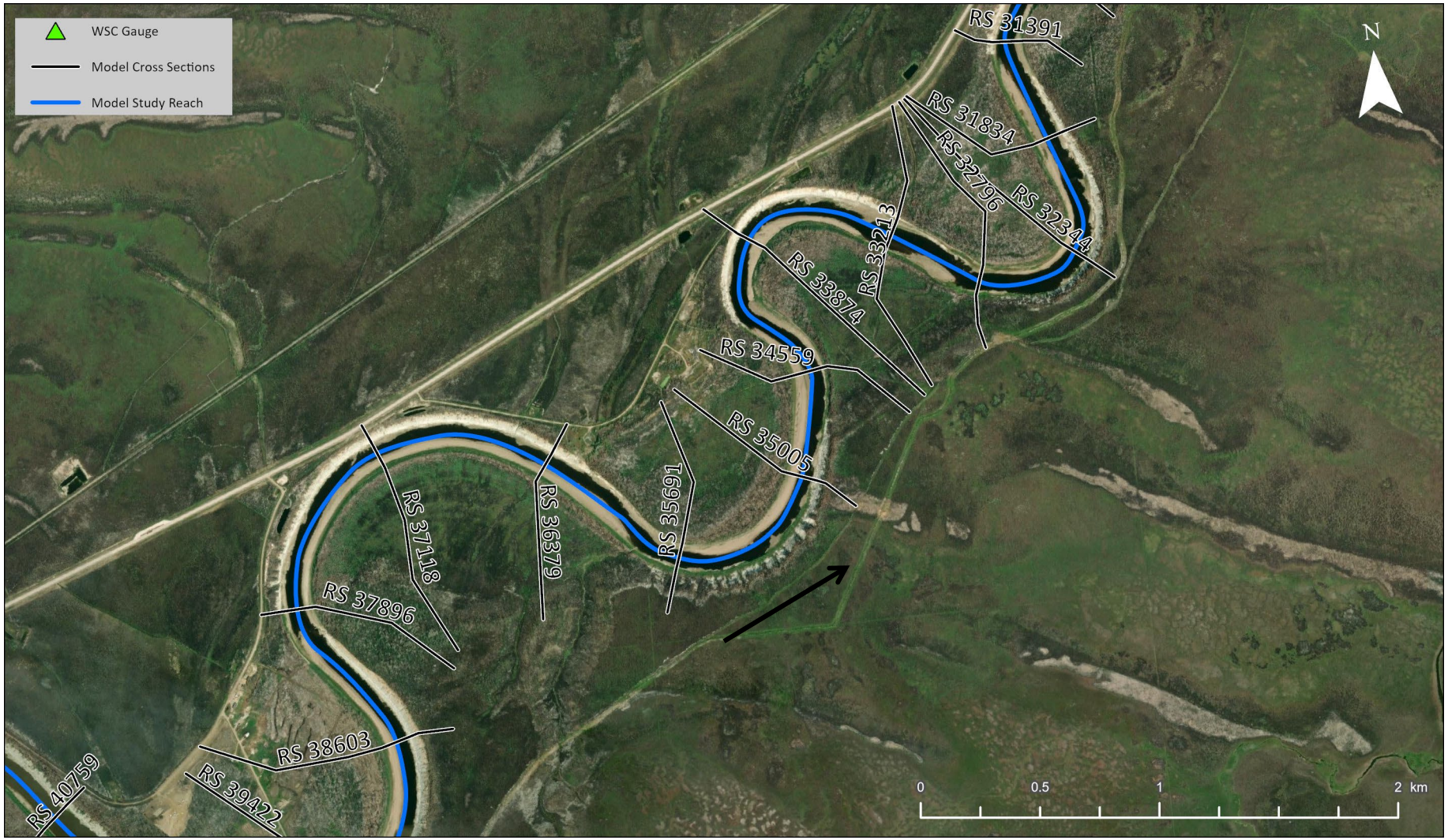

Notes: 1. RS refers to model cross section river stations in metres.

Government of Northwest Territories / Gouvernement des Territoires du Nord-Ouest; Canada; nhc	SCALE – AS SHOWN	KÁTŁ'ODEH (HAY RIVER) FLOOD HAZARD MAPPING STUDY
		RIVER CENTRELINES AND MODEL CROSS SECTIONS HAY RIVER MAIN CHANNEL (REACH 6 OF 8)
	Job: 1008469 / *Date: Feb-2025*	FIGURE 29

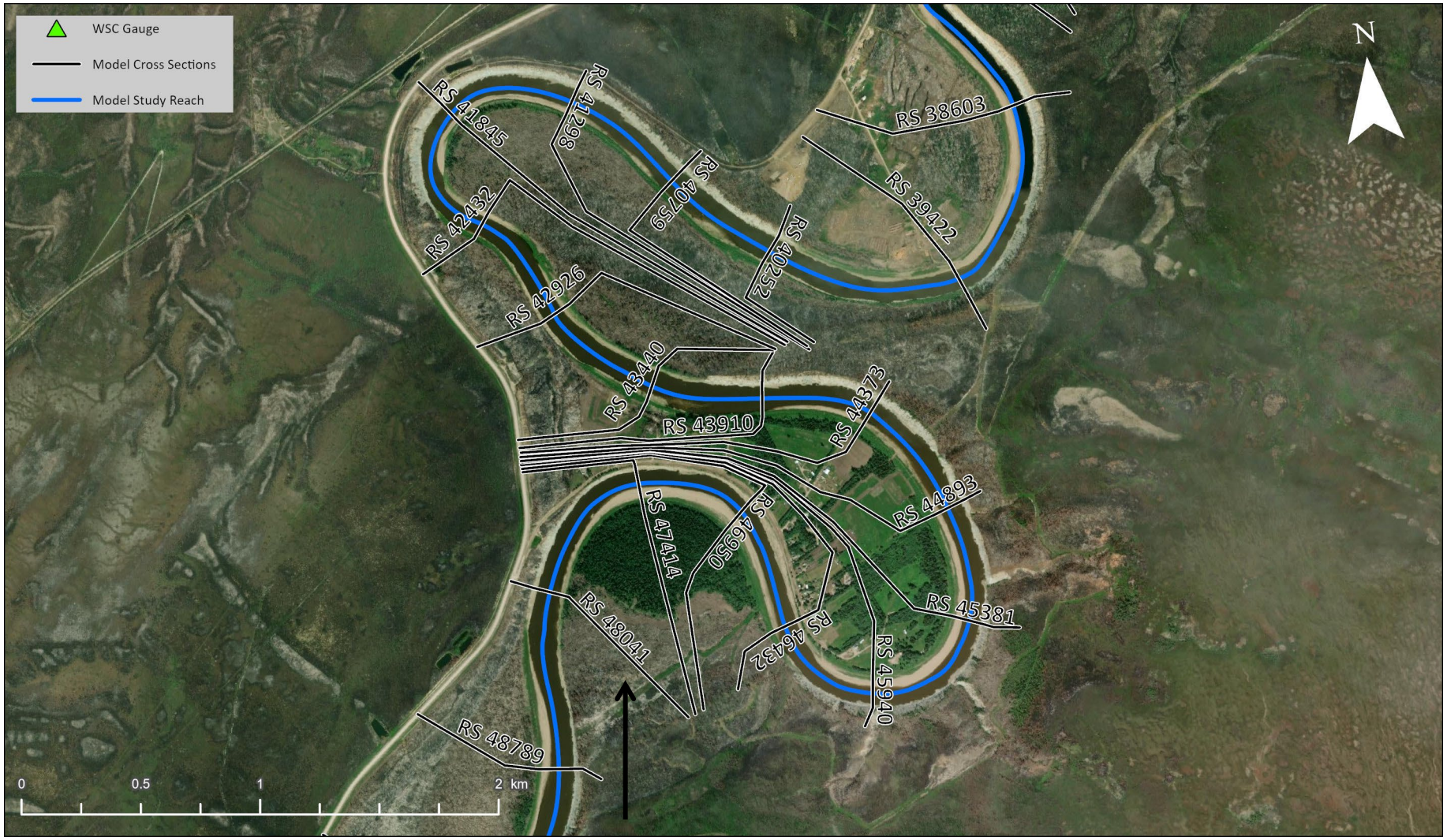

Notes: 1. RS refers to model cross section river stations in metres.

Government of Northwest Territories / Gouvernement des Territoires du Nord-Ouest; Canada; nhc	SCALE – AS SHOWN	KÁTŁ'ODEH (HAY RIVER) FLOOD HAZARD MAPPING STUDY
		RIVER CENTRELINES AND MODEL CROSS SECTIONS HAY RIVER MAIN CHANNEL (REACH 7 OF 8)
	Job: 1008469 / *Date: Feb-2025*	FIGURE 30

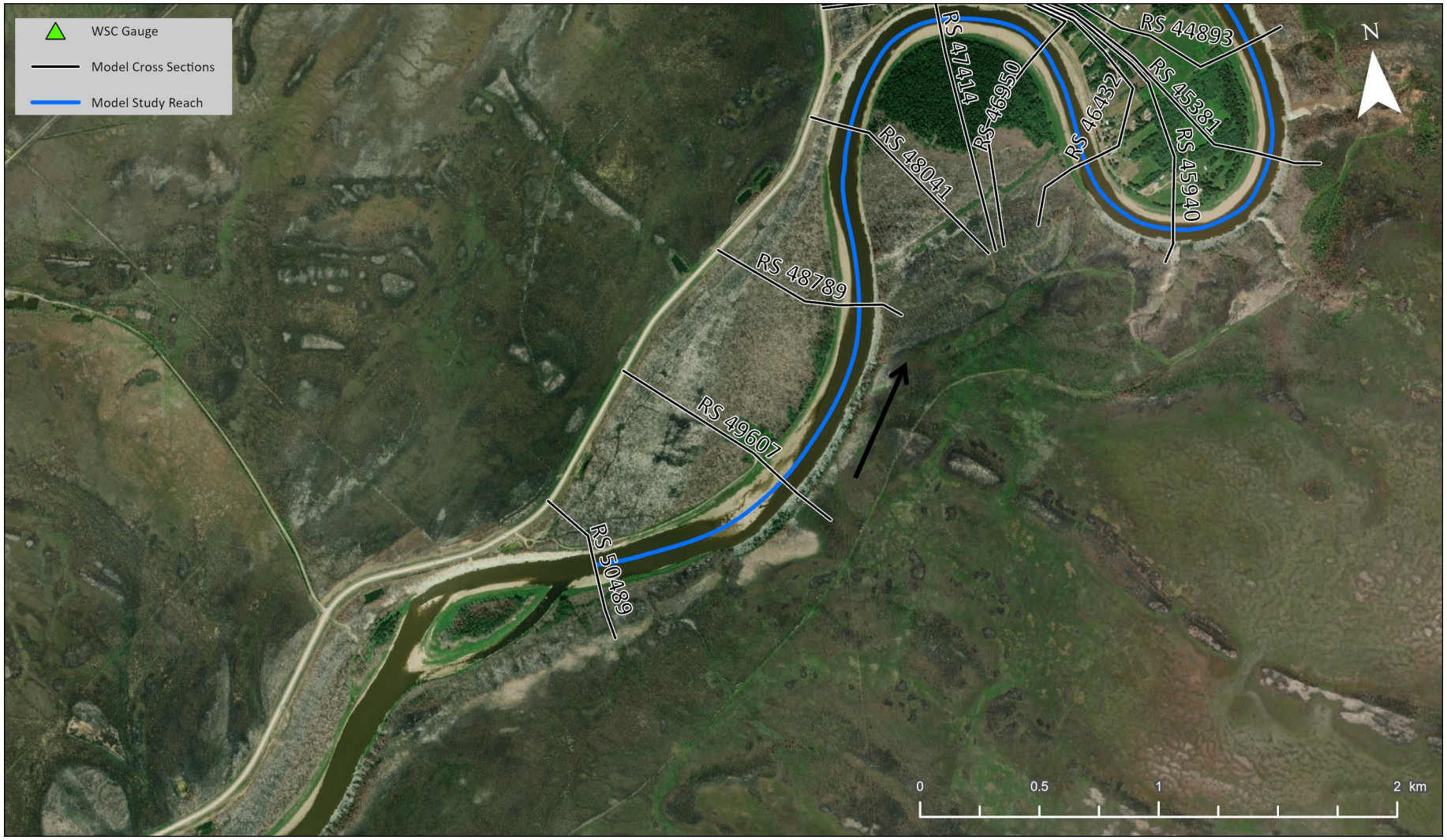

Notes: 1. RS refers to model cross section river stations in metres.

Government of Northwest Territories / Gouvernement des Territoires du Nord-Ouest; Canada; nhc	SCALE – AS SHOWN	KÁTŁ'ODEH (HAY RIVER) FLOOD HAZARD MAPPING STUDY
		RIVER CENTRELINES AND MODEL CROSS SECTIONS HAY RIVER MAIN CHANNEL (REACH 8 OF 8)
	Job: 1008469 / *Date: Feb-2025*	FIGURE 31

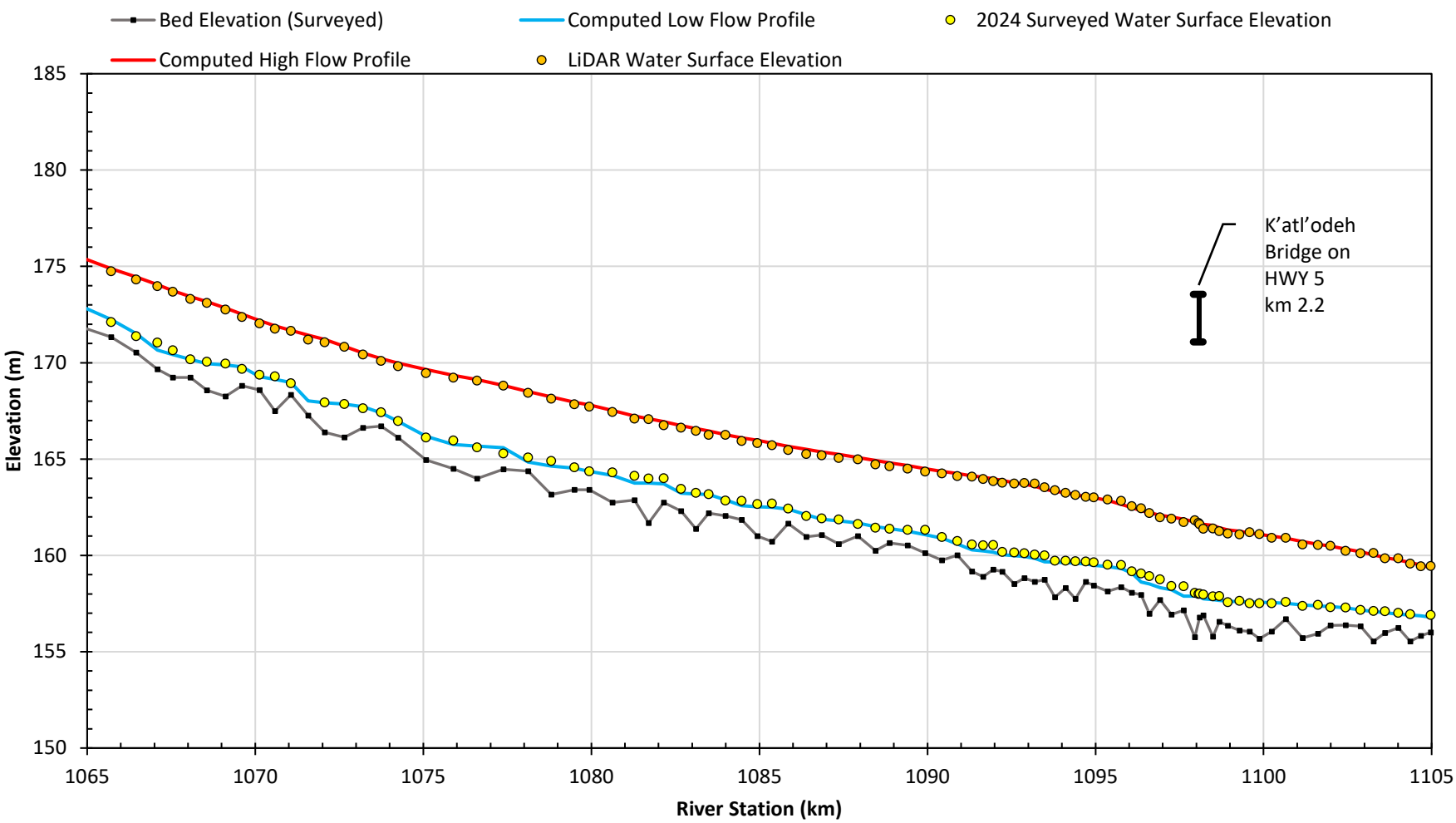

Government of Northwest Territories / Gouvernement des Territoires du Nord-Ouest

Canada

nhc

UNITS – AS SHOWN

VERTICAL ELEVATION DATUM: CGVD2013a

Job: 1008469

Date: Feb-2025

KÁTŁ'ODEH (HAY RIVER)
FLOOD HAZARD MAPPING STUDY

OPEN WATER CALIBRATION PROFILES
HAY RIVER MAIN CHANNEL

FIGURE 32

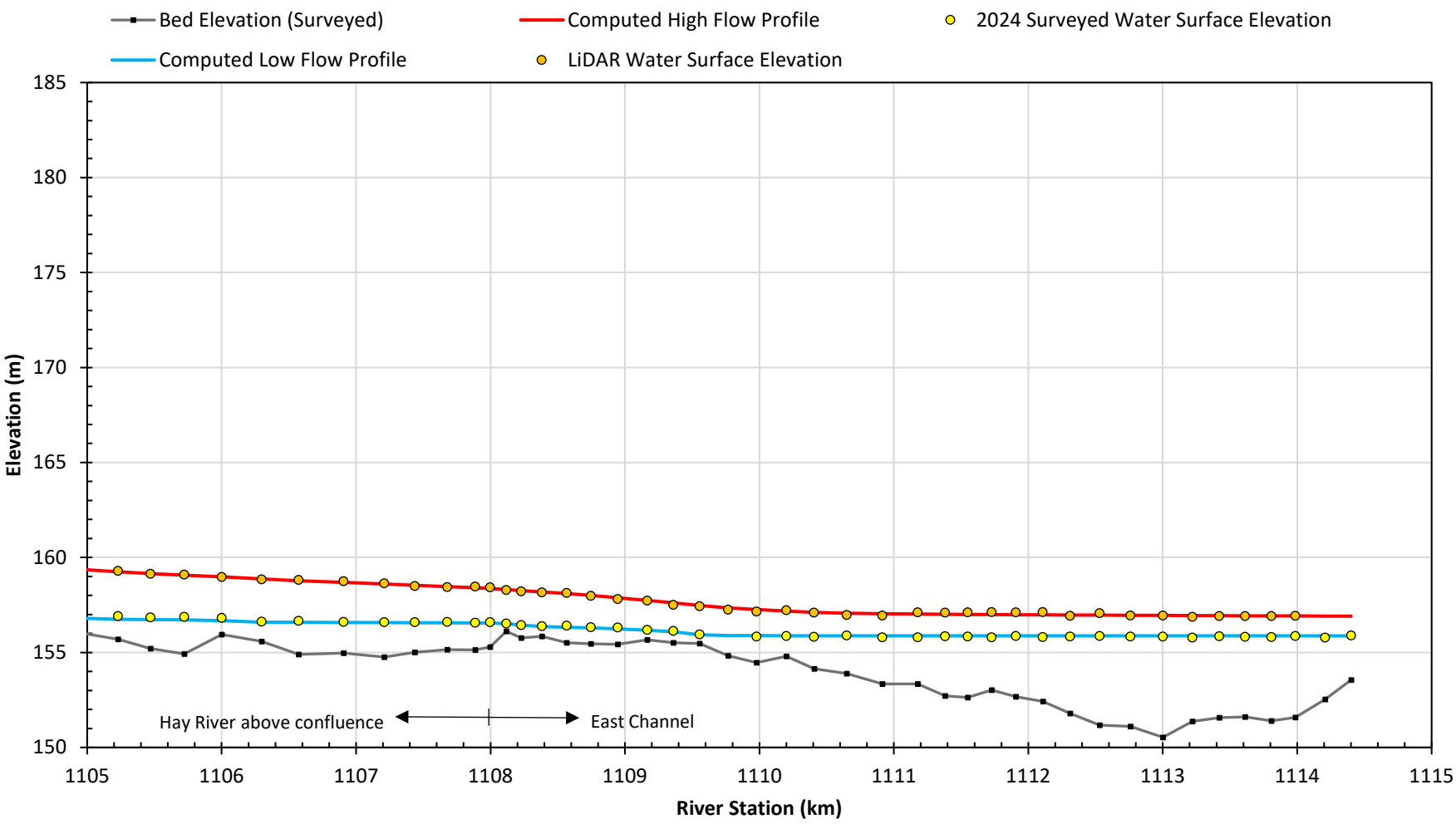

Government of Northwest Territories
Gouvernement des Territoires du Nord-Ouest

Canada

nhc

UNITS – AS SHOWN

VERTICAL ELEVATION DATUM: CGVD2013a

Job: 1008469

Date: Feb-2025

KÁTŁ'ODEH (HAY RIVER)
FLOOD HAZARD MAPPING STUDY

OPEN WATER CALIBRATION PROFILES
HAY RIVER MAIN AND EAST CHANNELS

FIGURE 33

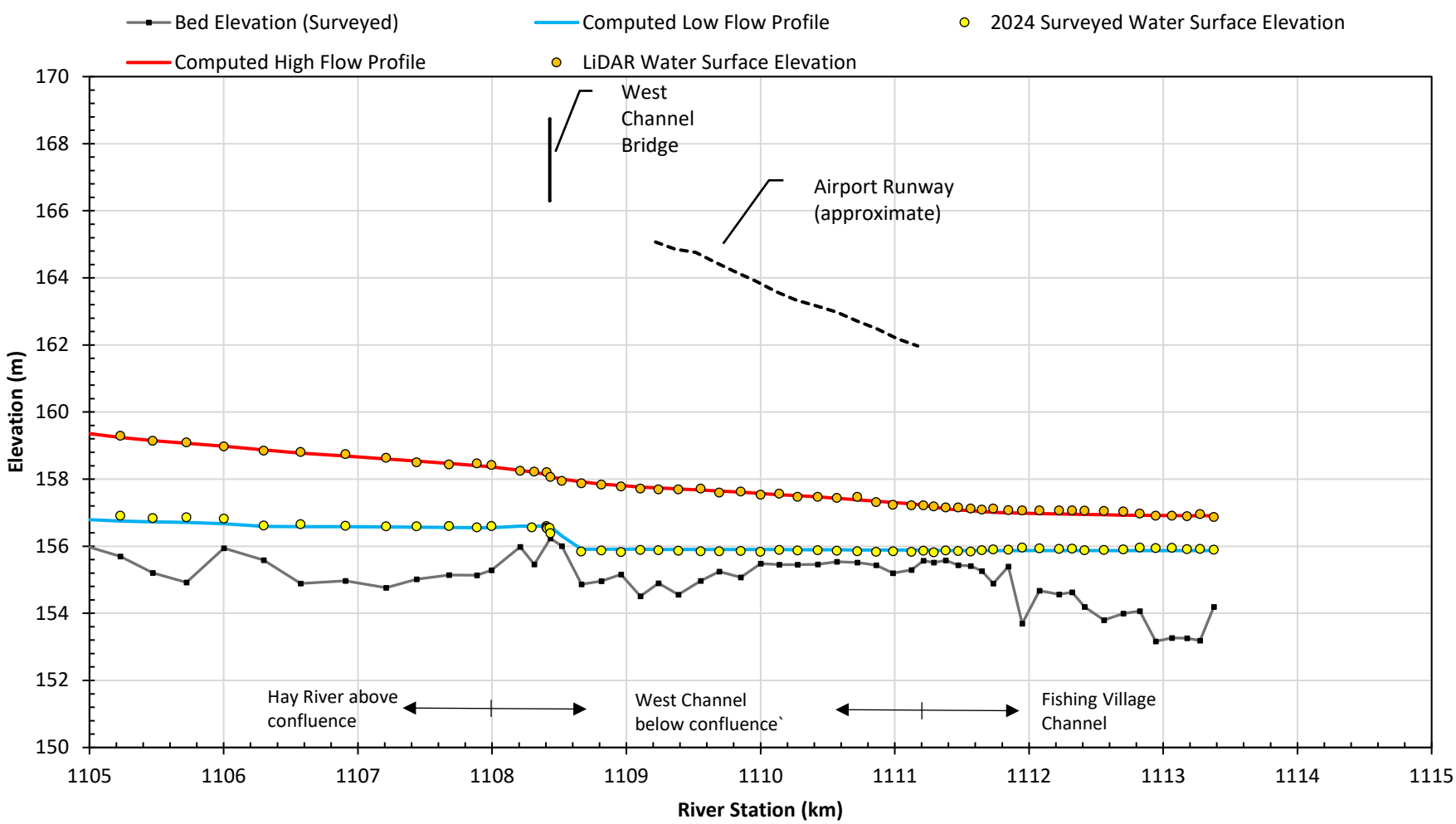

Government of Northwest Territories
Gouvernement des Territoires du Nord-Ouest

Canada

nhc

UNITS – AS SHOWN

VERTICAL ELEVATION DATUM: CGVD2013a

Job: 1008469

Date: Feb-2025

KÁTŁ'ODEH (HAY RIVER)
FLOOD HAZARD MAPPING STUDY

OPEN WATER CALIBRATION PROFILES
HAY RIVER WEST AND WEST FISHING VILLAGE CHANNELS

FIGURE 34

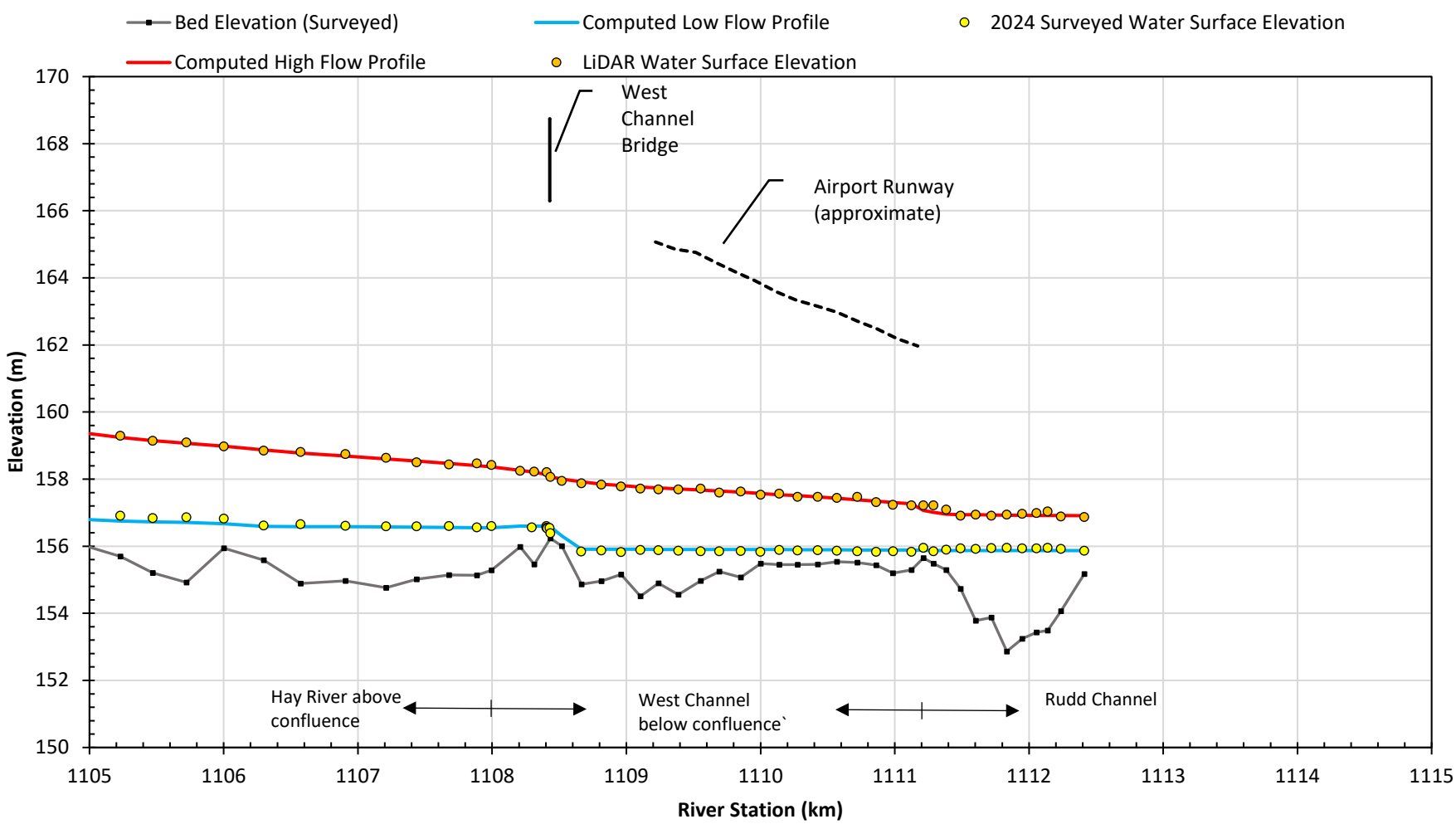

Government of Northwest Territories
Gouvernement des Territoires du Nord-Ouest

Canada

nhc

UNITS – AS SHOWN

VERTICAL ELEVATION DATUM: CGVD2013a

Job: 1008469

Date: Feb-2025

KÁTŁ'ODEH (HAY RIVER)
FLOOD HAZARD MAPPING STUDY

OPEN WATER CALIBRATION PROFILES
HAY RIVER WEST AND RUDD CHANNELS

FIGURE 35

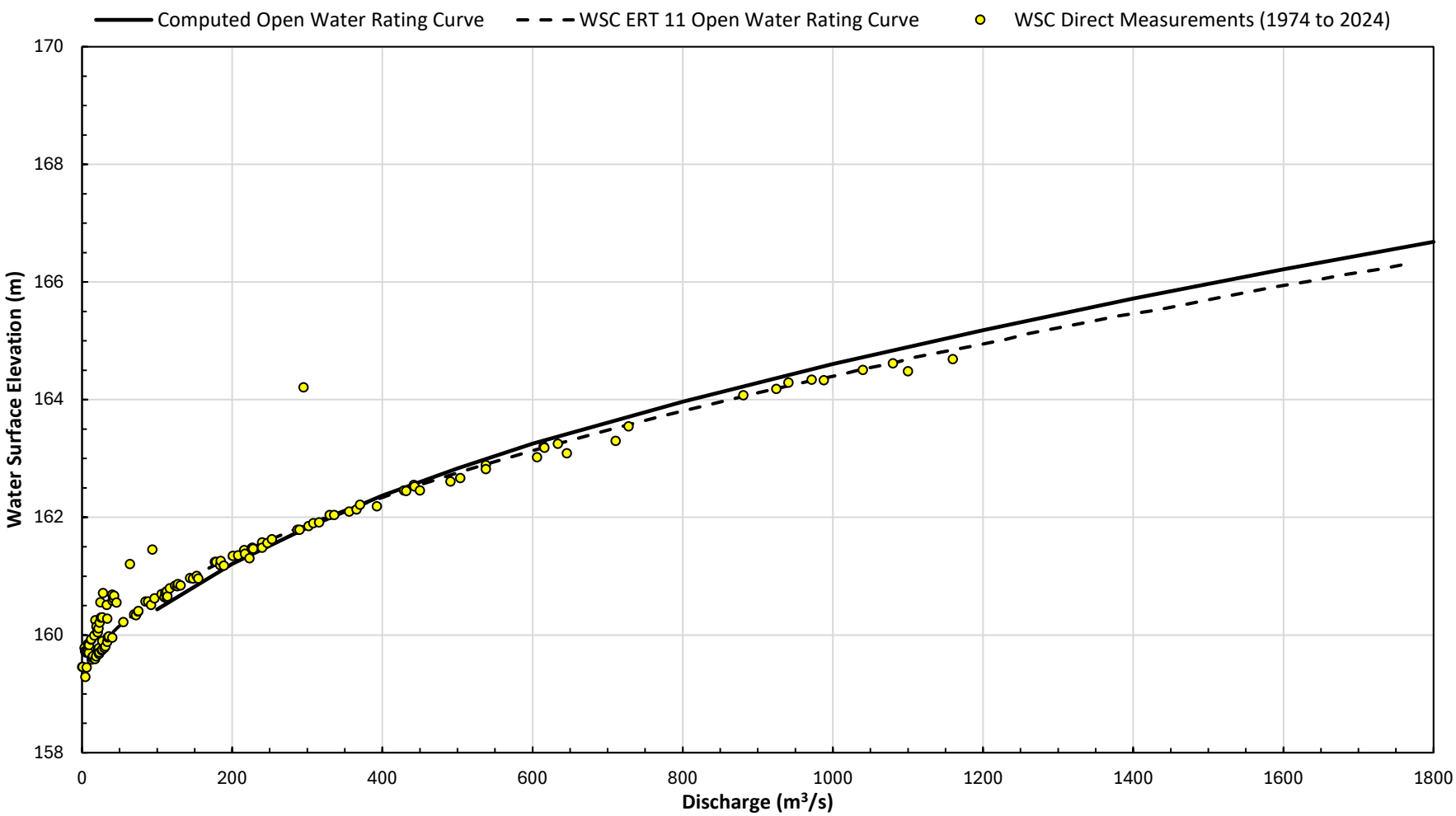

Notes: 1. WSC open water direct measurements are included for reference.

Government of Northwest Territories
Gouvernement des Territoires du Nord-Ouest

Canada

nhc

UNITS – AS SHOWN

VERTICAL ELEVATION DATUM: CGVD2013a

Job: 1008469

Date: Feb-2025

KÁTŁ'ODEH (HAY RIVER)
FLOOD HAZARD MAPPING STUDY

OPEN WATER RATING CURVE CALIBRATION RESULTS
#07OB001 HAY RIVER NEAR HAY RIVER

FIGURE 36

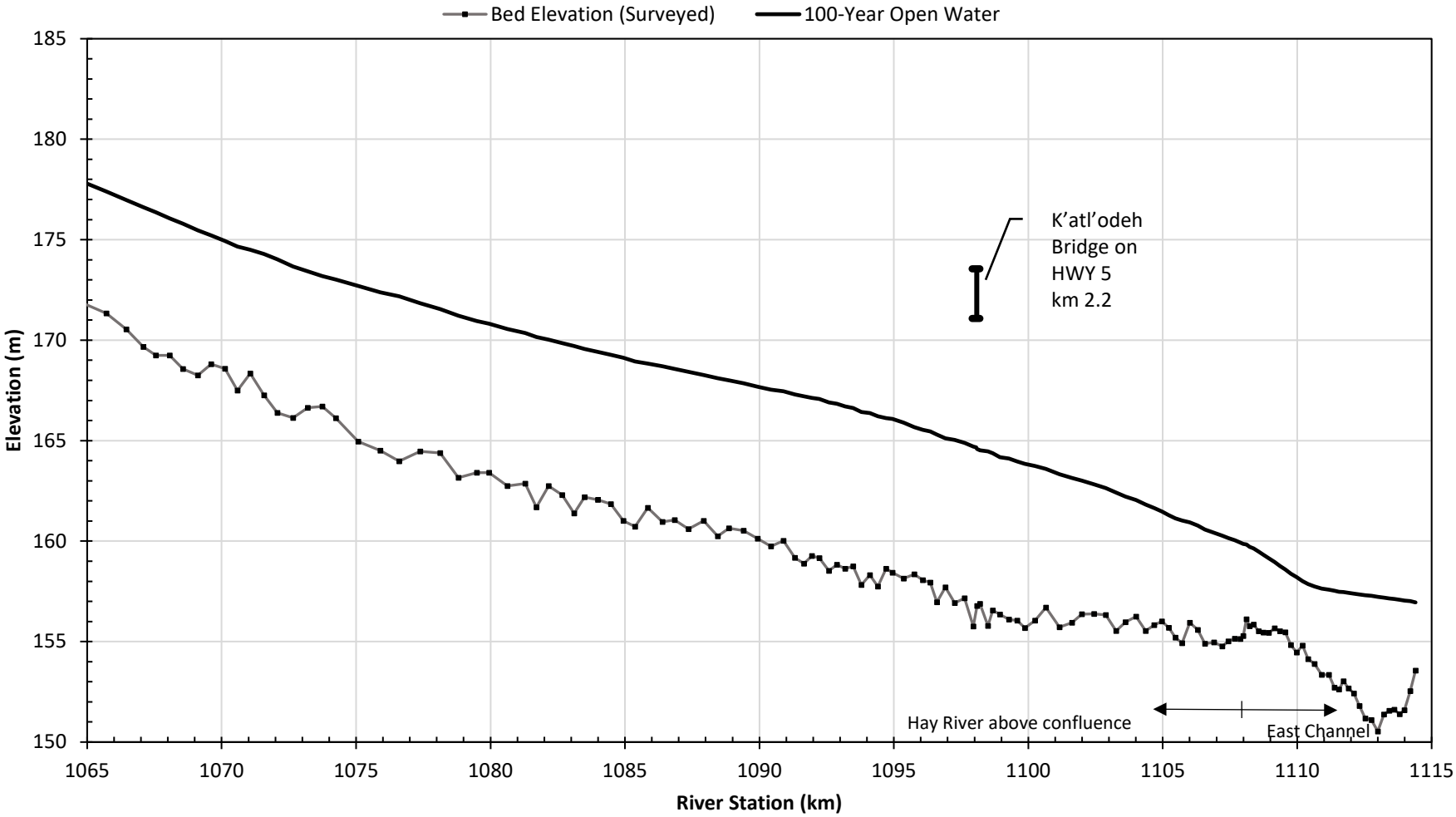

Government of Northwest Territories
Gouvernement des Territoires du Nord-Ouest

Canada

nhc

UNITS – AS SHOWN

VERTICAL ELEVATION DATUM: CGVD2013a

Job: 1008469

Date: Feb-2025

KÁTŁ'ODEH (HAY RIVER)
FLOOD HAZARD MAPPING STUDY

100-YEAR OPEN WATER FLOOD FREQUENCY PROFILE
HAY RIVER MAIN AND EAST CHANNELS

FIGURE 37

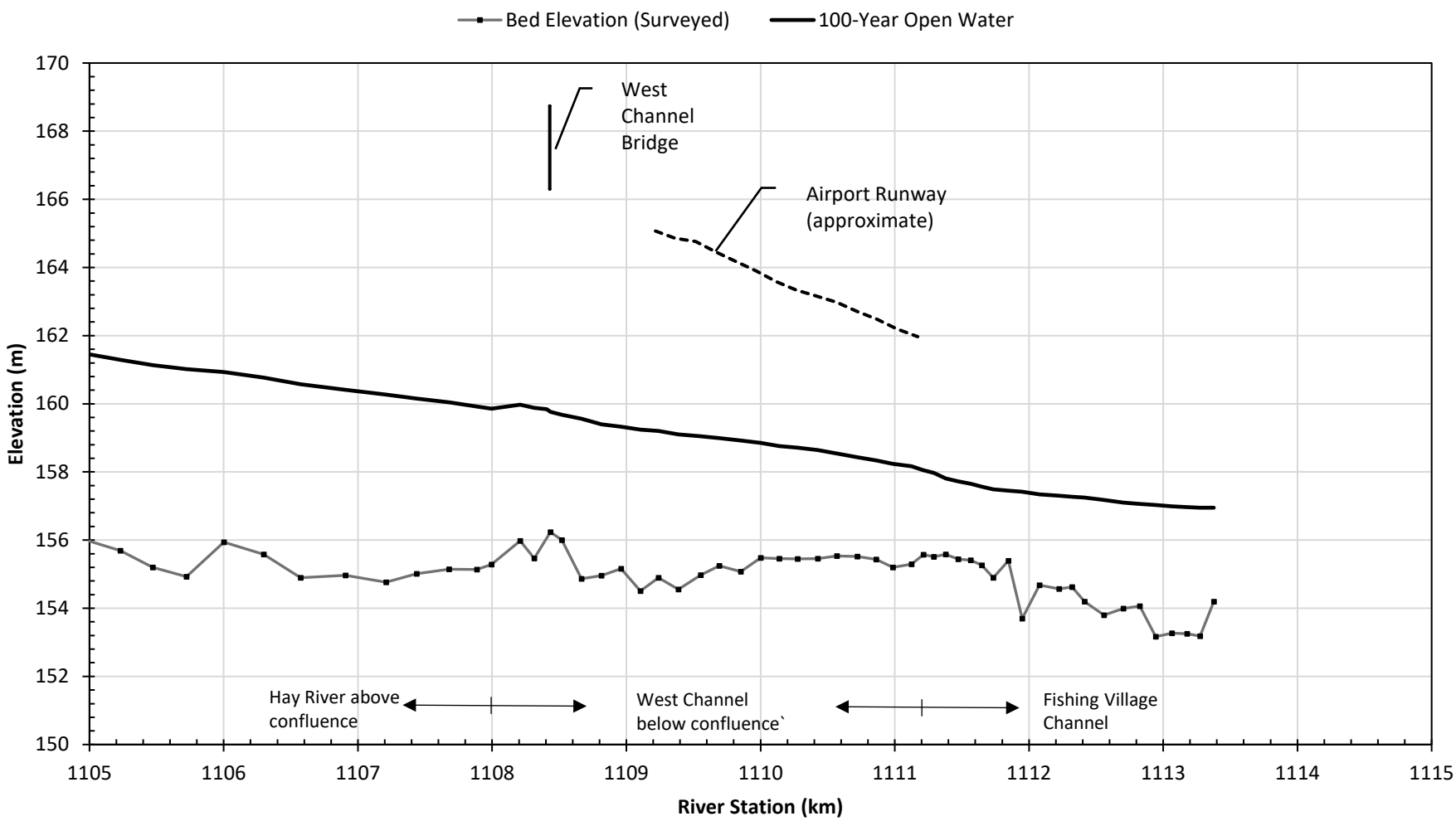

Government of Northwest Territories
Gouvernement des Territoires du Nord-Ouest

Canada

nhc

UNITS – AS SHOWN

VERTICAL ELEVATION DATUM: CGVD2013a

Job: 1008469

Date: Feb-2025

KÁTŁ'ODEH (HAY RIVER)
FLOOD HAZARD MAPPING STUDY

100-YEAR OPEN WATER FLOOD FREQUENCY PROFILE HAY RIVER WEST AND WEST FISHING VILLAGE CHANNELS

FIGURE 38

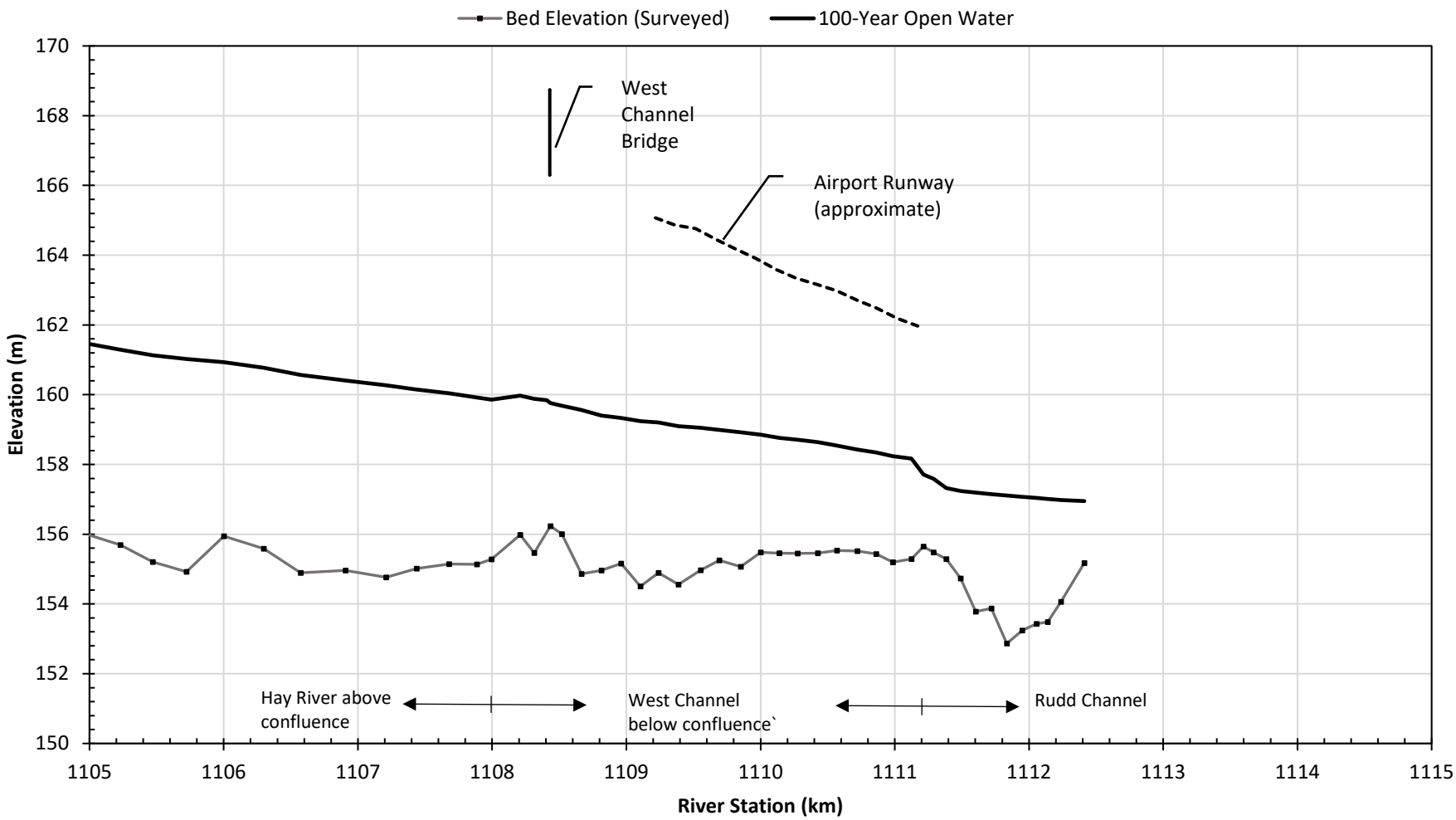

Government of Northwest Territories
Gouvernement des Territoires du Nord-Ouest

Canada

nhc

UNITS – AS SHOWN

VERTICAL ELEVATION DATUM: CGVD2013a

Job: 1008469

Date: Feb-2025

KÁTŁ'ODEH (HAY RIVER)
FLOOD HAZARD MAPPING STUDY

100-YEAR OPEN WATER FLOOD FREQUENCY PROFILE HAY RIVER WEST AND RUDD CHANNELS

FIGURE 39

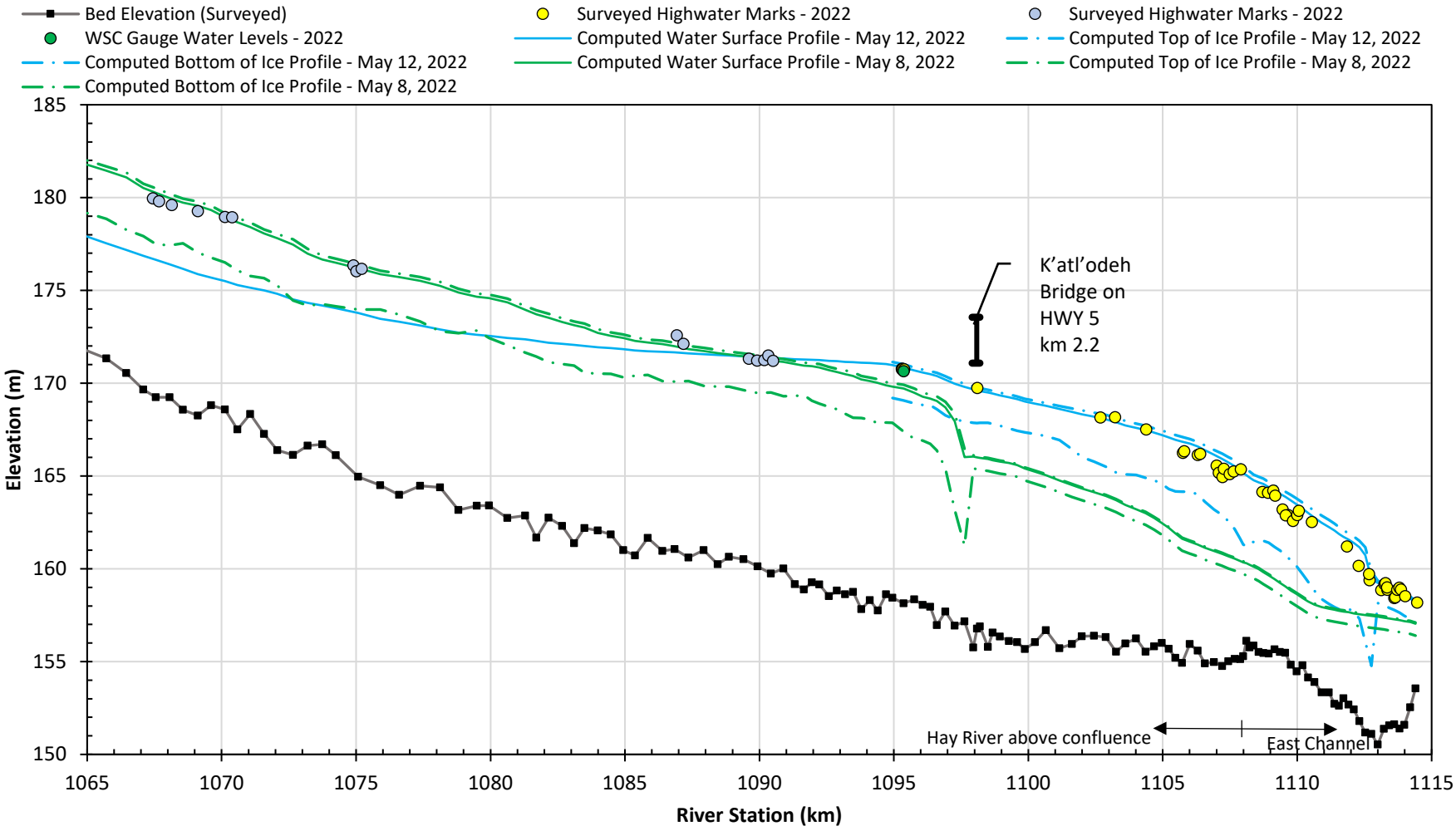

Government of Northwest Territories
Gouvernement des Territoires du Nord-Ouest

Canada

nhc

UNITS – AS SHOWN

VERTICAL ELEVATION DATUM: CGVD2013a

Job: 1008469

Date: Feb-2025

KÁTŁ'ODEH (HAY RIVER)
FLOOD HAZARD MAPPING STUDY

2022 ICE JAM CALIBRATION PROFILES
HAY RIVER MAIN AND EAST CHANNELS

FIGURE 40

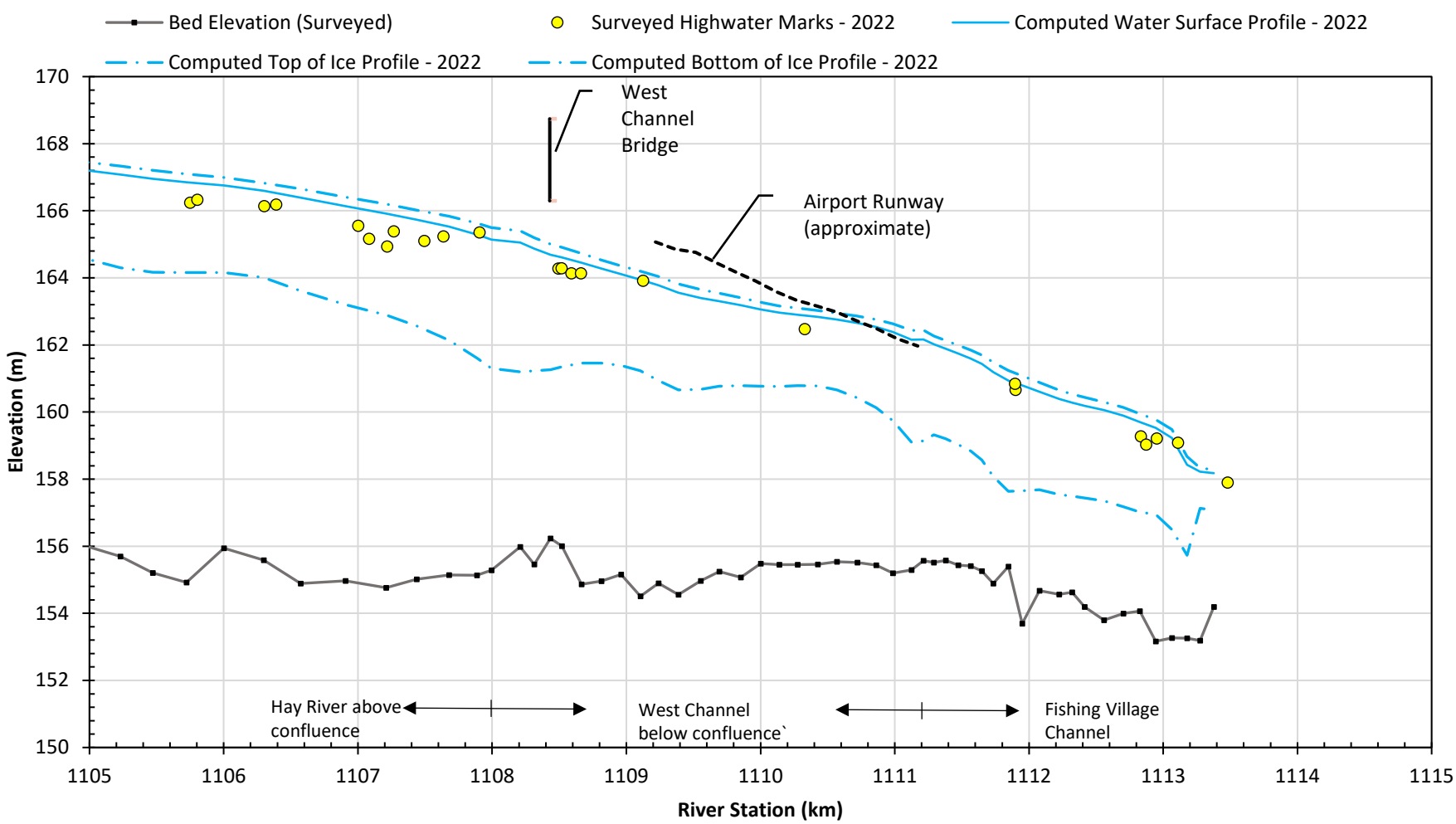

Government of Northwest Territories / Gouvernement des Territoires du Nord-Ouest

Canada

nhc

UNITS – AS SHOWN

VERTICAL ELEVATION DATUM: CGVD2013a

Job: 1008469

Date: Feb-2025

KÁTŁ'ODEH (HAY RIVER)
FLOOD HAZARD MAPPING STUDY

2022 ICE JAM CALIBRATION PROFILE
HAY RIVER WEST AND WEST FISHING VILLAGE CHANNELS

FIGURE 41

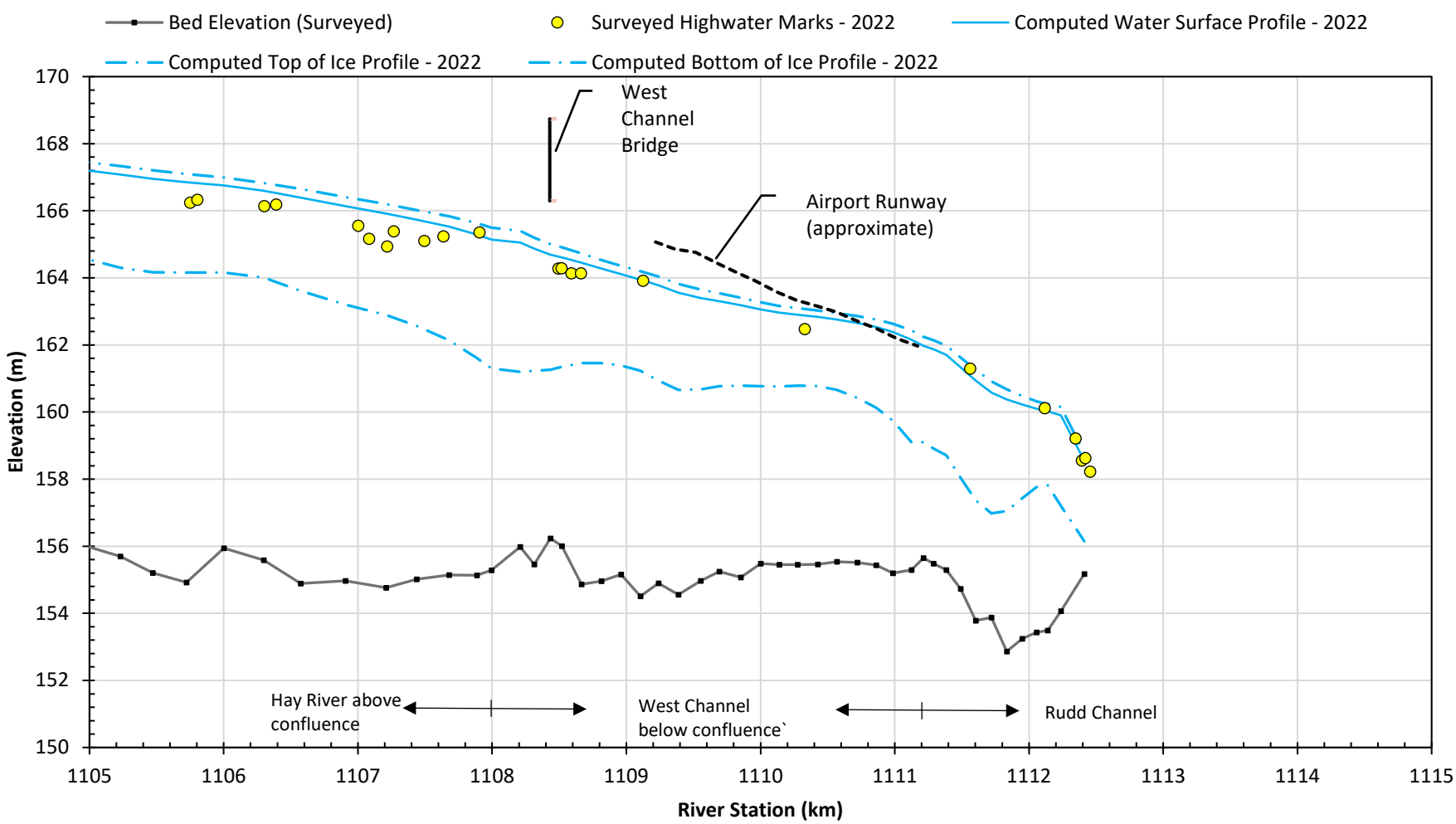

Government of Northwest Territories / Gouvernement des Territoires du Nord-Ouest

Canada

nhc

UNITS – AS SHOWN

VERTICAL ELEVATION DATUM: CGVD2013a

Job: 1008469

Date: Feb-2025

KÁTŁ'ODEH (HAY RIVER)
FLOOD HAZARD MAPPING STUDY

2022 ICE JAM CALIBRATION PROFILE
HAY RIVER WEST AND RUDD CHANNELS

FIGURE 42

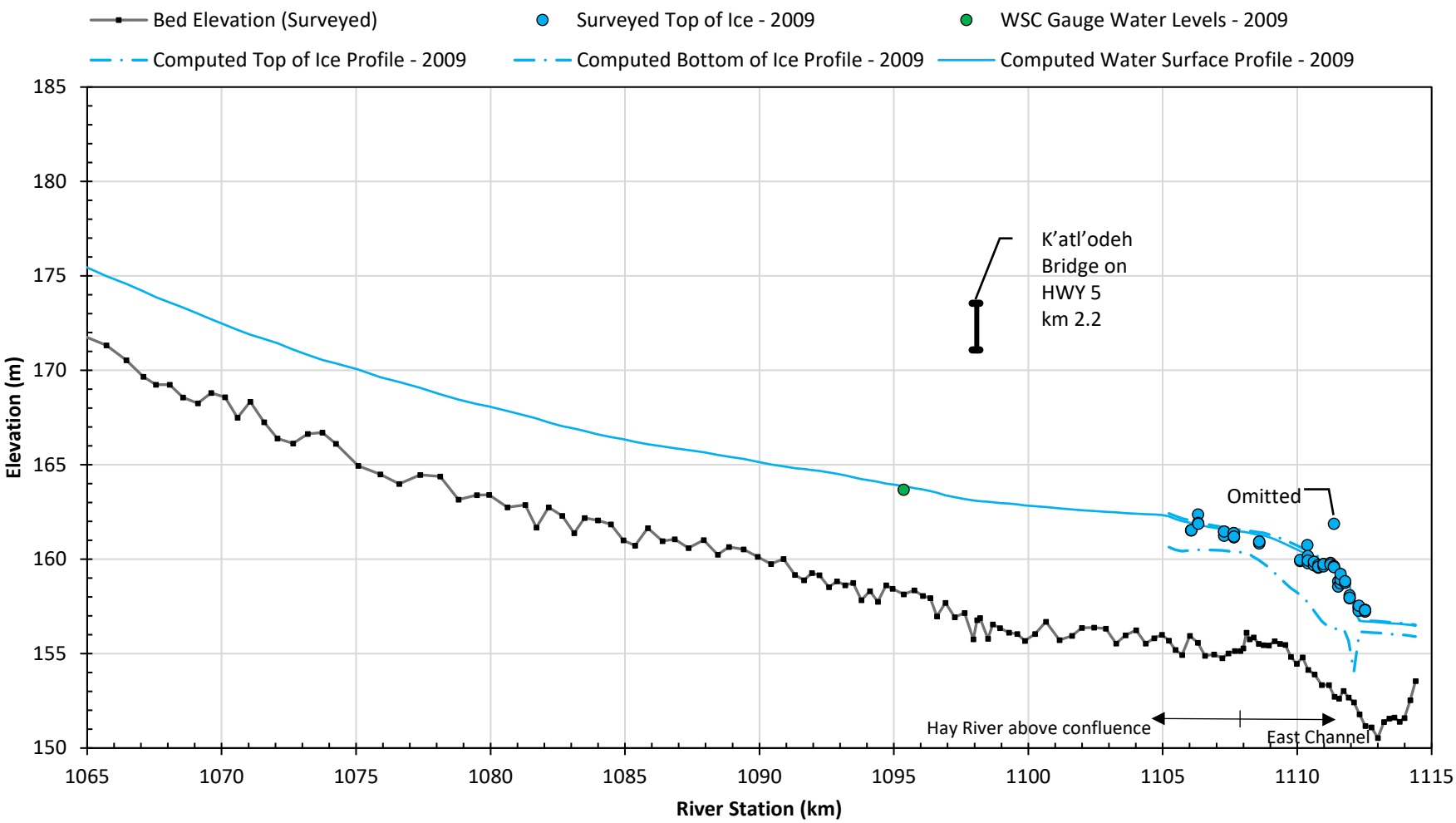

Notes: 1. The data point labelled "omitted" was excluded from NHC's ice jam calibration as it appears inconsistent with expected top of ice profiles when compared to surrounding top of ice observations.

Government of Northwest Territories
Gouvernement des Territoires du Nord-Ouest

Canada

nhc

UNITS – AS SHOWN

VERTICAL ELEVATION DATUM: CGVD2013a

Job: 1008469

Date: Feb-2025

KÁTŁ'ODEH (HAY RIVER)
FLOOD HAZARD MAPPING STUDY

2009 ICE JAM CALIBRATION PROFILE
HAY RIVER MAIN AND EAST CHANNELS

FIGURE 43

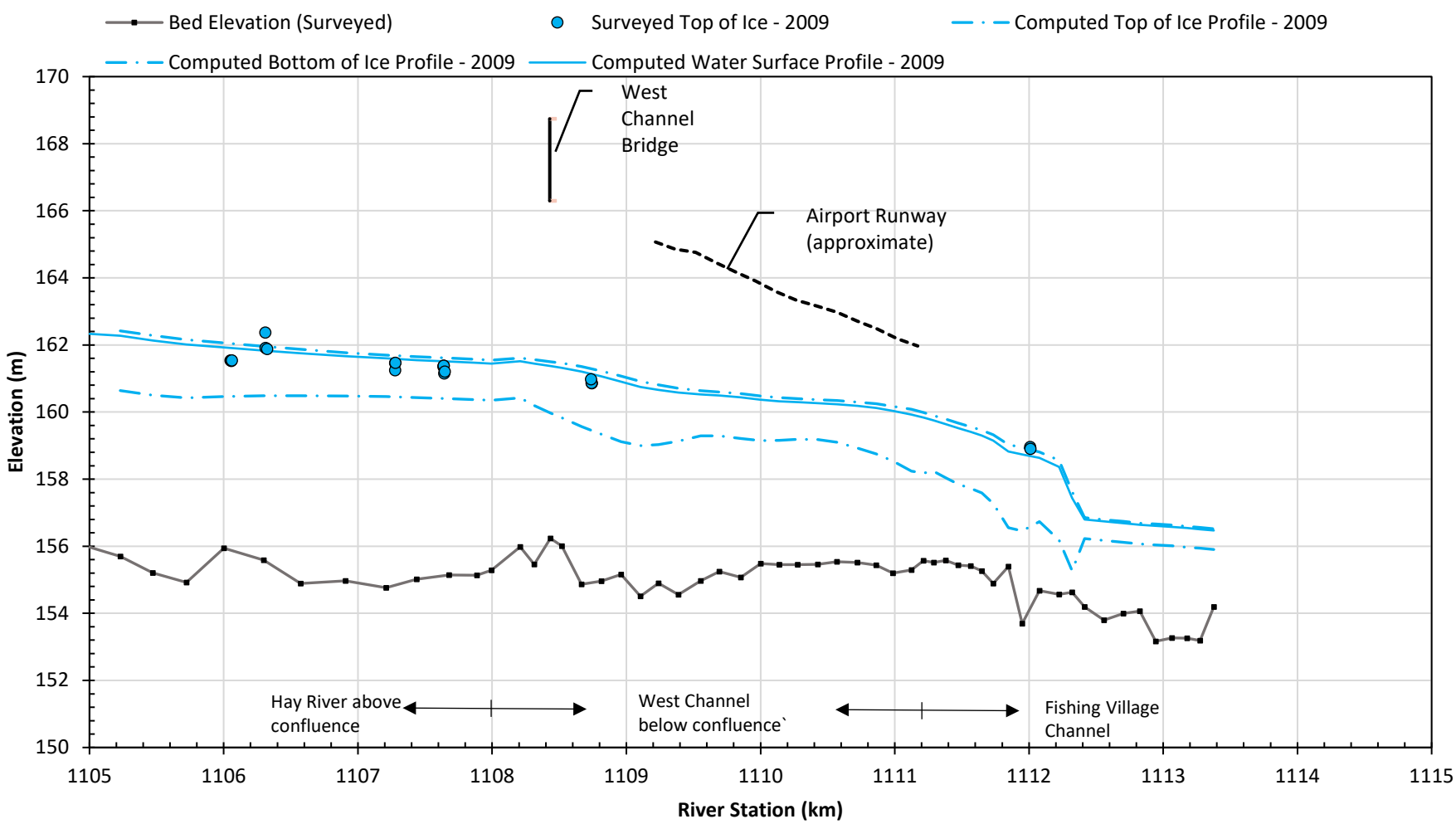

Government of Northwest Territories
Gouvernement des Territoires du Nord-Ouest

Canada

nhc

UNITS – AS SHOWN

VERTICAL ELEVATION DATUM: CGVD2013a

Job: 1008469

Date: Feb-2025

KÁTŁ'ODEH (HAY RIVER)
FLOOD HAZARD MAPPING STUDY

2009 ICE JAM CALIBRATION PROFILE
HAY RIVER WEST AND WEST FISHING VILLAGE CHANNELS

FIGURE 44

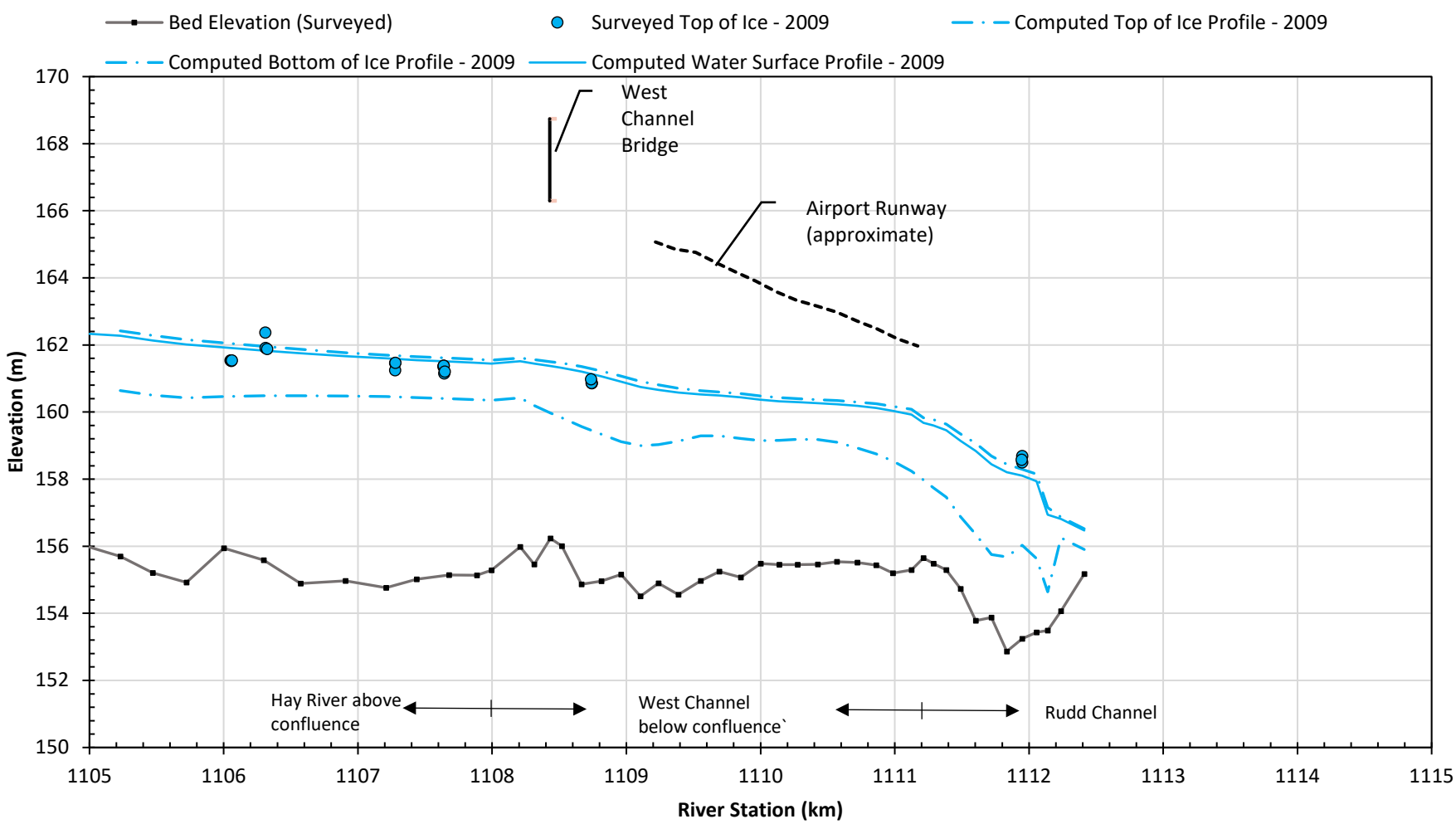

Government of Northwest Territories
Gouvernement des Territoires du Nord-Ouest

Canada

nhc

UNITS – AS SHOWN

VERTICAL ELEVATION DATUM: CGVD2013a

Job: 1008469

Date: Feb-2025

KÁTŁ'ODEH (HAY RIVER)
FLOOD HAZARD MAPPING STUDY

2009 ICE JAM CALIBRATION PROFILE
HAY RIVER WEST AND RUDD CHANNELS

FIGURE 45

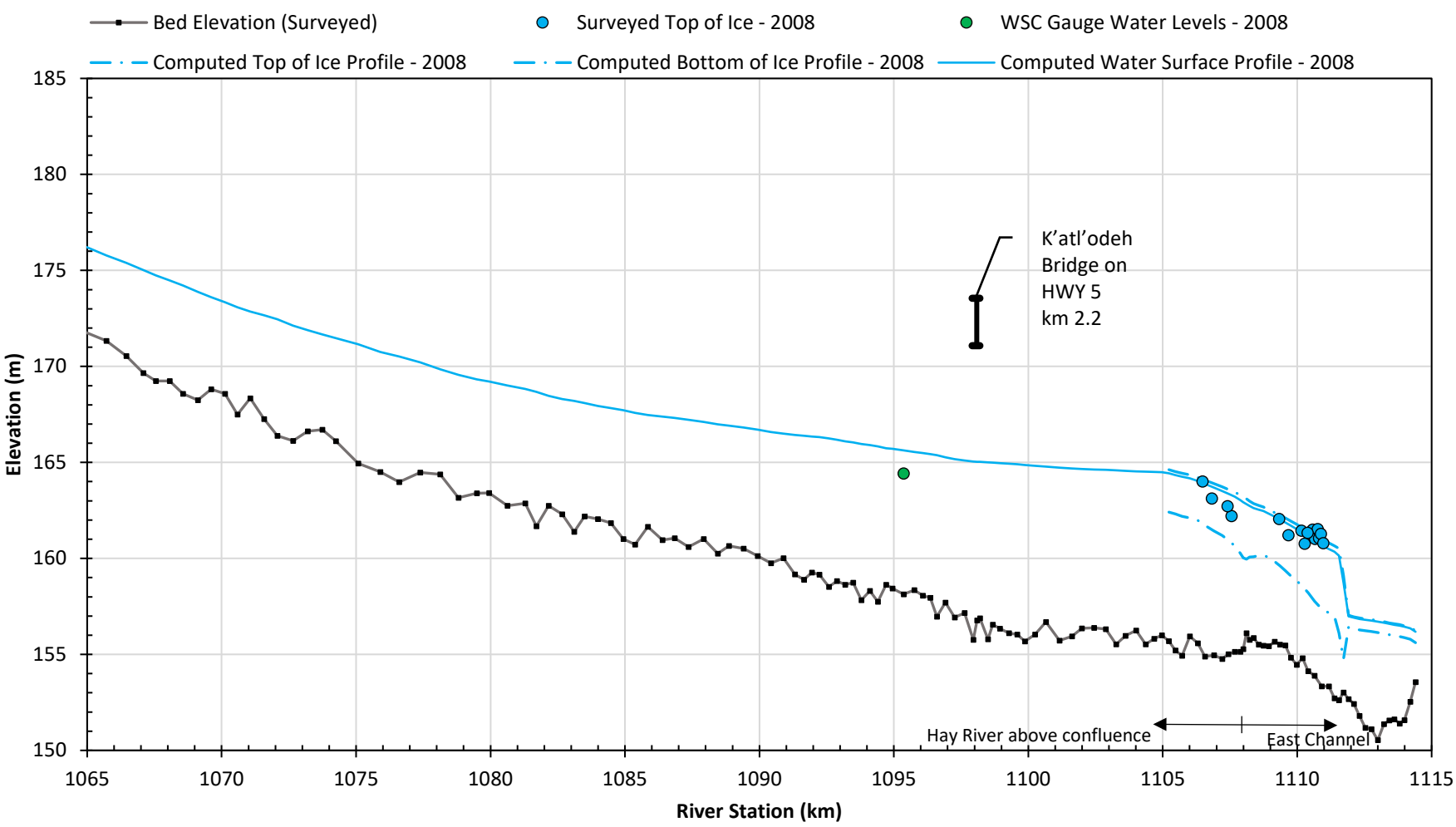

Government of Northwest Territories / Gouvernement des Territoires du Nord-Ouest

Canada

nhc

UNITS – AS SHOWN

VERTICAL ELEVATION DATUM: CGVD2013a

Job: 1008469

Date: Feb-2025

KÁTŁ'ODEH (HAY RIVER)
FLOOD HAZARD MAPPING STUDY

2008 ICE JAM CALIBRATION PROFILE
HAY RIVER MAIN AND EAST CHANNELS

FIGURE 46

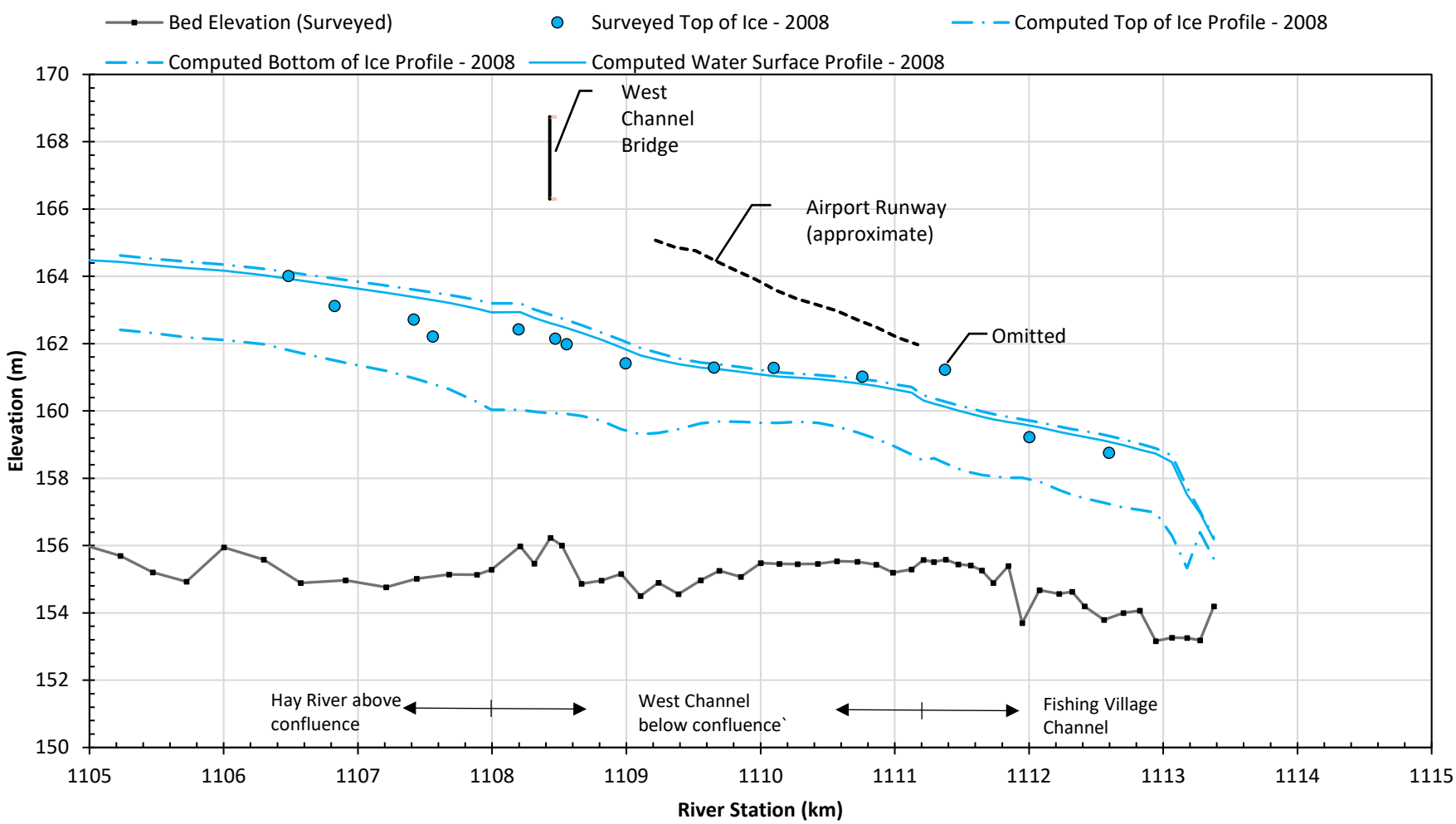

Notes: 1. The data point labelled “omitted” was excluded from NHC’s ice jam calibration as it appears inconsistent with expected top of ice profiles when compared to surrounding top of ice observations.

Government of Northwest Territories / Gouvernement des Territoires du Nord-Ouest

Canada

nhc

UNITS – AS SHOWN

VERTICAL ELEVATION DATUM: CGVD2013a

Job: 1008469

Date: Feb-2025

KÁTŁ’ODEH (HAY RIVER)
FLOOD HAZARD MAPPING STUDY

2008 ICE JAM CALIBRATION PROFILE
HAY RIVER WEST AND WEST FISHING VILLAGE CHANNELS

FIGURE 47

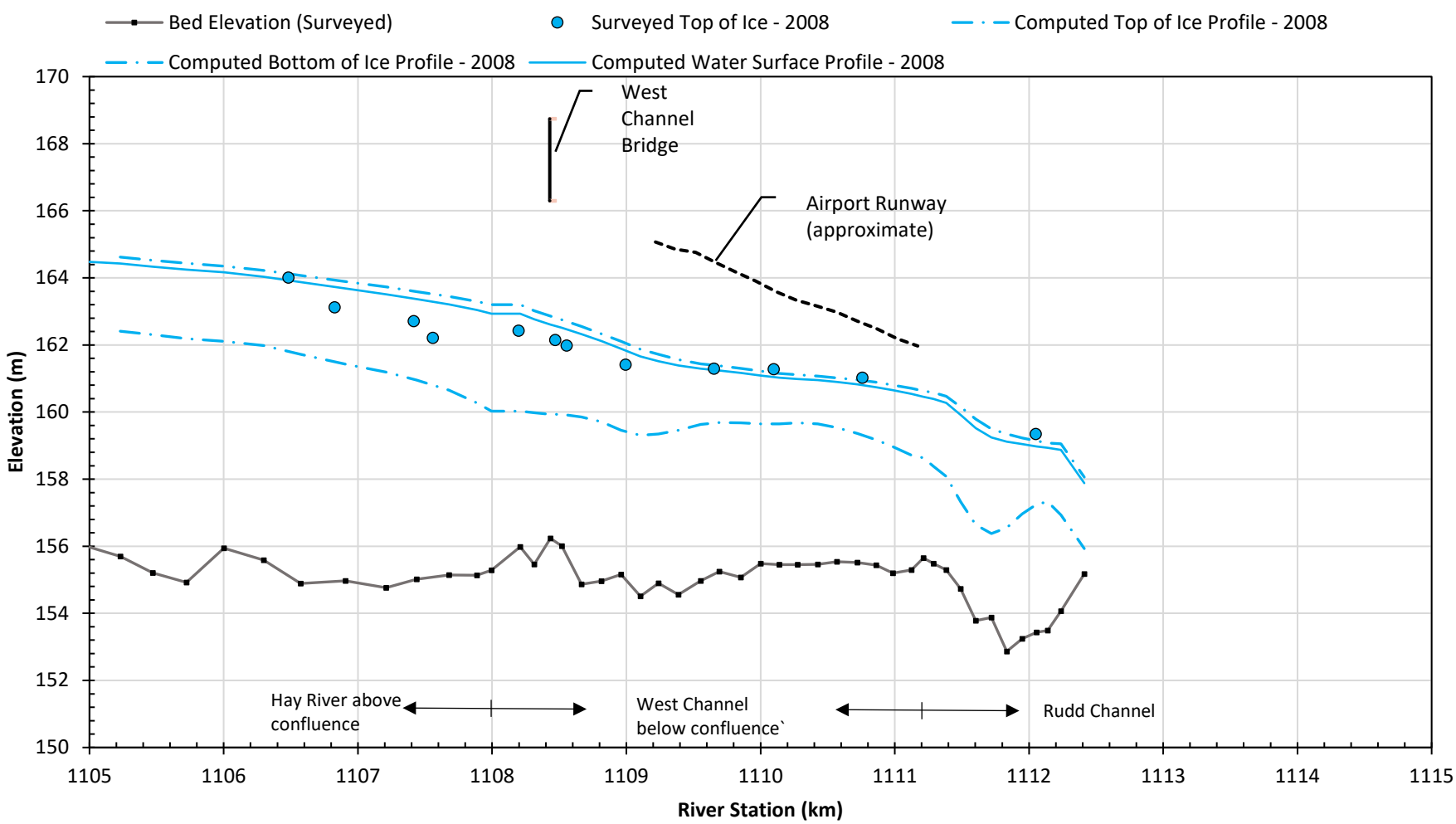

Government of Northwest Territories / Gouvernement des Territoires du Nord-Ouest

Canada

nhc

UNITS – AS SHOWN

VERTICAL ELEVATION DATUM: CGVD2013a

Job: 1008469

Date: Feb-2025

KÁTŁ'ODEH (HAY RIVER)
FLOOD HAZARD MAPPING STUDY

2008 ICE JAM CALIBRATION PROFILE
HAY RIVER WEST AND RUDD CHANNELS

FIGURE 48

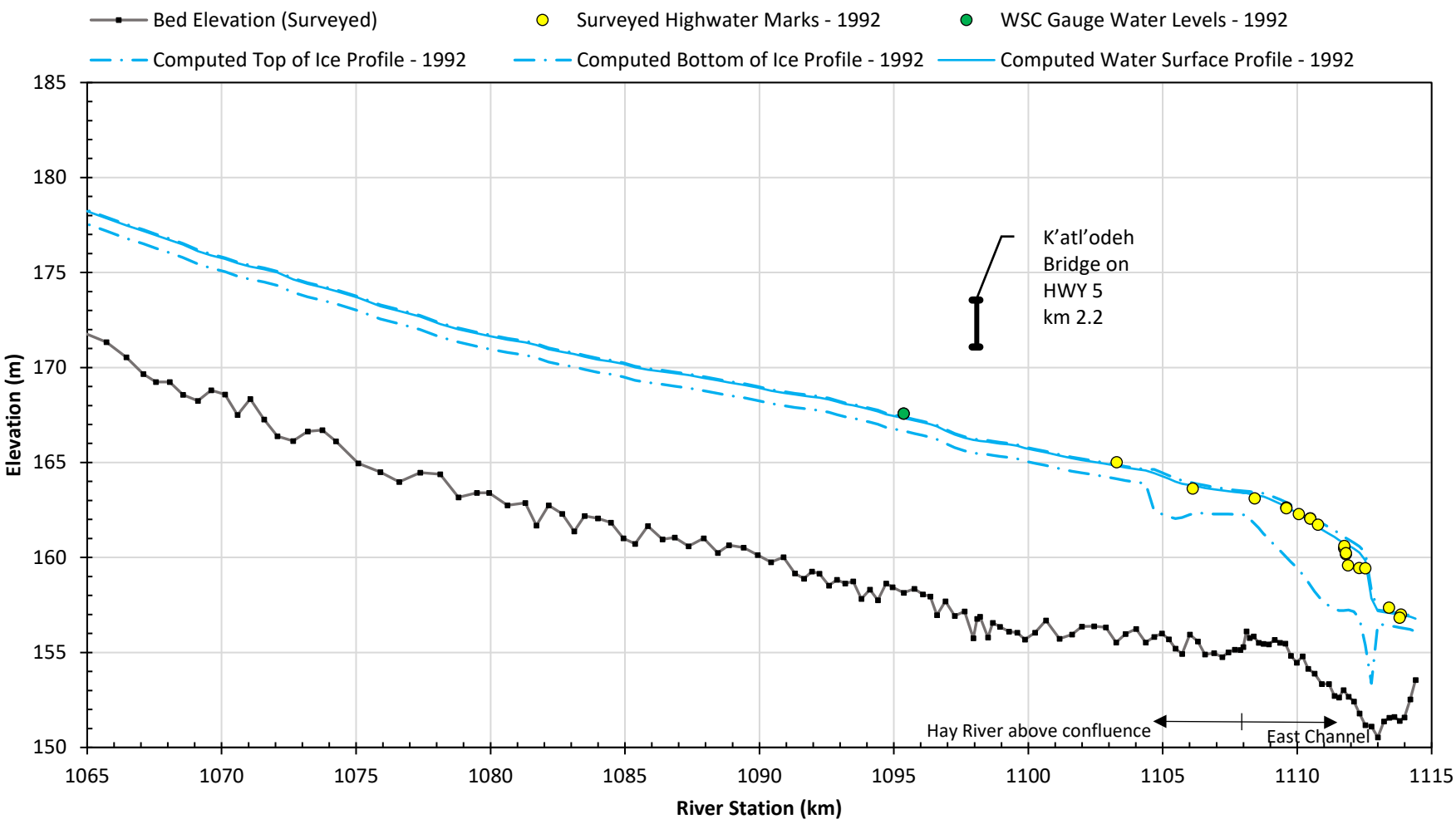

Government of Northwest Territories / Gouvernement des Territoires du Nord-Ouest

Canada

nhc

UNITS – AS SHOWN

VERTICAL ELEVATION DATUM: CGVD2013a

Job: 1008469

Date: Feb-2025

KÁTŁ'ODEH (HAY RIVER)
FLOOD HAZARD MAPPING STUDY

1992 ICE JAM CALIBRATION PROFILE
HAY RIVER MAIN AND EAST CHANNELS

FIGURE 49

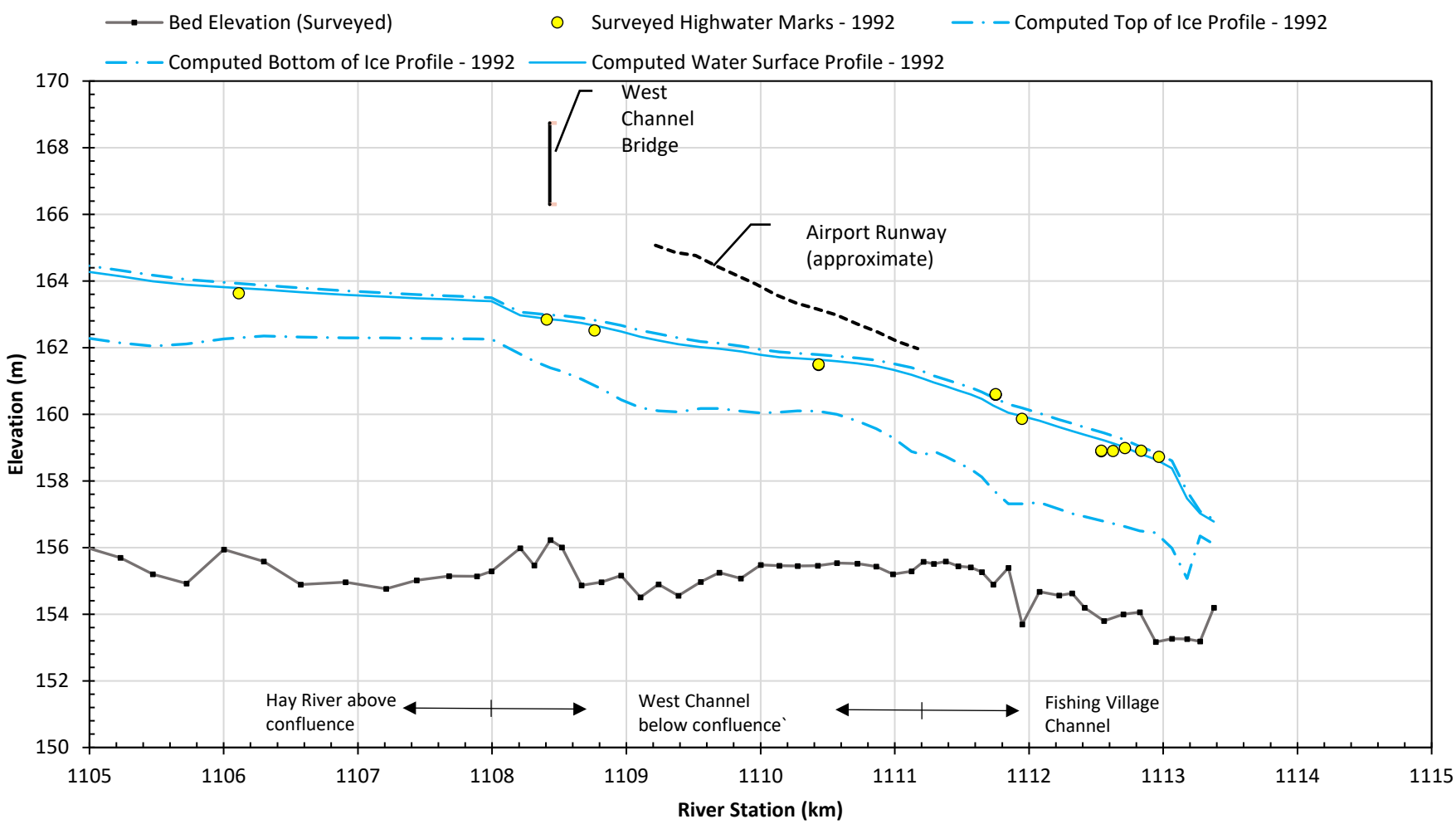

Government of Northwest Territories
Gouvernement des Territoires du Nord-Ouest

Canada

nhc

UNITS – AS SHOWN

VERTICAL ELEVATION DATUM: CGVD2013a

Job: 1008469

Date: Feb-2025

KÁTŁ'ODEH (HAY RIVER)
FLOOD HAZARD MAPPING STUDY

1992 ICE JAM CALIBRATION PROFILE
HAY RIVER WEST AND WEST FISHING VILLAGE CHANNELS

FIGURE 50

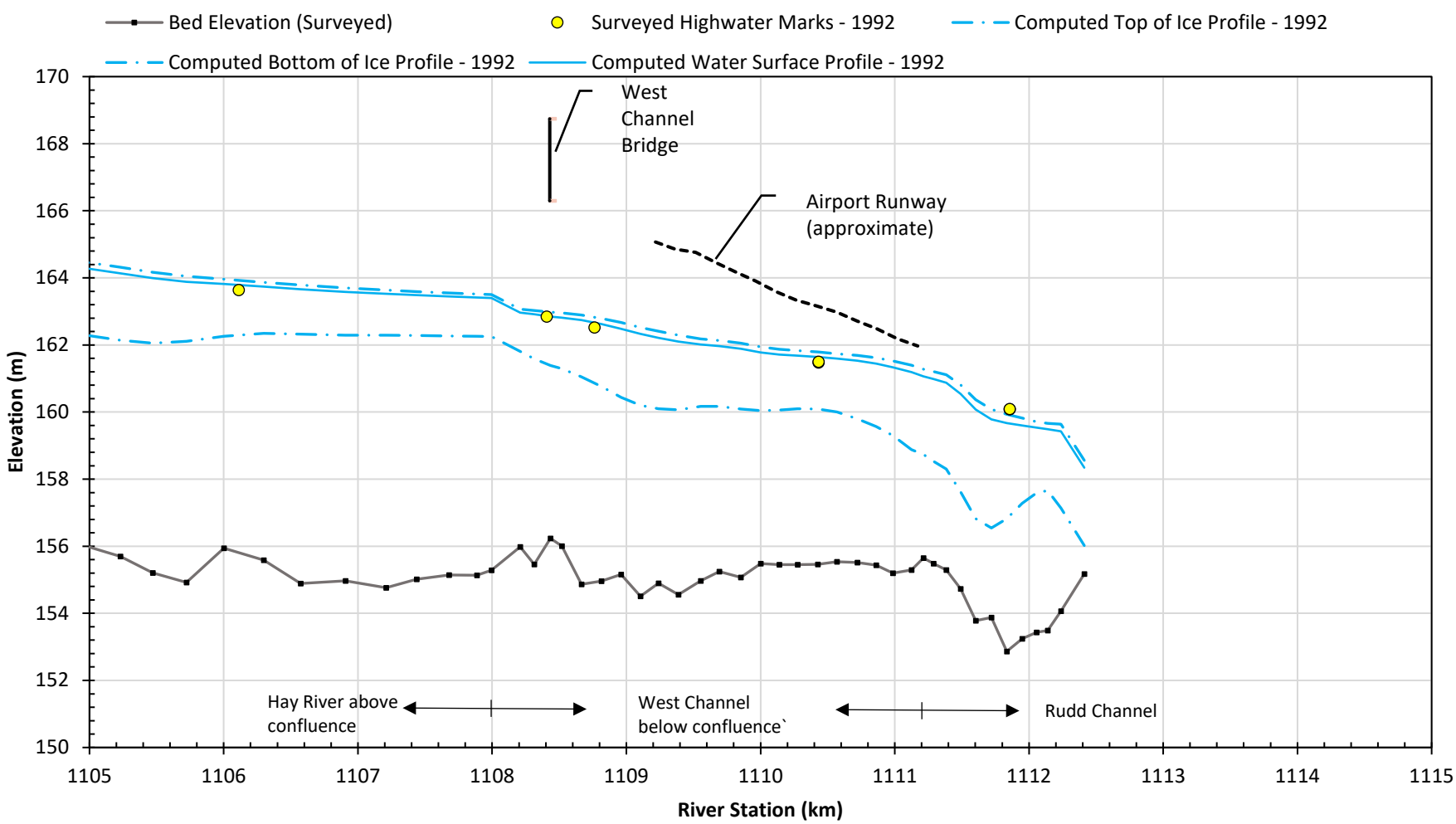

Government of Northwest Territories / Gouvernement des Territoires du Nord-Ouest

Canada

nhc

UNITS – AS SHOWN

VERTICAL ELEVATION DATUM: CGVD2013a

Job: 1008469

Date: Feb-2025

KÁTŁ'ODEH (HAY RIVER)
FLOOD HAZARD MAPPING STUDY

1992 ICE JAM CALIBRATION PROFILE
HAY RIVER WEST AND RUDD CHANNELS

FIGURE 51

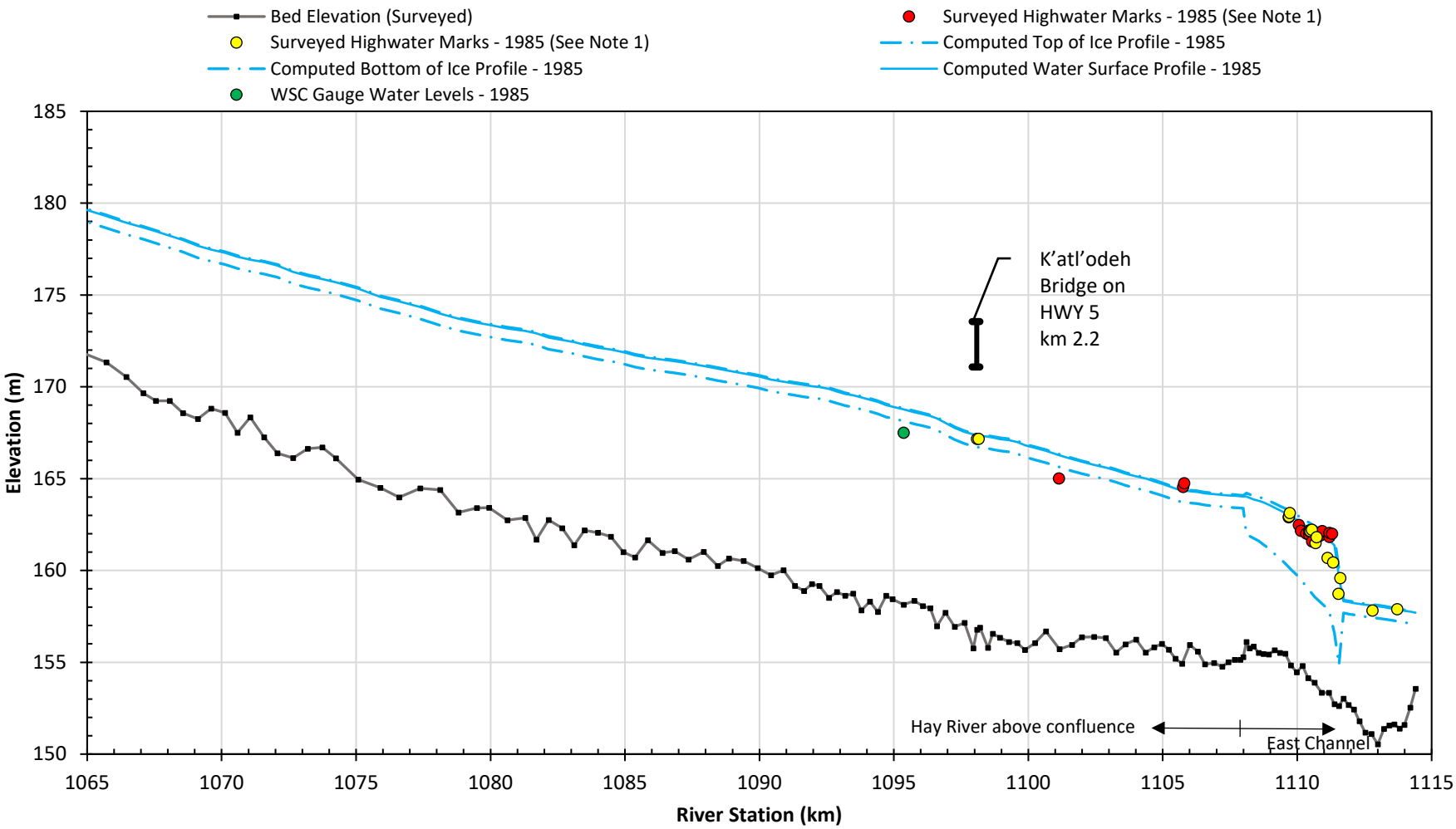

Notes: 1. NHC's ice jam calibration followed highwater marks (yellow points) that were considered to result from active river flow and associated with the peak water level. NHC excluded highwater marks (red points) from calibration that were due to overtopping of intact structures (i.e., roads and berms), top of ice data, or collected after the water receded, as indicated in the Underhill Engineering Ltd. (1985) report.

Government of Northwest Territories / Gouvernement des Territoires du Nord-Ouest

Canada

nhc

UNITS – AS SHOWN

VERTICAL ELEVATION DATUM: CGVD2013a

Job: 1008469

Date: Feb-2025

KÁTŁ'ODEH (HAY RIVER)
FLOOD HAZARD MAPPING STUDY

1985 ICE JAM CALIBRATION PROFILE
HAY RIVER MAIN AND EAST CHANNELS

FIGURE 52

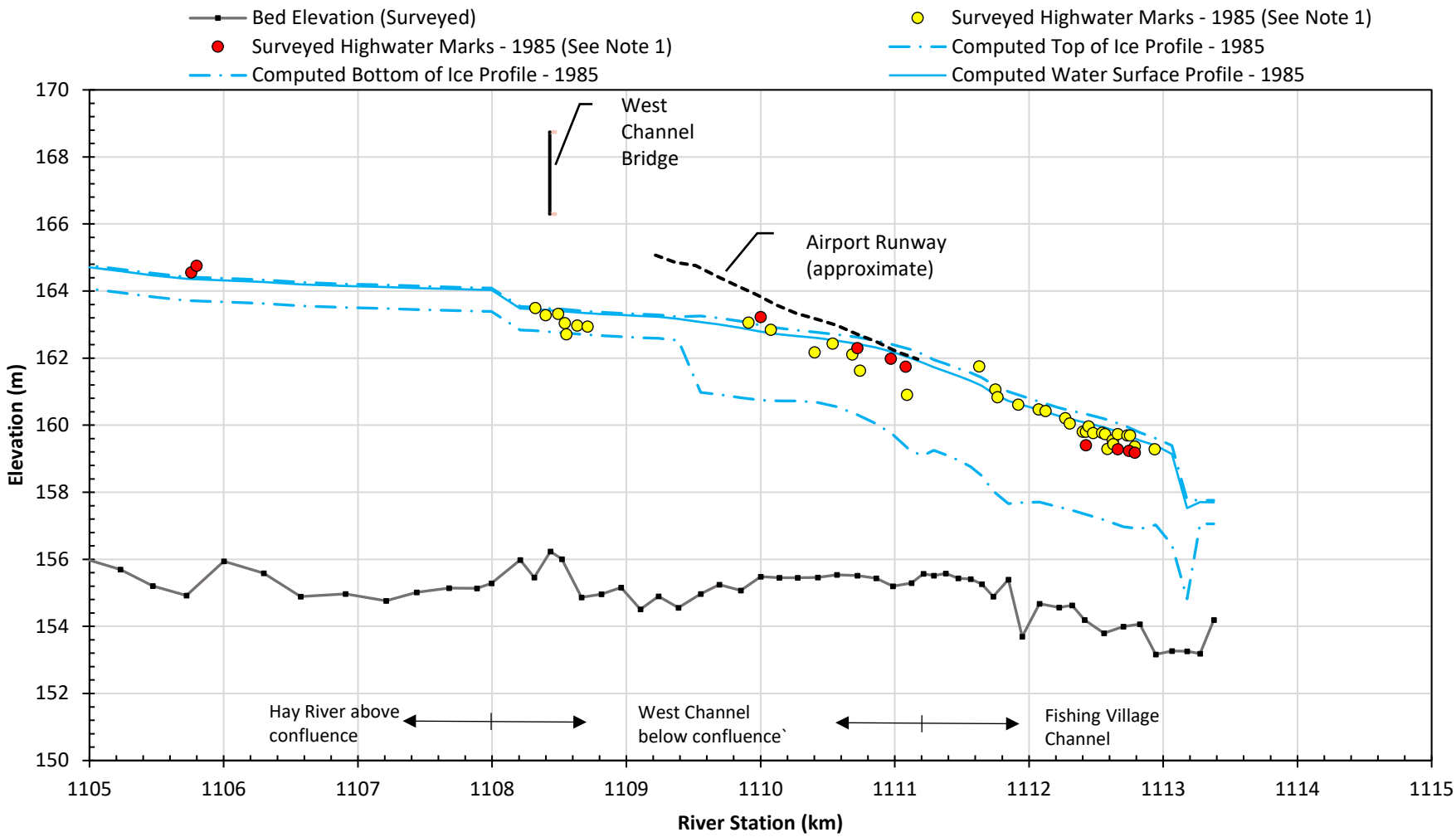

Notes: 1. NHC's ice jam calibration followed highwater marks (yellow points) that were considered to result from active river flow and associated with the peak water level. NHC excluded highwater marks (red points) from calibration that were due to overtopping of intact structures (i.e., roads and berms), top of ice data, or collected after the water receded, as indicated in the Underhill Engineering Ltd. (1985) report.

Government of Northwest Territories / Gouvernement des Territoires du Nord-Ouest

Canada

nhc

UNITS – AS SHOWN

VERTICAL ELEVATION DATUM: CGVD2013a

Job: 1008469

Date: Feb-2025

KÁTŁ'ODEH (HAY RIVER)
FLOOD HAZARD MAPPING STUDY

1985 ICE JAM CALIBRATION PROFILE HAY RIVER WEST AND WEST FISHING VILLAGE CHANNELS

FIGURE 53

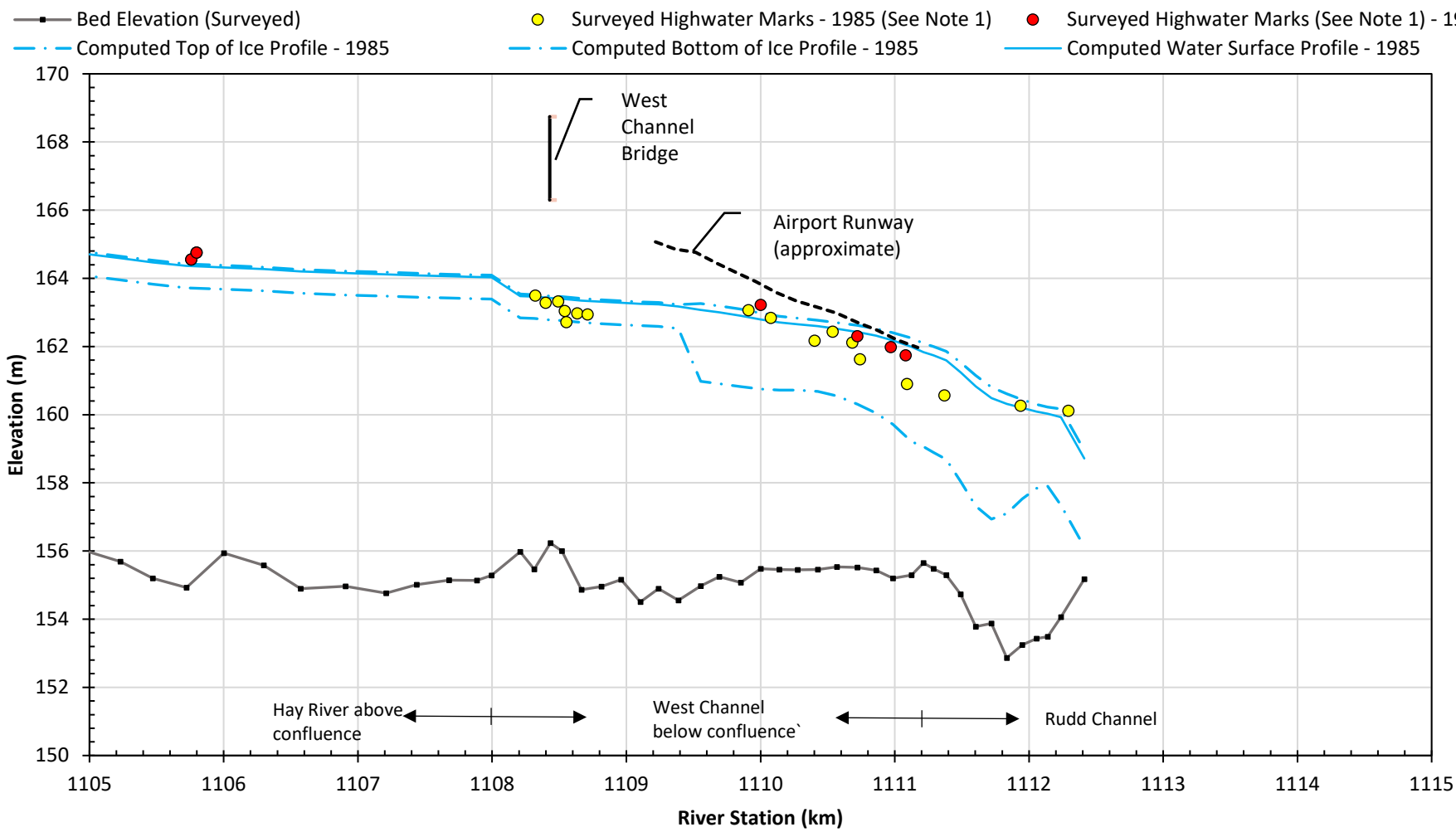

Notes: 1. NHC's ice jam calibration followed highwater marks (yellow points) that were considered to result from active river flow and associated with the peak water level. NHC excluded highwater marks (red points) from calibration that were due to overtopping of intact structures (i.e., roads and berms), top of ice data, or collected after the water receded, as indicated in the Underhill Engineering Ltd. (1985) report.

Government of Northwest Territories
Gouvernement des Territoires du Nord-Ouest
Canada
nhc

UNITS – AS SHOWN
VERTICAL ELEVATION DATUM: CGVD2013a

Job: 1008469 | *Date: Feb-2025*

KÁTŁ'ODEH (HAY RIVER)
FLOOD HAZARD MAPPING STUDY

1985 ICE JAM CALIBRATION PROFILE
HAY RIVER WEST AND RUDD CHANNELS

FIGURE 54

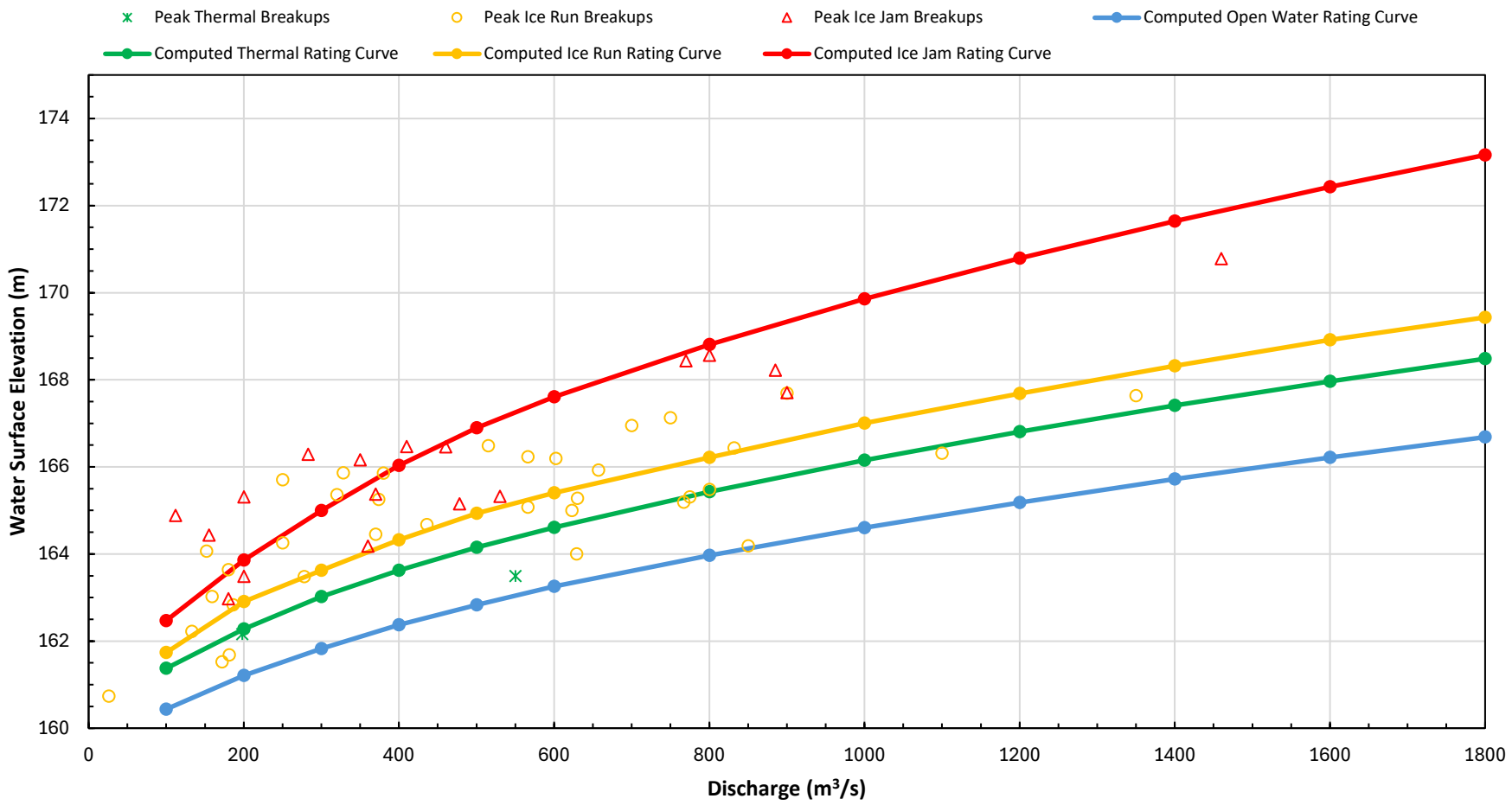

Breakup Type		Number of Historic Events	Percentage of Historic Events
Thermal		3	5%
Mechanical	Ice Run	36	63%
	Ice Jam	18	32%

Notes: 1. Breakup flood levels and discharge were not available for all documented historic breakup events.

Government of Northwest Territories
Gouvernement des Territoires du Nord-Ouest

Canada

nhc

UNITS – AS SHOWN

VERTICAL ELEVATION DATUM: CGVD2013a

Job: 1008469

Date: Feb-2025

KÁTŁ'ODEH (HAY RIVER)
FLOOD HAZARD MAPPING STUDY

BREAKUP RATING CURVES AT #07OB001 HAY RIVER NEAR HAY RIVER

FIGURE 55

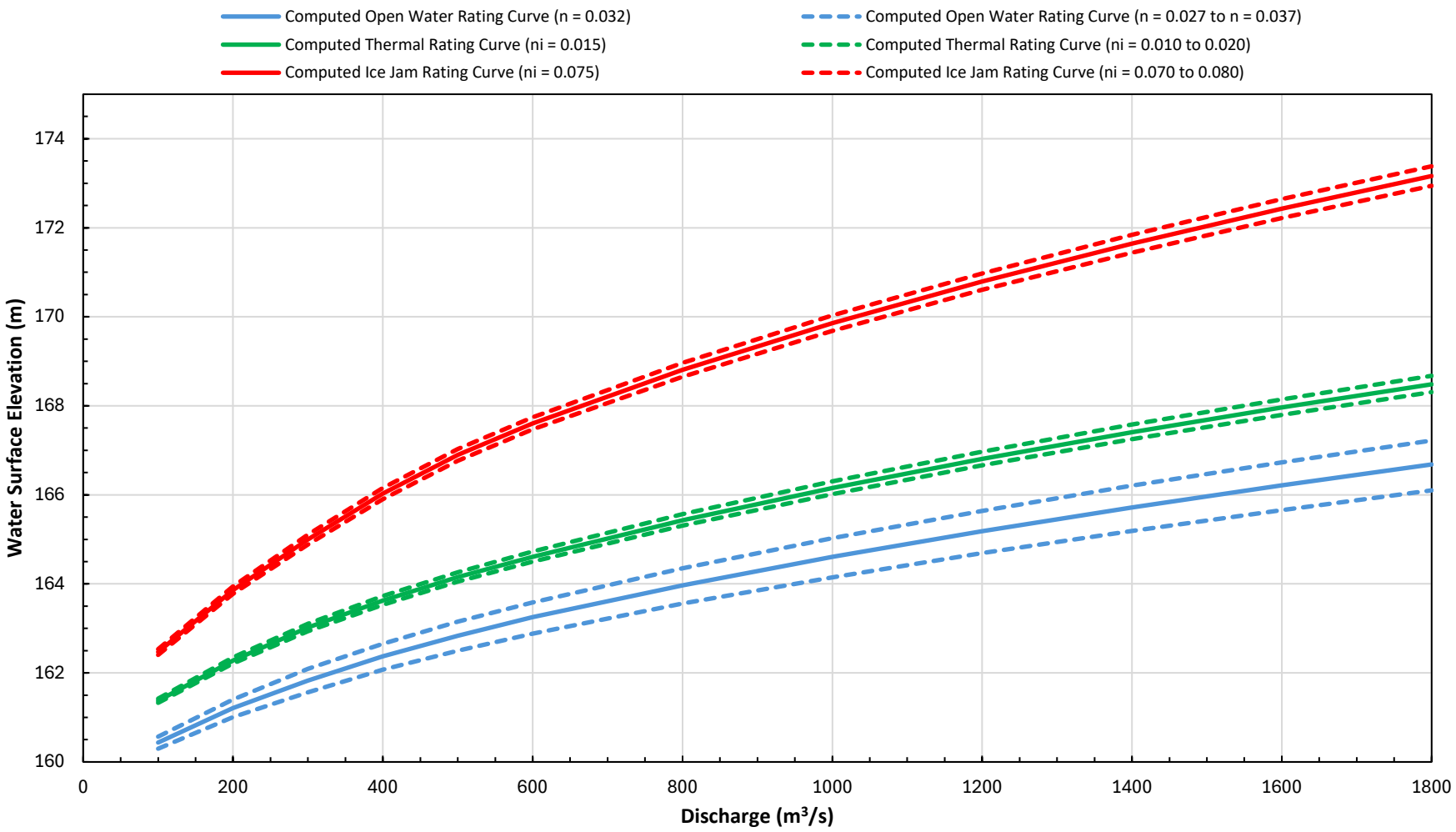

Government of Northwest Territories
Gouvernement des Territoires du Nord-Ouest

Canada

nhc

UNITS – AS SHOWN

VERTICAL ELEVATION DATUM: CGVD2013a

Job: 1008469

Date: Feb-2025

KÁTŁ'ODEH (HAY RIVER)
FLOOD HAZARD MAPPING STUDY

MANNING'S ROUGHNESS SENSITIVITY ANALYSIS AT #07OB001 HAY RIVER NEAR HAY RIVER

FIGURE 56

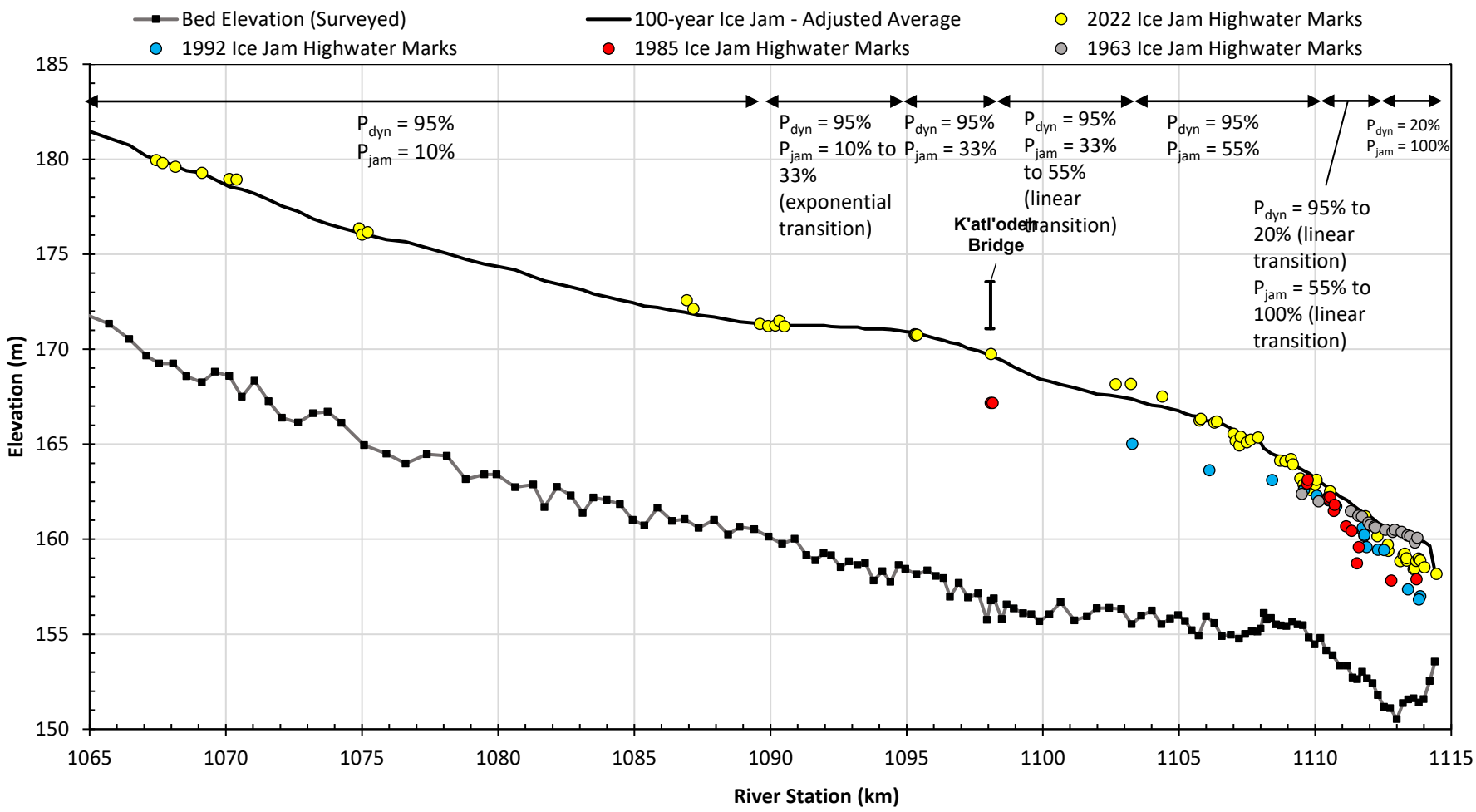

Government of Northwest Territories
Gouvernement des Territoires du Nord-Ouest

Canada

nhc

UNITS – AS SHOWN

VERTICAL ELEVATION DATUM: CGVD2013a

Job: 1008469

Date: Feb-2025

KÁTŁ'ODEH (HAY RIVER)
FLOOD HAZARD MAPPING STUDY

100-YEAR ICE JAM FLOOD FREQUENCY PROFILE
HAY RIVER MAIN AND EAST CHANNELS

FIGURE 57

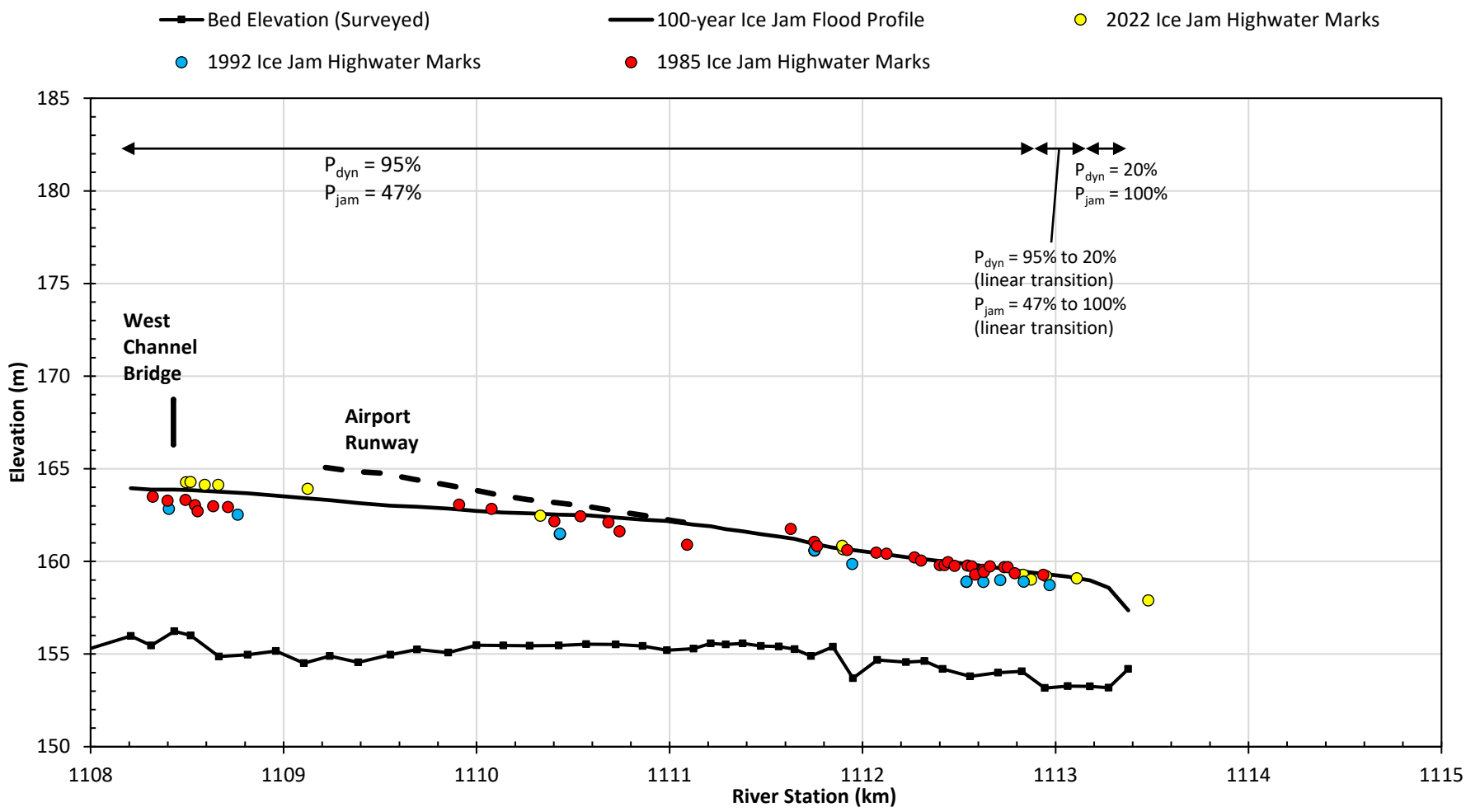

Government of Northwest Territories
Gouvernement des Territoires du Nord-Ouest

Canada

nhc

UNITS – AS SHOWN

VERTICAL ELEVATION DATUM: CGVD2013a

Job: 1008469

Date: Feb-2025

KÁTŁ'ODEH (HAY RIVER)
FLOOD HAZARD MAPPING STUDY

100-YEAR ICE JAM FLOOD FREQUENCY PROFILE HAY RIVER WEST AND WEST FISHING VILLAGE CHANNELS

FIGURE 58

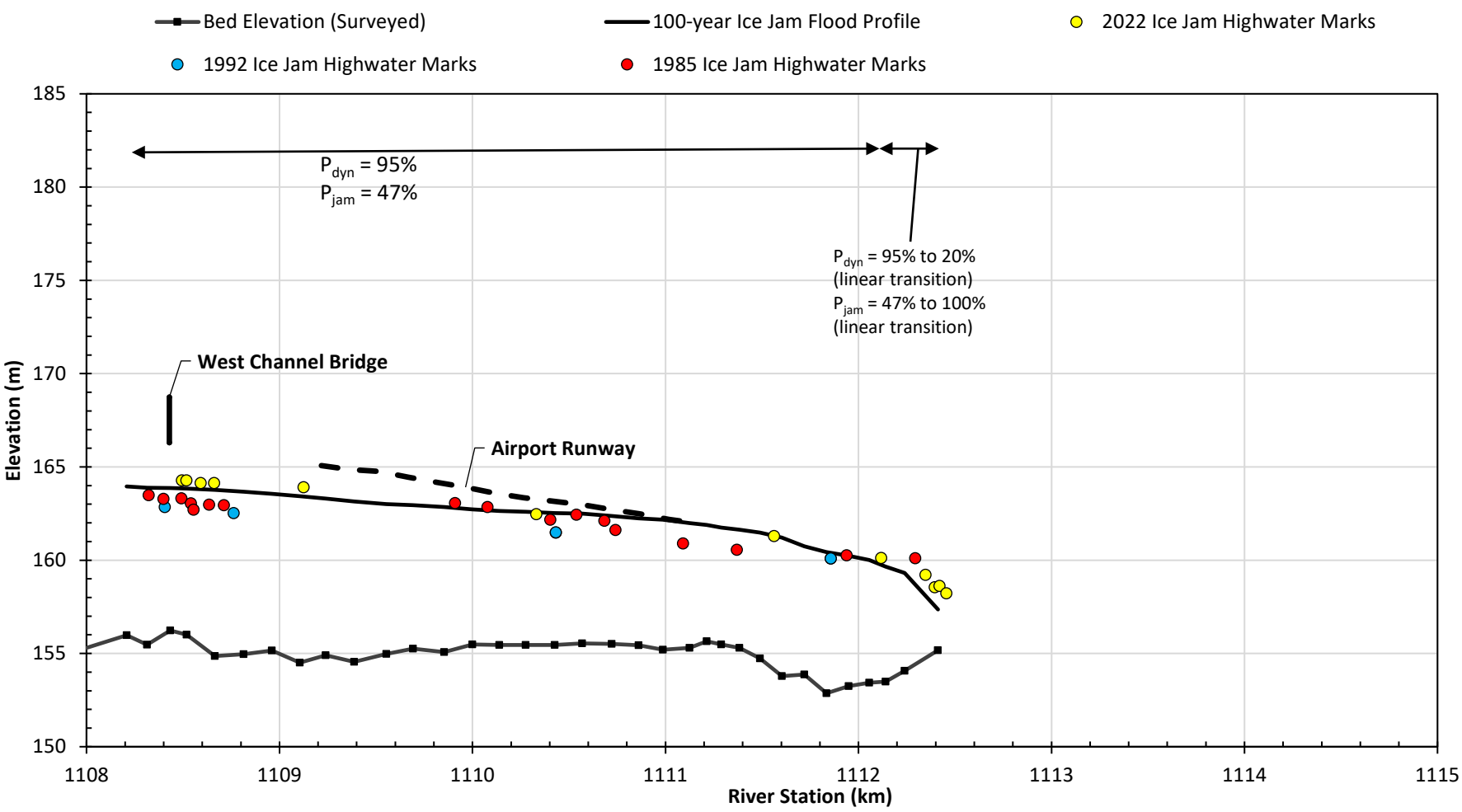

Notes: 1. Design elevations at Hay River Rudd Chanel cross sections were adopted from calculated design elevations at adjacent Hay River West Fishing Village Channel cross sections (model cross sections are shown in Figure 21).

Government of Northwest Territories / Gouvernement des Territoires du Nord-Ouest; Canada; nhc	UNITS – AS SHOWN VERTICAL ELEVATION DATUM: CGVD2013a	KÁTŁ'ODEH (HAY RIVER) FLOOD HAZARD MAPPING STUDY ***100-YEAR ICE JAM FLOOD FREQUENCY PROFILE HAY RIVER WEST AND RUDD CHANNELS***
	Job: 1008469 / *Date: Feb-2025*	FIGURE 59

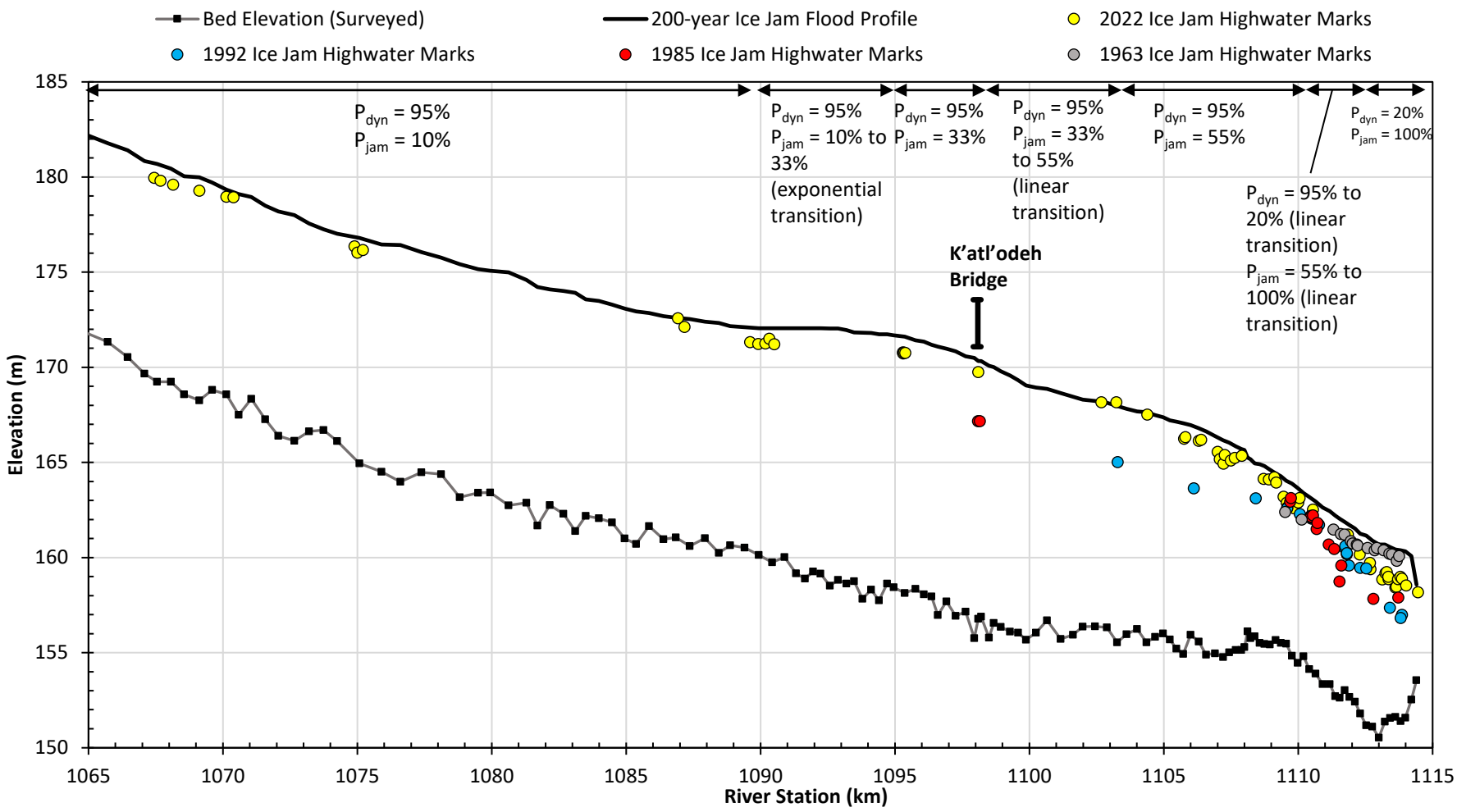

Government of Northwest Territories
Gouvernement des Territoires du Nord-Ouest

Canada

nhc

UNITS – AS SHOWN

VERTICAL ELEVATION DATUM: CGVD2013a

Job: 1008469

Date: Feb-2025

KÁTŁ'ODEH (HAY RIVER)
FLOOD HAZARD MAPPING STUDY

200-YEAR ICE JAM FLOOD FREQUENCY PROFILE
HAY RIVER MAIN AND EAST CHANNELS

FIGURE 60

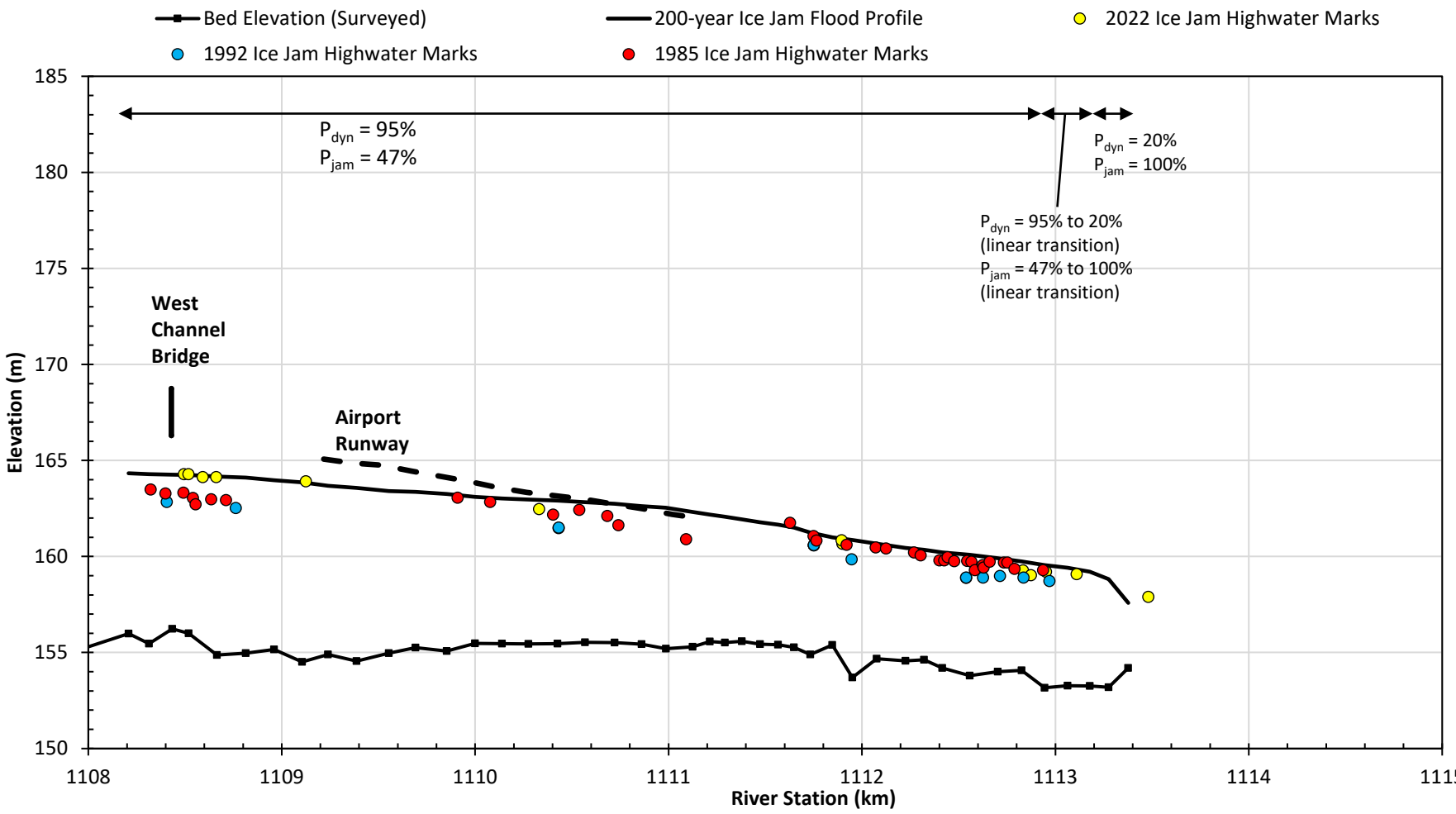

Government of Northwest Territories
Gouvernement des Territoires du Nord-Ouest

Canada

nhc

UNITS – AS SHOWN

VERTICAL ELEVATION DATUM: CGVD2013a

Job: 1008469

Date: Feb-2025

KÁTŁ'ODEH (HAY RIVER)
FLOOD HAZARD MAPPING STUDY

200-YEAR ICE JAM FLOOD FREQUENCY PROFILE HAY RIVER WEST AND WEST FISHING VILLAGE CHANNELS

FIGURE 61

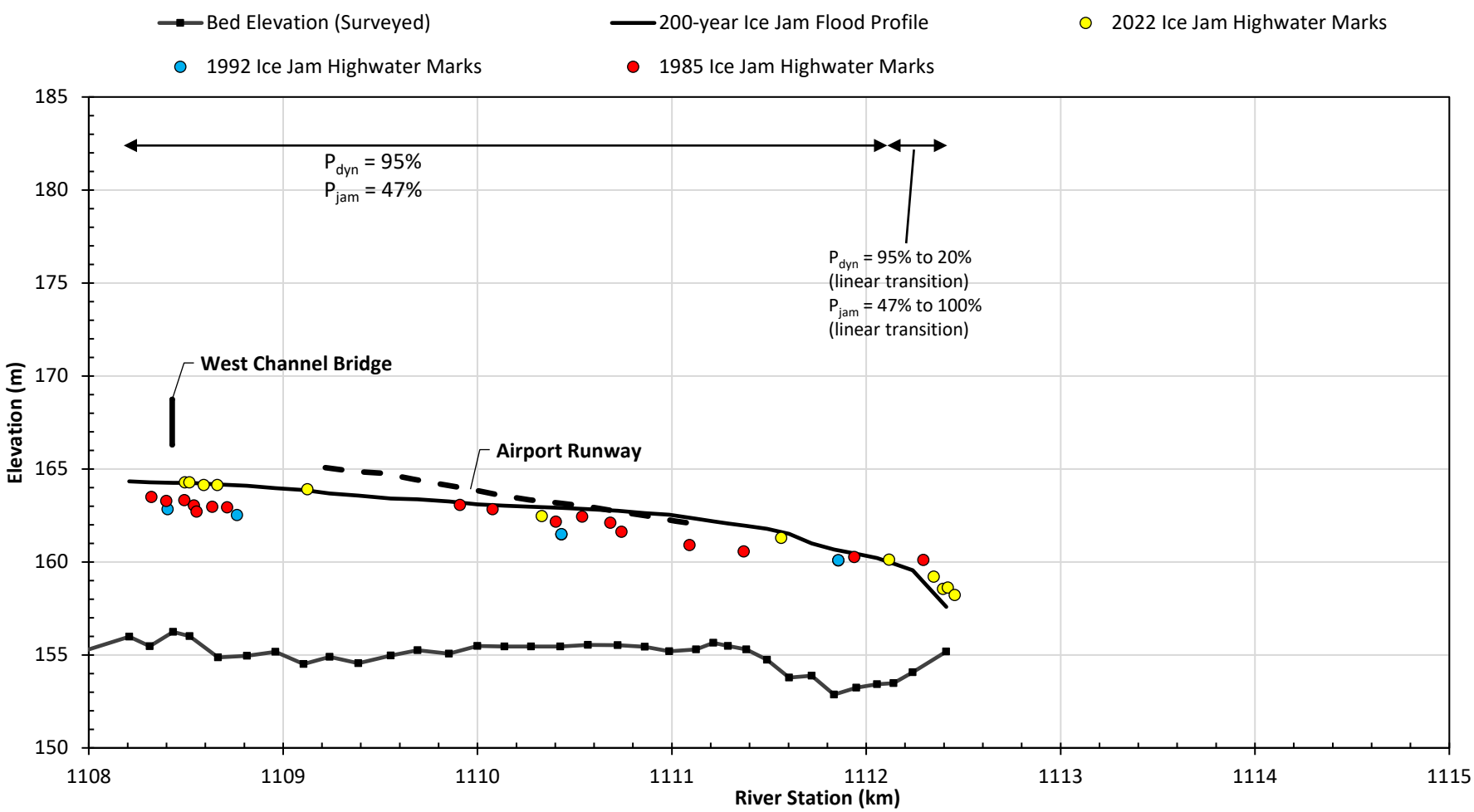

Notes: 1. Design elevations at Hay River Rudd Chanel cross sections were adopted from calculated design elevations at adjacent Hay River West Fishing Village Channel cross sections (model cross sections are shown in Figure 21).

Government of Northwest Territories / Gouvernement des Territoires du Nord-Ouest; Canada; nhc	UNITS – AS SHOWN VERTICAL ELEVATION DATUM: CGVD2013a	KÁTŁ'ODEH (HAY RIVER) FLOOD HAZARD MAPPING STUDY ***200-YEAR ICE JAM FLOOD FREQUENCY PROFILE HAY RIVER WEST AND RUDD CHANNELS***
	Job: 1008469 *Date: Feb-2025*	FIGURE 62

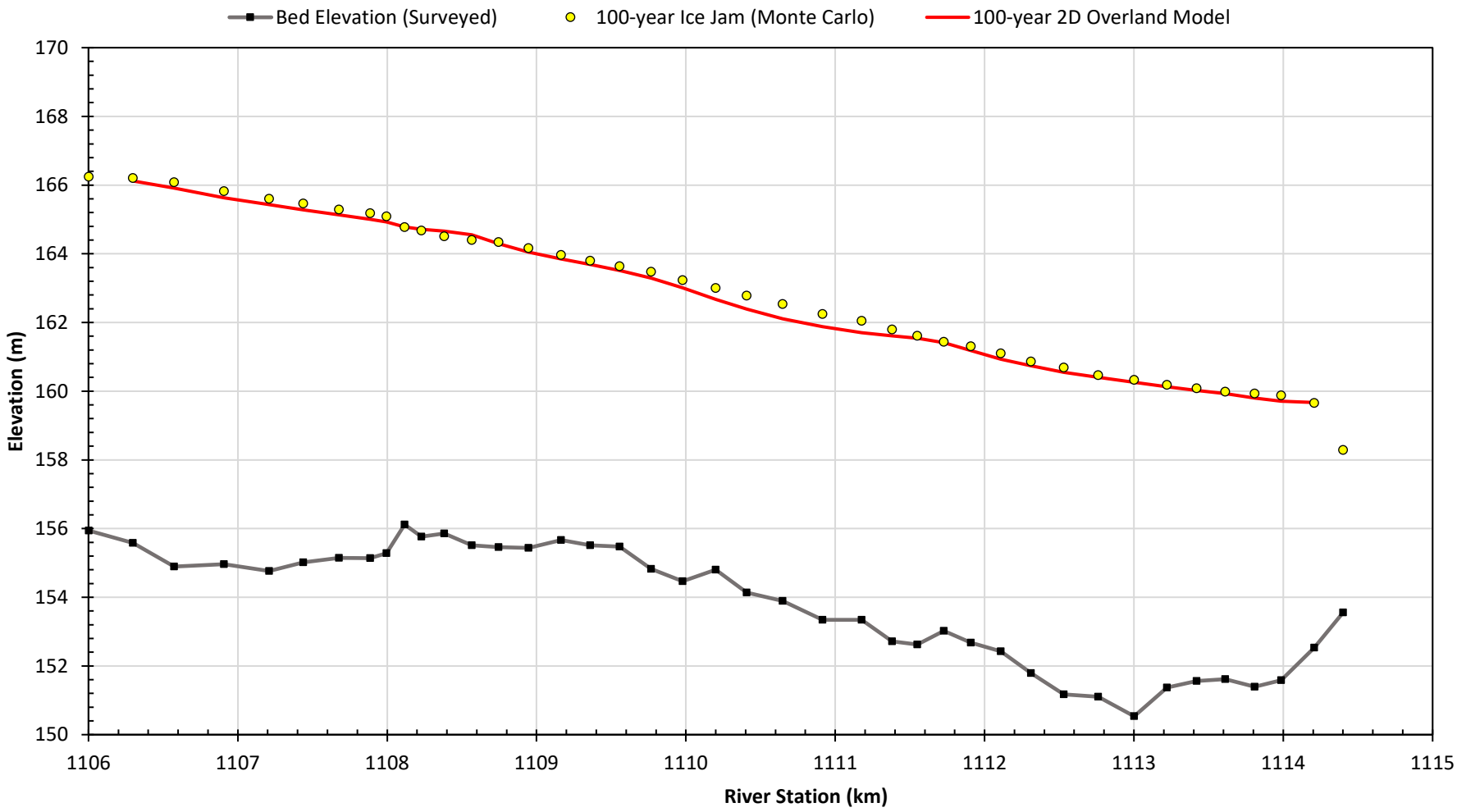

Government of Northwest Territories
Gouvernement des Territoires du Nord-Ouest

Canada

nhc

UNITS – AS SHOWN

VERTICAL ELEVATION DATUM: CGVD2013a

Job: 1008469

Date: Feb-2025

KÁTŁ'ODEH (HAY RIVER)
FLOOD HAZARD MAPPING STUDY

COMPARISON OF 100-YEAR ICE JAM OVERLAND MODELLING AND FLOOD FREQUENCY RESULTS HAY RIVER MAIN AND EAST CHANNELS

FIGURE 63

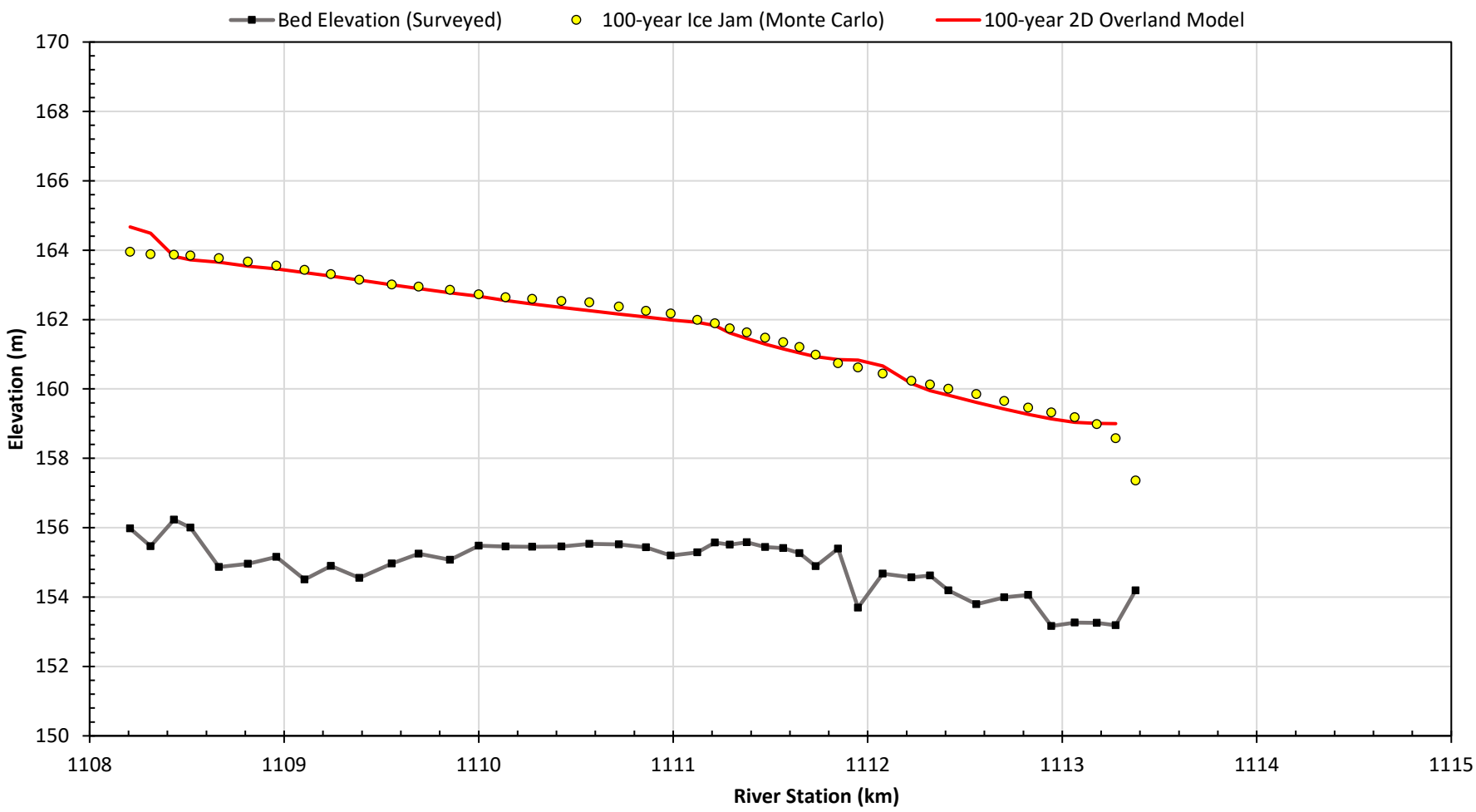

Government of Northwest Territories
Gouvernement des Territoires du Nord-Ouest

Canada

nhc

UNITS – AS SHOWN

VERTICAL ELEVATION DATUM: CGVD2013a

Job: 1008469

Date: Feb-2025

KÁTŁ'ODEH (HAY RIVER)
FLOOD HAZARD MAPPING STUDY

COMPARISON OF 100-YEAR ICE JAM OVERLAND MODELLING AND FLOOD FREQUENCY RESULTS HAY RIVER WEST AND WEST FISHING VILLAGE CHANNELS

FIGURE 64

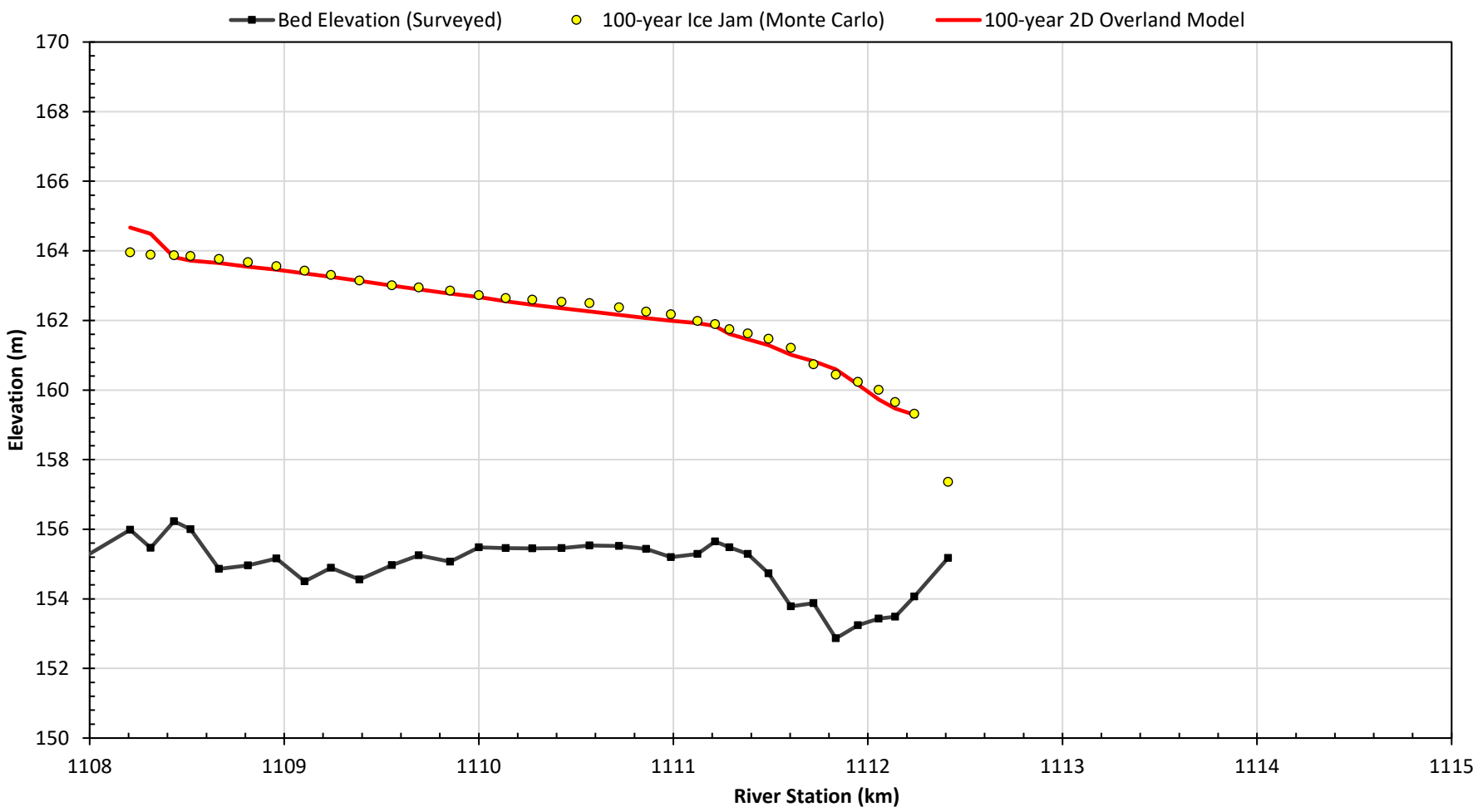

Notes: 1. Design elevations at Hay River Rudd Chanel cross sections were adopted from calculated design elevations at adjacent Hay River West Fishing Village Channel cross sections (model cross sections are shown in Figure 21).

Government of Northwest Territories
Gouvernement des Territoires du Nord-Ouest
Canada
nhc

UNITS – AS SHOWN

VERTICAL ELEVATION DATUM: CGVD2013a

Job: 1008469 | *Date: Feb-2025*

KÁTŁ'ODEH (HAY RIVER)
FLOOD HAZARD MAPPING STUDY

COMPARISON OF 100-YEAR ICE JAM OVERLAND MODELLING AND FLOOD FREQUENCY RESULTS HAY RIVER WEST AND RUDD CHANNELS

FIGURE 65

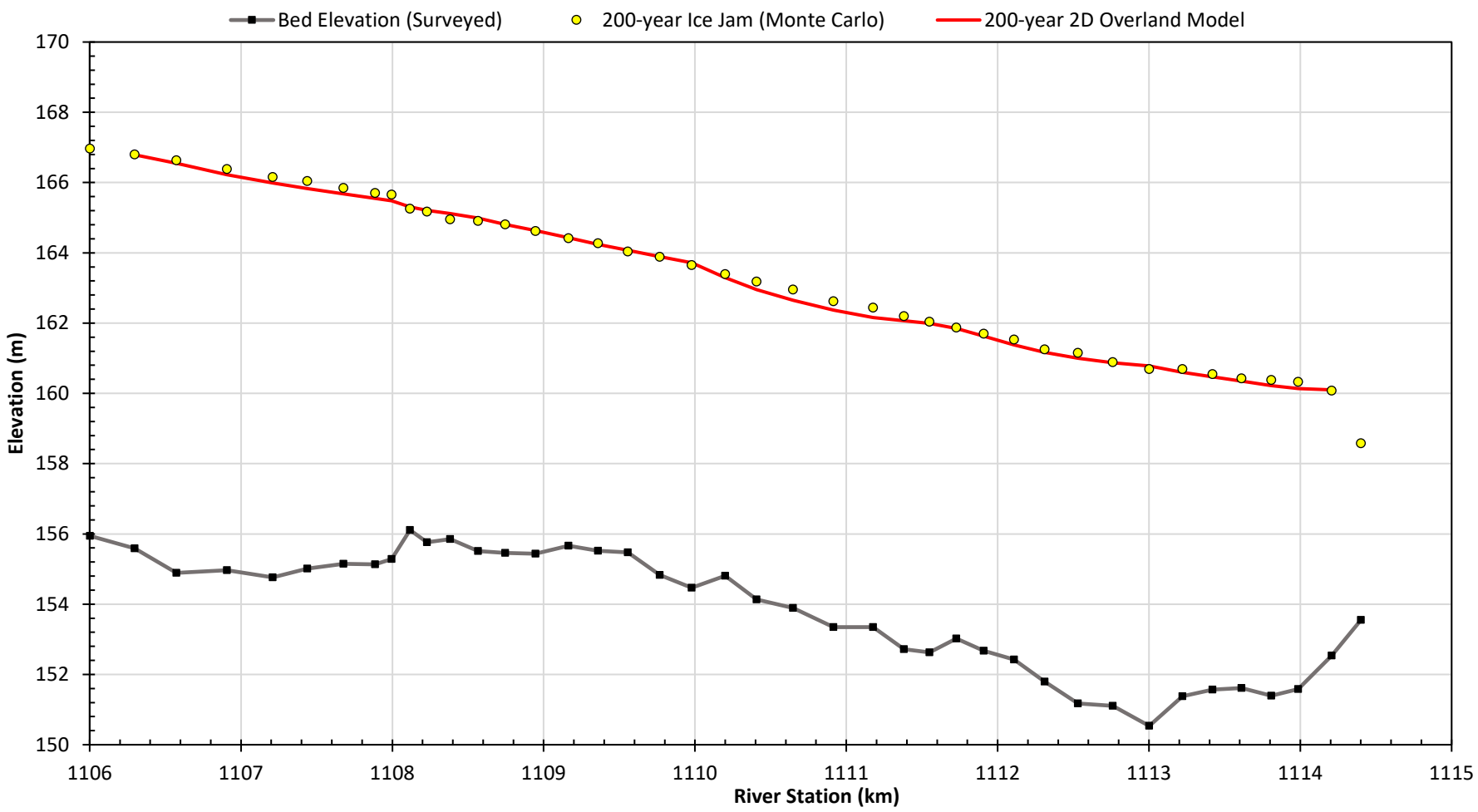

Government of Northwest Territories
Gouvernement des Territoires du Nord-Ouest

Canada

nhc

UNITS – AS SHOWN

VERTICAL ELEVATION DATUM: CGVD2013a

Job: 1008469

Date: Feb-2025

KÁTŁ'ODEH (HAY RIVER)
FLOOD HAZARD MAPPING STUDY

COMPARISON OF 200-YEAR ICE JAM OVERLAND MODELLING AND FLOOD FREQUENCY RESULTS HAY RIVER MAIN AND EAST CHANNELS

FIGURE 66

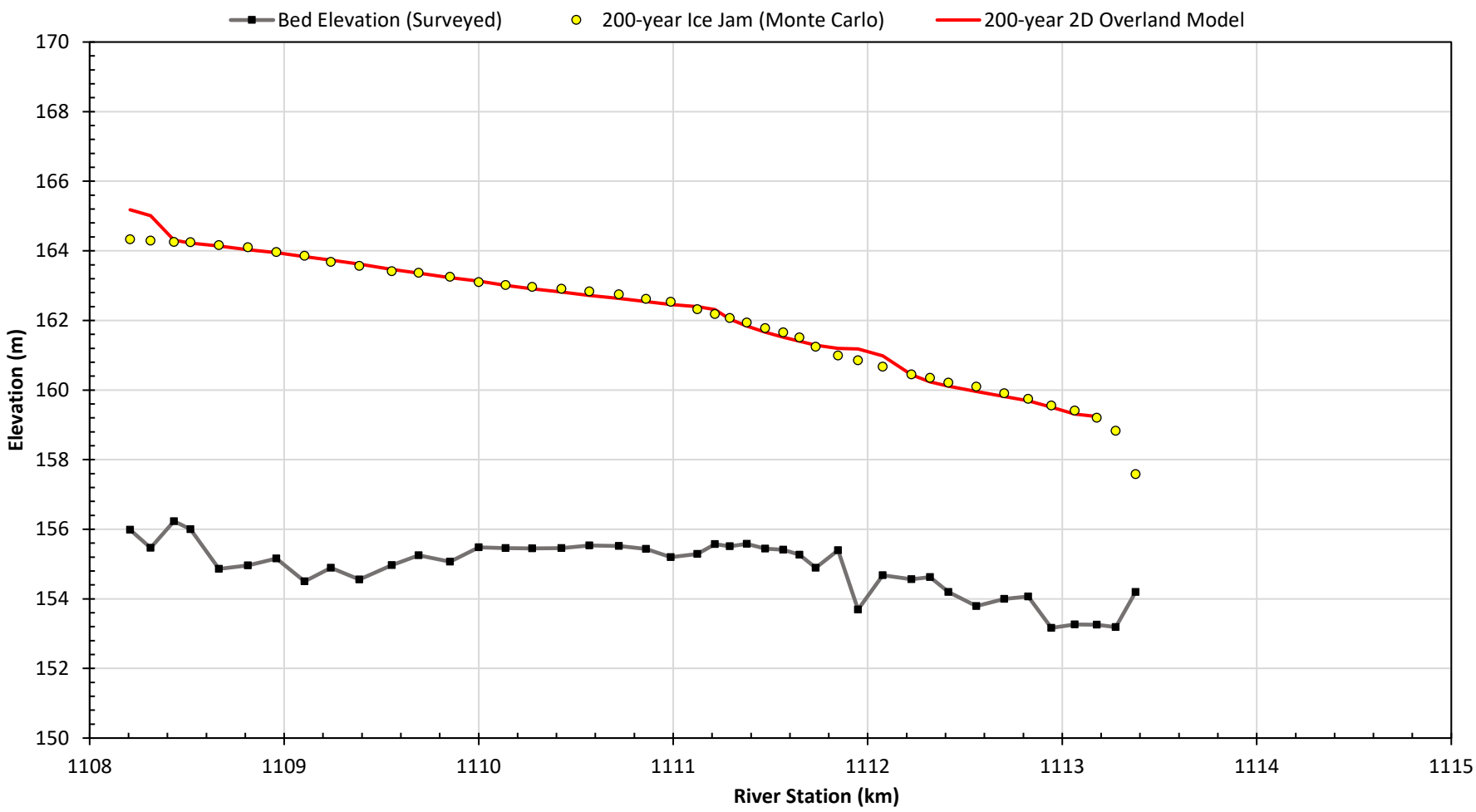

Government of Northwest Territories
Gouvernement des Territoires du Nord-Ouest

Canada

nhc

UNITS – AS SHOWN

VERTICAL ELEVATION DATUM: CGVD2013a

Job: 1008469

Date: Feb-2025

KÁTŁ'ODEH (HAY RIVER)
FLOOD HAZARD MAPPING STUDY

COMPARISON OF 200-YEAR ICE JAM OVERLAND MODELLING AND FLOOD FREQUENCY RESULTS HAY RIVER WEST AND WEST FISHING VILLAGE CHANNELS

FIGURE 67

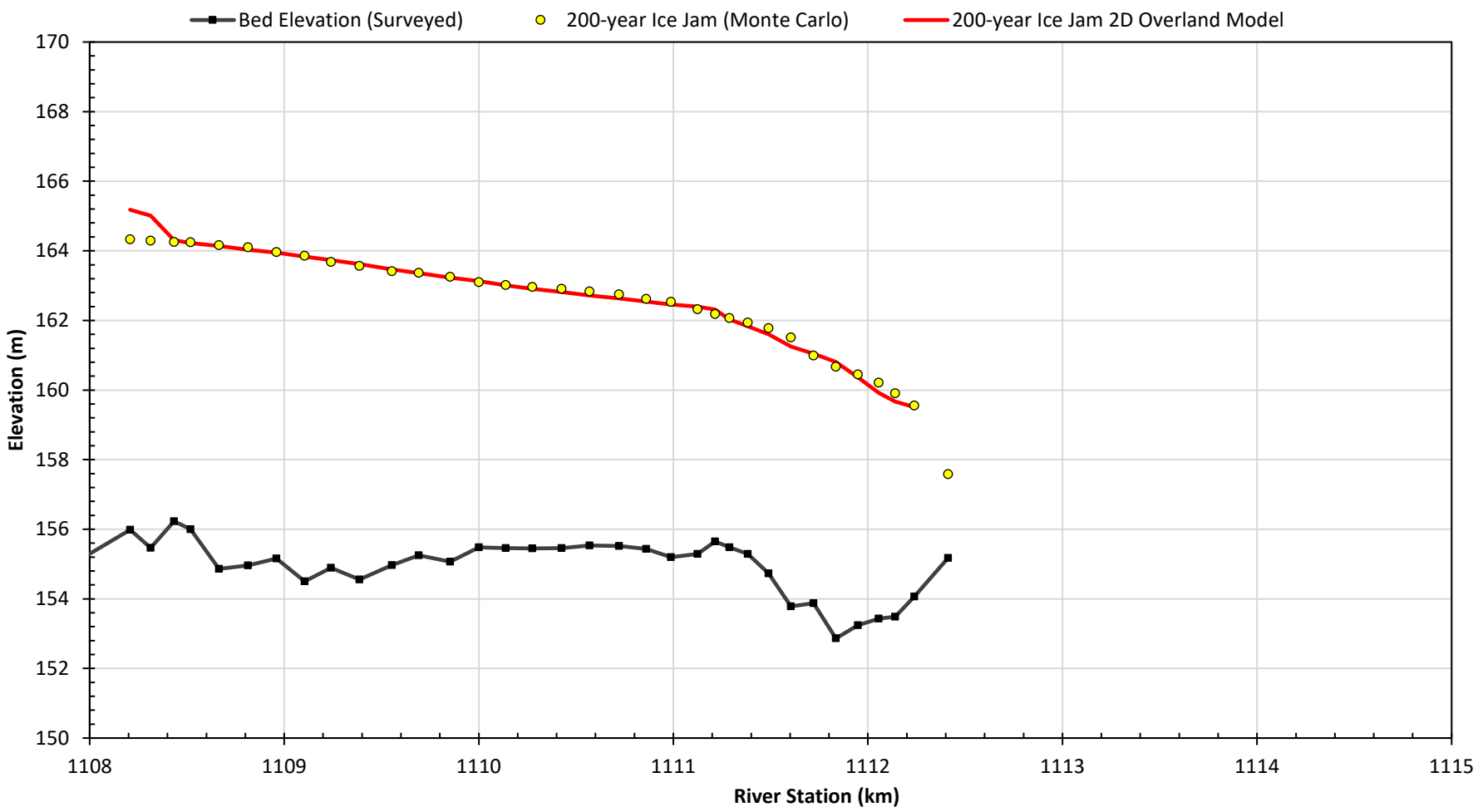

Notes: 1. Design elevations at Hay River Rudd Chanel cross sections were adopted from calculated design elevations at adjacent Hay River West Fishing Village Channel cross sections (model cross sections are shown in Figure 21).

Government of Northwest Territories
Gouvernement des Territoires du Nord-Ouest

Canada

nhc

UNITS – AS SHOWN

VERTICAL ELEVATION DATUM: CGVD2013a

Job: 1008469

Date: Feb-2025

KÁTŁ'ODEH (HAY RIVER)
FLOOD HAZARD MAPPING STUDY

COMPARISON OF 200-YEAR ICE JAM OVERLAND MODELLING AND FLOOD FREQUENCY RESULTS HAY RIVER WEST AND RUDD CHANNELS

FIGURE 68

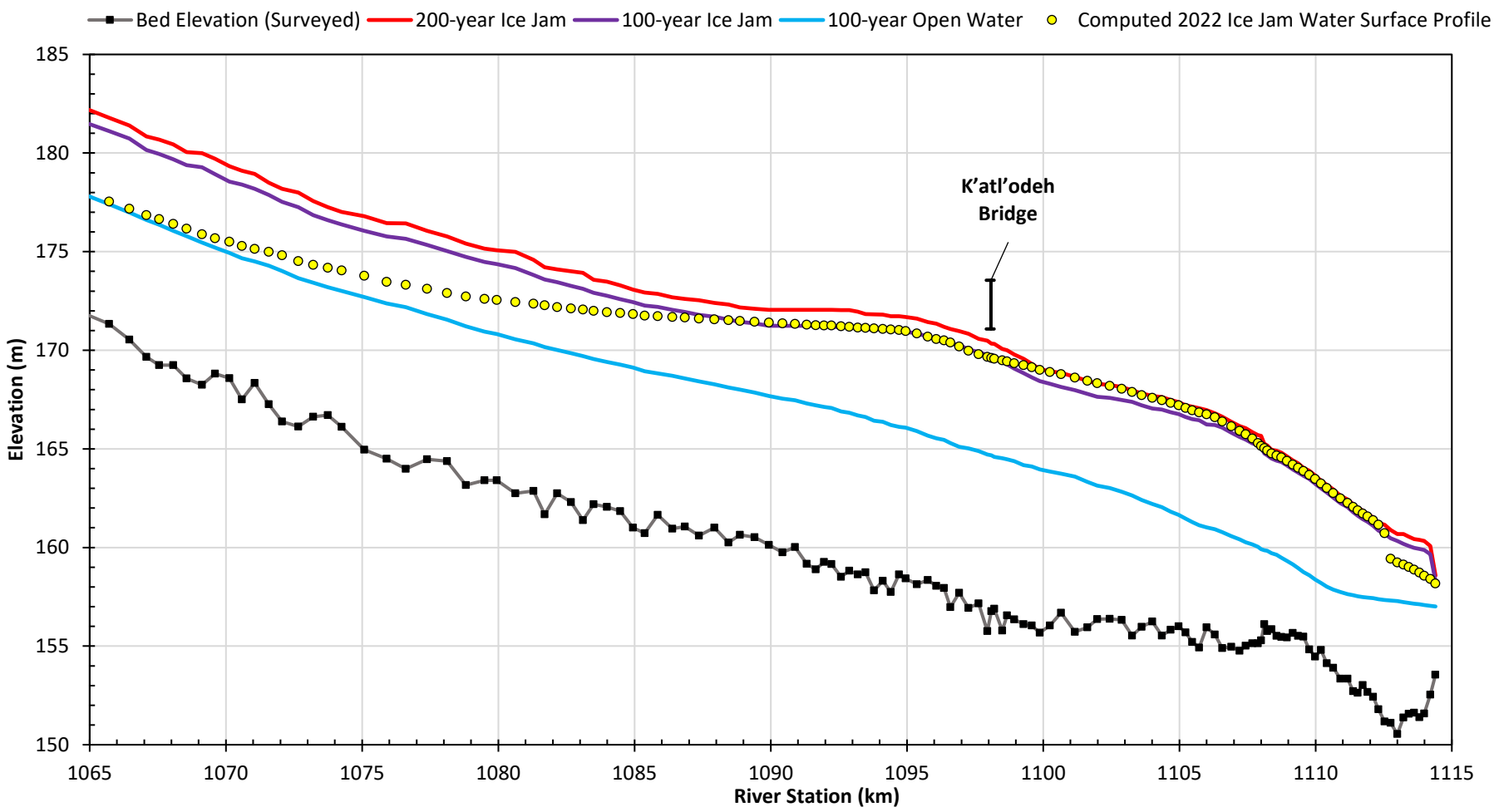

Notes: 1. The computed 2022 ice jam water surface elevations as per the Northwest Territories Ice Jam Flood Mapping Case Studies report (NHC 2023b).

Government of Northwest Territories / Gouvernement des Territoires du Nord-Ouest

Canada

nhc

UNITS – AS SHOWN

VERTICAL ELEVATION DATUM: CGVD2013a

Job: 1008469

Date: Feb-2025

KÁTŁ'ODEH (HAY RIVER)
FLOOD HAZARD MAPPING STUDY

FLOOD FREQUENCY PROFILES
HAY RIVER MAIN AND EAST CHANNELS

FIGURE 69

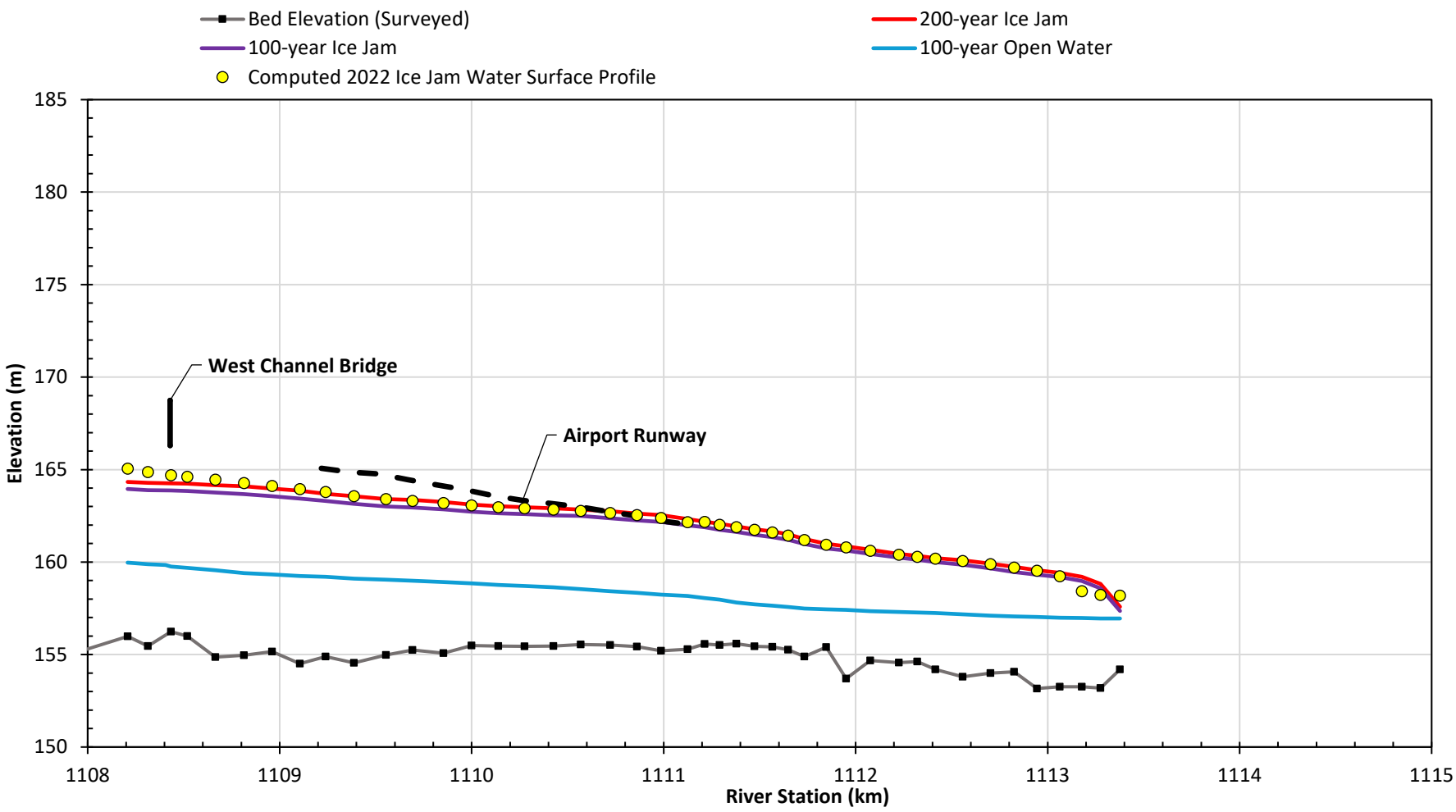

Notes: 1. The computed 2022 ice jam water surface elevations as per the Northwest Territories Ice Jam Flood Mapping Case Studies report (NHC 2023b).

Government of Northwest Territories / Gouvernement des Territoires du Nord-Ouest

Canada

nhc

UNITS – AS SHOWN

VERTICAL ELEVATION DATUM: CGVD2013a

Job: 1008469

Date: Feb-2025

KÁTŁ'ODEH (HAY RIVER)
FLOOD HAZARD MAPPING STUDY

FLOOD FREQUENCY PROFILES
HAY RIVER WEST AND WEST FISHING VILLAGE CHANNELS

FIGURE 70

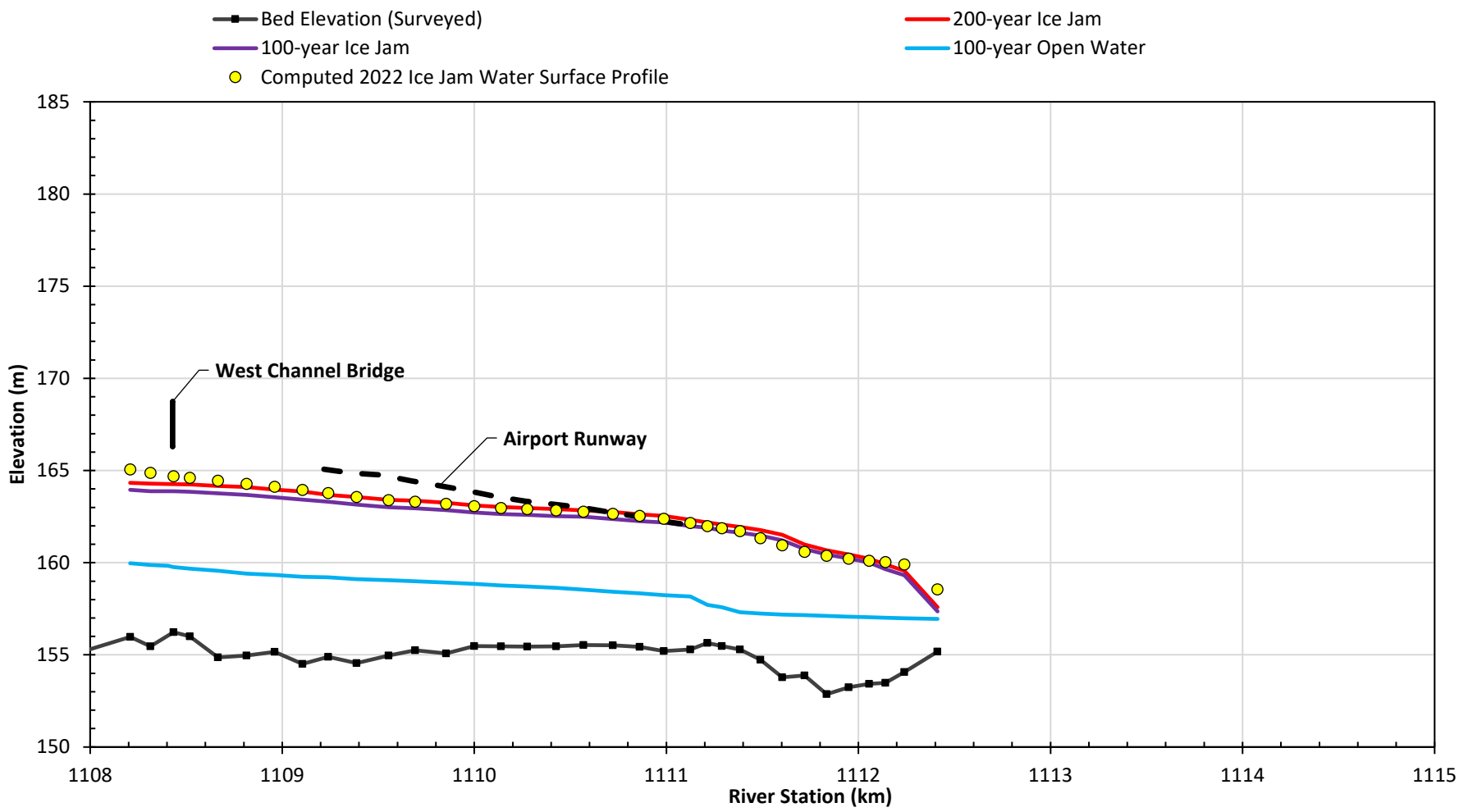

Notes: 1. The computed 2022 ice jam water surface elevations as per the Northwest Territories Ice Jam Flood Mapping Case Studies report (NHC 2023b).

Government of Northwest Territories / Gouvernement des Territoires du Nord-Ouest; Canada; nhc	UNITS – AS SHOWN VERTICAL ELEVATION DATUM: CGVD2013a	KÁTŁ'ODEH (HAY RIVER) FLOOD HAZARD MAPPING STUDY ***FLOOD FREQUENCY PROFILES*** ***HAY RIVER WEST AND RUDD CHANNELS***
	Job: 1008469 / *Date: Feb-2025*	FIGURE 71

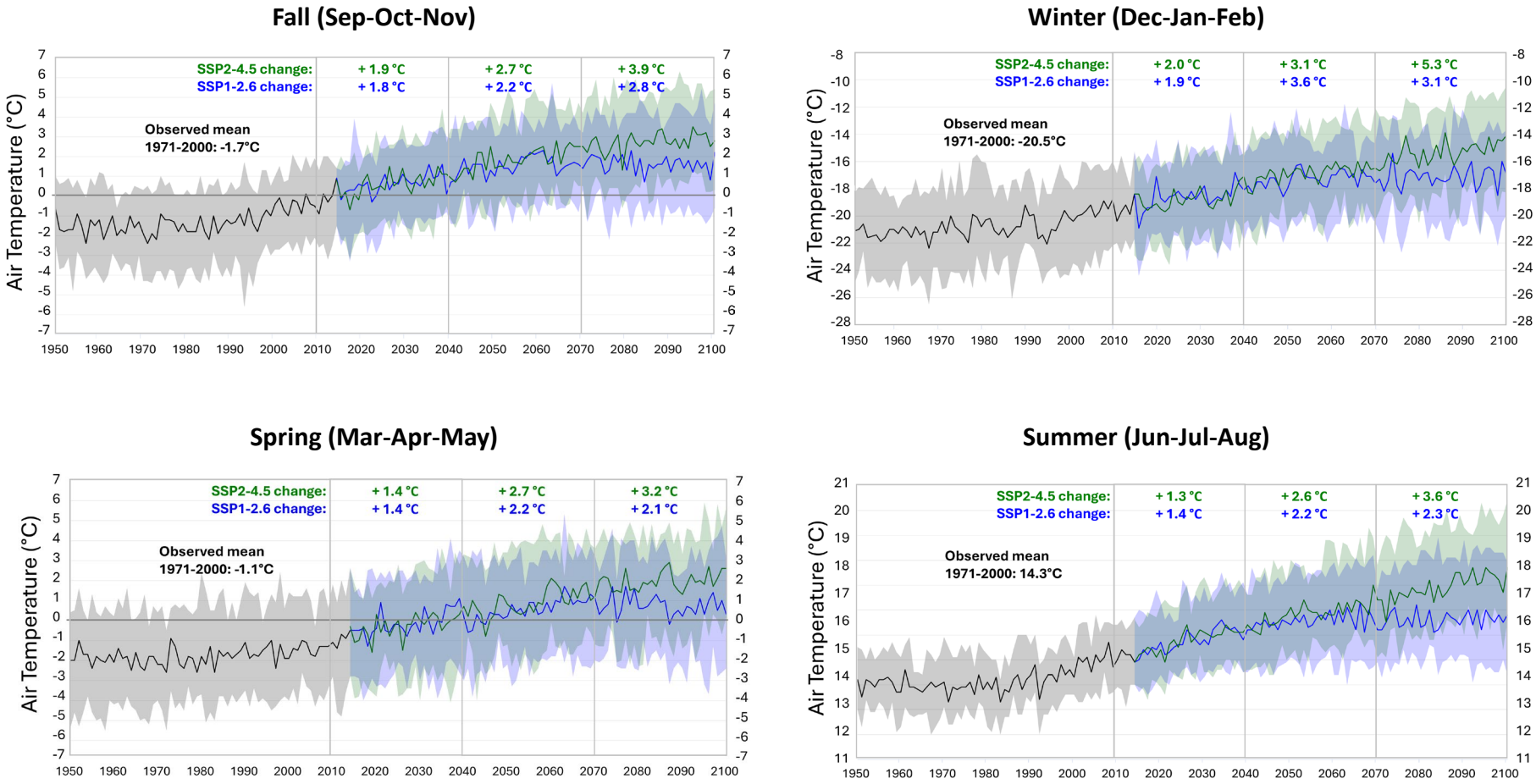

Notes: 1. The values annotated are for periods 2011-2040, 2041-2070 and 2071-2100, relative to 1971-2000.

Government of Northwest Territories / Gouvernement des Territoires du Nord-Ouest; Canada; nhc	UNITS – AS SHOWN	KÁTŁ'ODEH (HAY RIVER) FLOOD HAZARD MAPPING STUDY ***PROJECTED AIR TEMPERATURE TREND FOR THE LOWER HAY RIVER***
	Job: 1008469 / *Date: Feb-2025*	FIGURE 72

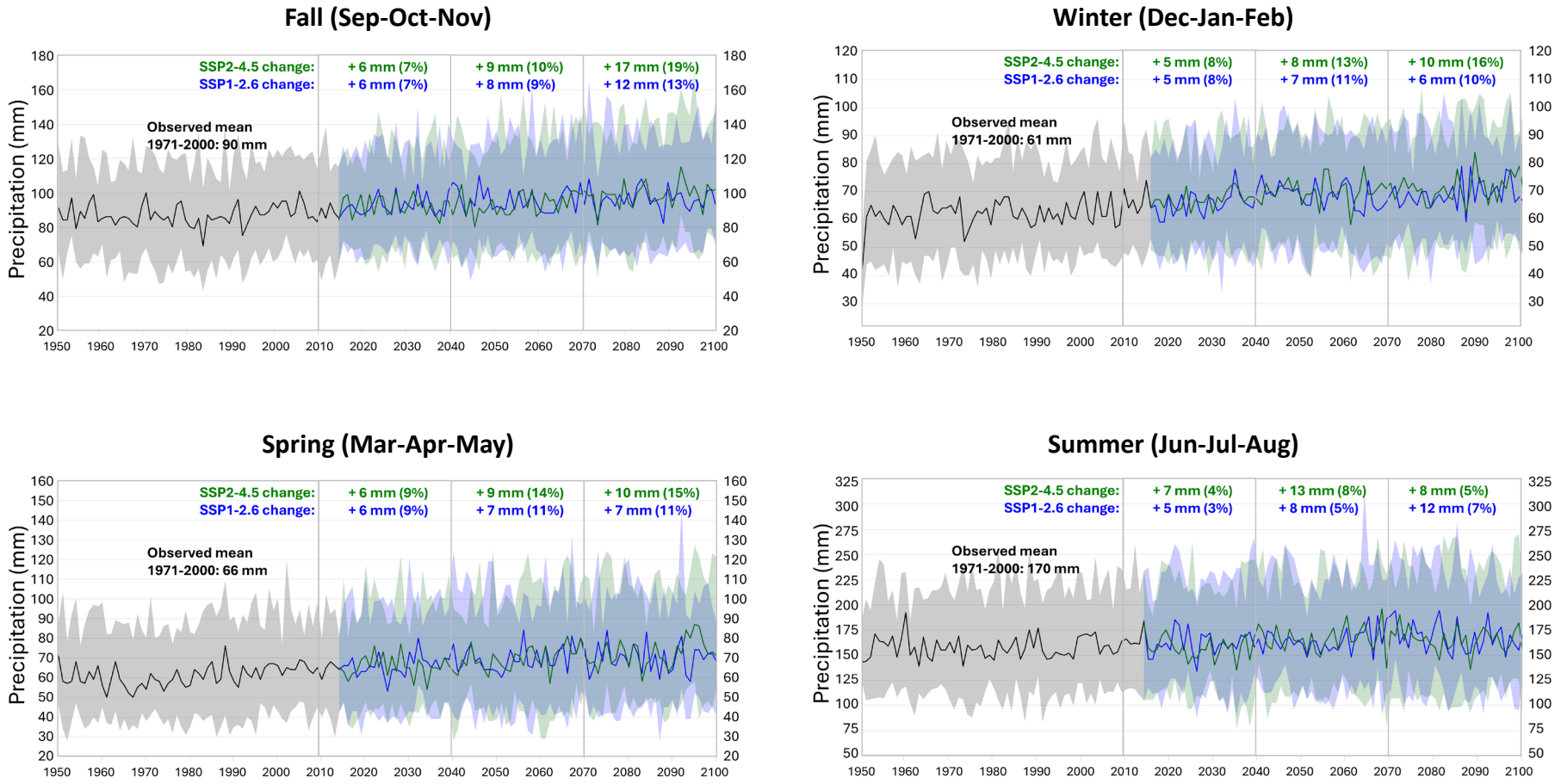

Notes: 1. The values annotated are for periods 2011-2040, 2041-2070 and 2071-2100, relative to 1971-2000.

Government of Northwest Territories
Gouvernement des Territoires du Nord-Ouest

Canada

nhc

UNITS – AS SHOWN

KÁTŁ'ODEH (HAY RIVER)
FLOOD HAZARD MAPPING STUDY

PROJECTED PRECIPITATION TREND FOR THE LOWER HAY RIVER

Job: 1008469

Date: Feb-2025

FIGURE 73

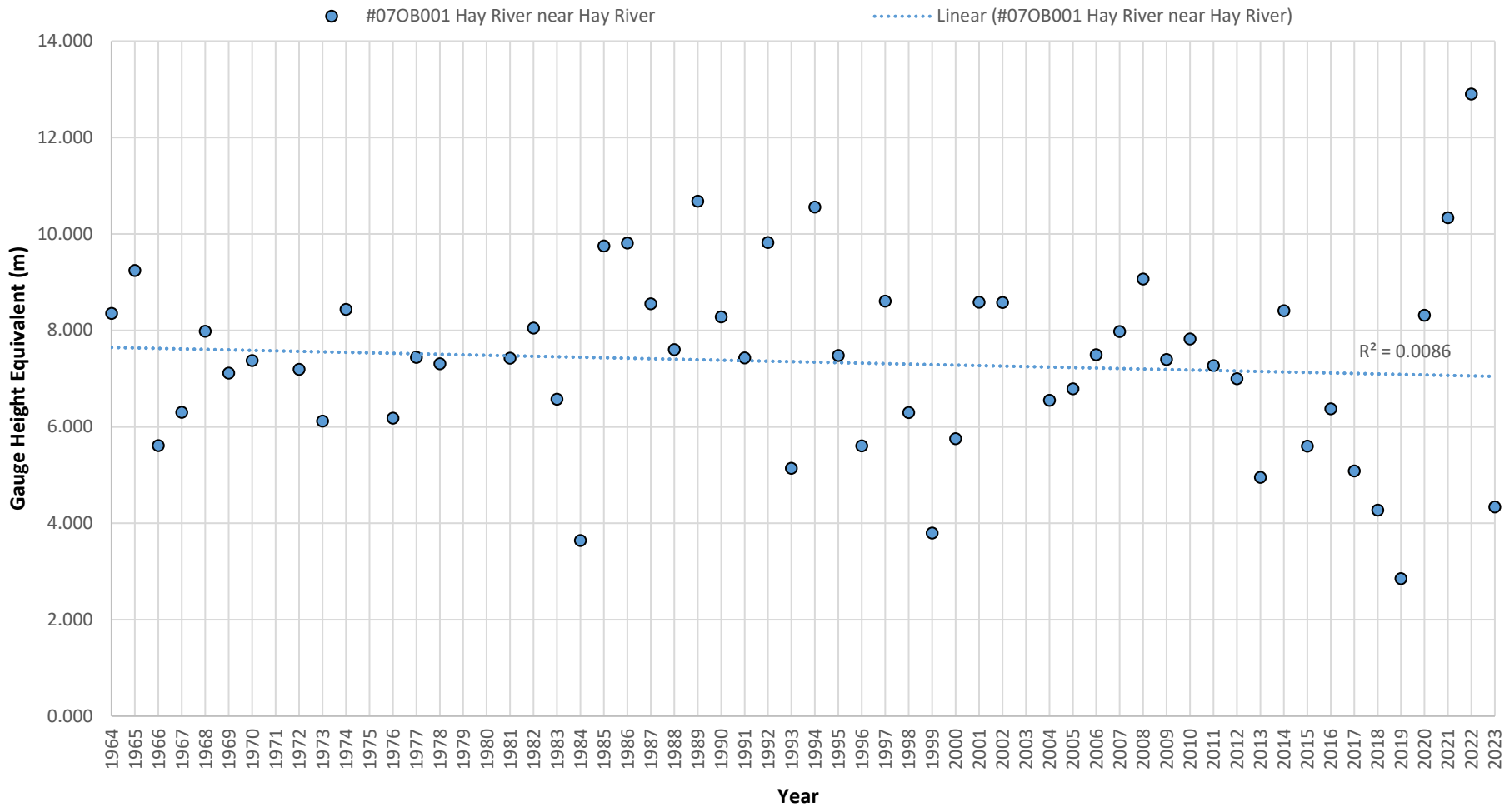

Notes: 1. A conversion to a gauge height equivalent has been adopted based off a gauge height adjustment (1985) during the years of record. The gauge height equivalent is equal to the CGVD28 elevation minus 158.000 m.

Government of Northwest Territories / Gouvernement des Territoires du Nord-Ouest

Canada

nhc

UNITS – AS SHOWN

VERTICAL ELEVATION DATUM: GAUGE HEIGHT EQUIVALENT

Job: 1008469

Date: Feb-2025

KÁTŁ'ODEH (HAY RIVER)
FLOOD HAZARD MAPPING STUDY

RECORDED PEAK BREAKUP WATER LEVELS TREND AT #07OB001 HAY RIVER NEAR HAY RIVER

FIGURE 74

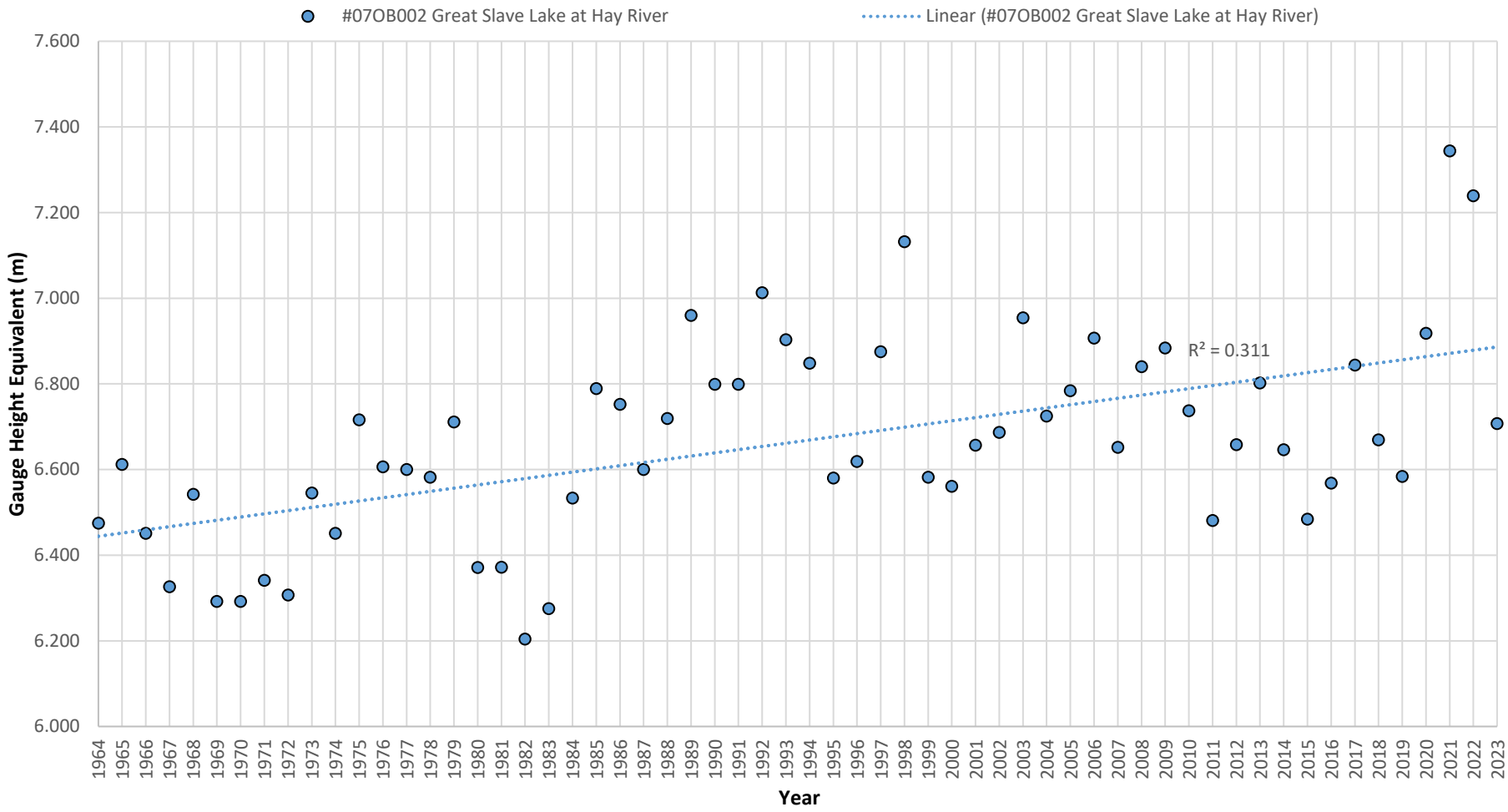

Notes: 1. A conversion to a gauge height equivalent has been adopted based off a gauge height adjustment (1985) during the years of record. The gauge height equivalent is equal to the CGVD28 elevation minus 150.000 m.

Government of Northwest Territories / Gouvernement des Territoires du Nord-Ouest

Canada

nhc

UNITS – AS SHOWN

VERTICAL ELEVATION DATUM: GAUGE HEIGHT EQUIVALENT

Job: 1008469

Date: Feb-2025

KÁTŁ'ODEH (HAY RIVER)
FLOOD HAZARD MAPPING STUDY

RECORDED SPRING BREAKUP WATER LEVELS TREND AT #07OB002 GREAT SLAVE LAKE AT HAY RIVER

FIGURE 75

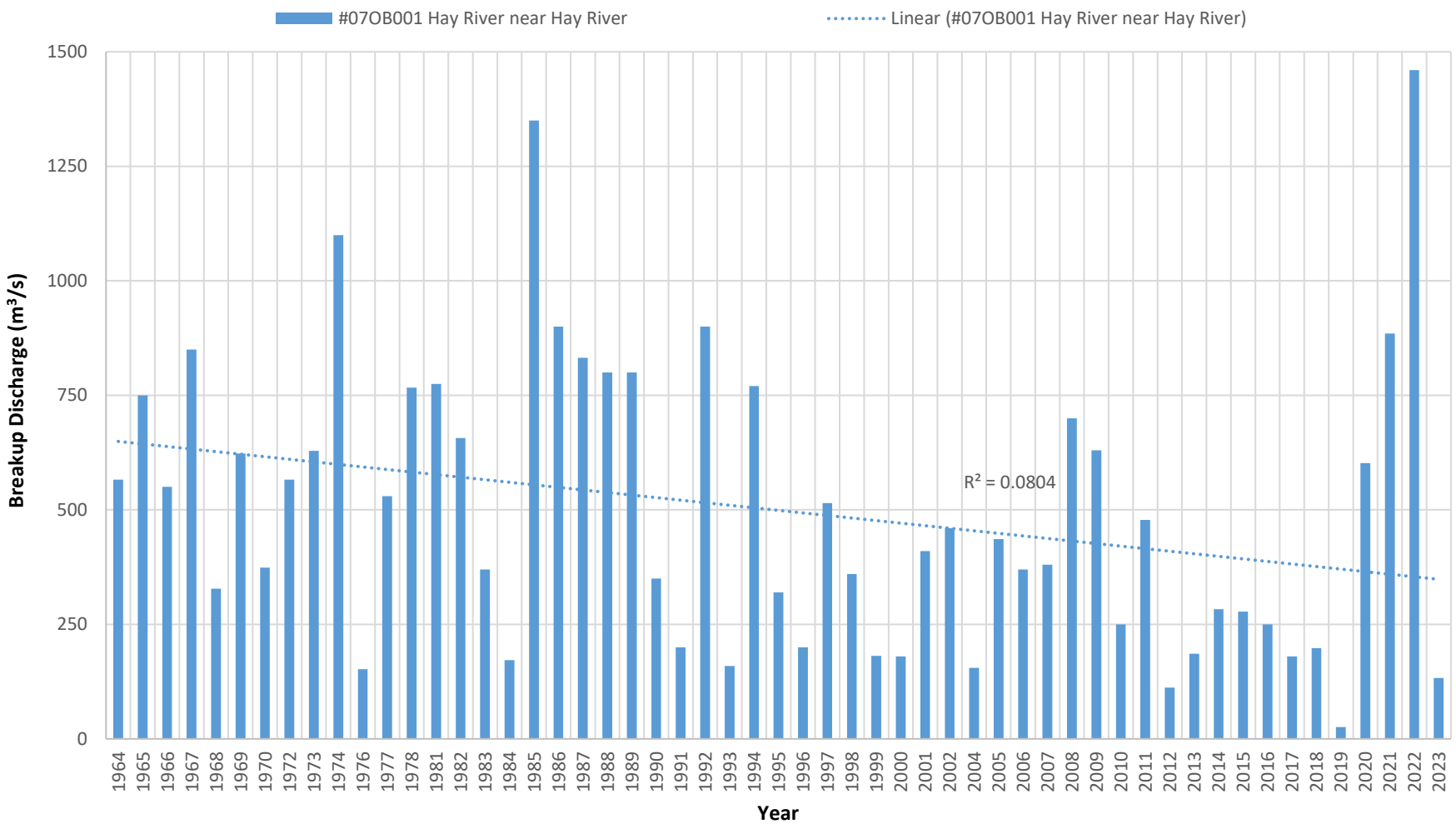

Government of Northwest Territories
Gouvernement des Territoires du Nord-Ouest

Canada

nhc

UNITS – AS SHOWN

Job: 1008469

Date: Feb-2025

KÁTŁ'ODEH (HAY RIVER)
FLOOD HAZARD MAPPING STUDY

RECORDED PEAK BREAKUP DISCHARGES TREND AT #07OB001 HAY RIVER NEAR HAY RIVER

FIGURE 76

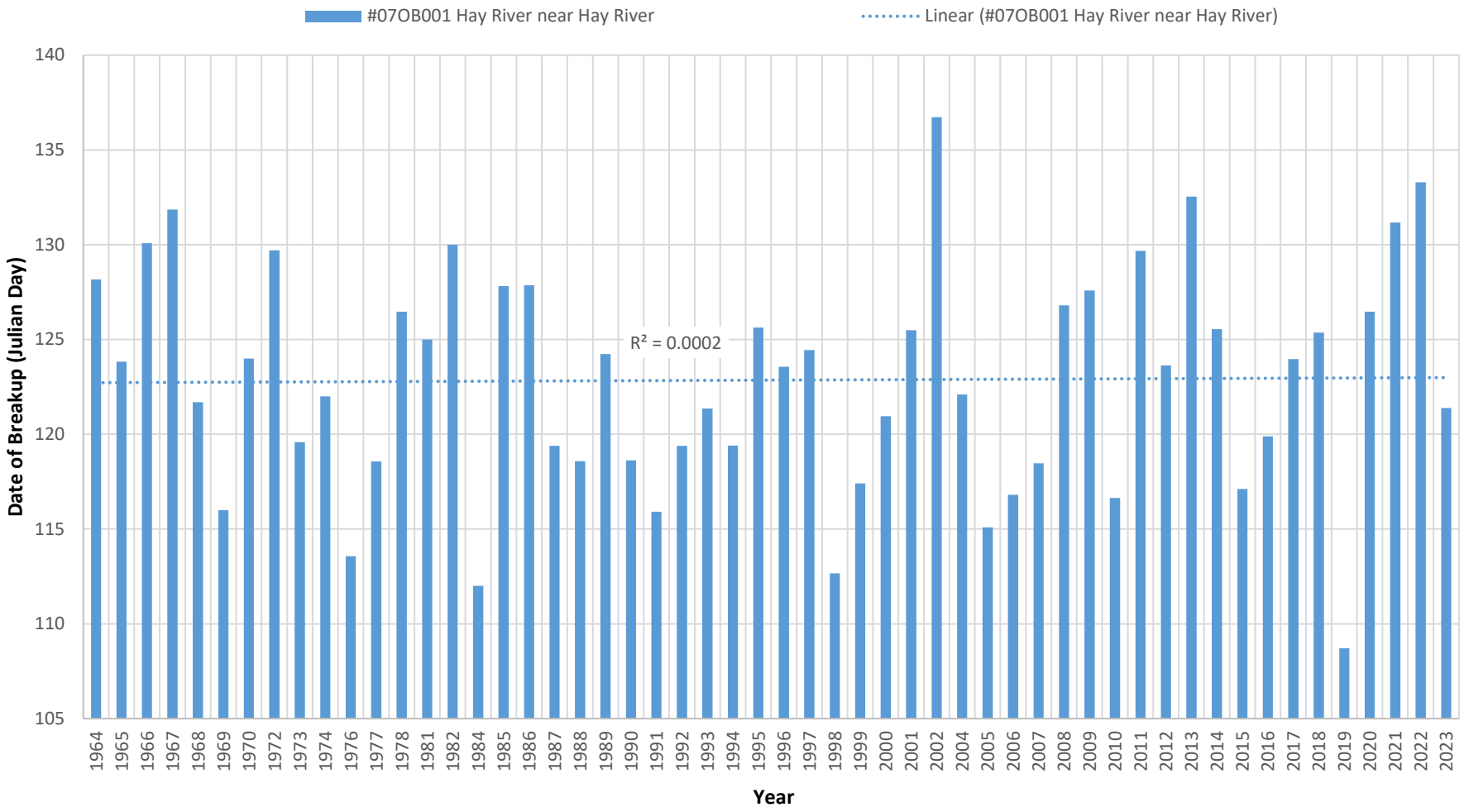

Government of Northwest Territories
Gouvernement des Territoires du Nord-Ouest

Canada

nhc

UNITS – AS SHOWN

KÁTŁ'ODEH (HAY RIVER)
FLOOD HAZARD MAPPING STUDY

RECORDED PEAK BREAKUP TIMING TREND AT #07OB001 HAY RIVER NEAR HAY RIVER

Job: 1008469

Date: Feb-2025

FIGURE 77

APPENDIX A

SURVEY DATA

Provided as an electronic file in ESRI geodatabase format (HayRiverSurvey2024.gdb)

APPENDIX B

REACH REPRESENTATIVE PHOTOS

1) Looking downstream from RS 44893 of the Hay River Main Channel near Paradise Gardens.

2) Looking downstream from RS 17583 of the Hay River Main Channel.

3) Looking upstream at K'atl'odeh Bridge from RS 16005 of the Hay River Main Channel.

4) Looking upstream at the West Channel Bridge from RS 4835 of the Hay River West Channel.

5) Looking upstream from RS 3808 of the Hay River West Channel.

6) Looking downstream from RS 896 of the Hay River Rudd Channel.

Note:

Photos taken by NHC during site visit May 27 through June 4.

Government of Northwest Territories

Hay River Flood Study

Reach Representative Photos

1008469	April 2025	**B-1**

7) Looking upstream at the highwater channel near RS 798 of the Hay River West Fishing Village Channel.

8) Looking upstream from RS 675 of the Hay River West Fishing Village Channel.

9) Looking downstream towards Great Slave Lake from RS 436 of the Hay River West Fishing Village Channel.

10) Looking upstream at the Island B side channel from RS 2963 of the Hay River East Channel.

11) Looking downstream towards Great Slave Lake from RS 1969 of the Hay River East Channel.

12) Looking upstream at the Island A side channel from RS 1279 of the Hay River West Fishing Village Channel.

Note:

Photos taken by NHC during site visit May 27 through June 4.

Government of Northwest Territories

Hay River Flood Study

Reach Representative Photos

1008469	April 2025	**B-2**

APPENDIX C

COMPUTED DESIGN FLOOD LEVELS

Table 1 Hay River Main Channel Computed Flood Frequency Water Levels

Project River Station (km)	Model RS (m)	Flood Return Period		
		100-year Open Water	100-year Ice Jam	200-year Ice Jam
		Water Surface Elevation (m)		
1064.0	50489	178.32	182.18	182.89
1064.9	49607	177.85	181.52	182.23
1065.7	48789	177.40	181.11	181.78
1066.5	48041	176.98	180.73	181.40
1067.1	47414	176.61	180.16	180.84
1067.6	46950	176.36	179.96	180.68
1068.1	46432	176.06	179.68	180.44
1068.6	45940	175.79	179.39	180.04
1069.1	45381	175.46	179.27	179.99
1069.6	44893	175.21	178.93	179.71
1070.1	44373	174.94	178.55	179.33
1070.6	43910	174.66	178.41	179.10
1071.1	43440	174.50	178.19	178.95
1071.6	42926	174.29	177.87	178.50
1072.1	42432	174.02	177.52	178.19
1072.7	41845	173.66	177.26	177.99
1073.2	41298	173.42	176.85	177.56
1073.7	40759	173.19	176.59	177.26
1074.2	40252	173.01	176.38	177.01
1075.1	39422	172.70	176.06	176.80
1075.9	38603	172.38	175.77	176.45
1076.6	37896	172.18	175.65	176.43
1077.4	37118	171.84	175.34	176.05
1078.1	36379	171.55	175.04	175.77
1078.8	35691	171.22	174.73	175.41
1079.5	35005	170.95	174.47	175.15
1079.9	34559	170.82	174.37	175.07

Project River Station (km)	Model RS (m)	Flood Return Period		
		100-year Open Water	100-year Ice Jam	200-year Ice Jam
		Water Surface Elevation (m)		
1080.6	33874	170.56	174.17	174.99
1081.3	33213	170.35	173.81	174.58
1081.7	32796	170.16	173.59	174.21
1082.2	32344	170.02	173.45	174.10
1082.7	31834	169.85	173.27	174.01
1083.1	31391	169.71	173.12	173.92
1083.5	31006	169.56	172.91	173.57
1084.0	30509	169.41	172.76	173.49
1084.5	30027	169.27	172.59	173.29
1084.9	29560	169.12	172.45	173.08
1085.4	29123	168.94	172.27	172.93
1085.9	28646	168.83	172.20	172.86
1086.4	28106	168.70	172.05	172.69
1086.9	27647	168.57	171.95	172.60
1087.4	27139	168.42	171.79	172.54
1087.9	26571	168.27	171.70	172.40
1088.4	26051	168.11	171.56	172.32
1088.9	25631	168.00	171.44	172.17
1089.4	25089	167.85	171.37	172.10
1089.9	24567	167.68	171.24	172.05
1090.4	24071	167.54	171.24	172.05
1090.9	23608	167.46	171.24	172.05
1091.3	23178	167.30	171.24	172.05
1091.7	22847	167.21	171.24	172.05
1092.0	22546	167.13	171.24	172.05
1092.2	22275	167.07	171.19	172.05
1092.6	21920	166.90	171.17	172.04
1092.9	21615	166.83	171.17	172.04
1093.2	21308	166.70	171.17	171.95

Project River Station (km)	Model RS (m)	Flood Return Period		
		100-year Open Water	100-year Ice Jam	200-year Ice Jam
		Water Surface Elevation (m)		
1093.5	21017	166.62	171.06	171.83
1093.8	20710	166.43	171.06	171.82
1094.1	20390	166.37	171.06	171.80
1094.4	20094	166.21	171.04	171.73
1094.7	19791	166.12	170.98	171.73
1095.0	19550	166.08	170.93	171.68
1095.4	19138	165.90	170.87	171.60
1095.8	18740	165.67	170.69	171.42
1096.1	18424	165.54	170.56	171.34
1096.4	18145	165.46	170.46	171.18
1096.6	17901	165.3	170.35	171.08
1096.9	17583	165.11	170.27	170.97
1097.3	17240	165.03	170.04	170.83
1097.6	16875	164.89	169.91	170.58
1098.0	16548	164.71	169.75	170.49
1098.1	16436	164.67	-	-
1098.1	16402	164.59	169.62	170.33
1098.2	16294	164.52	169.60	170.33
1098.5	16005	164.47	169.41	170.07
1098.7	15821	164.38	169.28	170.01
1098.9	15560	164.17	169.07	169.79
1099.3	15219	164.11	168.83	169.57
1099.6	14916	163.96	168.62	169.32
1099.9	14622	163.85	168.44	169.04
1100.2	14255	163.74	168.31	168.94
1100.7	13843	163.59	168.14	168.86
1101.2	13340	163.33	167.97	168.65
1101.6	12878	163.14	167.79	168.45
1102.0	12512	163.01	167.64	168.30

Project River Station (km)	Model RS (m)	Flood Return Period		
		100-year Open Water	100-year Ice Jam	200-year Ice Jam
		Water Surface Elevation (m)		
1102.4	12055	162.83	167.58	168.23
1102.9	11619	162.64	167.48	168.14
1103.3	11232	162.41	167.38	167.97
1103.6	10887	162.21	167.21	167.82
1104.0	10495	162.05	167.04	167.68
1104.4	10138	161.82	166.99	167.63
1104.7	9820	161.65	166.86	167.48
1105.0	9528	161.47	166.77	167.38
1105.2	9271	161.29	166.61	167.21
1105.5	9028	161.13	166.50	167.14
1105.7	8778	161.02	166.46	167.05
1106.0	8498	160.93	166.39	166.96
1106.3	8202	160.77	166.21	166.80
1106.6	7927	160.57	166.08	166.63
1106.9	7592	160.41	165.82	166.38
1107.2	7290	160.27	165.60	166.16
1107.4	7062	160.15	165.47	166.04
1107.7	6822	160.04	165.29	165.85
1107.9	6614	159.92	165.18	165.70
1108.0	6504	159.86	165.09	165.65

Notes:

1. Model RS refers to the HEC-RAS river station values, while the adopted project river stations follows NHC's adopted river stationing convention for the project

Table 2 Hay River East Channel Computed Flood Frequency Water Levels

Project River Station (km)	Model RS (m)	Flood Return Period		
		100-year Open Water	100-year Ice Jam	200-year Ice Jam
		Water Surface Elevation (m)		
1108.1	6383	159.83	164.77	165.25
1108.2	6271	159.71	164.68	165.17
1108.4	6117	159.63	164.51	164.95
1108.6	5934	159.48	164.40	164.91
1108.7	5754	159.32	164.34	164.81
1108.9	5554	159.15	164.16	164.62
1109.2	5335	158.96	163.96	164.42
1109.4	5141	158.76	163.80	164.27
1109.6	4944	158.59	163.64	164.04
1109.8	4732	158.38	163.48	163.89
1110.0	4521	158.20	163.23	163.65
1110.2	4300	158.01	163.00	163.39
1110.4	4092	157.86	162.78	163.18
1110.6	3851	157.74	162.54	162.95
1110.9	3585	157.64	162.24	162.62
1111.2	3322	157.58	162.04	162.44
1111.4	3118	157.53	161.79	162.20
1111.5	2950	157.48	161.61	162.04
1111.7	2773	157.46	161.43	161.87
1111.9	2592	157.43	161.30	161.70
1112.1	2392	157.38	161.10	161.53
1112.3	2189	157.34	160.86	161.25
1112.5	1969	157.31	160.69	161.15
1112.8	1740	157.28	160.47	160.89
1113.0	1499	157.23	160.33	160.69
1113.2	1279	157.19	160.18	160.69
1113.4	1079	157.15	160.08	160.55

Project River Station (km)	Model RS (m)	Flood Return Period		
		100-year Open Water	100-year Ice Jam	200-year Ice Jam
		Water Surface Elevation (m)		
1113.6	888	157.12	159.98	160.42
1113.8	692	157.08	159.93	160.38
1114.0	514	157.04	159.88	160.33
1114.2	293	157.01	159.65	160.08
1114.4	99	156.95	158.29[1]	158.58[1]

Notes:

1. Computed flood frequency water levels were not used for flood hazard mapping.
2. Model RS refers to the HEC-RAS river station values, while the adopted project river stations follows NHC's adopted river stationing convention for the project

Table 3 Hay River West Channel Computed Flood Frequency Water Levels

Project River Station (km)	Model RS (m)	Flood Return Period		
		100-year Open Water	100-year Ice Jam	200-year Ice Jam
		Water Surface Elevation (m)		
1108.2	5292	159.97	163.95[1]	164.33[1]
1108.3	5186	159.88	163.88[1]	164.29[1]
1108.4	5094	159.84	-	-
1108.4	5066	159.76	163.87	164.26
1108.5	4981	159.68	163.84	164.25
1108.7	4835	159.56	163.77	164.16
1108.8	4686	159.40	163.67	164.10
1109	4540	159.33	163.56	163.97
1109.1	4395	159.24	163.43	163.86
1109.2	4260	159.20	163.31	163.68
1109.4	4113	159.10	163.15	163.56
1109.6	3946	159.05	163.01	163.41
1109.7	3808	158.99	162.95	163.36
1109.9	3647	158.92	162.85	163.25
1110	3500	158.85	162.73	163.10
1110.1	3361	158.76	162.64	163.02
1110.3	3224	158.71	162.60	162.96
1110.4	3074	158.64	162.53	162.91
1110.6	2931	158.54	162.50	162.83
1110.7	2779	158.43	162.37	162.75
1110.9	2639	158.34	162.25	162.62
1111	2513	158.24	162.18	162.53
1111.1	2375	158.17	161.99	162.32
1111.2	2286	158.05	161.89	162.18
1111.3	2209	157.97	161.74	162.07
1111.4	2121	157.81	161.63	161.93
1111.5	2027	157.72	161.47	161.78

Project River Station (km)	Model RS (m)	Flood Return Period		
		100-year Open Water	100-year Ice Jam	200-year Ice Jam
		Water Surface Elevation (m)		
1111.6	1934	157.65	161.35	161.65
1111.6	1851	157.57	161.21	161.51
1111.7	1767	157.49	160.98	161.24
1111.8	1653	157.45	160.74	160.99
1112	1550	157.42	160.62	160.85
1112.1	1423	157.34	160.44	160.67
1112.2	1275	157.30	160.24	160.44
1112.3	1179	157.27	160.12	160.35
1112.4	1085	157.25	160.00	160.21
1112.6	942	157.18	159.85	160.09
1112.7	798	157.10	159.65	159.91
1112.8	675	157.06	159.46	159.74
1112.9	556	157.03	159.32	159.56
1113.1	436	156.99	159.18	159.41
1113.2	322	156.97	158.98	159.20
1113.3	225	156.95	158.58[1]	158.83[1]
1113.4	123	156.95	157.36[1]	157.58[1]

Notes:

1. Computed flood frequency water levels were not used for flood hazard mapping.
2. Model RS refers to the HEC-RAS river station values, while the adopted project river stations follows NHC's adopted river stationing convention for the project

Table 4 Hay River Rudd Channel Computed Flood Frequency Water Levels

Project River Station (km)	Model RS (m)	Flood Return Period		
		100-year Open Water	100-year Ice Jam	200-year Ice Jam
		Water Surface Elevation (m)		
1111.2	1286	157.71	161.89	162.18
1111.3	1211	157.59	161.74	162.07
1111.4	1117	157.32	161.63	161.93
1111.5	1010	157.24	161.47	161.78
1111.6	896	157.19	161.21	161.51
1111.7	780	157.15	160.74	160.99
1111.8	665	157.11	160.44	160.67
1111.9	551	157.07	160.24	160.44
1112.1	444	157.04	160.00	160.21
1112.1	360	157.01	159.65	159.91
1112.2	261	156.98	159.32	159.56
1112.4	88	156.95	157.36[1]	157.58[1]

Notes:

1. Computed flood frequency water levels were not used for flood hazard mapping.
2. Model RS refers to the HEC-RAS river station values, while the adopted project river stations follows NHC's adopted river stationing convention for the project

APPENDIX D

100-YEAR OPEN WATER FLOOD HAZARD MAP

Provided under separate cover.

APPENDIX E

100-YEAR ICE JAM FLOOD HAZARD MAP

Provided under separate cover.

APPENDIX F

200-YEAR ICE JAM FLOOD HAZARD MAP

Provided under separate cover.

APPENDIX G

CLIMATE CHANGE SUPPORTING INFORMATION

CLIMATE CHANGE SUPPORTING INFORMATION

GNWT Climate Change Strategic Framework

The Government of the Northwest Territories Climate Change Strategic Framework[1] has three goals: (1) Transition to a strong, healthy economy that uses less fossil fuel, thereby reducing greenhouse gas emissions by 30% below 2005 levels by 2030; (2) Improve knowledge of the climate change impacts occurring in the NWT; and (3) Build resilience and adapt to a changing climate. Goal 2 is most relevant to this work, details on the goal are provided below.

Goal #2- Improve knowledge of the climate change impacts occurring in the NWT

"Improving knowledge of climate change impacts occurring in the NWT is the second goal of the Framework. To address climate change, there is a need for greater understanding of the impacts to the natural environment, residents' health, safety, culture and heritage, and the territory's infrastructure. The integrated use and management of traditional, local and scientific knowledge to determine knowledge gaps, set and implement research and monitoring requirements, and obtain current and timely information, is essential.

"The warming climate is leading to gradual shifts within ecosystems and more extreme events affecting the natural environment. Thawing of permafrost, changes to water quality and quantity, altered forests and tundra vegetation, and impacts on wildlife, fish and marine mammal health and distribution, have been observed for several years and are intensifying.

"The effects of climate change on the natural environment can directly impact the health of NWT residents, both physically (such as increases in respiratory problems due to extreme weather) and mentally (such as stress or effects on well-being due to impacts on traditional harvesting sites and activities).

"Safety of the general public is also a central concern, from erosion of coastlines leading to building instability, to increased flood risks in certain communities, to less predictable winter travel conditions, all leading to a heightened risk of injury and death.

"Effects on the territory's culture and heritage, from risks to heritage resources such as archeological sites due to permafrost thaw and wildland fires, to impacts on traditional economies such as trapping, are evident and will likely continue to intensify. Indigenous people and other residents of the NWT are particularly vulnerable to climate related changes since, for generations, they have depended on the land, water and wildlife for their livelihood and sustenance.

"The NWT's infrastructure (buildings, roads, pipelines, transmission lines, etc.) has been and continues to be impacted by climate change. Permafrost thaw and extreme weather events can have significant effects on infrastructure. Coastal erosion is also a concern in the northern parts of the NWT, threatening important infrastructure such as roads and buildings.

"Developing a better understanding of current and future impacts and opportunities will support informed decision-making on how to build resilience and adapt to a changing climate."

Source: GNWT Climate Change Strategic Framework[1]

[1] https://www.gov.nt.ca/ecc/en/services/climate-change/2030-nwt-climate-change-strategic-framework

Available Research and Climate Projection Data

Emission Scenarios

Anthropogenic activities around the globe release greenhouse gases into the earth's atmosphere – CO_2 being the principal one, followed by nitrous oxide – and these interfere with the earth's energy balance creating a trend towards higher air temperatures. At any given geographic location, natural climatic variability continues exhibiting colder years as well as warmer years, but an underlying tendency towards progressively higher mean temperatures over time is projected for the future. A warming trend is found in observational records of recent decades at most global locations.

The magnitude of future global emissions of greenhouse gases cannot be predicted with any certainty, but scientists have developed a number of scenarios for possible future emissions. The ESMs included in the CMIP6 projections dataset were run under these scenarios. However, the IPCC does not attempt to attribute comparative likelihoods to the different scenarios. In this, it follows the tradition established in CMIP3, where the Special Report on Emission Scenarios (Nakićenović, N. et al., 2000) presented all scenarios as *"equally valid with no assigned probabilities of occurrence"*. The scenarios used in CMIP5 were defined on the basis of hypothetical future greenhouse gas concentrations in the earth's atmosphere, i.e., "representative concentrations pathways" (RCPs), where *"no likelihood or preference is attached to any of the individual scenarios in the set"* while they included a very wide range of possibilities described as *"...the full range of emission scenarios available in the current scientific literature, with and without climate policy"* (van Vuuren et al., 2011). No explanations (whether socio-economic, technologic or demographic) were associated with any of the RCPs, until CMIP6.

In CMIP6, explanatory storylines were sought, called "shared socio-economic pathways" (SSPs), and these SSPs were developed to correspond with the RCPs, i.e., a storyline (SSP) was associated with specific greenhouse gas concentrations (RCP). The SSPs represent scenarios of future evolution of human societies and were developed by multidisciplinary teams including economists and energy specialists. Each SSP is based on a storyline of demographic, economic, technological and political evolution involving the world countries.

Five different classes of SSPs were developed with key differences in their narratives (Table 1-1) More complete descriptions are given in Riahi et al. (2017), O'Neill et al. (2014) and van Vuuren et al. (2011). Four of those were used by a large number of ESMs, and SSP4 was used for a smaller number of ESMs and the SSP4 results are not available through the CMIP6 data portals. The main scenario of each SSP is indicated in the last column of Table 1-1.

The numbers in the name of each SSP identify the class as well as the projected global energy imbalance it corresponds to in year 2100. For example, SSP1-2.6 belongs to class SSP1 and corresponds to an energy imbalance of 2.6 Watt per square meter in year 2100. Thus, SSP2-4.5

leads to a higher energy imbalance than SSP1-2.6, therefore more intense warming of the earth's atmosphere, due to higher greenhouse emissions in the course of this century.

Table 1-1 The five classes of SSP global emission scenarios and the main scenario of each class. Class descriptions are repeated from Riahi et al. (2017).

SSP Class	Class Description	Main scenario of each SSP
SSP1 Low emissions	The world shifts gradually, but pervasively, toward a more sustainable path, emphasizing more inclusive development that respects perceived environmental boundaries. Management of the global commons slowly improves, educational and health investments accelerate the demographic transition, and the emphasis on economic growth shifts toward a broader emphasis on human well-being. Driven by an increasing commitment to achieving development goals, inequality is reduced both across and within countries. Consumption is oriented toward low material growth and lower resource and energy intensity.	SSP1-2.6
SSP2 Moderate emissions	The world follows a path in which social, economic, and technological trends do not shift markedly from historical patterns. Development and income growth proceeds unevenly, with some countries making relatively good progress while others fall short of expectations. Global and national institutions work toward but make slow progress in achieving sustainable development goals. Environmental systems experience degradation, although there are some improvements and overall the intensity of resource and energy use declines. Global population growth is moderate and levels off in the second half of the century. Income inequality persists or improves only slowly and challenges to reducing vulnerability to societal and environmental changes remain.	SSP2-4.5
SSP3 High emissions	A resurgent nationalism, concerns about competitiveness and security, and regional conflicts push countries to increasingly focus on domestic or, at most, regional issues. Policies shift over time to become increasingly oriented toward national and regional security issues. Countries focus on achieving energy and food security goals within their own regions at the expense of broader-based development. Investments in education and technological development decline. Economic development is slow, consumption is material-intensive, and inequalities persist or worsen over time. Population growth is low in industrialized and high in developing countries. A low international priority for addressing environmental concerns leads to strong environmental degradation in some regions.	SSP3-7.0
SSP4 Very high emissions	Highly unequal investments in human capital, combined with increasing disparities in economic opportunity and political power, lead to increasing inequalities and stratification both across and within countries. Over time, a gap widens between an internationally-connected society that contributes to knowledge- and capital-intensive sectors of the global economy, and a fragmented collection of lower-income, poorly educated societies that work in a labor intensive, low-tech economy. Social cohesion degrades and conflict and unrest become increasingly common. Technology development is high in the high-tech economy and sectors. The globally connected energy sector diversifies, with investments in both carbon-intensive fuels like coal and unconventional oil, but also low-carbon energy sources. Environmental policies focus on local issues around middle and high income areas.	unavailable

SSP Class	Class Description	Main scenario of each SSP
SSP5 Extreme emissions	This world places increasing faith in competitive markets, innovation and participatory societies to produce rapid technological progress and development of human capital as the path to sustainable development. Global markets are increasingly integrated. There are also strong investments in health, education, and institutions to enhance human and social capital. At the same time, the push for economic and social development is coupled with the exploitation of abundant fossil fuel resources and the adoption of resource and energy intensive lifestyles around the world. All these factors lead to rapid growth of the global economy, while global population peaks and declines in the 21st century. Local environmental problems like air pollution are successfully managed. There is faith in the ability to effectively manage social and ecological systems, including by geo-engineering if necessary.	SSP5-8.5

Figure 1.1 shows the evolution over time of our planet's energy imbalance (known as "radiative forcing") and mean global temperature corresponding to each SSP and RCP. This figure also shows the relationship between the RCP scenarios from CMIP5 and the SSP scenarios of CMIP6.

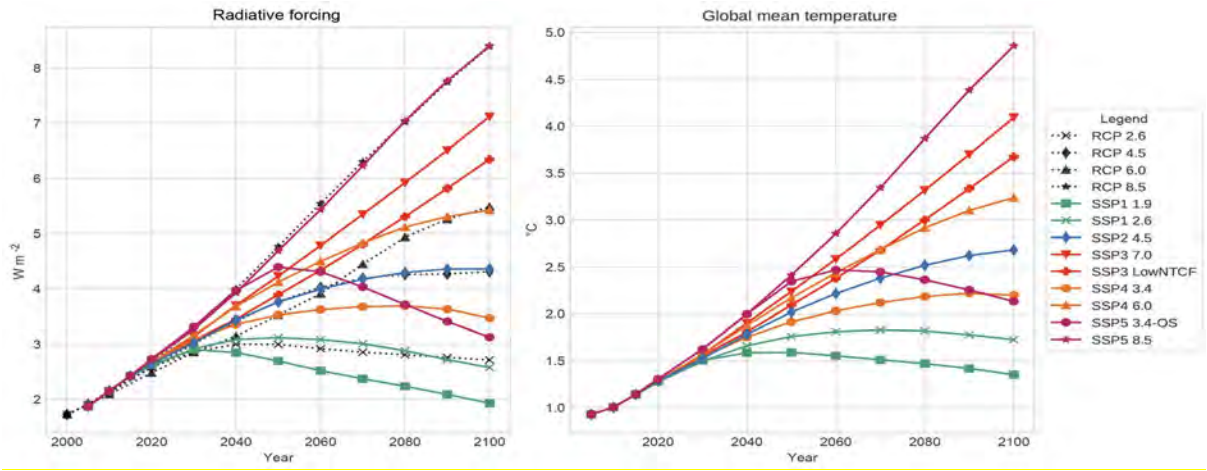

Figure 1.1 Radiative forcing or global energy imbalance (left panel) and global mean temperature (right panel) for each RCP and SSP. Figure source: Gidden et al. (2019).

Downscaled climate projections

The downscaled projections are from an ensemble of 24 earth system models (ESMs) and were made available on the Canadian government data portal[2], for SSP1-2.6, SSP2-4.5 and SSP5-8.5. An empirical-statistical methodology – briefly described below – was used to obtain these projections. Other sources provide downscaled projections in gridded format (e.g., the Pacific

[2] https://climatedata.ca

Climate Impacts Consortium data portal[3]) but, to our knowledge, this one[Error! Bookmark not defined.] is unique in providing projections by watershed.

The outputs from earth system models must undergo a process of "downscaling" before they can be used in impact assessment studies. Downscaling serves two purposes: (1) It provides a higher resolution spatial scale, and (2) it provides climatic values that are in better agreement with observations. The increased spatial resolution is necessary because grid cells of earth system models (ESMs) cover considerably large areas, ranging from a few hundred km^2 in some ESMs to several thousand km^2 in others. Resolutions desired for impact assessment studies are typically in the order of 1/8°x 1/8° (less than 150 km^2) or 1/12°x 1/12° (less than 70 km^2).

The higher spatial resolution may be obtained by statistical methods or dynamical models:

(a) Empirical-statistical downscaling models (ESDMs) establish a statistical relationship between the coarse-resolution ESM output for a historical period for a given geographical region and the finer-resolution observations-based gridded data representing that period over that region. The observations-based gridded data may have been obtained by statistical interpolation of ground observations or using a weather model that assimilates those ground observations to create a "Reanalysis" data set.

(b) Dynamical downscaling uses regional climate models (RCMs), which have higher spatial resolution than ESMs and better represent land topography and coastlines. The output from the RCMs typically needs to be statistically downscaled (as in (a) above) to remove the bias present in most RCM data.

While option (b), dynamical downscaling, is scientifically superior than option (a), empirical-statistical downscaling, it involves computationally (and financially) costly runs of regional climate models. For this reason, dynamically-downscaled projections are not readily available for large ESM ensembles.

Selection of SSP scenarios for this study

Projections for two SSPs are consulted in this study. They are SSP1-2.6 and SSP2-4.5. This section explains the reasons for this selection of SSPs instead of others. Similar to previous IPCC assessment reports, no probabilities or relative likelihoods were assigned to the SSPs (Riahi et al., 2017). Thus, the user is to make their own evaluation. Difficulties resulting from this approach have been reviewed e.g. by Huard et al. (2022), however various scientists have argued from early on that it is not possible to assign probabilities to future emissions because they represent

[3] https://www.pacificclimate.org/data/statistically-downscaled-climate-scenarios

"unknowable knowledge" and depend on subjective opinions about future developments which are unpredictable (e.g., Dessai and Hulme, 2004).

Despite the reluctance to assign probabilities to SSPs, the first chapter of the IPCC Sixth Assessment report (Chen et al., 2021) does discuss their likelihood. It concludes that SSP5-8.5 and SSP3-7.0, both of which consider completely unregulated and unabated future emissions (in violation of commitments already in place today), should be considered counter-factual scenarios. It also concludes that policies currently agreed upon would lead to an energy imbalance by year 2100 roughly close to 4.5 Watt/m^2 – thus making SSP2-4.5 a likely scenario.

Concerning SSP3-7.0, Shiogama et al. (2023) warns it is not intended for impact studies. It clarifies that SSP3–7.0 was designed to have different characteristics compared with the other scenarios for purposes of increasing scientific understanding of the impacts of aerosols and land use. SSP3-7.0 assumes high-aerosol emissions incompatible with air quality policies and assumes very large deforestation rates.

Other researchers have tried to independently obtain some approximate answers to the question of SSP probabilities. Huard et al. (2022) presented a methodology that allows calculating SSP probabilities, where the first step involves calculating the greenhouse gas emissions rates compatible with each SSP, and the second step involves "integrated assessment models". Unfortunately, the first step is highly uncertain given the complexity of indirect emissions resulting from carbon cycle feedbacks (for example, the carbon emissions from permafrost thaw). Nevertheless, their estimation of a very low probability for SSP5-8.5 (the most extreme SSP) in the second half of this century appears to be a robust result. Another, more uncertain result of their study is that SSP2-4.5 is the most likely pathway for this century.

The recent work of Venmans and Carr (2024) offered a different approach, which focuses on the emission-reduction policies which have already been approved by different governments around the world. This includes individual policies as well as international accords. Assuming those policies will indeed be implemented, they demonstrate that the most likely energy imbalance reached in year 2100 is close to 4.5 Watt/m^2, making SSP2-4.5 the most likely. This result agrees with that of Huard et al. (2022) mentioned above. They also agree with Huard et al. (2022) in estimating a very low probability for SSP5-8.5, on the basis that the costs of renewable energies have fallen far more rapidly in recent years than had been anticipated; the global coal consumption has stagnated since 2013 (and the International Energy Agency (IEA) projects it will fall by another 25% before year 2050 as a result of policies already agreed on and given the fall in price of shale gas); and the cost of batteries has also dropped, lowering the demand for oil (which the IEA projects will stagnate around year 2030). Moreover, as they point out, the price of carbon in the European Union Emission Trading Scheme increased sharply (from 5/tCO_2 in 2017 to over 80/tCO_2 in 2023); the United States have rejoined the Paris Accord; and in 2021 China launched the largest emission trading scheme of all time so far.

Earlier this year, a publication by Nathan Gillett from ECCC (Gillett, 2024) argued that the uncertainty associated with future greenhouse gas emissions has roughly halved in the past decade, on the basis of their analysis of the progress made in climate policy and climate science. The conclusion presented is that *"…the range of plausible future emissions is now lower and narrower than it was in 2013 … and can reasonably be bracketed by the SSP1-1.9 and SSP2-4.5 scenarios"* (Gillett, 2024).

Uncertainty Associated with Climate Projections

While there is a need to provide climate projections for planning purposes, the underlying projections of climate change are subject to large and unquantifiable uncertainty. The projections of air temperature and precipitation presented below should therefore be considered as plausible representations of the future, given the best current scientific information, and do not represent specific predictions. The actual future realizations of these variables over the areas studied will differ from any of the projections considered here, and their differences compared to historical climate may be greater or smaller than the differences in the projections considered. Uncertainty is particularly great for precipitation projections, where even the sign of change (increase or decrease) often differs between earth system models. Precipitation processes have chaotic behavior and involve multiple spatial scales including scales finer than the resolution of earth system models.

The main sources of uncertainty are unknown future emissions of greenhouse gases (addressed in the preceding section); limitations of current scientific knowledge and the formulation of the earth system models used; and the natural variability of climate, in particular the great variability of precipitation from year to year and at longer scales such as decadal scale. An additional source of uncertainty is the use of spatial downscaling of the precipitation and temperature time series simulated by earth system models. Extreme precipitation additionally depends on a major non-climatic factor, which is the local atmospheric concentrations of different types of aerosols.

Adding to the uncertainty of climate projections, the effects of the Great Slave Lake on regional climate as the lake's ice cover period lengthens are not well represented by CMIP6 earth systems models. The lake's presence, due to its thermal inertial across the seasons, could moderate seasonal climatic changes (Huziy and Sushama, 2017). The lake's presence could also lead to increased snowfall in the ice-free fall season, known as "lake effect snow".

Review of Literature on Ice Jam Flooding Related to the Hay River and Fort Simpson

Ice jams on the lower Hay River have been studied over time, and Burrell et al. (2015) provides a list of 16 different studies, spanning 1959 to 2012. Notable from this list are theses and peer-reviewed publications by students of Prof. Faye Hicks at University of Alberta, dating from 2011 and 2012. NHC consulted these studies for the present assessment, having found that the doctoral thesis by Zhao (2012) contains important observations-based interpretation of the hydro-climatic factors associated with ice jam flooding on the Hay River.

A good number of peer-reviewed publications address specifically the effects of climate change on ice jam flooding frequency and severity. Some of these publications themselves represent literature reviews, including Turcotte et al. (2019), while others focus on particular aspects of river ice formation, thickening, ice break, ice jams, etc., most of them with a focus on tributaries of the Mackenzie River.

Climate change will impact ice jam flooding risk through a number of processes that this section attempts to separate into subsections.

Thresholds Between Mechanical and Thermal Breakup of River Ice Cover

Due to the clarity of its exposition, Beltaos (2003) is quoted directly below:

"The breakup of river ice is triggered by mild weather and encompasses a variety of processes associated with thermal deterioration, initial fracture, movement, fragmentation, transport, jamming, and final clearance of the ice. Though several or all of these processes may be occurring simultaneously within a given reach, it is convenient to visualize the breakup period as a succession of distinct phases such as ***pre-breakup, onset, drive, wash****. During the pre-breakup phase, the ice cover becomes more susceptible to fracture and movement via thermally induced reductions in thickness and strength (excepting premature breakup events, as discussed later). At the same time, the warming weather brings about increased flow discharges, due to snowmelt or rainfall or both. The increasing hydrodynamic forces and rising water levels fracture the ice cover and reduce its attachment to the riverbanks while the increased flow velocities cause it to move and break down into relatively small blocks. This is the onset of breakup, and is followed by the drive, that is, the transport of ice blocks and slabs by the current.*

"The onset is governed by many factors, including channel morphology, which is highly variable along the river. It is thus typical to find reaches where breakup has started alternating with reaches where the winter ice cover has not yet moved. This configuration is the almost exclusive cause of breakup jamming: ice blocks moving down the river eventually encounter stationary ice cover and begin to pile up behind it, initiating a jam. In this case, the upstream drive has been stalled at a reach that is still in the pre-breakup phase, and which may well be followed by another that is in the drive, or even wash, phase. As the flow continues to increase and thermal deterioration advances, ice jams release, thus generating major ice runs and surging flows. The wash may begin after the passage of an ice run and typically involves re-floating and transporting ice blocks that may have been left stranded on shallow areas near the banks or mid-channels bars and islands.

"Depending on hydrometeorological conditions, the severity of a breakup event can vary between two extremes, those of the thermal or overmature breakup and the premature breakup. The former type occurs when mild weather is accompanied by low runoff, due to gradual slow melt and lack of rain. The ice cover deteriorates in place and eventually disintegrates under the limited forces applied by the modest current. Ice jamming is minimal, if any, and water levels remain low. Premature breakup on the other hand, is associated with rapid runoff, usually due to a combination of rapid melt and heavy rain. The hydrodynamic forces are sufficient to lift and break

segments of the ice cover before significant thermal deterioration can occur. Ice jams are now the most persistent because they are held in place by sheet ice that retains its strength and thickness. This is aggravated by the high river flows caused by the intense runoff, rendering premature events the most severe in terms of flooding and damages. Usually, a breakup event falls somewhere between these two extremes, and involves a combination of thermal effects and mechanical fracture of the ice. The term mechanical breakup is used herein to denote all nonthermal events because they are 'at least partly' governed by the mechanical properties of the ice cover.

"The conditions that determine whether a breakup event will be thermal or mechanical have never been examined or quantified, despite their practical significance in flood forecasting and warning, and in hydroclimatic studies of river ice processes. Using current understanding of breakup initiation mechanisms, a first attempt to develop physics-based criteria for this threshold has been carried out and is presented herein. The resulting relationships are tested with case studies in three different rivers, and their practical implications are discussed.

"Onset of mechanical breakup:

"Defining the onset of the breakup event at any particular location along a river as the time when the winter ice cover is set in sustained motion, a number of onset criteria have been formulated in the past few decades (e.g. see Beltaos, 1995). Most are completely empirical, relying on various combinations of water level, ice thickness, freeze-up conditions, and air temperature indices such as degree-days of thaw. A common criterion that incorporates past empirical findings (…) is:

$$H_B - H_F = k \cdot h_0 - F(S) \qquad (1)$$

in which H_B = water surface elevation at which the ice cover starts to move; H_F = water surface elevation at which the ice cover formed during the preceding freeze-up event = freeze-up level; h_0 = ice cover thickness prior to the start of melt, or "initial" thickness for the pre-breakup period; F = a site-specific function of S, the latter being an index of thermal effects on the ice cover, often taken as the cumulative heat flux to the ice or simply the accumulated degreedays of thaw; and k = site-specific coefficient, so far known to take on values between 2 and 10. Note that this type of criterion does not apply to thermal breakup events.

"Eq. (1) and others like it do not explicitly account for hydrodynamic or morphological effects; hence, they can only be applied to the particular river site at which they have been calibrated, i.e. they are site-specific."

Snow Accumulation and Snowmelt

Future warming leads to the **shortening of the snow accumulation period**. However, winter temperatures will remain well below freezing throughout this century and **winter precipitation is projected to increase**. There will be a possible increase in snowfall as the Great Slave Lake experiences a shortening of its ice cover period. The known **"lake effect snow"** refers to the enhancement of snowfall after a cold air mass passes through open water and becomes

saturated with moisture. Rühland et al. (2023) presented a recent account of the climatic changes affecting the Great Slave Lake.

Snow falling in river water frequently leads to the formation of slush, later resulting in thicker river ice cover (Turcotte et al., 2012). A thicker and denser snowpack promotes the formation of thicker river ice due to higher albedo (Bush and Lemmen, 2019).

Streamflow Hydrograph

As a result of warming in the fall and spring, seasonal flows throughout the southern Mackenzie River upstream of Fort Simpson, including the Hay River, will experience changes in their seasonal means and seasonal peak flow frequencies. Warming of the fall season, where the average air temperature is crossing above 0°C, implies a progressive transition from snowfall to rainfall and higher mean seasonal flows and peak flows in this season. A trend toward earlier arrival of the spring freshet was detected throughout the Mackenzie River basin (Von de Wall et al., 2010).

The progressive thawing of permafrost will increase infiltration capacity and amplify the subsurface component of the hydrograph (e.g., St. Jacques and Sauchyn, 2009), which may augment minimum flows in winter. An observed decline in minimum flows in the Liard River basin was detected already 20 years ago (Burn et al., 2004). It also has potential implications for channel stability. However, permafrost thaw can also amplify surface runoff response and therefore peak flows, due to increased surface connectivity. This phenomenon was studied specifically for the Liard River basin by Connon et al. (2014), and this publication is reviewed in section0.

Land cover changes may occur as a result of permafrost thaw and warming, including not only a shift in tree species but also an increased incidence of forest fires instigated by pine beetle infestations that kill trees, producing fuel for fires. The proliferation of pine beetles is inhibited by very low minimum air temperatures. Strong rains in the years following a fire can produce exceptional runoff peaks, due to hydrophobic soils in addition of lesser canopy interception. Such runoff peaks may lead to dynamic ice breakup.

Streamflow changes have important consequences for channel morphology, ice formation and ice break-up, as highlighted in each of the subsections below.

Channel Morphology

Most geomorphological change occurs during the dynamic periods of freezup and breakup. Pulses of high sediment concentration typically peak shortly after the arrival of the peak surface concentration of ice. An increase in frequency and magnitude of ice jams, associated with a changing climate, will tend to intensify erosion and sedimentation processes.

The thawing of permafrost as well as possible increases in the frequency of freeze-thaw cycles are expected to decrease bank resistance (Ettema and Daly, 2004), increasing erosion and sediment supply to the channel. Increased sediment transport is expected to lead to morphological changes (Turcotte et al., 2011), but the impact of such changes on ice jams is uncertain and site specific. Turcotte et al. (2019) writes: *"A modification of any channel geometry parameter (i.e., channel avulsion, channel widening, bank incision), alignment (i.e., meander migration acceleration) or profile (i.e., increased spacing between pools) could either reinforce or reverse the intensity and frequency of the [ice] generating process through an alteration of ice-cover or ice-jam mobilization resisting and driving forces. The location of ice jams could also be impacted."*

Ice Formation

Freeze-up conditions in a warmer climate are important to study because they help determine ice cover thickness and ice resistance at breakup, thereby influencing ice jam flood risk. Future changes in air temperature will influence freeze-up conditions through multiple avenues:

(a) Higher flows in late autumn and early winter **delay and prolong the river freezing-over process and the development of a consolidated river ice cover** by preventing ice congestion and slowing down progression of the ice front (e.g., Prowse et al., 2007; Burrell et al., 2023). Prowse et al. (2007) indicates that higher streamflows during freeze-up could translate into an increased initial ice thickness, promoting addition of ice vertically instead of horizontally in the upstream direction, thus delaying the upstream advance of the freeze-up front. According to Prowse et al. (2007), this would result in a **heterogeneous ice cover thickness from upstream to downstream**, which could **lower the thresholds for ice breakup** (Burrell et al., 2023).

(b) Because freeze-up time is prolonged, there is **more formation of frazil ice** instead of an ice layer. Higher flows are more turbulent – which promotes mixing and precludes thermal stratification of the water column, thereby requiring that a larger volume of water be cooled before ice can be produced (e.g., Prowse et al., 2007; Beltaos and Prowse, 2009).

(c) Beltaos and Prowse (2009) suggest that higher streamflows can also lead to more frequent occurrence of a process (termed "**telescoping**") where the initial ice cover undergoes a process of collapsing, thickening and shortening; and that he combination of higher flows with higher air temperatures can increase the severity of **freeze-up jamming**.

(d) Importantly, higher streamflows cause ice to be formed at higher stage levels in the stream channel. The **higher freeze-up stage** will require a higher streamflow threshold capable of initiating ice breakup in the spring. This higher threshold can **potentially reduce the frequency of ice jams during break-up** (Beltaos et al., 2006; Turcotte et al., 2019), especially if spring flows are reduced due to lesser snow accumulation given a

shorter cold season. On the other hand, the higher threshold does ensure that **an ice jam flood, if it does occur, will be of significant magnitude.**

Ice Thickness

After ice formation, which in this region historically occurs in the fall, ice continues to grow during the winter but at declining rates. This is because the ice sheet itself, and the snow cover, provide thermal insulation. Beltaos and Burrel (2002) remark that *"In the colder parts of Canada, ice thickness hardly changes during the latter part of the winter. A general rise in air temperatures would then produce a relatively small reduction in the pre-breakup ice thickness, which is the value that influences the breakup process."* Burrell et al. (2023), citing studies by Brown and Duguay (2010) and Dibike et al. (2011), indicates that trends in ice thickness are associated not only with air temperature but also snow cover, with the thickest ice corresponding to the smallest snow depth, and vice versa.

The simplest established approach for representing the dependence of maximum ice thickness (Z_{ice}) on air temperature is the Stefan equation (Stefan, 1891; Jumikis, 1977), which represents a linear dependence on the square root of the accumulated freezing degree days ($AFDD$). The Stefan equation is $Z_{ice} = \alpha\sqrt{AFDD}$. The multiplication factor (α) is to be obtained empirically for the specific site of interest, and is sometimes called the "insulation coefficient". Its values have been found to vary between 7 and 27 (according to Turcotte et al., 2019 citing Michel, 1971, and Beltaos, 1995b). Factor α depends on the conditions of snowpack and wind as well as characteristics of the water body. While additional factors, such as streamflow and latent heat fluxes, also influence Z_{ice}, their effect is much smaller (Beltaos and Prowse, 2009). The Stefan equation was used e.g. by Das et al. (2020) for obtaining Z_{ice} projections for the Athabasca River at Fort McMurray, Alberta, under future climate conditions.

For the lower Peace River, Beltaos and Bonsal (2021) obtained an empirical relationship between Z_{ice} and $AFDD$ that differed from the Stefan equation by having an $AFDD$ exponent of 0.59 (instead of 0.5). The empirical value of α was a non-linear function of total winter snowfall. Based on this equation, they used projected $AFDD$ and projected snowfall to obtain projected ice thickness, which indicated a reduction of about 0.2 meters between the 1980s and 2050s and by an additional 0.1 m by the 2080s under the RCP8.5 emissions scenario.

Ice growth in southern rivers of the pan-Arctic domain depends more strongly on air temperature, while in more northern rivers snowpack depth plays a more important role (Burrell et al., 2023, citing the work of Park et al., 2016). In the southern Mackenzie River basin, air temperature is expected to dominate, hence ice is likely to become thinner, regardless of the uncertain future of snow accumulation. Beltaos (2007) showed a reduction by about 10 cm in the maximum ice thickness on the Peace River in the period 1962-2006 – a finding in line with separate studies at a few other North American locations and Russia. As ice thickness declines, the volume of ice available for forming a jam is smaller, reducing the flood risk it poses (Rokaya et al., 2022).

Ice Breakup

The initiation of ice breakup results when the driving force is greater than the resisting force of the ice. In a "dynamic breakup", the driving force is provided by the moving water under the ice cover, while the resistance force depends on the ice cover strength in the downstream direction. In a "thermal breakup", the driving force is a strong radiative balance, brought by increasing air temperature and sunlight in spring. Broken ice may get washed out of the reach and may form an ice jam farther downstream. The warming projected for spring does suggest that rain on snow might become a common occurrence in future, with runoff peaks occurring while the ice still maintains its thickness due to the relatively early date in the year.

Turcotte et al. (2019) provides conceptual graphic representations (reproduced in 1.2) of the evolution of driving and resisting forces from fall to spring, for (a) a cold winter, (b) a less cold and shorter winter, and (c) a very mild winter. As the winter season warms and shortens, the number of ice-jam events may increase due to higher streamflows but cold enough temperatures for ice cover to regrow and regain strength (Figure 1.2b). As warming continues, multiple mid-winter runoff events may break the ice, while air temperatures are insufficiently cold to build a resistance ice cover – resulting in a single and minor ice-jam event in spring (Figure 1.2c). Mid-winter breakup events may occur more frequently as a result of higher peak flows in winter – see e.g. evidence from (Beltaos, 2002).

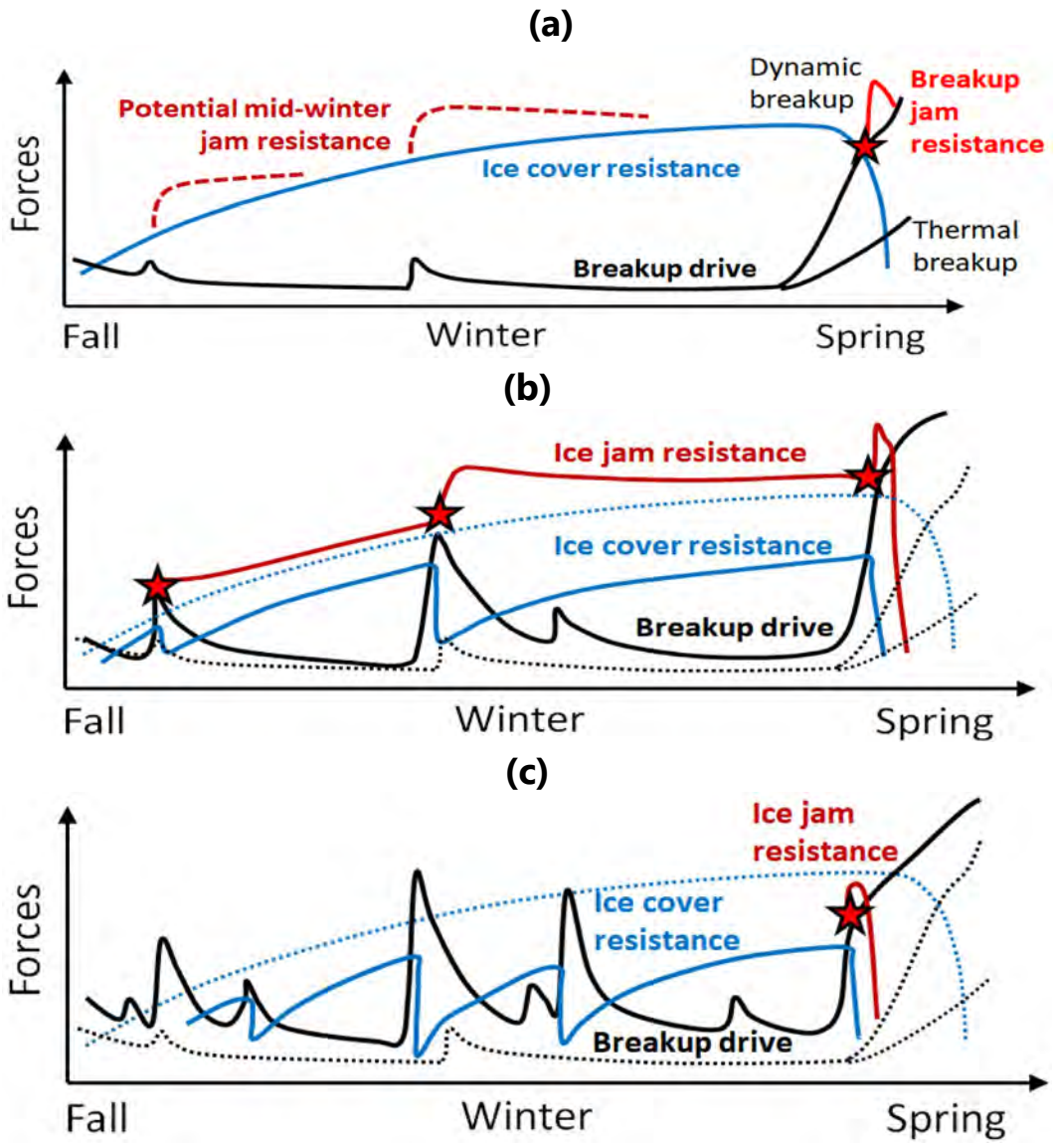

Figure 1.2 Conceptual graphs showing how resisting forces (blue for intact ice cover, red for ice jams) and driving forces (black lines) may evolve under climate warming. The figure panels are reproduced from Turcotte et al. (2019) and they show:

(a) A specific winter scenario characterized by minor mid-winter runoff events.

(b) A shorter winter characterized by major mid-winter runoff events and cold enough temperatures, followed by a dynamic spring breakup event. Three ice-jam events are represented by red stars. Compare to dotted lines from panel a.

(c) A very mild winter characterized by multiple mid-winter runoff events and air temperatures too mild to generate a resistant ice cover. Only one minor ice-jam event is represented by a red star. Compare to dotted lines from panel a.

Turcotte et al. (2019) recommends to use **streamflow** as the best single indicator of the driving forces. He admonishes against using **degree days of thaw (DDT)** as an indicator of high streamflow from spring snowmelt because DDT's strongest effect is through the weakening of the ice cover. In other words, DDT is best used as an indicator of (weakened) resisting forces, though it may also enhance the driving force.

Approaches to Determine Climate Change Impacts on Ice Jam Flooding

Turcotte et al. (2019) describes five different approaches:

1. Statistical analysis of historical water-level trends during the presence of ice
2. Climate-simulation outputs, hydrological models, and river-ice-jam models
3. Climate-simulation outputs and hydromorphologic-climatic transfer
4. Climate-simulation outputs and river ice-jam parameters
5. Climate-simulation outputs and conceptual river ice-jam models

Rather than repeat the descriptions here, we can refer directly to Turcotte et al. (2019).

Hay River Study by Zhao (2012)

The climatic factors associated with severe and moderate flooding at Town of Hay River were investigated empirically in the doctoral thesis by Zhao (2012), from which Figure 1.3 is reproduced. The variables and gauge locations mentioned in Figure 1.3 are given in Table 1-2.

Table 1-2 Definition of variables and gauge name acronyms from Zhao (2012).

Variable	Description
$ADDF_w$	Accumulated degree-days of freezing for the winter at a climate station. Defined as the sum of the negative degree-days for the winter period, which begins on D_{OF} and ends on D_{OT}. This is considered as an index of the winter severity and late winter ice cover condition.
API	Antecedent precipitation index. This is the accumulated precipitation during the previous summer (between July 1 and September 30). It is considered as an index of soil moisture that affects the spring snowmelt runoff process.
$DECAY$	Index variable to account for potential ice strength decay during pre-breakup. $DECAY$ is set to 0, unless D_i is 7 or more days after D_{OT}, in which case it is set to 1. The choice of 7 days is based on the estimated time required for the ice cover to become isothermal before starting to decay.
D_i	Date of measurement of t_i (usually in mid-April).
D_{OF}	Date of onset of freezing degree-days at a climate station.
D_{OT}	Date of onset of thawing degree-days at a climate station.
H_{OF}	Daily water level on the date of onset of freeze-up at a WSC gauge. This variable gives a general idea of the required water level to initiate the

	breakup in spring. As a rule of thumb, the higher H_{OF} is, the greater the water level and snowmelt runoff required to initiate breakup. It is also an alternative of API, considered as a surrogate of soil infiltration capacity during the snowmelt period.
SWE_w	Snow water equivalent for the winter
t_i	Ice thickness from the last direct measurement by WSC near a gauge site at time D_i (usually conducted in mid-April).
Gauge/Station	**Location**
HRA	Hay River Airport
HL	Snow course near the town of High Level.
$HRHR$	Town of Hay River near Hay River

The following interpretation is provided by Zhao (2012) for the results in Figure 1.3:

"It appears that flooding events are associated with higher freeze-up levels, H_{OF}. As shown in [Figure 1.3(a)], when H_{OF} is above 2.8 m, the probability of flooding is high, with some or severe flooding occurring in 7 of 10 cases. The three exceptions (1998, 1993 and 1977) were associated with low snowmelt runoff events, specifically: 390, 159 and 530 m^3/s, respectively, all of which are below the average snowmelt runoff peak flow of 638 m^3/s. Flooding occurred in only 3 (18%) of the 17 years for which the freeze-up level, H_{OF} was below 2.1 m, and none of these events were significant in severity. These findings are consistent with the logic of breakup severity forecasting discussed by Beltaos (1995).

- *When H_{OF} is low: neither low nor high snowmelt runoff would be expected to induce severe flooding.*
- *When H_{OF} is high: a low snowmelt runoff would be more likely to result in a thermal breakup (no flooding), and a high snowmelt runoff would be expected to induce severe flooding.*

"A competent and thick ice cover is typically considered necessary for any significant breakup event. Therefore, the ice variables (t_i and $DECAY$) at the $HRHR$ gauge were also assessed for their potential as predictors of breakup severity. The results are shown in [Figure 1.3(b)], where the letter 'Y' indicates that some ice decay occurred prior to breakup. As the figure illustrates, there is no clear pattern. Two examples are 1977 and 2008: in 1977, the index ice thickness was relatively high (1.2 m) yet no flooding occurred; in 2008, the index ice thickness was 0.6 m (below the average of 0.7 m), yet severe flooding occurred. There also appears to be no particular trend towards lower breakup severity for those years in which decay was thought to have occurred prior to breakup.

> *"[Figure 1.3(c)] shows the freezing degree-days, $ADDF_w$, at the Hay River Airport [HRA], coded by breakup severity. It appears that most of the severe flooding events are associated with a higher $ADDF_w$: 7 of the 8 years (88%) with severe flooding have $ADDF_w$ exceeding the threshold 2,900. Considering that $ADDF_w$ is as an index of the winter severity and late winter ice cover condition, it makes sense that higher $ADDF_w$ may be indicative of a severe breakup. However, this indication is very weak: non-flooding events occurred as many times as flooding events when $ADDF_w$ exceeded this value. This*

suggests that the initial ice cover condition prior to deterioration plays a minor role in the case of Hay River breakup.

"It was also found that neither the API or SWE index variables were indicative of breakup severity, as exemplified by [Figure 1.3(d)] for the API at Hay River A station and [Figure 1.7(e)] for the SWE_w at the High Level snow course. This result implies that none of these variables are individually sufficiently representative of the late winter snowpack condition and runoff potential in the Hay River basin. This illustrates the need for the multi-layer modeling approach; their effects will be combined to facilitate inclusion of all SWE data sources and API in a Layer 3 breakup indicator.

"Based on the above results, the potential predictors for a long lead-time forecasting model of breakup severity include H_{OF}, $ADDF_w$, and a combination of the API and SWE variables to indicate the expected magnitude of snowmelt runoff, i.e. the breakup indicator in Layer 3. This will be discussed in details in Chapter 4."

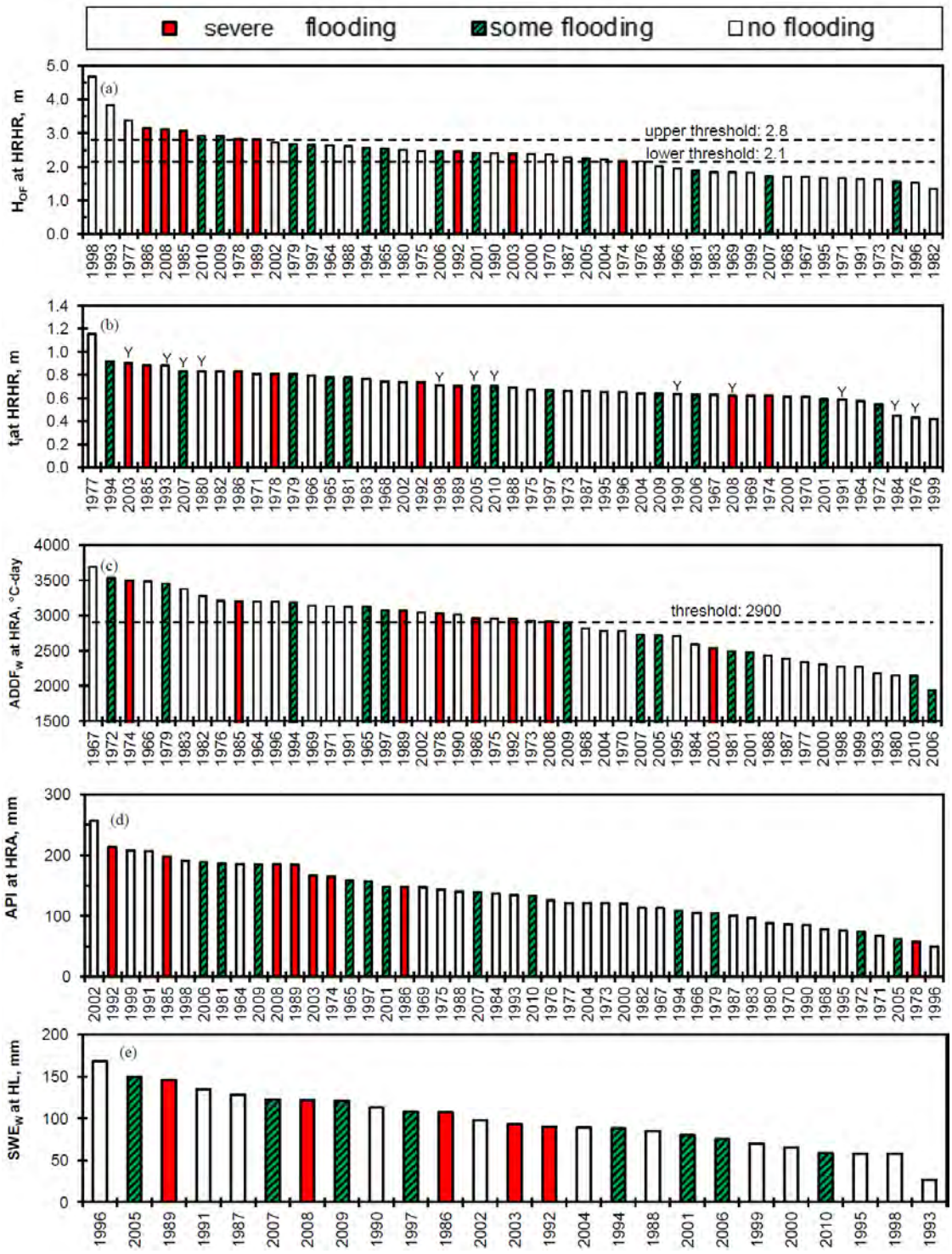

Note: the letter "Y" in panel (b) indicates that some ice decay occurred prior to breakup.

Figure 1.3 Potential predictors for breakup severity at the Town of Hay River. Variables are defined in Table 1-2. This figure is reproduced from Figure 2-5 in Zhao (2012).

Hay River Study by Turcotte (2021)

Turcotte (2021) the water stage records of a few rivers of northwest Canada, including the Hay River. Figure 1.4 plots stage against estimated discharge. The highest stage peaks are break-up peaks (red squares). Turcotte (2021) conveys the difficulty in estimating discharge during ice breakup, especially in the presence of ice jams, and which may explain the poor x-y correlation seen for the red squares plotted in the figure.

Figure 1.5 shows these data plotted chronologically. The variability and auto-correlation clearly exhibited by the data, and the relatively short duration of this record, give insufficient confidence to the trend estimates represented by the dashed lines.

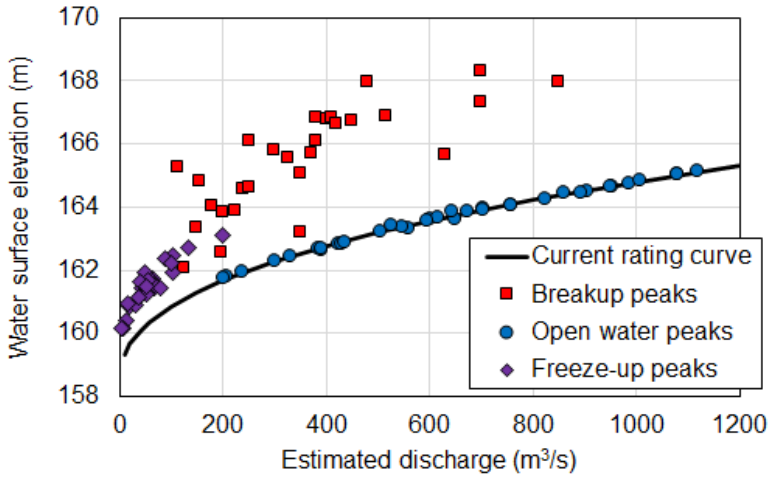

Figure 1.4 Approximate current rating curve, maximum breakup water levels, maximum open water levels and maximum freeze-up water levels between 1972 and 2021 (with several gaps) expressed as a function of the estimated discharge at station 07OB001 on the Hay River upstream of the town of Hay River, Northwest Territories. This figure and legend are reproduced from Turcotte (2021).

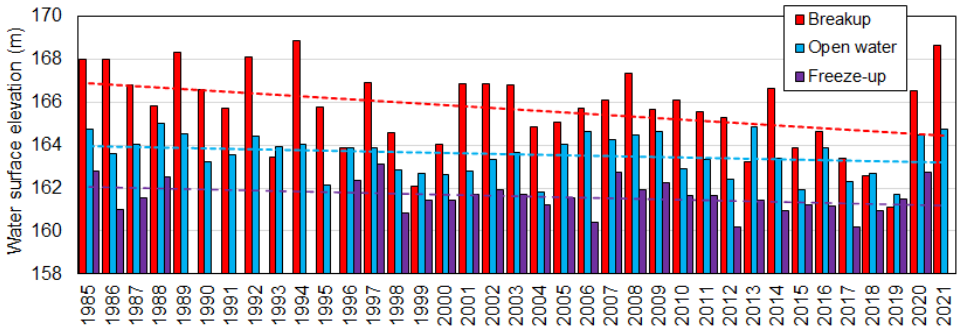

Figure 1.5 Historical annual maximum water levels at breakup, during the open water season, and at freeze-up between 1985 and 2021 at station 07OB001 on the Hay River upstream of the town of Hay River, Northwest Territories. Linear interpolation for freeze-up is presented for qualitative purposes. This figure and legend are reproduced from Turcotte (2021).